Title
Development of Bimetallic Heterogeneous Catalysts for Aqueous Perchlorate Reduction

Permalink
https://escholarship.org/uc/item/9620b0qc

Author
Ren, Changxu

Publication Date
2021

Peer reviewed|Thesis/dissertation

UNIVERSITY OF CALIFORNIA
RIVERSIDE

Development of Bimetallic Heterogeneous Catalysts for Aqueous Perchlorate Reduction

A Dissertation submitted in partial satisfaction
of the requirements for the degree of

Doctor of Philosophy

in

Chemical and Environmental Engineering

by

Changxu Ren

December 2021

Dissertation Committee:
     Dr. Jinyong Liu, Chairperson
     Dr. Kandis Leslie Abdul-Aziz
     Dr. Yun Shen

The Dissertation of Changxu Ren is approved:

Committee Chairperson

University of California, Riverside

ACKNOWLEDGMENTS

crystal diffraction. In addition, Xiaoge Su and Dr. Lihua Xu have been patient with me and helped me with DFT calculations in the past few years. These immense technical supports were exceedingly critical for my Ph.D. study. I feel honored and lucky to have them on the journey towards earning the degree.

Part of this dissertation has used paragraphs, sentences, figures, and tables from the following publications:

(1) Ren, C.; Liu, J. Bioinspired catalytic reduction of aqueous perchlorate by one single-metal site with high stability against oxidative deactivation. *ACS Catalysis*, 2021, 11, 6715−6725.

(2) Ren, C.; Yang, P.; Gao, J.; Huo, X.; Min, X.; Bi, E. Y.; Liu, Y.; Wang, Y.; Zhu, M.; Liu, J. Catalytic reduction of aqueous chlorate with MoOx immobilized on Pd/C. *ACS Catalysis*, 2020, 10, 8201−8211.

(3) Ren, C.; Yang, P.; Sun, J.; Bi, E. Y.; Gao, J.; Palmer, J.; Zhu, M.; Wu, Y.; Liu, J. A bioinspired molybdenum catalyst for aqueous perchlorate reduction. *Journal of the American Chemical Society*, 2021, 143, 7891−7896.

(4) Ren, C.; Bi, Y. E.; Gao, J.; Liu, J. Molybdenum-catalyzed perchlorate reduction: robustness, challenges, and solutions. *ACS ES&T Engineering*, 2021, DOI: 10.1021/acsestengg.1c00290.

ABSTRACT OF THE DISSERTATION

Development of Bimetallic Heterogeneous Catalysts for Aqueous Perchlorate Reduction

by

Changxu Ren

Doctor of Philosophy, Graduate Program in Chemical and Environmental Engineering
University of California, Riverside, December 2021
Dr. Jinyong Liu, Chairperson

As a powerful oxidizer, perchlorate (ClO_4^-) has found widespread use in many energetic materials. Over the past two decades, it has increasingly drawn public attention as a pervasive and persistent water pollutant due to the improper disposal of manufacturing waste. Because human exposure to ClO_4^- can cause thyroid malfunction, many states in the U.S. have set the limits for ClO_4^- at $0.8-18$ μg L^{-1} in drinking water. The interest in ClO_4^- treatment has been further fueled by the recent discovery of ClO_4^- on Mars, Moon, and meteorites, which collectively imply its wide distribution throughout the Solar System. Thus, ClO_4^- removal technologies are of great interest for water purification, disposal of hazardous materials, and human extraterrestrial exploration.

Currently, the commonly used strategy for ClO_4^- removal from drinking water is ion exchange. While selective resins are effective in physically removing ClO_4^-, challenges persist, particularly with the disposal of enriched waste brine and spent reins. Catalytic reduction offers a clean and complete reduction of ClO_4^- to Cl^-. However, the real-world application of the best ClO_4^- reduction catalyst (Re(*hoz*)$_2$–Pd/C) is hampered by using a rare-earth metal and its short lifespan in the oxidative environment. Therefore, it is

imperative to develop an effective, robust, practical, and economic heterogeneous catalyst for aqueous ClO_4^- reduction.

In this work, we have studied the structure-stability relationship of rhenium complexes and discovered that introducing a methyl group on the oxazoline moiety could significantly enhance the overall stability of the complex. Next, we screened a series of molybdenum (Mo) precursors to identify the active Mo species for oxygen atom transfer reaction. Sodium molybdate was found to increase the catalytic activity of virgin Pd/C by 55-fold. This doctoral study has culminated in discovering a simple and straightforward way to construct Mo catalyst for aqueous ClO_4^- reduction. The initial turnover frequency of (*L*)MoO$_x$−Pd/C (*L* = (NH$_2$)$_2$*bpy*) reached 165 h^{-1}, which is the highest among all reported abiotic ClO_4^- reduction catalysts. Lastly, we evaluated the performance of (*L*)MoO$_x$−Pd/C catalyst in synthetic waste brines mimicking ion-exchange resin regeneration. The catalyst has shown limited inhibition in concentrate salt solution and excellent stability under oxidative stress. At the same time, the challenges of deactivation by nitrate and ligand hydrogenation have been identified, and viable solutions were proposed. This doctoral research showcased the power of coordination chemistry in environmental technology innovation. It will guide the ongoing efforts to design catalysts for a wide range of oxygen atom transfer reactions.

TABLE OF CONTENTS

LIST OF FIGURES

LIST OF SCHEMES

LIST OF TABLES

Chapter 1. Introduction

1.1 Toxic Oxyanions in Water Resources

Oxyanions are a wide range of negatively charged polyatomic ions. They have a generic formula of $A_xO_y^{z-}$, in which A represents a chemical element and O represents an oxygen atom.[1] Depending on the pH and electrochemical potential, many metal and non-metal elements can transform into oxyanions in an aqueous phase.[2] Oxyanions of Cr^3, $As^{4,5}$, V^6, C^7, N^8, Si^9, P^{10}, S^7, $Cl^{11, 12}$, and Br^{13} are commonly found in various water systems. Some oxyanions (e.g., CO_3^{2-} and SO_4^{2-}) are benign to the environment and public health. However, other oxyanions are characterized by nonbiodegradability and/or carcinogenicity, which can cause severe health problems.[14]

The occurrence of toxic oxyanions in the aquatic system can be attributed to both natural and anthropogenic processes. For example, the primary sources of heavy metal ions are the natural weathering of mineral ores and improper disposal of manufacturing waste from industrial activities.[15] The contribution of the latter has increased significantly in recent years because of the growth of the microelectronics, electroplating, and battery manufacturing industry.[16] Non-metal oxyanions can form naturally in the atmospheric[17] and geological processes.[18-20] However, the discharge of oxyanion-containing waste from manufacturing plants and runoff from agriculture activities contribute most to the occurrence of non-metal oxyanions in the drinking water resources.[21, 22]

Due to their high solubility, mobility, and low retention capability in soil, oxyanions can be carried far away from the contamination sites by ground and surface water, which

leads to the widespread of these contaminants.[23] They can easily be transferred into living organisms through ingestion, inhalation, and skin absorption.[24] Because of the nonbiodegradability, oxyanions can accumulate in the food chain. Eventually, they will cause adverse health effects to the human being.[25] Regulations and guidelines at the national or state level have been established for oxyanions with confirmed toxicities. For example, the U.S. Environmental Protection Agency (EPA) has set the maximum contaminant level (MCL) for nitrite (NO_2^-), nitrate (NO_3^-), chlorite (ClO_2^-), bromate (BrO_3^-), and total chromium (including CrO_4^{2-}).[26] Some oxyanions are also regulated at the state level. For example, perchlorate (ClO_4^-) is regulated by Massachusetts[27] and California.[28] Considering their detrimental effects, removing toxic oxyanions from drinking water resources and wastewater has become a critical issue for environmental and public health protection. Among all the non-metal oxyanions, ClO_3^- and ClO_4^- are considered recalcitrant oxyanions.[29, 30] This doctoral research focuses on developing novel treatment methods to remove ClO_3^- and ClO_4^- anions in the aqueous phase.

1.2 Background of Chlorate

Chlorate has the formula of ClO_3^-, in which the chlorine atom is in the oxidation state of five. It is highly soluble in water with a solubility of 957 g L^{-1} at 20 ˚C. It has been detected in both surface and groundwater systems.[31]

Water disinfection using chlorine is a major anthropogenic source of ClO_3^- contamination in water. It is a disinfection byproduct (DBP) from the water treatment that uses chlorine compounds, such as chlorine gas, chlorine dioxide, and hypochlorite. As a

potent oxidizing agent, hypochlorite reacts with many components in the solution. It sanitizes a majority of microorganisms, such as bacteria, bacterial spores, and viruses.[32, 33] In comparison to the gaseous chlorine, the use of hypochlorite resulted in the increased formation of chlorate at a fairly high level despite its benefit of on-site generation, easy transportation, and storage.[32, 34, 35] In addition, the chlorate generation can also be exacerbated by the storage conditions, including temperature, UV exposure, and storage duration.[36] It is reported that about 30% of chlorine dioxide is converted to chlorate during the disinfection.[37, 38] Besides the formations related to water treatment processes, the use of herbicides, defoliants, bleaching agent production in the pulp and paper industry also contribute to the occurrence of chlorate in the environment.[39]

ClO_3^- may cause many health effects by inhalation and ingestion. It has shown adverse impacts, including gastrointestinal irritations, stomach ulcers, renal damage and failure, cyanosis, congenital disabilities.[12, 40-44] The lethal dose of ClO_3^- was reported to be 20-gram sodium chlorate or 230 milligrams per kilograms of body.[45] In the United States, the use of weed killers has resulted in reported cases of chlorate intoxication.[11] ClO_3^- can induce hematological responses and cause damages to the red blood cells, proteins, and amino acids. It is also responsible for the formation of methemoglobin by the oxidization state change of the iron center from +2 to +3, which weakens its oxygen transportability.[32, 44, 46] Furthermore, methemoglobin can intensify the inflammatory responses in the body by stimulating the release of cytokines and adhesion molecules, which can lead to acute renal injury.[47] Studies have also shown the carcinogenic effects of chlorate salts. Sub-chronic exposure of potassium and sodium chlorate was reported as promotors of renal tumors.[43]

Regulations for ClO_3^- have been reported and vary with different institutions. ClO_3^- is included in the U.S. EPA Third Contaminant Candidate List (CCL3) in 2014[41] and is reviewed as a DBP in 2016.[48] A health reference level of ClO_3^- in drinking water is 210 µg L^{-1}.[41] Although it is not yet regulated federally, the state of California has a notification level at 800 µg L^{-1}.[11]

1.3 Background of Perchlorate

Perchlorate (ClO_4^-) ion has a tetrahedron molecular geometry, in which chlorine atom is located at the center with four oxygen atoms that are located at the corners of a tetrahedron. In ClO_4^- ion, the chlorine atom is in its highest oxidation state (+VII). From a thermodynamic point of view, it is apparent that ClO_4^- ion is unstable concerning the lowest energy form of chlorine, chloride (Cl^-). However, the spontaneous reduction of ClO_4^- to Cl^- has never been observed in both laboratory and natural environments at ambient temperature.[49] Therefore, ClO_4^- ion is considered kinetically stable. Additional energy is required to overcome an activation barrier for its conversion to a lower free energy state.[14] It has been reported that mechanisms involving oxygen atom transfer and electron transfer are required for the reduction.[49] Because of its notorious lack of reactivity, ClO_4^- persists in the ground and surface water for a long time after entering the environment.

The atmospheric reactions between chlorine and ozone are the primary natural sources of ClO_4^-.[22, 50, 51] In addition to the natural production of ClO_4^-, human activities also contribute to the occurrence of ClO_4^- in the environment. Perchlorate salts have been

manufactured on a large scale for solid rocket fuel, fireworks, and safety flares.[22, 52-55] It has also been reported that water disinfection using chlorine products can generate a certain level of ClO_4^- as the DBP. Hypochlorite products degrade into ClO_4^- depending on the storage time, temperature, and humidity.[36, 56-58] For example, the concentration of ClO_4^- in a bleach product could rise from 390 µg L^{-1} to 8000 µg L^{-1} in two years, as reported by Munster.[59]

In the United States, the first report identifying ClO_4^- in the environment can be dated back to 1997.[60] One year later, the U.S. EPA placed ClO_4^- on the CCL1, indicating the interest in regulating ClO_4^- in drinking water.[61] The inclusion of ClO_4^- on the CCL1 was primarily triggered by the discovery of contamination in Lake Mead and Colorado River, which serve as water resources for multiple purposes by millions of people in California, Nevada, and Arizona.[60] Over the last two decades, studies have reported that ClO_4^- in over 50 states and ClO_4^- has been found in various environmental matrices.[22, 49] At present, ClO_4^- contamination is a global issue. It has been detected in many countries, including Canada[62], China[63], India[64], Japan[65], Korea[66], and Vietnam[67].

ClO_4^- has been found in water, vegetables, fruits, milk, and other dairy products, which poses a risk for populations. [32, 68-70] Because ClO_4^- and I^- have similar ion radius and charge, ClO_4^- can competitively inhibit the iodide uptake in the thyroid.[71] The low I^- level can lead to insufficient production of thyroid hormone. The thyroid hormone regulates growth and cellular metabolism. Patients without adequate storage of the thyroid hormones can suffer from goiter and hypothyroidism.[72] The lack of thyroid hormone can also cause neurological and cognitive deficits for infants.[73, 74]

Due to the toxicity and adverse health effects of ClO_4^-, efforts have been made to determine its environmental occurrence and evaluate its acceptable levels. In 2005, the U.S. National Academy of Science reported an acceptable concentration of 24.5 µg L^{-1} in drinking water, calculated based on a reference dose at 0.07 µg kg^{-1} day^{-1} and daily water ingestion at 2 liters.[75] In 2008, the U.S. EPA set a series of threshold levels from 2 to 25 µg L^{-1}.[75] ClO_4^- concentration in drinking water is also regulated by the state guidelines and regulations for water quality. For example, California has set the MCL of 6 µg L^{-1}, lower than the U.S. federal MCL of 15 µg L^{-1}. In addition, in 2015, the California Office of Environmental Health Hazard Assessment published a public health goal of 1 ppb in drinking water.[76, 77]

1.4 Current Treatments and Challenges

Since the ClO_4^- was added to the CCL1 by the U.S. EPA in 1998, numerous studies have been conducted for ClO_4^- treatment. Based on the working principles, reported ClO_4^- removal methods can be classified into physical, chemical, and biological approaches.

1.4.1 Adsorption by Granular Activated Carbon

Powdered or granular activated carbon has been widely used in water treatment facilities in the U.S. to remove a class of chemicals that gives bad odors or tastes to water. Using activated carbon (AC) for ClO_4^- removal would be easily achieved by retrofitting existing processes in water treatment facilities.[78] AC removes conventional contaminants through surface complexation and electrostatic forces between the contaminant species and the carbon surface. Virgin AC has a relatively large surface area and was expected to offer

a huge capacity to absorb ClO_4^- in water. Experiments using virgin AC for ClO_4^- removal have been conducted. It has been observed that virgin AC was not an effective adsorbent for ClO_4^-.[79] However, the surface property of AC is primarily determined by various functional groups such as carboxylic, lactonic, and phenolic.[80] Although virgin AC was ineffective for aqueous ClO_4^- removal, its adsorption capacity can be improved after appropriate surface modifications. Over the years, multiple effective strategies have been developed for surface modifications. Most surface modifiers are surfactants containing quaternary ammonium (QA) functional group because the permanent positive charge on QA enhances the electrostatic interaction between the carbon surface and the negative charged ClO_4^- ion. Some previously studied surfactants include decyl trimethyl ammonium bromide (DTAB), tributyl heptyl ammonium bromide (THAB), myristyl trimethyl ammonium bromide (MTAB), cetyl trimethyl ammonium chloride (CTAC), cetyl pyridinium chloride (CPC), cetyltrimethylammonium bromide (CTAB), and cetyltrimethylammonium chloride (CTAC).[81] The improvement of adsorption performance by surface modification is rather significant. For example, when using virgin AC for ClO_4^- removal in natural groundwater matrix, the effluent ClO_4^- concentration exceeds the limit after only 2100 bed volumes. In contrast, the surface-modified AC can treat 27000 to 35000 bed volumes before ClO_4^- can be detected in the effluent.[81] Because activated carbon surface is tailored to remove ClO_4^- selectively, additional measures are needed when co-contaminants exist. For instance, to remove arsenate and ClO_4^- in the groundwater, iron hydroxide can be used to eliminate arsenate selectively.[82]

To avoid frequent regeneration, surface modification of virgin AC is necessary. However, the decoration of cationic surfactants on the carbon surface will increase the manufacturing cost. Furthermore, the weak binding between modifiers and the carbon surface may cause surfactants to leach after a long treatment time, which needs additional treatment to prevent secondary pollution. Besides, ClO_4^- ions retained inside the activated carbon need further treatment.

1.4.2 Removal by Membrane Technologies

Membrane technology is an emerging and advanced water treatment process that has been widely used in desalination, disinfection, and removal of synthetic chemicals.[83] It simply uses a physical barrier to separate water molecules from the pollutants such as bacteria, viruses, organic and inorganic substances, and aqueous salts. Several types of membrane operations are commonly used in water treatment. They include microfiltration (MF), ultrafiltration (UF), nanofiltration (NF), and reverse osmosis (RO). Among these pressure-driven membrane operations, MF membranes have the largest pore size, which is typically used to remove large particles and microorganisms. RO can be considered non-porous, which can separate water molecules from aqueous salts and many organic chemicals. The membrane operations can be classified into high-pressure-driven and low-pressure-driven membrane operations.[84, 85] Clearly, operations with smaller membrane pore sizes (e.g., RO and NF) require higher pressure.

RO, NF, and UF have been extensively studied for aqueous ClO_4^- removal among all membrane technologies. The reported methods can be classified into charge-based and size-based exclusion based on the rejection mechanism.

For charge-based separation, a study has evaluated the rejection efficiency of ClO_4^- at a concentration of 100 ppb by NF and UF membranes.[86] In a water matrix without competing ions, the results indicated that the negatively charged membrane could reject ClO_4^- ion, even though the membrane pore size is greater than the size of ClO_4^- ion. This rejection capability might be attributed to the electrostatic interaction between the membrane surface and the ClO_4^- ion. However, they also found that this interaction is quickly lost when there are a sufficient amount of co-existing anions in the water matrix.

Besides charge-based separations, size-based exclusion has also been investigated. Among size-based separations, RO has no limit requirement on the size of an ion. RO membrane may reject all ions in the solution and only allows water molecules to pass through.[78] RO is effective. However, high pressure needs to be maintained for ClO_4^- separation, which may increase the operational cost. One alternative strategy is to use low-pressure membrane filtration in combination with chelate formation. One example is polyelectrolyte enhanced ultrafiltration (PEUF).[87] The operation of PEUF involves the addition of a water-soluble polyelectrolyte, which carries the opposite charge to that of the ions to be removed from the contaminated water. In the case of ClO_4^- removal, the polyelectrolyte should carry a positive charge. The complexation of ClO_4^- with polyelectrolytes leads to the formation of ClO_4^--polyelectrolyte complexes, which the UF membrane can reject. The removal efficiencies of ClO_4^- by multiple polyelectrolytes have

been studied. For example, a study reported that the removal efficiency of ClO_4^- ion by poly(diallyl dimethyl ammonium) chloride (PDADMAC)-enhanced ultrafiltration could reach 90% in a water matrix without competing ions.[81] However, with competing ions such as sulfate and nitrate, the removal rate was reduced to 60% to 80%. Later, a comparative study of poly (4-vinyl pyridine) (P4VP)- and PDADMAC-enhanced ultrafiltration for ClO_4^- removal was published. The authors discovered that the complexation between ClO_4^- and P4VP was affected by the solution pH, polyelectrolyte concentrations, and competing ions.[88]

Overall, pressure-driven membrane technology is a promising technology for eliminating ClO_4^- from drinking water. However, challenges remain. Efforts need to be made to prevent membrane fouling and address the issues of ClO_4^- in the retentate.

1.4.3 Removal by Ion-exchange

Ion exchange (IX) is another commonly used treatment method in water treatment plants. It is a process in which ions exchange between two electrolytes or between an electrolyte solution and a complex. In drinking and wastewater treatment processes, ion exchange resins have been widely used for the purification, separation, and decontamination of undesired ions.[89] Before ClO_4^- became a publicly concerned contaminant in drinking water, the strong base anion (SBA) exchange resins have been observed high affinity to ClO_4^-.[90] A study has investigated an array of fifteen commercial SBA resins for ClO_4^- removal.[91] These resins can be classified into three matrixes (e.g., polystyrene, polyvinyl pyridine, and polyacrylic) and nine functional groups. From the

isotherm experiments, the authors have determined the perchlorate-chloride separation factors for the selected 15 resins. They discovered that the separation factors could vary over three orders of magnitude. The resins of polystyrene-divinylbenzene polymer matrix with triethylamine and tripropyl amine functionalities have been identified as high selectivity for ClO_4^-. However, these resins also showed high selectivity toward nitrate. Therefore, these resins are not recommended for the treatment of water containing both nitrate and perchlorate. Besides nitrate, adsorption experiments of ClO_4^- were also conducted with other co-contaminants. Study by Gu et al. showed that the bifunctional resins, which contain both long and short trialkyl functional groups, outperformed the conventional monofunctional resins when the water has low ClO_4^- and high concentration of competing anions.[92] However, the desorption of ClO_4^- from the bifunctional resins by a HCl solution (0.01 M) was found to be ineffective.

IX is considered the most effective and promising method for removing trace ClO_4^- (10-100 ppb) from drinking water, but it has some intrinsic drawbacks.[78] First, the resins must be functionalized with various quaternary ammonium ions to increase the selectivity of ClO_4^-, which increases the manufacturing cost. Furthermore, a higher affinity between ClO_4^- and resins makes the regeneration of resins unattainable. Considering the high manufacturing cost of resins, one-time use of these resins makes IX economically unsustainable. In addition, direct disposal of the spent resins can reintroduce ClO_4^- back into the environment. The lack of an effective ClO_4^- decomposition method leaves no choice but to incinerate the spent resins when they exhaust.[93] For future researches, efforts can be made to address the effects of co-existing ions and the regeneration issues with

selective resins. Moreover, IX technology can be coupled with other novel methods to decompose ClO_4^- chemically.

1.4.4 Chemical and Biological Reduction

In comparison to physical removal processes, chemical and biological approaches can provide a complete solution if ClO_4^- is reduced to the innocuous Cl^- ion.

As discussed in the background section, the reduction of ClO_4^- in the aqueous solution is a thermodynamically favored reaction. The redox potential of ClO_4^- is +1.226 V.[49]

$$ClO_4^- + 2e^- + 2H^+ \rightarrow ClO_3^- + H_2O \qquad E = +1.226V$$
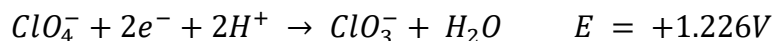
However, the kinetic measurements of the reduction rates indicate that the reactions are inhibited. No appreciable reaction rates have been observed at ambient temperature and pressure between ClO_4^- and common reducing agents used in environmental remediations. These reducing agents include sulfite,[94] dithionites,[94] and zero-valent iron[95]. With conventional reducing agents, harsh reaction conditions such as high temperature and pressure, excess reagents, and strong acidic conditions were usually used to achieve noticeable reaction rates.[49] It has been concluded that the kinetic inertness of ClO_4^- comes from its tetrahedral structure. The nucleophilic attack to the tetrahedrally bound chloride center may form a five-coordination reaction intermediate. The expansion from the tetrahedral to either trigonal bipyramidal or square pyramidal coordination geometry seems to be energetically unfavorable, causing reaction kinetics' overall sluggishness.[49]

In recent years, the biological reduction has shown promise for large-scale applications. Microorganisms have evolved sophisticated but highly efficient enzymatic machinery to utilize oxyanions as metabolism substrates.[96] A widely accepted perchlorate-reducing pathway is the following:

$$ClO_4^- \rightarrow ClO_3^- \rightarrow ClO_2^- \rightarrow Cl^- + O_2$$
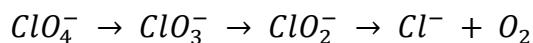
In this process, two key enzymes are involved. The (per)chlorate reductase fulfilled the reduction of ClO_4^- to ClO_2^-. Then, the transformation of ClO_2^- to Cl^- and O_2 is achieved by chlorite dismutase.[97] Inside the protein pocket of the enzymes, the active site for ClO_4^- reduction is the cofactor. Cofactors, mostly non-protein organic molecules or ligand-coordinated metals (e.g., Fe, Mg, Co, Cu, Zn, and Mo), assist enzymes in various biological activities.[97, 98] For example, a Fe-containing hemoprotein, cytochrome, plays a critical role in generating adenosine triphosphate (ATP).[99] Inside (per)chlorate reductase, a highly active molybdenum cofactor (Mo-co) that enables the OAT reaction from ClO_4^- to the Mo center.[100] Mo-co has been found in most living systems, including microorganisms, plants, and animals.[100] The structure contains an organic thiolate ligand.[97] Many OAT reactions associated with the metabolism of nitrogen, sulfur, chlorine, and carbon can be mediated by the Mo-co containing enzymes.[101]

A variety of perchlorate-reducing strains (PRS) have been isolated from the environment or bioreactors. The isolated PRSs are either chemoautotrophic or chemoheterotrophic bacteria. These bacteria are commonly used in the ex-situ treatment process, which is suitable for treating concentrate ClO_4^- waste streams. Ex-situ

bioremediations are commonly implemented by either fluidized-bed or fixed-bed biofilm reactors with ethanol, acetate, or lactate electron donors. [89] Granular activated carbon, glass beads, or buoyant polypropylene rings are employed as support media.[102, 103] Fix-bed bioreactors are effective in ClO_4^- removal. For example, when the influent concentration of ClO_4^- is 40 ppb, a complete reduction to Cl^- can be achieved with an empty bed contact time of 8 hours in a single-pass plug flow operation.[103] In addition, the effects of dissolved oxygen level[104], co-existing ions concentration[105, 106], and backwashing frequency[107] on the bioreactor performance have been studied by multiple researchers. Overall, bioremediation is a promising treatment method. To further explore the potential of biological reduction technology, it is desirable to increase the effectiveness of the biological process, shorten the operation cycle, and investigate the health effects associated with the microorganisms.

1.5 Catalytic Reduction of Perchlorate

1.5.1 Perchlorate Reduction with Hydrogenation Catalysts

Catalytic reduction by supported hydrogenation catalysts is another emerging and promising water treatment method. In reducing target species, hydrogenation metals generate highly reactive atomic hydrogen (H•) via dissociative adsorption of H_2 gas. Then, the reactive H• can reductively transform co-adsorbed water contaminant substrates. In practice, the hydrogenation metal nanoparticles (e.g., Cu^0, In^0, Au^0, Ir^0, Pd^0, Ru^0, Pt^0, and Rh^0) are commonly immobilized onto the heterogeneous supports to enhance metal dispersion and to facilitate catalyst handling. Common supports include activated carbon (C), alumina (Al_2O_3), and silica (SiO_2).[108-110]

These catalysts have shown effectiveness in reducing a variety of toxic oxyanions including ClO_3^-, ClO_4^-, BrO_3^-, and NO_3^-.[111] For instance, an Ir/C catalyst was prepared by impregnating mesoporous carbon support with solutions of H_2IrCl_6.[112] The resulted catalysts were evaluated for ClO_3^- reduction in concentrated solutions of NaCl, which mimics the NaCl brine in the chloralkali process. The reduction rate was dependent on the solution pH, Ir loading in the catalyst, dispersion, and distribution of Ir nanoparticles on the support. Among tested formulations, the catalyst with 5 wt % of Ir was identified to provide the best performance. The authors found that Ir catalysts are resistant to concentrate NaCl compared to other hydrogenation catalysts. The best catalyst was used for up to 18 rounds of ClO_3^- reduction and the authors claimed that the catalyst is stable during long-term testing.

When necessary, a second metal can also be immobilized onto the heterogeneous support to combine the desired properties of both metal catalysts. For instance, Cu-Pd and In-Pd bimetallic catalysts were prepared to reduce NO_3^- ions while improving the selectivity of nitrogen gas.[113] As discussed previously, a step involving the oxygen atom transfer is necessary for ClO_4^- reduction. In order to enhance the overall reduction rate, high-valent oxo transition metals were employed as the second metal catalyst. To date, the highest ClO_4^- reduction rate was achieved by a rhenium complex.[114] The brief history, activities, and imperfections of the rhenium complex are discussed in the following section.

1.5.2 Perchlorate Reduction with Rhenium Complexes and Challenges

Over decades of development, high-valent oxorhenium complexes have become one of the versatile tools in the toolbox of organic and inorganic chemists.[115-123] Because of their ability to transfer oxygen atom from oxygen donors to the substrates, oxorhenium complexes can catalyze a broad spectrum of oxidation reactions, including epoxidation of alkenes,[124, 125] syntheses of sulfoxide and sulfone,[126, 127], and oxidation of organosilanes.[128] Oxophilic rhenium (Re) complexes, on the other hand, are excellent oxygen atom acceptors. A variety of functional Re catalysts have been designed, studied, and utilized for the deoxygenation of carbonyl compounds,[129, 130] the deoxydehydration of renewable biomass derivatives[131-133], and the reduction of nonlabile oxyanions.[134, 135] Among the fascinating features of Re complexes, the most attractive one to environmental chemists is their remarkable ability to catalyze the reduction of ClO_4^-, which is a notoriously inert and pervasive water contaminant.[52, 136] The first report of the reduction of ClO_4^- by in-situ generated methylrhenium dioxide (MDO) can date back to 1995.[137] Later, ligands of 2-(2'-hydroxyphenyl)-2-oxazoline (*hoz*),[134, 138] 2-(2'-hydroxyphenyl)-2-thiazoline (*htz*),[139] and *N,N'*-bis(salicylidene)-1,3-diamino-2,2'-dimethylpropane (saldmpen)[134] were introduced to Re center to overcome the setbacks of MDO, such as facile polymerization, the requirement of highly acidic reaction environment (pH = 0) and the need of potent reducing agents to regenerate.[140] The outstanding catalytic activity of $Re^V(O)(L)_2Cl$ complexes (L = *hoz* or *htz*) motivates researchers to develop a water-compatible catalyst by heterogenization of Re active sites with supported hydrogenation metals (e.g., Pd^0/C and

Rh^0/C).[114, 141] Under 1 atm H_2 and room temperature, such catalysts enable complete reduction of ClO_4^- into Cl^- via OAT reaction.[141]

The development of functional oxorhenium complexes, however, is not without challenges. One major obstacle that jeopardizes their practical application is the deactivation of active sites via hydrolytic decomposition.[141, 142] Upon the reduction of ClO_4^-, $Re^V(O)$ active sites are transformed to the oxidized state, $Re^{VII}(O)_2$. Although reducing agents can quickly regenerate the active sites, the heterogenized $Re^{VII}(O)_2$ can react with water resulting in the formation of perrhenate (ReO_4^-) and free ligands, thus irreversibly loses the unsurpassed activity for ClO_4^- reduction.[139, 142] In most scenarios, the reduction and formation of $Re^{VII}(O)_2$ are in dynamic equilibrium, maintaining a low concentration of $Re^{VII}(O)_2$ species.[139] Therefore, the deactivation is not significant, which might explain why people often overlooked and a dearth of study has focused on the investigation of decomposition. Nevertheless, when the equilibrium is disrupted, for example, the formation rate of $Re^{VII}(O)_2$ is accelerated by reacting with a mass of reaction intermediates (e.g., ClO_x^-, x = 3, 2, 1), the accumulation of $Re^{VII}(O)_2$ can cause severe decomposition.[142] Although eternal catalysts do not exist, it is believed that minimizing the rate of deactivation can be highly beneficial to prevent a misinterpretation of kinetic results, to avoid a waste of Re element during the reaction, and to promote the real-world applications of the catalysts.

Recently, two strategies were developed to regulate the deactivation of the heterogenized $Re(O)(hoz)_2Cl$ complex. In the first approach,[142] a supported Rh^0 catalyst was used to scavenge highly active reaction intermediates because Rh^0 nanoparticles

exhibited higher reduction activity to ClO_x^- than Pd^0 catalyst.[111] This method mediates Re element leaching from 26 % to 5 % of total immobilized metal in the course of ClO_4^- reduction.[142] The strategy is straightforward and effective, but 5 % metal leaching is still unacceptable for any practical use. Also, Rh has a lower natural abundance than Pd, which further limits its practical viability.[143] The second approach involves the structural modification of the *hoz* ligand.[114] A heteroleptic Re(O)(*hoz*)(*htz*)Cl complex was synthesized by replacing one *hoz* ligand with *htz*. The substitution of the oxazoline O in *hoz* by the thiazoline S in *htz* leads to decreased electron density at the metal center, which detunes the OAT activity.[114, 140] The metal leaching detected in the reduction of 4 mM ClO_4^- with the hybrid complex is minimal (e.g., 1 % of the total immobilized complex). However, at the same time, because of the detuned activity Re(O)(*hoz*)(*htz*)Cl is expected to be less effective than Re(O)(*hoz*)$_2$Cl complex in the reduction of 1 mM ClO_4^-, where the decomposition is less prominent. Therefore, complex Re(O)(*hoz*)(*htz*)Cl is not suitable for ClO_4^- reduction with various initial concentrations.

Overall, the $Re^V(O)(L)_2Cl$ complexes are effective for aqueous ClO_4^- removal. However, the practical application of Re-Pd/C catalyst is greatly hindered by the use of rare-earth metal and its short lifespan. Therefore, ongoing needs are to design new Re complexes that are stable in challenging reaction conditions and find a relatively abundant metal that promotes the OAT reactions.

1.6 Research Objectives

This doctoral research aims to develop an effective, robust, practical, and economic heterogeneous catalyst for aqueous ClO_4^- reduction. The specific objectives are the following:

Objective 1: Investigate the structure-stability relationship of Re complexes and design new complexes with enhanced stability and activity.

Chapter 2 addresses **Objective 1** and showcases the significant effect of simple ligand modification in improving catalyst stability for ClO_4^- reduction. Insights on the heterogeneous catalyst design from Re-based catalysts provide the critical knowledge basis for developing Mo-based catalysts.

Objective 2: Identify active Mo species for oxygen atom transfer reaction.

The highly active Mo cofactor in metalloenzymes suggests a great promise of developing Mo-based ClO_4^- reduction catalysts. Limited work has been done to investigate the OAT activity of molybdate and its polyanions in the aqueous phase. In **Chapter 3**, a series of water-soluble Mo isopoly and heteropoly anions are studied for their OAT activity.

Objective 3: Achieve high catalytic ClO_4^- reduction activity and understand reaction mechanisms at the heterogeneous surface.

In biological systems, the assimilated molybdate oxyanion must be complexed with dithiolene ligands to gain biological activity. Inspired by biological systems, we enhanced the OAT activity of molybdate by introducing organic ligands. **Chapter 4** describes a

simple and straightforward way to construct highly reactive ClO_4^- reduction catalysts from molybdate and common nitrogen ligands. The catalyst characterization and heterogeneous reaction mechanisms are also discussed.

Objective 4: Evaluate critical aspects regarding the practical application of Mo-based heterogeneous catalyst.

Chapter 5 evaluates the catalysts' activity, stability, and longevity in the pertinent water treatment conditions. The challenges that are closely related to practical applications have been identified, and viable solutions were provided. The formulation of the catalysts was also optimized to improve the cost-effectiveness of the catalyst.

1.7 References

1.   Adegoke, H. I.; Adekola, F. A.; Fatoki, O. S.; Ximba, B. J., Sorptive Interaction of Oxyanions with Iron Oxides: A Review. *Polish Journal of Environmental Studies* **2013,** *22* (1).

2.   Cornelis, G.; Johnson, C. A.; Van Gerven, T.; Vandecasteele, C., Leaching mechanisms of oxyanionic metalloid and metal species in alkaline solid wastes: A review. *Applied Geochemistry* **2008,** *23* (5), 955-976.

3.   Campos, V.; Büchler, P. M., Removal of chromate from drinking water using powder carbon steel. *Environmental Geology* **2005,** *47* (7), 926-930.

4.   Das, J.; Sarkar, P., A new dipstick colorimetric sensor for detection of arsenate in drinking water. *Environmental Science: Water Research & Technology* **2016,** *2* (4), 693-704.

5.   Johnson, R. L.; Aldstadt, J. H., Quantitative trace-level speciation of arsenite and arsenate in drinking water by ion chromatography. *Analyst* **2002,** *127* (10), 1305-1311.

6.   Ding, W.; Hasegawa, T.; Hosaka, H.; Peng, D.; Takahashi, K.; Seko, Y., Effect of long-term treatment with vanadate in drinking water on KK mice with genetic non-insulin-dependent diabetes mellitus. *Biological Trace Element Research* **2001,** *80* (2), 159-174.

7.   Rylander, R., Drinking water constituents and disease. *The Journal of nutrition* **2008,** *138* (2), 423S-425S.

8.   Winton, E.; Tardiff, R.; McCabe, L., Nitrate in drinking water. *Journal-American Water Works Association* **1971,** *63* (2), 95-98.

9.   Li, B.; Trueman, B. F.; Rahman, M. S.; Gao, Y.; Park, Y.; Gagnon, G. A., Understanding the impacts of sodium silicate on water quality and iron oxide particles. *Environmental Science: Water Research & Technology* **2019,** *5* (8), 1360-1370.

10.   Vasudevan, S.; Sozhan, G.; Ravichandran, S.; Jayaraj, J.; Lakshmi, J.; Sheela, M., Studies on the removal of phosphate from drinking water by electrocoagulation process. *Industrial & Engineering Chemistry Research* **2008,** *47* (6), 2018-2023.

11.   Alfredo, K.; Stanford, B.; Roberson, J. A.; Eaton, A., Chlorate challenges for water systems. *Journal-American Water Works Association* **2015,** *107* (4), E187-E196.

12.   Righi, E.; Bechtold, P.; Tortorici, D.; Lauriola, P.; Calzolari, E.; Astolfi, G.; Nieuwenhuijsen, M. J.; Fantuzzi, G.; Aggazzotti, G., Trihalomethanes, chlorite, chlorate in drinking water and risk of congenital anomalies: a population-based case-control study in Northern Italy. *Environmental research* **2012,** *116*, 66-73.

13.   Matos, C. T.; Velizarov, S.; Reis, M. A.; Crespo, J. G., Removal of bromate from drinking water using the ion exchange membrane bioreactor concept. *Environmental science & technology* **2008,** *42* (20), 7702-7708.

14.   Yin, Y. B.; Guo, S.; Heck, K. N.; Clark, C. A.; Coonrod, C. L.; Wong, M. S., Treating water by degrading oxyanions using metallic nanostructures. *ACS Sustainable Chemistry & Engineering* **2018,** *6* (9), 11160-11175.

15.   Tchounwou, P. B.; Yedjou, C. G.; Patlolla, A. K.; Sutton, D. J., Heavy metal toxicity and the environment. *Molecular, clinical and environmental toxicology* **2012**, 133-164.

16.   Weidner, E.; Ciesielczyk, F., Removal of hazardous oxyanions from the environment using metal-oxide-based materials. *Materials* **2019,** *12* (6), 927.

17.   Orel, A. E.; Seinfeld, J. H., Nitrate formation in atmospheric aerosols. *Environmental Science & Technology* **1977,** *11* (10), 1000-1007.

18.   Bao, H.; Gu, B., Natural perchlorate has a unique oxygen isotope signature. *Environmental Science & Technology* **2004,** *38* (19), 5073-5077.

19.   Jackson, W. A.; Anderson, T.; Harvey, G.; Orris, G.; Rajagopalan, S.; Kang, N., Occurrence and formation of non-anthropogenic perchlorate. In *Perchlorate*, Springer: 2006; pp 49-69.

20.   Holloway, J. M.; Dahlgren, R. A., Geologic nitrogen in terrestrial biogeochemical cycling. *Geology* **1999,** *27* (6), 567-570.

21.   Bouchard, D. C.; Williams, M. K.; Surampalli, R. Y., Nitrate contamination of groundwater: sources and potential health effects. *Journal-American Water Works Association* **1992,** *84* (9), 85-90.

22.   Trumpolt, C. W.; Crain, M.; Cullison, G. D.; Flanagan, S. J.; Siegel, L.; Lathrop, S., Perchlorate: sources, uses, and occurrences in the environment. *Remediation Journal: The Journal of Environmental Cleanup Costs, Technologies & Techniques* **2005,** *16* (1), 65-89.

23.   Anthony, E. T.; Oladoja, N. A., Oxyanions in Groundwater System—Prevalence, Dynamics, and Management Strategies. In *Progress and Prospects in the Management of Oxyanion Polluted Aqua Systems*, Springer: 2021; pp 69-102.

24.   Hajji, S.; Montes-Hernandez, G.; Sarret, G.; Tordo, A.; Morin, G.; Ona-Nguema, G.; Bureau, S.; Turki, T.; Mzoughi, N., Arsenite and chromate sequestration onto ferrihydrite, siderite and goethite nanostructured minerals: Isotherms from flow-through reactor experiments and XAS measurements. *Journal of hazardous materials* **2019,** *362*, 358-367.

25.   Zghida, H.; Baouab, M. H. V.; Gauthier, R., Sorption of chromium oxy-anions onto cationized ligno-cellulosic material. *Journal of applied polymer science* **2003,** *87* (10), 1660-1665.

26.   Acrylamide, O., National Primary Drinking Water Regulations. *Kidney* **2009,** *2* (4-D), 0.07.

27.   Charnley, G., Perchlorate: overview of risks and regulation. *Food and Chemical Toxicology* **2008,** *46* (7), 2307-2315.

28.   Tikkanen, M. W., Development of a drinking water regulation for perchlorate in California. *Analytica Chimica Acta* **2006,** *567* (1), 20-25.

29.   Jung, B.; Sivasubramanian, R.; Batchelor, B.; Abdel-Wahab, A., Chlorate reduction by dithionite/UV advanced reduction process. *International Journal of Environmental Science and Technology* **2017,** *14* (1), 123-134.

30.   Simon, R.; Weber, E. J., Reduction of perchlorate in river sediment. *Environmental Toxicology and Chemistry: An International Journal* **2006,** *25* (4), 899-903.

31.   Robbins, W. W.; Crafts, A. S.; Ray-nor, R. N., Weed control. A textbook and manual. *Weed control. A textbook and manual.* **1942**.

32.   McCarthy, W. P.; O'Callaghan, T. F.; Danahar, M.; Gleeson, D.; O'Connor, C.; Fenelon, M. A.; Tobin, J. T., Chlorate and other oxychlorine contaminants within the dairy supply chain. *Comprehensive reviews in food science and food safety* **2018,** *17* (6), 1561-1575.

33.   Bremer, P. J.; Seale, R. B., Clean-in-Place (CIP). *Encyclopedia of Industrial Biotechnology: Bioprocess, Bioseparation, and Cell Technology* **2009**, 1-8.

34.   Bolyard, M.; Fair, P. S.; Hautman, D. P., Occurrence of chlorate in hypochlorite solutions used for drinking water disinfection. *Environmental science & technology* **1992,** *26* (8), 1663-1665.

35.   Nieminski, E. C.; Chaudhuri, S.; Lamoreaux, T., The occurrence of DBPs in Utah drinking waters. *Journal-American Water Works Association* **1993,** *85* (9), 98-105.

36.   Garcia-Villanova, R. J.; Leite, M. V. O. D.; Hierro, J. M. H.; de Castro Alfageme, S.; Hernandez, C. G., Occurrence of bromate, chlorite and chlorate in drinking waters disinfected with hypochlorite reagents. Tracing their origins. *Science of the Total Environment* **2010,** *408* (12), 2616-2620.

37.   Bolyard, M.; Fair, P. S.; Hautman, D. P., Sources of chlorate ion in US drinking water. *Journal-American Water Works Association* **1993,** *85* (9), 81-88.

38.   Couri, D.; Abdel-Rahman, M. S.; Bull, R. J., Toxicological effects of chlorine dioxide, chlorite and chlorate. *Environmental Health Perspectives* **1982,** *46*, 13-17.

39.   Ali, S. N.; Ahmad, M. K.; Mahmood, R., Sodium chlorate, a herbicide and major water disinfectant byproduct, generates reactive oxygen species and induces oxidative damage in human erythrocytes. *Environmental Science and Pollution Research* **2017,** *24* (2), 1898-1909.

40.   Singelmann, E.; Wetzel, E.; Adler, G.; Steffen, C., Erythrocyte membrane alterations as the basis of chlorate toxicity. *Toxicology* **1984,** *30* (2), 135-147.

41.   USEPA, X., Announcement of Preliminary Regulatory Determination for Contaminants on the Third Drinking Water Contaminant Candidate List. *Federal Register* **2014,** *79* (202), 62716.

42.   Hooth, M. J.; Deangelo, A. B.; George, M. H.; Gaillard, E. T.; Travlos, G. S.; Boorman, G. A.; Wolf, D. C., Subchronic sodium chlorate exposure in drinking water results in a concentration-dependent increase in rat thyroid follicular cell hyperplasia. *Toxicologic pathology* **2001,** *29* (2), 250-259.

43.   McCauley, P.; Robinson, M.; Daniel, F. B.; Olson, G. R., The effects of subchronic chlorate exposure in Sprague-Dawley rats. *Drug and Chemical Toxicology* **1995,** *18* (2-3), 185-199.

44.   Ali, S. N.; Ansari, F. A.; Khan, A. A.; Mahmood, R., Sodium chlorate, a major water disinfection byproduct, alters brush border membrane enzymes, carbohydrate metabolism and impairs antioxidant system of Wistar rat intestine. *Environmental toxicology* **2017,** *32* (5), 1607-1616.

45.   Council, N. R.; Committee, S. D. W., Drinking Water and Health: Volume 1. **1977**.

46.   Al-Otoum, F.; Al-Ghouti, M. A.; Ahmed, T. A.; Abu-Dieyeh, M.; Ali, M., Disinfection by-products of chlorine dioxide (chlorite, chlorate, and trihalomethanes): Occurrence in drinking water in Qatar. *Chemosphere* **2016,** *164*, 649-656.

47.   Chain, E. P. o. C. i. t. F., Risks for public health related to the presence of chlorate in food. *EFSA Journal* **2015,** *13* (6), 4135.

48.   Agency, U. E. P., Announcement of final regulatory determinations for contaminants on the Third Drinking Water Contaminant Candidate List. *Federal Register* **2016,** *81* (1), 13-19.

49.   Gu, B.; Coates, J. D., *Perchlorate: environmental occurrence, interactions and treatment*. Springer Science & Business Media: 2006.

50.   Walvoord, M. A.; Phillips, F. M.; Stonestrom, D. A.; Evans, R. D.; Hartsough, P. C.; Newman, B. D.; Striegl, R. G., A reservoir of nitrate beneath desert soils. *Science* **2003,** *302* (5647), 1021-1024.

51.   Dasgupta, P. K.; Martinelango, P. K.; Jackson, W. A.; Anderson, T. A.; Tian, K.; Tock, R. W.; Rajagopalan, S., The origin of naturally occurring perchlorate: the role of atmospheric processes. *Environmental Science & Technology* **2005,** *39* (6), 1569-1575.

52.   Cao, F.; Jaunat, J.; Sturchio, N.; Cancès, B.; Morvan, X.; Devos, A.; Barbin, V.; Ollivier, P., Worldwide occurrence and origin of perchlorate ion in waters: A review. *Science of the Total Environment* **2019,** *661*, 737-749.

53.   Wu, Q.; Zhang, T.; Sun, H.; Kannan, K., Perchlorate in tap water, groundwater, surface waters, and bottled water from China and its association with other inorganic anions and with disinfection byproducts. *Archives of environmental contamination and toxicology* **2010,** *58* (3), 543-550.

54.   Mendiratta, S. K.; Dotson, R. L.; Brooker, R. T., Perchloric acid and perchlorates. *Kirk-Othmer Encyclopedia of Chemical Technology* **2000**.

55.   Silva, M., Safety flares threaten water quality with perchlorate. *Santa Clara Valley Water District* **2003**.

56.   Stanford, B. D.; Pisarenko, A. N.; Snyder, S. A.; Gordon, G., Perchlorate, bromate, and chlorate in hypochlorite solutions: Guidelines for utilities. *Journal-American Water Works Association* **2011,** *103* (6), 71-83.

57.   Asami, M.; Kosaka, K.; Yoshida, N., Occurrence of chlorate and perchlorate in bottled beverages in Japan. *Journal of health science* **2009,** *55* (4), 549-553.

58.   Dasgupta, P. K.; Dyke, J. V.; Kirk, A. B.; Jackson, W. A., Perchlorate in the United States. Analysis of relative source contributions to the food chain. *Environmental science & technology* **2006,** *40* (21), 6608-6614.

59.   Munster, J. E., *Nonpoint sources of nitrate and perchlorate in urban land use to groundwater, Suffolk County, NY*. State University of New York at Stony Brook: 2008.

60.   Brandhuber, P.; Clark, S.; Morley, K., A review of perchlorate occurrence in public drinking water systems. *Journal-American Water Works Association* **2009,** *101* (11), 63-73.

61.   USEPA, Announcement of the drinking water contaminant candidate list. *Fed. Reg.* **1998,** *63* (40), 10273.

62.   Wang, Z.; Forsyth, D.; Lau, B. P.-Y.; Pelletier, L.; Bronson, R.; Gaertner, D., Estimated dietary exposure of Canadians to perchlorate through the consumption of fruits and vegetables available in Ottawa markets. *Journal of agricultural and food chemistry* **2009,** *57* (19), 9250-9255.

63.   Liao, Z.; Cao, D.; Gao, Z.; Zhang, S., Occurrence of perchlorate in processed foods manufactured in China. *Food Control* **2020,** *107*, 106813.

64.   Kannan, K.; Praamsma, M. L.; Oldi, J. F.; Kunisue, T.; Sinha, R. K., Occurrence of perchlorate in drinking water, groundwater, surface water and human saliva from India. *Chemosphere* **2009,** *76* (1), 22-26.

65.   Kosaka, K.; Asami, M.; Matsuoka, Y.; Kamoshita, M.; Kunikane, S., Occurrence of perchlorate in drinking water sources of metropolitan area in Japan. *Water research* **2007,** *41* (15), 3474-3482.

66.   Her, N.; Jeong, H.; Kim, J.; Yoon, Y., Occurrence of perchlorate in drinking water and seawater in South Korea. *Archives of environmental contamination and toxicology* **2011,** *61* (2), 166-172.

67.   Eguchi, A.; Kunisue, T.; Wu, Q.; Trang, P. T. K.; Viet, P. H.; Kannan, K.; Tanabe, S., Occurrence of perchlorate and thiocyanate in human serum from e-waste recycling and reference sites in Vietnam: association with thyroid hormone and iodide levels. *Archives of environmental contamination and toxicology* **2014,** *67* (1), 29-41.

68.   Murray, C. W.; Egan, S. K.; Kim, H.; Beru, N.; Bolger, P. M., US Food and Drug Administration's Total Diet Study: dietary intake of perchlorate and iodine. *Journal of Exposure Science & Environmental Epidemiology* **2008,** *18* (6), 571-580.

69.   Calderón, R.; Godoy, F.; Escudey, M.; Palma, P., A review of perchlorate (ClO 4−) occurrence in fruits and vegetables. *Environmental monitoring and assessment* **2017,** *189* (2), 82.

70.   El Aribi, H.; Le Blanc, Y. J.; Antonsen, S.; Sakuma, T., Analysis of perchlorate in foods and beverages by ion chromatography coupled with tandem mass spectrometry (IC-ESI-MS/MS). *Analytica Chimica Acta* **2006,** *567* (1), 39-47.

71.   Di Bernardo, J.; Iosco, C.; Rhoden, K. J., Intracellular anion fluorescence assay for sodium/iodide symporter substrates. *Analytical biochemistry* **2011,** *415* (1), 32-38.

72.   Niziński, P.; Błażewicz, A.; Kończyk, J.; Michalski, R., Perchlorate–properties, toxicity and human health effects: an updated review. *Reviews on Environmental Health* **2020**.

73.   Savin, S.; Cvejic, D.; Nedic, O.; Radosavljevic, R., Thyroid hormone synthesis and storage in the thyroid gland of human neonates. *Journal of Pediatric Endocrinology and Metabolism* **2003,** *16* (4), 521-528.

74.   Dowling, A. L.; Martz, G. U.; Leonard, J. L.; Zoeller, R. T., Acute changes in maternal thyroid hormone induce rapid and transient changes in gene expression in fetal rat brain. *Journal of Neuroscience* **2000,** *20* (6), 2255-2265.

75.   Luis, S. J.; Miesner, E. A.; Enslin, C. L.; Heidecorn, K., Review of perchlorate occurrence in large public drinking water systems in the United States of America. *Water Supply* **2019,** *19* (3), 681-694.

76.   Department of Toxic Substances Control, Human and Ecological Risk Office, Perchlorate https://dtsc.ca.gov/perchlorate/ (accessed October 20, 2021).

77.   California Water Boards, Perchlorate in Drinking Water https://www.waterboards.ca.gov/drinking_water/certlic/drinkingwater/Perchlorate.html (accessed October 20, 2021).

78.   Xie, Y.; Ren, L.; Zhu, X.; Gou, X.; Chen, S., Physical and chemical treatments for removal of perchlorate from water–a review. *Process Safety and Environmental Protection* **2018,** *116*, 180-198.

79.   Na, C.; Cannon, F. S.; Hagerup, B., Perchlorate removal via iron-preloaded GAC and borohydride regeneration. *Journal-American Water Works Association* **2002,** *94* (11), 90-102.

80.   Mahmudov, R.; Huang, C. P., Perchlorate removal by activated carbon adsorption. *Separation and Purification Technology* **2010,** *70* (3), 329-337.

81.   Parette, R.; Cannon, F. S., The removal of perchlorate from groundwater by activated carbon tailored with cationic surfactants. *Water Research* **2005,** *39* (16), 4020-4028.

82.   Jang, M.; Cannon, F. S.; Parette, R. B.; Yoon, S.-j.; Chen, W., Combined hydrous ferric oxide and quaternary ammonium surfactant tailoring of granular activated carbon for concurrent arsenate and perchlorate removal. *Water research* **2009,** *43* (12), 3133-3143.

83.   Jacangelo, J. G.; Trussell, R. R.; Watson, M., Role of membrane technology in drinking water treatment in the United States. *Desalination* **1997,** *113* (2-3), 119-127.

84.   Fane, A. T.; Wang, R.; Jia, Y., Membrane technology: past, present and future. In *Membrane and Desalination Technologies*, Springer: 2011; pp 1-45.

85.   Baker, R. W., *Membrane technology and applications*. John Wiley & Sons: 2012.

86.   Yoon, Y.; Amy, G.; Cho, J.; Her, N.; Pellegrino, J., Transport of perchlorate (ClO4−) through NF and UF membranes. *Desalination* **2002,** *147* (1-3), 11-17.

87.   Korus, I.; Loska, K., Removal of Cr (III) and Cr (VI) ions from aqueous solutions by means of polyelectrolyte-enhanced ultrafiltration. *Desalination* **2009,** *247* (1-3), 390-395.

88.   Roach, J. D.; Lane, R. F.; Hussain, Y., Comparative study of the uses of poly (4-vinylpyridine) and poly (diallyldimethylammonium) chloride for the removal of perchlorate from aqueous solution by polyelectrolyte-enhanced ultrafiltration. *water research* **2011,** *45* (3), 1387-1393.

89.   Ye, L.; You, H.; Yao, J.; Su, H., Water treatment technologies for perchlorate: a review. *Desalination* **2012,** *298*, 1-12.

90.   Freeman, D. H., Thermodynamics of Binary Ion-Exchange Systems. *The Journal of Chemical Physics* **1961,** *35* (1), 189-191.

91.   Tripp, A. R.; Clifford, D. A., Ion exchange for the remediation of perchlorate-contaminated drinking water. *Journal-American Water Works Association* **2006,** *98* (4), 105-114.

92.   Gu, B.; Ku, Y.-K.; Brown, G. M., Sorption and desorption of perchlorate and U (VI) by strong-base anion-exchange resins. *Environmental science & technology* **2005,** *39* (3), 901-907.

93.   Choe, J. K.; Mehnert, M. H.; Guest, J. S.; Strathmann, T. J.; Werth, C. J., Comparative assessment of the environmental sustainability of existing and emerging perchlorate treatment technologies for drinking water. *Environmental science & technology* **2013,** *47* (9), 4644-4652.

94.   Vellanki, B. P.; Batchelor, B., Perchlorate reduction by the sulfite/ultraviolet light advanced reduction process. *Journal of hazardous materials* **2013,** *262*, 348-356.

95.   Huang, H.; Sorial, G. A., Perchlorate remediation in aquatic systems by zero valent iron. *Environmental engineering science* **2007,** *24* (7), 917-926.

96.   Karl, D. M., Microbially mediated transformations of phosphorus in the sea: new views of an old cycle. *Annual review of marine science* **2014,** *6*, 279-337.

97.   Coates, J. D.; Achenbach, L. A., Microbial perchlorate reduction: rocket-fuelled metabolism. *Nature Reviews Microbiology* **2004,** *2* (7), 569-580.

98.   Hashim, O. H.; Adnan, N. A., Coenzyme, cofactor and prosthetic group: ambiguous biochemical jargon. *Biochemical education* **1994,** *22* (2), 93-94.

99.   Waterhouse, N. J.; Goldstein, J. C.; Von Ahsen, O.; Schuler, M.; Newmeyer, D. D.; Green, D. R., Cytochrome c maintains mitochondrial transmembrane potential and ATP generation after outer mitochondrial membrane permeabilization during the apoptotic process. *The Journal of cell biology* **2001,** *153* (2), 319-328.

100.	Holm, R., The biologically relevant oxygen atom transfer chemistry of molybdenum: from synthetic analogue systems to enzymes. *Coordination chemistry reviews* **1990,** *100*, 183-221.

101.	Cramer, S.; Wahl, R.; Rajagopalan, K., Molybdenum sites of sulfite oxidase and xanthine dehydrogenase. A comparison by EXAFS. *Journal of the American Chemical Society* **1981,** *103* (26), 7721-7727.

102.	Choi, Y. C.; Li, X.; Raskin, L.; Morgenroth, E., Chemisorption of oxygen onto activated carbon can enhance the stability of biological perchlorate reduction in fixed bed biofilm reactors. *Water research* **2008,** *42* (13), 3425-3434.

103.	Choi, H.; Silverstein, J., Effluent recirculation to improve perchlorate reduction in a fixed biofilm reactor. *Biotechnology and bioengineering* **2007,** *98* (1), 132-140.

104.	Brown, J. C.; Snoeyink, V. L.; Raskin, L.; Lin, R., The sensitivity of fixed-bed biological perchlorate removal to changes in operating conditions and water quality characteristics. *Water Research* **2003,** *37* (1), 206-214.

105.	Herman, D. C.; Frankenberger Jr, W. T. *Bacterial reduction of perchlorate and nitrate in water*; 0047-2425; Wiley Online Library: 1999.

106.	Xu, J.; Trimble, J. J.; Steinberg, L.; Logan, B. E., Chlorate and nitrate reduction pathways are separately induced in the perchlorate-respiring bacterium Dechlorosoma sp. KJ and the chlorate-respiring bacterium Pseudomonas sp. PDA. *Water Research* **2004,** *38* (3), 673-680.

107.	Choi, Y. C.; Li, X.; Raskin, L.; Morgenroth, E., Effect of backwashing on perchlorate removal in fixed bed biofilm reactors. *Water research* **2007,** *41* (9), 1949-1959.

108.	Soares, O. S. G.; Órfão, J. J.; Pereira, M. F. R., Nitrate reduction in water catalysed by Pd–Cu on different supports. *Desalination* **2011,** *279* (1-3), 367-374.

109.	Sikora, E.; Karacs, G.; Kocserha, I.; Muránszky, G.; Fiser, B.; Viskolcz, B.; Vanyorek, L., Hydrogenation of chlorate ions by commercial carbon supported palladium catalysts—a comparative study. *Reaction Kinetics, Mechanisms and Catalysis* **2020,** *131* (1), 129-137.

110.	Gao, J.; Ren, C.; Huo, X.; Ji, R.; Wen, X.; Guo, J.; Liu, J., Supported palladium catalysts: A facile preparation method and implications to reductive catalysis technology for water treatment. *ACS ES&T Engineering* **2020,** *1* (3), 562-570.

111.	Chen, X.; Huo, X.; Liu, J.; Wang, Y.; Werth, C. J.; Strathmann, T. J., Exploring beyond palladium: Catalytic reduction of aqueous oxyanion pollutants with alternative

platinum group metals and new mechanistic implications. *Chemical Engineering Journal* **2017,** *313*, 745-752.

112.   Kuznetsova, L. I.; Kuznetsova, N. I.; Koscheev, S. V.; Zaikovskii, V. I.; Lisitsyn, A. S.; Kaprielova, K. M.; Kirillova, N. V.; Twardowski, Z., Carbon-supported iridium catalyst for reduction of chlorate ions with hydrogen in concentrated solutions of sodium chloride. *Applied Catalysis A: General* **2012,** *427*, 8-15.

113.   Jung, J.; Bae, S.; Lee, W., Nitrate reduction by maghemite supported Cu-Pd bimetallic catalyst. *Applied Catalysis B: Environmental* **2012,** *127*, 148-158.

114.   Liu, J.; Han, M.; Wu, D.; Chen, X.; Choe, J. K.; Werth, C. J.; Strathmann, T. J., A new bioinspired perchlorate reduction catalyst with significantly enhanced stability via rational tuning of rhenium coordination chemistry and heterogeneous reaction pathway. *Environmental science & technology* **2016,** *50* (11), 5874-5881.

115.   Bandari, C.; Nicholas, K. M., Oxo-Rhenium-Catalyzed Radical Addition of Benzylic Alcohols to Olefins. *The Journal of Organic Chemistry* **2020,** *85* (5), 3320-3327.

116.   Lambic, N. S.; Sommer, R. D.; Ison, E. A., Tuning catalytic activity in the hydrogenation of unactivated olefins with transition-metal oxos as the lewis base component of frustrated lewis pairs. *ACS Catalysis* **2017,** *7* (2), 1170-1180.

117.   Hayne, D. J.; White, J. M.; McLean, C. A.; Villemagne, V. L.; Barnham, K. J.; Donnelly, P. S., Synthesis of oxorhenium (V) and oxotechnetium (V) complexes that bind to amyloid-β plaques. *Inorganic chemistry* **2016,** *55* (16), 7944-7953.

118.   Lippert, C. A.; Arnstein, S. A.; Sherrill, C. D.; Soper, J. D., Redox-Active Ligands Facilitate Bimetallic O2 Homolysis at Five-Coordinate Oxorhenium (V) Centers. *Journal of the American Chemical Society* **2010,** *132* (11), 3879-3892.

119.   Morrill, C.; Grubbs, R. H., Highly selective 1, 3-isomerization of allylic alcohols via rhenium oxo catalysis. *Journal of the American Chemical Society* **2005,** *127* (9), 2842-2843.

120.   Naruto, M.; Agrawal, S.; Toda, K.; Saito, S., Catalytic transformation of functionalized carboxylic acids using multifunctional rhenium complexes. *Scientific reports* **2017,** *7* (1), 1-12.

121.   Sherry, B. D.; Loy, R. N.; Toste, F. D., Rhenium (V)-catalyzed synthesis of 2-deoxy-α-glycosides. *Journal of the American Chemical Society* **2004,** *126* (14), 4510-4511.

122.   Valla, M.; Stadler, D.; Mougel, V.; Copéret, C., Switching on the Metathesis Activity of Re Oxo Alkylidene Surface Sites through a Tailor-Made Silica–Alumina Support. *Angewandte Chemie International Edition* **2016,** *55* (3), 1124-1127.

123.   Zhang, Y.; Fanna, D. J.; Shepherd, N. D.; Karatchevtseva, I.; Lu, K.; Kong, L.; Price, J. R., Dioxo-vanadium (V), oxo-rhenium (V) and dioxo-uranium (VI) complexes with a tridentate Schiff base ligand. *RSC advances* **2016,** *6* (79), 75045-75053.

124.   Terfassa, B.; Schachner, J. A.; Traar, P.; Belaj, F.; Zanetti, N. C. M., Oxorhenium (V) complexes with naphtholate-oxazoline ligands in the catalytic epoxidation of olefins. *Polyhedron* **2014,** *75*, 141-145.

125.   Dinda, S.; Drew, M. G.; Bhattacharyya, R., Oxo-rhenium (V) complexes with bidentate phosphine ligands: Synthesis, crystal structure and catalytic potentiality in epoxidation of olefins using hydrogen peroxide activated bicarbonate as oxidant. *Catalysis Communications* **2009,** *10* (5), 720-724.

126.   Zhang, B.; Li, S.; Yue, S.; Cokoja, M.; Zhou, M.-D.; Zang, S.-L.; Kuehn, F. E., Imidazolium perrhenate ionic liquids as efficient catalysts for the selective oxidation of sulfides to sulfones. *Journal of Organometallic Chemistry* **2013,** *744*, 108-112.

127.   Wojaczynska, E.; Wojaczynski, J., Enantioselective synthesis of sulfoxides: 2000− 2009. *Chemical reviews* **2010,** *110* (7), 4303-4356.

128.   Ison, E. A.; Corbin, R. A.; Abu-Omar, M. M., Hydrogen production from hydrolytic oxidation of organosilanes using a cationic oxorhenium catalyst. *Journal of the American Chemical Society* **2005,** *127* (34), 11938-11939.

129.   Bernando, J. R.; Florindo, P. R.; Wolff, M.; Machura, B.; Fernandes, A. C., Reduction of aldehydes catalyzed by oxo-rhenium (V) complexes containing heterocyclic ligands. *Tetrahedron letters* **2015,** *56* (2), 414-418.

130.   Bernardo, J. R.; Fernandes, A. C., Deoxygenation of carbonyl compounds using an alcohol as an efficient reducing agent catalyzed by oxo-rhenium complexes. *Green Chemistry* **2016,** *18* (9), 2675-2681.

131.   Raju, S.; Van Slagmaat, C. A.; Li, J.; Lutz, M.; Jastrzebski, J. T.; Moret, M.-E.; Klein Gebbink, R. J., Synthesis of cyclopentadienyl-based trioxo-rhenium complexes and their use as deoxydehydration catalysts. *Organometallics* **2016,** *35* (13), 2178-2187.

132.   Cao, J.; Tamura, M.; Nakagawa, Y.; Tomishige, K., Direct synthesis of unsaturated sugars from methyl glycosides. *ACS Catalysis* **2019,** *9* (4), 3725-3729.

133.   Shiramizu, M.; Toste, F. D., Deoxygenation of Biomass-Derived Feedstocks: Oxorhenium-Catalyzed Deoxydehydration of Sugars and Sugar Alcohols. *Angewandte Chemie International Edition* **2012,** *51* (32), 8082-8086.

134.   Abu-Omar, M. M.; McPherson, L. D.; Arias, J.; Béreau, V. M., Clean and efficient catalytic reduction of perchlorate. *Angewandte Chemie* **2000,** *112* (23), 4480-4483.

135.   Zhang, Y.; Hurley, K. D.; Shapley, J. R., Heterogeneous catalytic reduction of perchlorate in water with Re− Pd/C catalysts derived from an oxorhenium (V) molecular precursor. *Inorganic chemistry* **2011,** *50* (4), 1534-1543.

136.   Liu, J.; Choe, J. K.; Sasnow, Z.; Werth, C. J.; Strathmann, T. J., Application of a Re–Pd bimetallic catalyst for treatment of perchlorate in waste ion-exchange regenerant brine. *Water research* **2013,** *47* (1), 91-101.

137.   Abu-Omar, M. M.; Espenson, J. H., Facile abstraction of successive oxygen atoms from perchlorate ions by methylrhenium dioxide. *Inorganic chemistry* **1995,** *34* (25), 6239-6240.

138.   Arias, J.; Newlands, C. R.; Abu-Omar, M. M., Kinetics and mechanisms of catalytic oxygen atom transfer with oxorhenium (V) oxazoline complexes. *Inorganic chemistry* **2001,** *40* (9), 2185-2192.

139.   McPherson, L. D.; Drees, M.; Khan, S. I.; Strassner, T.; Abu-Omar, M. M., Multielectron atom transfer reactions of perchlorate and other substrates catalyzed by rhenium oxazoline and thiazoline complexes: Reaction kinetics, mechanisms, and density functional theory calculations. *Inorganic chemistry* **2004,** *43* (13), 4036-4050.

140.   Abu-Omar, M. M., Swift oxo transfer reactions of perchlorate and other substrates catalyzed by rhenium oxazoline and thiazoline complexes. *Chemical communications* **2003,** (17), 2102-2111.

141.   Liu, J.; Choe, J. K.; Wang, Y.; Shapley, J. R.; Werth, C. J.; Strathmann, T. J., Bioinspired complex-nanoparticle hybrid catalyst system for aqueous perchlorate reduction: Rhenium speciation and its influence on catalyst activity. *ACS Catalysis* **2015,** *5* (2), 511-522.

142.   Liu, J.; Chen, X.; Wang, Y.; Strathmann, T. J.; Werth, C. J., Mechanism and mitigation of the decomposition of an oxorhenium complex-based heterogeneous catalyst for perchlorate reduction in water. *Environmental science & technology* **2015,** *49* (21), 12932-12940.

143.   Schlesinger, M.; Paunovic, M., *Modern electroplating*. John Wiley & Sons: 2011; Vol. 55.

Chapter 2. Bioinspired Catalytic Reduction of Aqueous Perchlorate by One Single-Metal Site with High Stability Against Oxidative Deactivation

This chapter is based on, or in part a reprint of the material as it appears in Ren, C.; Liu, J. Bioinspired catalytic reduction of aqueous perchlorate by one single-metal site with high stability against oxidative deactivation. *ACS Catalysis*, 2021, 11, 6715−6725.

2.1 Abstract

Reduction of perchlorate (ClO_4^-) with an active and stable catalyst is of great importance for environmental, energy, and space technologies. However, after the rate-limiting oxygen atom transfer (OAT) from inert ClO_4^-, the much more reactive ClO_x^- ($x \leq 3$) intermediates can cause catalyst deactivation. The previous Re−Pd/C catalyst contained a $[Re^V(O)(hoz)_2]^+$ site (H*hoz* = 2-(2'-hydroxyphenyl)-2-oxazoline) and readily reduced ClO_4^-, but ClO_x^- intermediates led to rapid formation and hydrolysis of $[Re^{VII}(O)_2(hoz)_2]^+$. While microbes use delicate enzymatic machinery to survive the oxidative stress during ClO_4^- reduction, a synthetic catalyst needs a straightforward self-protective design. In this work, we introduced a methyl group on the ligand oxazoline moiety and achieved a substantial enhancement of catalyst stability without sacrificing the performance of ClO_4^- reduction. A suite of kinetics measurement, XPS characterization, reaction modeling, stopped-flow photospectrometry, and ^{1}H NMR monitoring revealed the underlying mechanism. The most critical and unexpected effect of the methyl group is the deceleration (for two orders-of-magnitude) of OAT from ClO_3^- to $[Re^V(O)(\mathbf{Me}hoz)_2]^+$. However, the rate of OAT with ClO_4^- was not affected. The methyl group also slowed down the

hydrolysis of $[Re^{VII}(O)_2(\textbf{Me}hoz)_2]^+$, and allowed the introduction of methoxy onto the phenolate moiety to further accelerate ClO_4^- reduction. With 1 atm H_2 at 20°C, the Re−Pd/C catalyst used $[Re^V(O)(\textbf{Me}hoz\textbf{OMe})_2]^+$ as the only reaction site to reduce multiple spikes of 10 mM ClO_4^- into Cl^- without decomposition. This work showcases the significant effect of simple ligand modification in improving catalyst stability for high-performance ClO_4^- reduction.

2.2 Introduction

Over the past two decades, perchlorate (ClO_4^-) has increasingly drawn public attention as a pervasive and persistent water pollutant due to the improper disposal of energetic materials and natural atmospheric formation.[1-4] Because excess exposure to ClO_4^- can cause thyroid malfunction,[5] many states in the U.S. have set the limits for ClO_4^- at 0.8−18 µg L^{-1} in drinking water.[3, 6] The interest in ClO_4^- has been further stimulated by the recent discovery of ClO_4^- on Mars,[7-10] Moon,[11] and meteorites,[11, 12] which collectively imply its wide distribution throughout (and perhaps beyond) the Solar System.[11, 13] Thus, the reduction and utilization of ClO_4^- have considerable importance for human's extraterrestrial exploration by removing chemical hazard, improving soil habitability, providing life support, and fueling vehicle operations.[14]

While ClO_4^- is highly inert under ambient conditions, microorganisms have developed delicate enzymatic machinery for ClO_4^- reduction (**Figure 2.1a**). The sequential 2e⁻ reduction of ClO_4^- to ClO_3^- and ClO_2^- are fulfilled by (per)chlorate reductase, which contains a molybdopterin-coordinated Mo cofactor as the active site.[15] A series of Fe-S

clusters, heme complexes, and electron shuttle compounds enable the electron transfer and redox cycling of the Mo cofactor.[16-18] The further reduction of ClO_2^- in the same pathway will generate highly reactive $HClO/ClO^-$ (pKa 7.5), which can irreversibly inactivate the enzyme by reacting with both the metal factors and the protein.[19] Thus, a second enzyme, chlorite dismutase, uses a *heme* factor to convert ClO_2^- into innocuous Cl^- and O_2.[20] However, ClO^- can still be released from approximately 1 out of 100 reaction cycles.[19] Another defense mechanism against ClO^- is realized by a methionine-rich periplasmic protein.[21] The oxidized sulfoxide product is regenerated by a methionine sulfoxide reductase that uses a Mo cofactor.[22] Therefore, the rapid and robust microbial reduction of ClO_4^- is achieved through the cooperation of all components and functions.[23]

Significant efforts have been taken to design synthetic metal catalysts that mimic biochemical principles to reduce ClO_4^- and other oxyanions.[24-30] In particular, we have developed a bioinspired Re−Pd/C catalyst, in which the single-site $[Re^V(O)(hoz)_2]^+$ complex (hoz = 2-(2′-hydroxyphenyl)-2-oxazoline), Pd^0 nanoparticles with H_2 gas, and the porous carbon (**Figure 2.1b**) mimic the three essential components of the enzyme system-the Mo cofactor, the electron transfer chain, and the protein support.[28] While homogeneous metal catalysts are moisture-sensitive[24, 29, 30] or require special electron donors such as hydrazine, ferrocene, sulfide, and phosphine,[24-26] the heterogeneous Re−Pd/C platform enables rapid reduction of aqueous ClO_4^- by 1 atm H_2 at 20 °C.[28] However, upon rapid oxidation by the highly reactive ClO_x^- intermediates, accumulated $[Re^{VII}(O)_2(hoz)_2]^+$ in the $Re^{V/VII}$ cycle is subject to irreversible hydrolysis (**Figure 2.1c**).[31] Because simplicity is essential for both bioinspired design and practical application, the multi-component

defense mechanism used by microbes cannot be readily mimicked in a synthetic catalyst system. Therefore, a novel "self-defense" mechanism for the Re site against oxidative deactivation is of great interest to both catalytic science and engineering. In other words, can we develop a single-metal site that is both active and stable without a multi-component protection mechanism? If yes, how simple is the design of such a metal site?

In this contribution, we report on the discovery and elucidation of a surprising and advantageous structure-stability feature. Without lowering the rate of ClO_4^- reduction, the introduction of a methyl group to the original *hoz* ligand substantially slowed down (1) the oxidation of the Re^V site by ClO_x^- intermediates and (2) the hydrolysis of the Re^{VII} site. The "evolved" catalyst exhibited high stability against oxidative deactivation and thus significantly enhanced the performance in ClO_4^- reduction. This simple ligand modification provided effective protection of the reactive site, demonstrating a novel strategy to design catalysts with a single-metal site against deactivation by reaction intermediates.
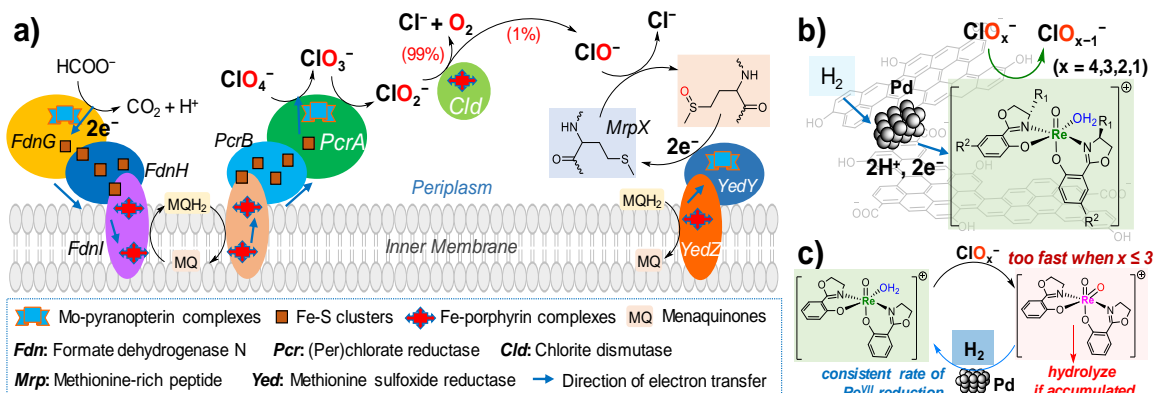
Figure 2.1 (a) Overall microbial reduction of ClO_4^- including electron harvest from organic donors, (per)chlorate reduction, chlorite dismutation, and hypochlorite scavenging; (b) the simplified bioinspired design of Re−Pd/C; and (c) the mechanistic challenge of the previous catalyst.

2.3 Materials and Methods

2.3.1 General Information

All chemicals and solvents were purchased from Alfa-Aesar, Sigma-Aldrich, and Ark Pharm. Without specific notes, chemicals were used as received. Nuclear magnetic resonance (NMR) and X-ray single-crystal structure determination were conducted at the Analytical Chemistry Instrumentation Facility (ACIF) at the University of California, Riverside. Elemental analyses were conducted by the Microanalysis Laboratory at the University of Illinois at Urbana-Champaign. Both the HL_{N-O} ligands and $Re^V(O)(L_{N-O})_2Cl$ complexes are stable under air. Unless noted, all experimental procedures were conducted under air. **SAFETY NOTE**: Although $NaClO_4$ and $LiClO_4$ are not categorized as explosive chemicals, cautions should be taken after they are mixed with metal complexes in organic solutions. One cannot exclude the possibility of forming potentially unstable products after a long-term storage of the mixture.

2.3.2 Preparation of H$L_{\text{N--O}}$ Ligands

The corresponding 2-hydroxybenzonitrile (1.5 mmol), amino alcohol (1.6 mmol), ZnCl$_2$ (4.1 mg, 0.03 mmol), and toluene (3 mL) were loaded in a 15-mL glass pressure vessel. The mixture was refluxed at 110 °C for 24 h. After the reaction, the solvent was removed by rotavap. The crude product was extracted with 3 mL of Et$_2$O five times. The combined organic phase was dried, and the residue was re-dissolved in a minimal amount of EtOAc. Silica gel flash chromatography was used to isolate the product with an eluent of 4:1 hexanes/EtOAc. Solvent removal by rotavap afforded a yellowish oil, which solidified after being placed under –20°C overnight and remained solid at room temperature.

H*hoz* (*L1*). The starting materials were 2-hydroxybenzonitrile and ethanolamine. Synthesis and characterization data have been reported previously.[28]

H*hoz*(5MeO) (*L2*). The starting materials were 2-hydroxy-5-methoxybenzonitrile (224 mg, 1.5 mmol) and ethanolamine (98 mg, 1.6 mmol). Yield: 243 mg (84 %). ^{1}H NMR (600 MHz, CDCl$_3$) δ 11.72 (br, 1H), 7.15 (d, *J* = 3.2 Hz, 1H), 6.98 (dd, *J* = 9.0, 3.1 Hz, 1H), 6.94 (d, *J* = 8.9 Hz, 1H), 4.42 (t, *J* = 9.5 Hz, 2H), 4.11 (t, *J* = 9.4 Hz, 2H), 3.77 (s, 3H). ^{13}C NMR (151 MHz, CDCl$_3$) δ 166.14, 154.25, 151.90, 121.08, 117.72, 111.04, 110.41, 66.92, 56.01, 53.69.

HMe*hoz* (*L3*). The starting materials were 2-hydroxybenzonitrile and (*S*)-(+)-2-amino-1-propanol (L-alaninol). Synthesis and characterization data have been reported previously.[32]

HMe*hoz*(5MeO) (*L*4). The starting materials were 2-hydroxy-5-methoxybenzonitrile (224 mg, 1.5 mmol) and (*S*)-(+)-2-amino-1-propanol (L-alaninol, 124 mg, 1.6 mmol). Yield: 270 mg (87 %). ^{1}H NMR (400 MHz, CDCl$_3$) δ 11.78 (br, 1H), 7.13 (d, *J* = 2.9 Hz, 1H), 7.01 – 6.90 (m, 2H), 4.51 (dd, *J* = 9.3, 7.6 Hz, 1H), 4.48 – 4.38 (m, 1H), 3.95 (t, *J* = 7.3 Hz, 1H), 3.77 (s, 3H), 1.36 (d, *J* = 6.3 Hz, 3H). ^{13}C NMR (101 MHz, CDCl$_3$) δ 164.91, 154.35, 151.91, 121.15, 117.70, 111.00, 110.34, 73.42, 61.04, 55.99, 21.58.

2.3.3 Preparation of Re^V(O)(*L*$_{N–O}$)$_2$Cl Complexes

The corresponding *L*$_{N–O}$ ligand (0.324 mmol) and Re(O)(OPPh$_3$)(SMe$_2$)Cl$_3$ (100 mg, 0.154 mmol) were first dissolved in EtOH (3 mL) in a 15 mL glass pressure vessel. Then 2,6-lutidine (38 µL, 35 mg, 0.324 mmol) was diluted in 0.5 mL EtOH and added dropwise by a syringe. Upon heating in a 78°C-oil bath, the mixture turned into a green solution within 10−15 min, and the green solid gradually precipitated out. After reflux for 24 h, the suspension was cooled in an ice-water bath and filtered through a glass funnel. The green powder was sequentially washed with EtOH (1 mL × 3) and Et$_2$O (1 mL × 3).

Re^V(O)(*hoz*)$_2$Cl (1a). The ligand used was *L*1. Synthesis and characterization data have been reported previously. In particular, an excess amount of 2,6-lutidine (5 molar equivalents to Re) was necessary to ensure complete conversion of the *N,N-cis* isomer into the desired *N,N-trans* isomer.

Re^V(O)[*hoz*(5MeO)]$_2$Cl (1b). The ligand used was *L*2. The product was a dark green solid with minimal solubilities in common solvents, such as dichloromethane,

chloroform, EtOAc, and acetonitrile, and methanol. ^{1}H NMR characterization showed a mixture of two isomers. The limited solubility made it very difficult to conduct further purification or isomer conversion. The stained-glass frit filter was effectively cleaned with concentrated nitric acid, which quickly oxidized the green Re^V stains into red Re^{VII}. Then the Re^{VII} product quickly hydrolyzed into a colorless mixture of ReO_4^- and the free ligand.

$Re^V(O)(Mehoz)_2Cl$ (2a). The ligand used was **L3**. Synthesis and characterization data have been reported previously.[33] An excess amount of 2,6-lutidine was not needed.

$Re^V(O)[Mehoz(5MeO)]_2Cl$ (2b). The ligand used was **L4** (67 mg, 0.324 mmol). Yield: 90 mg (90 %). ^{1}H NMR (400 MHz, CDCl$_3$) δ 7.30 (d, J = 3.3 Hz, 1H), 7.17 (d, J = 3.1 Hz, 1H), 7.08 (dd, J = 9.2, 3.3 Hz, 1H), 6.87 (dd, 1H), 6.84 (d, J = 9.3 Hz, 1H), 6.72 (d, J = 9.1 Hz, 1H), 5.43 – 5.29 (m, 1H), 5.03 (t, J = 8.6 Hz, 1H), 4.78 (t, J = 8.6 Hz, 1H), 4.71 (dd, J = 8.6, 3.8 Hz, 1H), 4.61 – 4.48 (m, 1H), 4.48 (dd, J = 8.1, 6.0 Hz, 1H), 3.81 (s, 3H), 3.76 (s, 3H), 1.74 (d, J = 6.5 Hz, 3H), 1.71 (d, J = 6.6 Hz, 3H). Elemental analysis ($C_{22}H_{24}ClN_2O_7Re$) Theoretical: C, 40.65%; H, 3.72%; N, 4.31%; Cl, 5.45%; Re, 28.64%, found: C, 40.86%; H, 3.77%; N, 4.33%; Cl, 5.14%; Re, 28.32%.

2.3.4 Preparation of Heterogeneous Re−Pd/C Catalysts

The preparation of bimetallic Re−Pd/C catalysts followed the direct aqueous adsorption approach.[28] The information on the Pd/C material and mass transfer considerations are available in our previous report. Specifically, Re(O)($L_{N–O})_2$Cl (containing 1.25 mg Re), 25 mg of Pd/C, a magnetic stir bar, and 50 mL of deionized (DI) water (pH adjusted to 3.0 by addition of 2N H$_2$SO$_4$) were sequentially loaded in a 50 mL

pear-shaped flask. Then, the flask was sealed with a rubber stopper and sonicated for 5 min

to disperse $Re(O)(L_{N-O})_2Cl$ and Pd/C. Two stainless steel needles (16-gauge in diameter,

6-inch in length) were inserted into the flask through the rubber stopper. The needle with

the tip submerged in the water was the inlet of H_2 gas. The other needle had the tip above

the water as the gas outlet to the fume hood and the sampling port. The suspension was

stirred at 1100 rpm under 1 atm H_2 headspace for at least 4 h. This process yielded a

suspension of $Re(O)(L_{N-O})_2-$Pd/C catalyst (0.5 g L^{-1}, 5 wt % Pd and 5 wt % Re) for ClO_4^-

reduction experiments. The >95% of chloride ion release from the $Re(O)(L_{N-O})_2Cl$

precursor **1a**, **2a**, and **2b** was the indicator for the immobilization and activation of

$Re^V(O)(L_{N-O})_2$ sites on the carbon support.[28]

2.3.5 Catalytic Reduction of Aqueous Perchlorate and Sample Analysis

Catalytic reduction of 1 mM (or 10 mM) ClO_4^- was initiated by adding 0.25 mL

(or 2.5 mL) of $NaClO_4$ stock solution (0.2 M) into the catalyst suspension through the H_2

outlet needle. The H_2 flow rate was adjusted to about 1 mL min^{-1} (1−2 bubbles per second

from the 16-gauge needle tip). A higher H_2 flow rate did not accelerate the reactions. For

the reduction of ClO_3^-, a 0.2 M $NaClO_3$ stock solution was used. Aliquots were collected

using 3-mL plastic syringes through the H_2 outlet needle and immediately filtered through

a 0.22-μm cellulose membrane to quench reactions. Ion chromatography (Dionex ICS-

5000 system with a conductivity detector and a 25 μL sample injection loop) was used to

quantify the concentrations of ClO_4^-, ClO_3^-, and Cl^- in aqueous samples. The best

separation for ClO_4^- was achieved by Dionex IonPac AS 16 analytical column using 65

mM KOH as eluent. For ClO_3^- and Cl^-, IonPac AS 19 analytical column was used as the

stationary phase and 20 mM KOH as the eluent. In all analytical conditions, the column temperature was maintained at 30°C, and the flow rate of eluents was 1 mL min^{-1}.

2.3.6 Calculation of the Turnover Number (TON) and Initial Turnover Frequency (TOF$_0$)

For the typical reaction setting that contains 0.5 g L^{-1} of 5 wt% Re–5 wt% Pd/C catalyst in water, the concentration of Re in the system is 0.134 mM. Our previous study on **1a'** observed that the rate constant kept increasing from 0.29 to 3.5 h^{-1} when the Re percentage increased from 1 to 10 wt%,[28] thus one can assume that all immobilized Re participate in the catalysis. The TON for the Re-catalyzed oxygen atom transfer (OAT) from 1 mM ClO$_4^-$ is thus 7.5. Because the direct reduction of ClO$_x^-$ intermediates by Pd/C without Re is slower than by the Re complex, one can assume that Re participates in all four steps of OAT through the formation of Cl$^-$. Thus, the corresponding TON is 30. Note that the TON values reported in **Table S2.1** in the **Appendix A** are for one batch of reaction rather than the total number of redox cycles upon reaching the life limit of all Re sites. The calculation of TOF$_0$ approximated the reduction of the first 5% of ClO$_4^-$ in a zeroth-order pattern. The time for achieving 5% reduction (i.e., C/C$_0$ = 0.95) was calculated with first-order kinetics: $T_{5\%} = \ln(0.95)/-k$, where k is the experimentally measured pseudo-first-order rate constant. Because Re has higher reactivities with ClO$_x^-$ intermediates than with ClO$_4^-$ and no ClO$_x^-$ product was observed, one can assume that Re sites will reduce ClO$_x^-$ intermediates before reducing another ClO$_4^-$. Therefore, TOF$_0$ = 0.05×C$_0$×4/0.134/$T_{5\%}$.

2.3.7 X-Ray Photoelectron Spectroscopy (XPS) Analysis

For the characterization of fresh catalysts, the $Re(O)(L_{N-O})_2-Pd/C$ catalysts were prepared as described above. Upon disconnecting from the H_2 supply (still with the rubber stopper to prevent air intrusion), the catalyst suspension was quickly transferred into an anaerobic glove bag (Coy Laboratories, filled with 98 % N_2 and 2 % H_2). The immobilized Re complexes are sensitive to air.[28] For the characterization of used $Re(O)(L_{N-O})_2-Pd/C$ catalysts, prior to the disconnection from the H_2 supply, samples were analyzed by IC to confirm that the reduction of ClO_4^- (or ClO_3^-) was complete. A ceramic funnel loaded with Whatman qualitative filter paper was used to filter the catalyst suspension under vacuum. The black cake on the filter paper was transferred into a 20-mL glass scintillation vial, which was placed in a sand bath at 100 °C to remove moisture from the catalyst powder. The dried powder was then loaded onto a copper conductive tape on the XPS stub and stored in an anaerobic chamber secured with Klein Flange. The chamber was transferred from UC Riverside to the XPS facility at UC Irvine Material Research Institute (IMRI), where XPS measurements were conducted on the Kratos AXIS Supra surface analysis instrument. The binding energy was calibrated by setting the sp^2 C 1s peak to 284.48 eV. Raw spectra were fit using CasaXPS (version 2.3.19). Spectra of Pd 3d (5 scans) and Re 4f (90 scans) were fit with constrained separations of spin-orbital coupling doublets (5.27 eV for Pd and 2.43 eV for Re) and doublet peak areas ratio (3:2 for 3d spectra and 4:3 for 4f spectra). The detection of Re^{VII} in all samples is probably attributed to the introduction of trace O_2 during road transportation with elevation changes.

2.3.8 Kinetic Measurement of $[Re^{VII}(O)_2(L_{N–O})_2]^+$

Hydrolysis by NMR. In an anhydrous glove box (VTI Super, filled with N_2, moisture <0.01 ppm), 3,4,5-trichloropyridine (TC*Py*, 1.9 mg, 10.53 μmol) and silver triflate (AgOTf, 3.0 mg, 11.58 μmol) were dissolved in 1 mL of deuterated acetonitrile (CD_3CN) in a 7-mL scintillation vial. TC*Py* was selected as the inert internal standard because its singlet peak (δ 8.57 ppm) does not overlap with any peaks of interest. The solution was added into another 7-mL scintillation vial, which had been loaded with $Re^V(O)(L_{N–O})_2Cl$ (10.53 μmol). A vigorous shake was applied to the vial, and the reaction turned the solution into dark green (for **1a⁺** and **2a⁺**) or brown (for **2b⁺**). After 3 min, white AgCl precipitated at the vial bottom, and the organic phase turned clear. The $[Re^V(O)(L_{N–O})_2][OTf]$ solution was obtained by filtration through a glass pipette filled with glass wool. In order to prepare $[Re^{VII}(O)_2(L_{N–O})_2][OTf]$, $LiClO_4$ (0.3 mg, 2.6 μmol) was added in the $[Re^V(O)(L_{N–O})_2][OTf]$ solution. Vigorous shake was applied until the solution turned into dark red. Afterward, 475 μL of the CD_3CN solution containing ~10.53 mM $[Re^{VII}(O)_2(L_{N–O})_2][OTf]$ was loaded into a 5-mm NMR tube. The tube cap was further sealed with Parafilm, and quickly transferred to the NMR lab. ^1H NMR spectra were collected on Bruker Avance spectrometer (600 MHz for ^1H). Before the addition of D_2O, a spectrum was collected and labeled as "Before D_2O addition". Then 25 μL of D_2O was added into the NMR tube to initiate the hydrolysis. Immediately after a vigorous horizontal shake, the NMR tube was injected into the instrument again. A quick shimming for the 95/5 CD_3CN/D_2O media was conducted before collecting spectra at selected time intervals.

2.3.9 Kinetic Analyses with Stopped-Flow Spectrophotometry

Oxidation of $[Re^V(O)(L_{N-O})_2]^+$. In the anhydrous glove box, 0.5 mM of $[Re^V(O)(L_{N-O})_2]^+$ and various concentrations of $LiClO_4$ and pyridine N-oxide (*Py*O) (e.g., 5−1000 mM) were prepared in anhydrous acetonitrile. The solution of $NaClO_3$ was prepared under air with 90/10 CH_3CN/H_2O mixed solvent. The reactions between $[Re^V(O)(L_{N-O})_2]^+$ and oxidants were monitored on a stopped-flow spectrophotometer (Applied Photophysics SX20). To minimize the hydrolytic decomposition during the reactions, the flow circuit and optical cell were flushed with anhydrous CH_3CN. The solutions were loaded into the instrument immediately after they were taken out of the glove box. For the collected time-dependent kinetic data, the initial rate constants were fitted over ~5% conversion on Pro-Data Viewer (Applied Photophysics). The dependence of initial rate constants on the concentrations of oxidants exhibited a plateau at the high range. Nonlinear-least-squares fittings of saturation kinetics were conducted on SigmaPlot 12.5 to obtain coordination equilibrium constants (K_1) and first-order rate constants for OAT (k_2).

Reduction of $[Re^{VII}(O)_2(L_{N-O})_2]^+$. The anhydrous solutions of 0.5 mM $[Re^V(O)(L_{N-O})_2]^+$ and 0.5 mM *Py*O were prepared as described above. The solutions of the homogeneous reductant, dimethyl sulfide (DMS), were prepared at various concentrations (5−20 mM). To minimize the hydrolysis during sample transfer under air, $[Re^{VII}(O)_2(L_{N-O})_2]^+$ was generated on-site by mixing 0.5 mM $[Re^V(O)(L_{N-O})_2]^+$ and 0.5 mM *Py*O in the aging loop of the sequential mixing stopped-flow spectrophotometer. After a preset aging time (determined from the oxidation kinetics), the reduction was initiated by the subsequent

45

mixing with DMS. The reaction process was followed to completion through monitoring the maximum absorbance of $[Re^{VII}(O)_2(L_{N-O})_2]^+$. Plots of initial rate constants (k_φ) versus [DMS] were linear, and the slopes indicated the second-order rate constants (k_3) for individual $[Re^{VII}(O)_2(L_{N-O})_2]^+$.

2.4 Results and Discussion

2.4.1 Catalyst Preparation and Basic Performance

To interrogate the effects of ligand structure modification on catalyst performance, we synthesized new N,O-bidentate ligands (HL_{N-O}) derived from the original H*hoz* ligand (H*L1*, **Figure 2.2a**). The oxazolinylphenolate structure is naturally occurring in microbial siderophores.[33] The HL_{N-O} ligands were synthesized via one-step construction of the oxazoline ring from specific benzonitriles and amino alcohols. The $Re^V(O)(L_{N-O})_2Cl$ complexes were prepared with our established method[32] and used as the precursor for Re−Pd/C catalysts. Detailed procedures are described in **Section 2.3 Materials and Methods**.

To enhance the reactivity of Re^V with ClO_4^-, we first introduced an electron-donating −OMe to the phenol moiety of H*hoz* (**L2**). However, the synthesis of $Re^V(O)(L2)_2Cl$ (**1b**) yielded a mixture of two products with poor solubility in most solvents, preventing further isolation and characterization. To increase the solubility and restrict the isomerization,[27] we introduced a methyl group on the oxazoline moiety (**L3** and **L4**) by switching the amino alcohol building block from glycinol to *L*-alaninol.[32] The corresponding $Re^V(O)(L_{N-O})_2Cl$ products (**2a** and **2b**) showed good solubilities in

dichloromethane and chloroform. Comparison of ^{1}H NMR spectra with the previously characterized **2a** (**Figure 2.2b,** δ 4.0−5.5 for H's on the oxazoline ring and δ 1.7 for H's of the methyl group) confirmed the exclusive yield of *N,N-trans* Re^V(O)(L_{N-O})$_2$Cl.[32] Single crystallography of **2b** (**Figure S2.1** in the **Appendix A,** not refined due to high-level disorders) also confirmed the *N,N-trans* configuration. For comparison, the original *L1* led to the formation of both *N,N-cis* and *N,N-trans* Re^V(O)(*hoz*)$_2$Cl (**1a**). Previous studies have confirmed that *N,N-cis* isomers are much less active than the *N,N-trans* counterparts for ClO$_4$$^-$ reduction.[27] Therefore, the use of the minimally steric –Me on the oxazoline moiety mimics the biochemical replacement of glycine with alanine, and ensures the exclusive formation of the desirable *N,N-trans* Re complexes.

To evaluate the activity and stability of Re−Pd/C catalysts (labeled as **1a'**, **2a'**, and **2b'**), we immobilized corresponding Re^V(O)(L_{N-O})$_2$Cl precursor (**1a**, **2a**, and **2b**) in Pd/C with an aqueous deposition method.[28] Briefly, the powders of Re complex and Pd/C were sonicated and stirred in water suspension under 1 atm H$_2$. Transiently dissolved Re complex in water was adsorbed into porous carbon and immobilized by hydrophobic and electrostatic interactions.[28] We observed >95% of Cl$^-$ in all three precursors released in water, indicating a near-complete immobilization and activation of Re for the reduction of aqueous ClO$_4$$^-$.[28] All Re−Pd/C catalysts exhibited a rapid reduction of 1 mM ClO$_4$$^-$ by 1 atm H$_2$ at 20°C (**Figure 2.2c**). The –Me substitution on oxazoline did not alter the rate of ClO$_4$$^-$ reduction (**1a'** versus **2a'**). The –OMe substitution provided a 68% faster ClO$_4$$^-$ reduction (**2b'** versus **2a'**). As the oxygen atom transfer (OAT) from ClO$_4$$^-$ to Re^V decreases the electron density of Re, an electron-rich ligand can promote this process.[34]

The chlorine balance was closed by ClO_4^- and Cl^- (**Figure 2.2d**). The initial 0.13 mM of Cl^- was released from the precursor **2b** (0.134 mM was added). More than 99.99% of 1 mM ClO_4^- was completely reduced to Cl^- within 1 h. The turnover number (TON) on each Re site was 7.5 for the reduction of ClO_4^- (or 30 if all four oxygen atoms were abstracted by the same OAT mechanism). The absence of a hydrogen-bonding motif (e.g., amino acid residues in enzymes[13] or the secondary coordination sphere in an artificial Fe complex[24]) for the metal-bound oxyanion required a slightly acidic environment (e.g., pH 3.0) to enable OAT.[28, 35]

Before we further discuss the kinetics, we note that the heterogeneous nature of Re−Pd/C catalysts has been confirmed in previous studies.[28, 31] The direct use of Re complex **1a**[28] or **2b** did not show ClO_4^- reduction in the pure aqueous medium (**Figure S2.2** in the **Appendix A**) for two reasons: (1) the solubility of $Re(O)(L)_2Cl$ in water is low and (2) the $Re(O)(L)_2Cl$ precursor cannot spontaneously release the chloro ligand to allow the coordination with ClO_4^-. The hydrophobic and electrostatic interactions between the Re complex and carbon surface provides unique advantages for the heterogeneous system. When cationic **1a⁺** and **2a⁺** (the Cl^- in **1a** and **2a** was removed by AgOTf) were dissolved in acetonitrile for homogeneous $LiClO_4$ reduction by alkyl sulfides, **2a⁺** was quickly inhibited by the Cl^- from ClO_4^- reduction, whereas the activity of **1a⁺** sustained longer (**Figure S2.3** in the **Appendix A**). Product inhibition by Cl^- was also observed from a homogeneous Fe catalyst.[24, 25] In stark comparison, **1a'** and **2a'** showed almost identical activity (**Figure 2.2c**). The immobilized Re complexes interact more strongly with the carbon surface than with aqueous Cl^-. During the aqueous deposition process, >95% of Cl^-

in $Re^V(O)(L_{N-O})_2Cl$ precursors were expelled into the aqueous phase. Compared to the high sensitivity of $[Re^V(O)(L_{N-O})_2]^+$ with Cl^- in the acetonitrile solution, the 0.13 mM of Re in Re−Pd/C catalysts was only partially inhibited even in the presence of 10−50 mM Cl^- (*vide infra*).
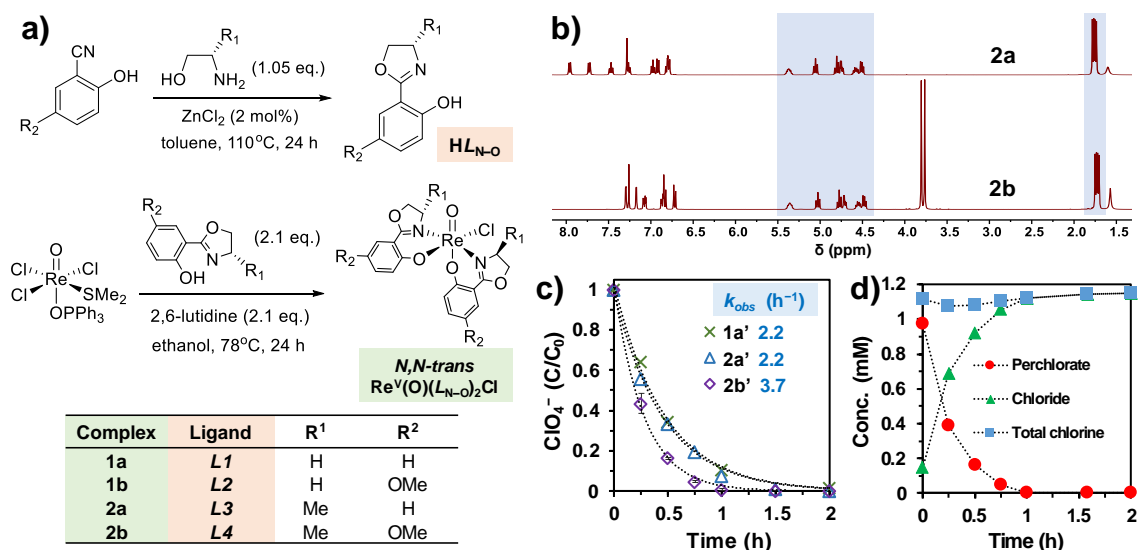
Figure 2.2 (a) Synthesis of HL_{N-O} ligands and $Re^V(O)(L_{N-O})_2Cl$ complexes; (b) comparison of ^1H NMR spectra for **2a**[32] and **2b** with signals of the two 4-methyloxazoline moieties highlighted in blue; (c) degradation profile of 1 mM ClO_4^- by Re−Pd/C catalysts (0.5 g L^{-1}, 5 wt% Re and 5 wt% Pd, pH 3.0, 1 atm H_2, 20°C); and (d) the chlorine balance using the Re−Pd/C prepared from **2b**.

2.4.2 Catalyst Stability Against Oxidative Deactivation

While the higher activity of **2b'** than **1a'** was expected, to our surprise, **2b'** exhibited high stability against oxidative deactivation. For the reduction of 1 mM ClO_4^-, the apparent first-order rate constant by **2b'** was 68% higher than that by **1a'** (**Figure 2.2c**). However, the rate constants for 10 mM ClO_4^- (TON=75 for ClO_4^- or 300 for abstracting all four oxygen atoms) by **2a'** and **2b'** were 8.6 and 9.7 folds higher than that by **1a'**,

respectively (**Figure 2.3a**). This significant difference in reducing concentrated ClO_4^- implies that the Re site in **2a'** and **2b'** are much more stable than in **1a'**.

We systematically assessed the catalyst stability by conducting two sets of kinetic experiments (**Figure 2.3b**). In the first set, each Re−Pd/C catalyst was used to reduce 10 mM ClO_4^- for 24 h, so that even the least active **1a'** could complete the reduction (**Figure 2.3a**). To probe whether the Re sites were still active, we added another spike of 1 mM ClO_4^- to the used catalysts and measured the reduction kinetics. Because the generation of 10 mM Cl^- can slightly inhibit the Re−Pd/C catalyst by competing with ClO_4^- for the reactive site,[31] in the second set of control experiments, we measured the reduction of 1 mM ClO_4^- by freshly prepared Re−Pd/C catalysts in the presence of 10 mM NaCl (mimicking the generation of Cl^- from 10 mM ClO_4^-). The significant disparity between the two experiments for **1a'** (**Figure 2.3c**) suggests a major deactivation of Re sites during the reduction of 10 mM ClO_4^-. In stark contrast, **2a'** and **2b'** showed negligible difference between the two experiments (**Figures 2.3d** and **2.3e**). Hence, the reduction of 10 mM ClO_4^- by **2a'** and **2b'** did not lead to a noticeable activity loss. For a single batch of 10 mM ClO_4^-, >97% and >99.98% reduction was achieved by **2b'** within 2 h and 4 h, respectively. The initial turnover frequency (TOF_0) calculated from the reduction of the first 5% of 10 mM ClO_4^- was 109 h^{-1} (or 436 h^{-1} for abstracting all four oxygen atoms, see **Section 2.3 Materials and Methods** for TOF_0 calculation).

The high stability of catalyst **2b'** was further verified by reusing it for reducing five spikes of 10 mM ClO_4^- (**Figure 2.3f**). Each ClO_4^- spike was completely reduced using 24 h before the next spike. The kinetics of the 5th spike was almost the same as the control

experiment, where freshly prepared **2b'** reduced 10 mM ClO_4^- in the presence of 40 mM NaCl (mimicking the four earlier ClO_4^- spikes). Hence, the gradual decrease of catalyst activity was solely attributed to the significant build-up of Cl^- in the water. This high stability makes **2b'** the most active catalyst for aqueous ClO_4^- reduction among all chemical reduction systems reported to date (**Table S2.1** and **Table S2.2** in the **Appendix A**).[34, 36-44]

As elucidated in previous studies, the OAT from ClO_x^- oxidizes $[Re^V(O)(L_{N-O})_2]^+$ into $[Re^{VII}(O)_2(L_{N-O})_2]^+$ (steps *i* and *ii* in **Scheme 2.1**).[28, 45] Organic sulfide (in the homogeneous system) or Pd-activated H_2 (in the heterogeneous system) removes one oxo group and thus reduces Re^{VII} back to Re^V (step *iii*). If the oxidation is faster than the reduction, the accumulated $[Re^{VII}(O)_2(L_{N-O})_2]^+$ is subject to hydrolytic decomposition into $Re^{VII}O_4^-$ and $[H_2L_{N-O}]^+$ (step *iv*).[31] Because ClO_4^- is much more inert than ClO_x^- intermediates, we attributed the catalyst deactivation to the highly reactive ClO_3^-, ClO_2^-, and ClO^- intermediates. When the initial concentration of ClO_4^- was elevated, the concentrations of ClO_x^- intermediates from the first-order reduction of ClO_4^- were also proportionally elevated, thus imposing higher oxidative "stress" to the Re sites. To confirm this mechanistic insight, we further challenged Re−Pd/C catalysts by directly exposing them to ClO_3^- (**Figure 2.4a**). The one-time addition of 0.5−1.0 mM ClO_3^- imposed substantially higher oxidative stress than the gradual generation (accompanied with rapid degradation) of ClO_3^- from the pseudo-first-order decay of 10 mM ClO_4^-. As shown in **Figures 2.4c** and **2.4d**, the one-time addition of 0.5 mM ClO_3^- did not deactivate catalyst **2a'** and **2b'** in the following reduction of 1 mM ClO_4^-. When ClO_3^- was increased to 1

mM, we observed deactivation to a limited extent. In stark comparison, **1a'** was severely

deactivated by 0.5 and 1 mM ClO_3^- (**Figure 2.4b**).

We used X-ray photoelectron spectroscopy (XPS) to probe the evolution of Re

speciation in the Re−Pd/C catalysts after use under various conditions. The fresh catalyst

1a' contained three Re species with $4f_{7/2}$ binding energies (BE) of 42.8 eV, 44.0 eV, and

45.2 eV (**Figure 2.4e**), which are consistent with reported Re^{III}, Re^V, and Re^{VII},

respectively.[28] The detection of Re^{III} was attributed to the reduction of the oxo group in

$[Re^V(O)(L_{N–O})_2]^+$ by Pd-activated H_2 (heterogeneous) or by PPh_3 (homogeneous).[28]

Interestingly, **2a'** and **2b'** contained little Re^{III} (**Figures 2.4i** and **2.4m**), probably due to

the steric effect of methyl groups in **L3** and **L4**. However, this difference did not cause

different catalytic activities by **1a'** and **2a'** (**Figure 2.2c**). The detection of Re^{VII} is caused

by the trace amount of O_2 during the sample preparation and transfer (see **Section 2.3**

Materials and Methods). After the reduction of 10 mM ClO_4^-, two new Re $4f_{7/2}$ peaks at

40.7 eV and 41.6 eV showed up in **1a'** (**Figure 2.4f**). To understand these two species, we

prepared the ReO_x−Pd/C catalyst from $KReO_4$ with the same aqueous deposition method.[28]

The ClO_4^- reduction activity of this catalyst (**Figure 2.5a**) was 150 and 257 fold lower than

1a' and **2b'**, respectively. The $Re^{VII}O_4^-$ is reductively immobilized into low-valent ReO_x

species.[46-48] The XPS spectrum of ReO_x−Pd/C contained a minor peak for Re^{III} (42.6 eV)

and two major peaks at 40.8 eV and 41.7 eV (**Figure 2.5b**), which have been identified as

two different Re^I structures.[47, 49] Thus, the two new peaks found in **Figures 2.4f** confirmed

the decomposition of active Re sites into $Re^{VII}O_4^-$ and the subsequent reduction into Re^I.

The two Re^I species took 42% of the total immobilized Re (**Table S2.3** in the **Appendix**

A). The XPS spectra after reducing 0.5 and 1.0 mM ClO_3^- also showed the two Re^I species, taking 35% and 56% of the total Re (**Figures 2.4g** and **2.4h**, **Table S2.3** in the **Appendix A**). Therefore, direct exposure to ClO_3^- caused more severe damage to the active Re sites than treating concentrated ClO_4^-. Moreover, the decomposition of Re sites into $Re^{VII}O_4^-$ and free L_{N-O} is a permanent deactivation because the use of $Re^{VII}O_4^-$ and *L4* (the ligand for **2b**) did not yield a higher activity than ReO_x–Pd/C (**Figure 2.5a**). The Re speciations were not the same (**Figure 2.5c** versus **2.5b** and versus **4m−4p**). This aspect also shows that, during the catalyst preparation and normal catalysis, the $Re(L_{N-O})_2$ complex remained intact rather than underwent "dissociation and reassembly" of Re metal and free L_{N-O} ligands on the carbon surface.

In stark contrast, the surface Re speciation in catalyst **2a'** and **2b'** did not show an increase of Re^I species after reducing either 10 mM ClO_4^- or 0.5 mM ClO_3^- (**Figures 2.4i−2.4p** and **Table S2.3** in the **Appendix A**). A small increase of Re^I species was observed after the reaction with 1 mM ClO_3^- (**Figures 2.4l** and **2.4p** and **Table S2.3** in the **Appendix A**). Thus, XPS characterization results are consistent with the kinetic data shown in **Figures 2.4b−2.4d**, providing spectroscopic evidence for the high stability of Re sites in **2a'** and **2b'**. We did not further test ClO_2^- or ClO^- as the more challenging substrates because their side reactions in acidic media[50] may complicate the analysis and understanding. Moreover, the stepwise reduction from ClO_4^- is less likely to accumulate ClO_2^- or ClO^- in high concentrations.
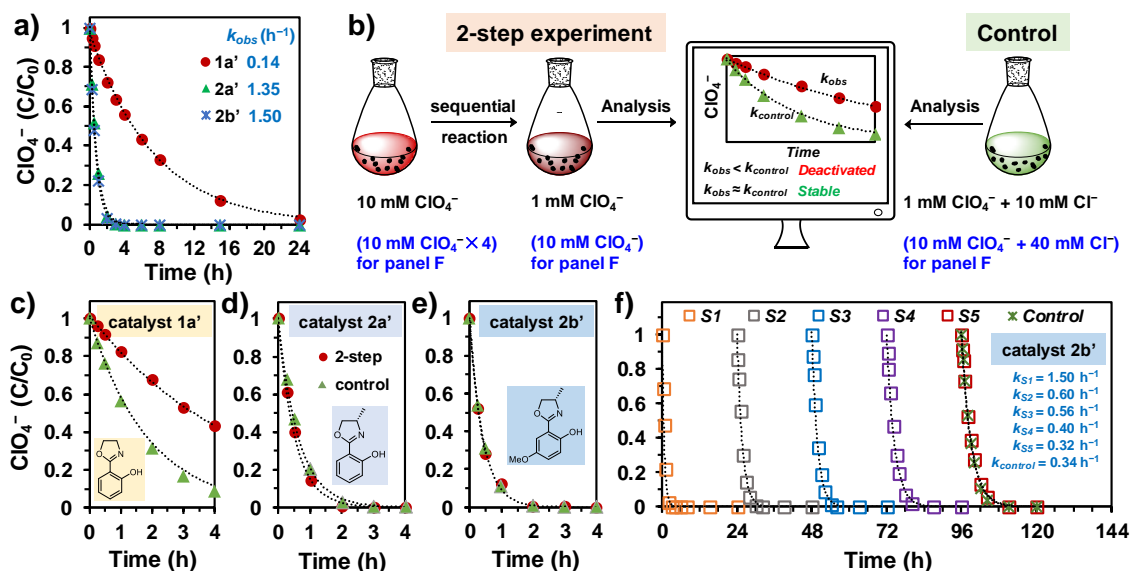
Figure 2.3 (a) Degradation profile of 10 mM ClO_4^- by Re−Pd/C catalysts (0.5 g L^{-1}, 5 wt% Re and 5 wt% Pd, pH 3.0, 1 atm H_2, 20°C); (b) illustration of the two-step stability test and the control experiment; (c−e) results of the stability test showing the effect of L_{N-O} structure (the common legend is in panel d); and (f) stability challenge of catalyst **2b'** with five spikes of 10 mM ClO_4^-.
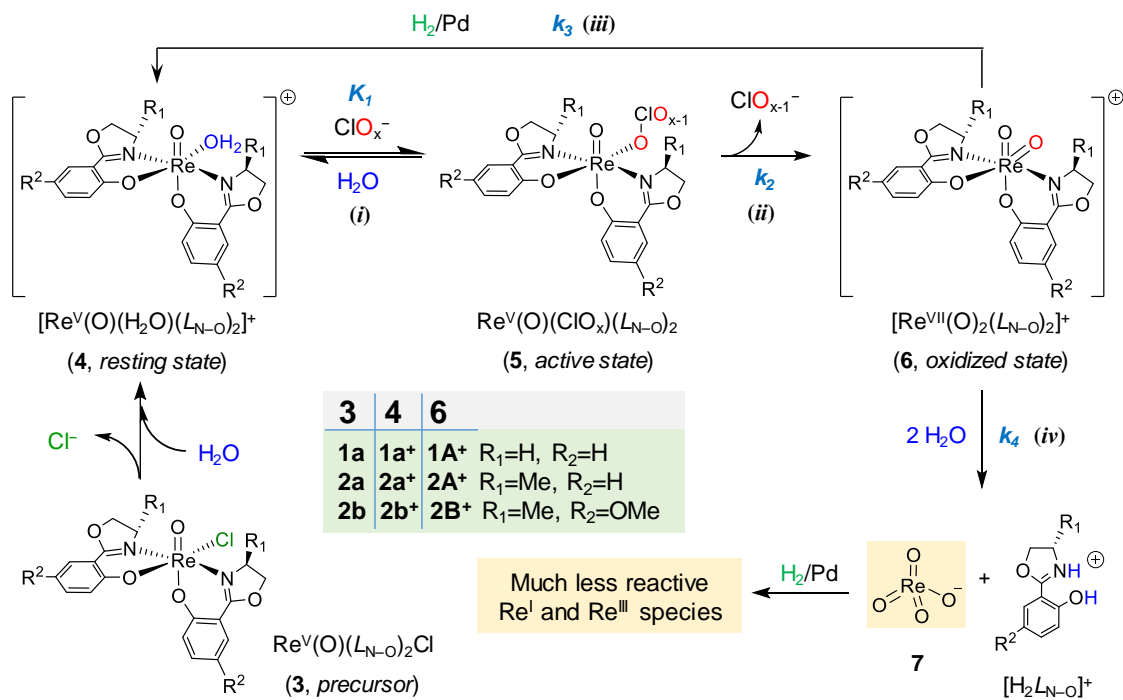
Scheme 2.1 Proposed transformation of molecular Re species at the carbon-water interface.

The scheme shows the following species and transformations:

Top pathway: H₂/Pd, k_3 (*iii*)

$[Re^V(O)(H_2O)(L_{N-O})_2]^+$ (**4**, *resting state*) → $Re^V(O)(ClO_x)(L_{N-O})_2$ (**5**, *active state*) → $[Re^{VII}(O)_2(L_{N-O})_2]^+$ (**6**, *oxidized state*)

Step (*i*): K_1, ClO_x^-, H_2O
Step (*ii*): k_2, ClO_{x-1}^-

Table:

	3	**4**	**6**	
1a	1a⁺	1A⁺	R₁=H, R₂=H
2a	2a⁺	2A⁺	R₁=Me, R₂=H
2b	2b⁺	2B⁺	R₁=Me, R₂=OMe

$Re^V(O)(L_{N-O})_2Cl$ (**3**, *precursor*)

Cl⁻, H₂O

2 H₂O, k_4 (*iv*)

7 + $[H_2L_{N-O}]^+$

Much less reactive Re^I and Re^III species ← H₂/Pd
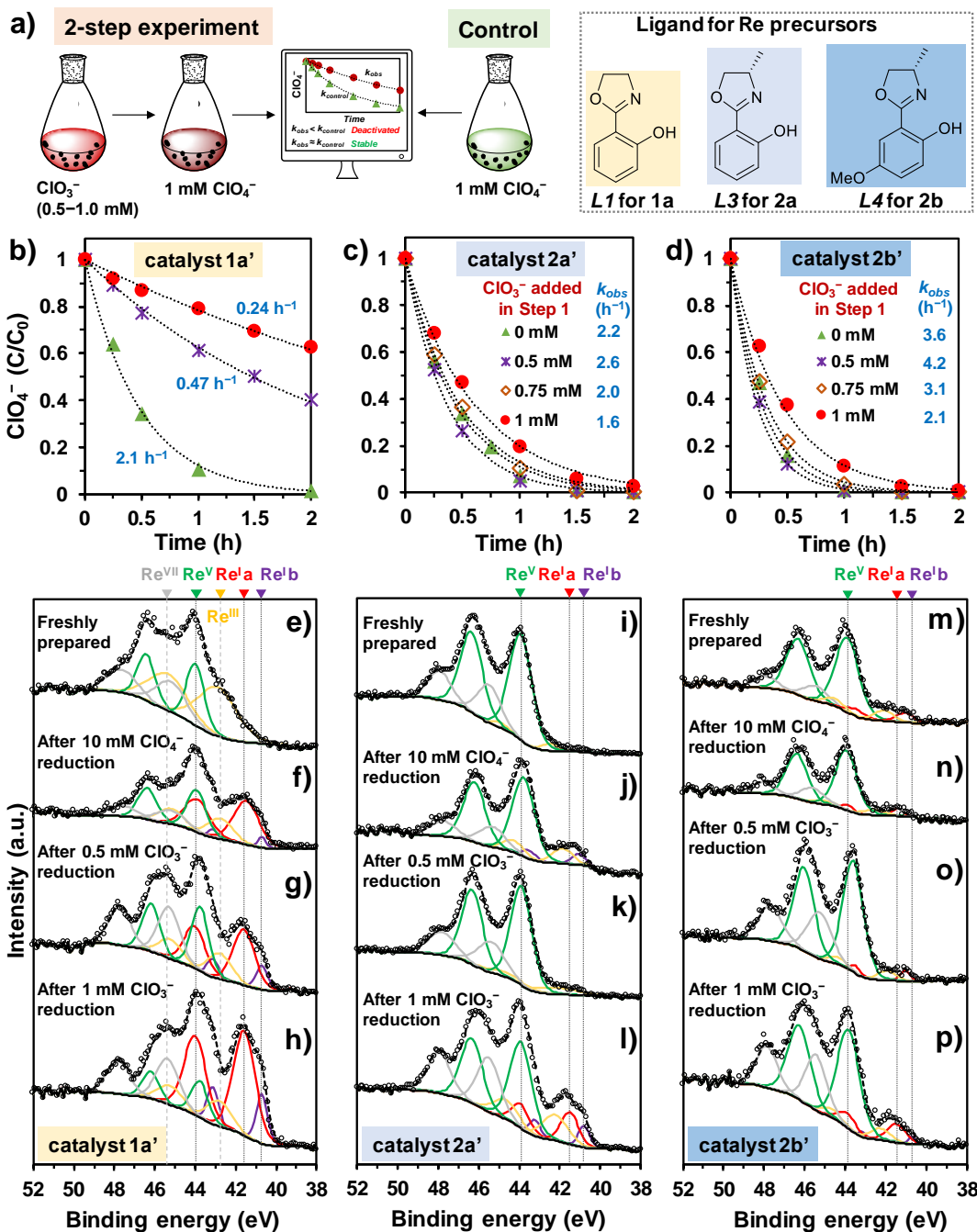
Figure 2.4 (a) Illustration of the two-step stability test using ClO_3^- and the control experiment; (b−d) results of the stability tests (the common legend is shown in panels c or d, 0.5 g L^{-1} of 5 wt% Re and 5 wt% Pd, pH 3.0, 1 atm H_2, 20°C); and (e−p) Re 4f XPS spectra of the three catalysts under various conditions. The Re $4f_{7/2}$ peaks are highlighted with dotted lines.
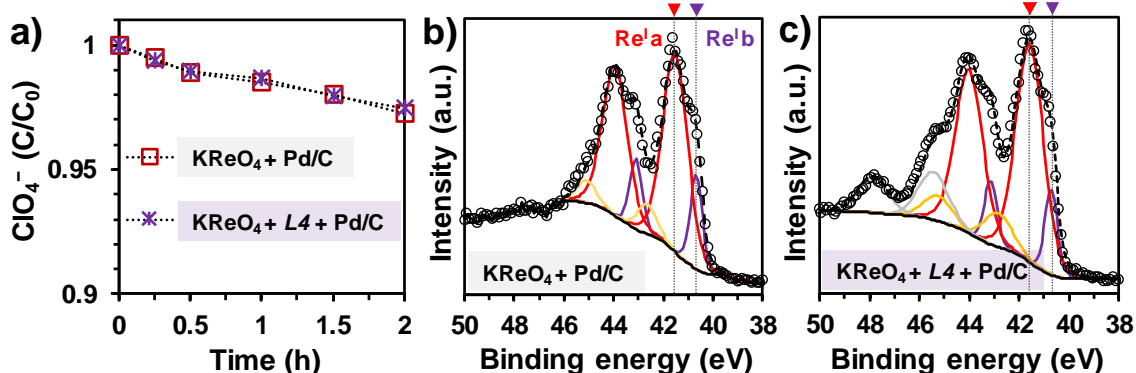
Figure 2.5 (a) Reduction of 1 mM ClO_4^- by Re−Pd/C catalysts prepared from $KReO_4$ with and without **L4** and (b+c) Re 4f XPS spectra of the two as-prepared catalysts. Reaction conditions: 0.5 g L^{-1} of 5 wt% Re and 5 wt% Pd, molar ratio of **L4**:Re = 2:1, pH 3.0, 1 atm H_2, 20°C. Note the y-axis in panel a starts from $C/C_0 = 0.9$.

2.4.3 Mechanisms for the Enhanced Catalyst Stability

Based on **Scheme 2.1**, we developed a quasi-steady-state equation to model the rate of removing $Re(L_{N-O})_2$ sites from the catalytic cycle into decomposition (**Eq. 2.1,** detailed derivation steps provided in **Text S2.1** in the **Appendix A**):

$$\frac{d[\mathbf{6}]}{dt} = -\frac{K_1 k_2 k_4}{k_3}[XO][Re]_T \qquad (Eq.\,2.1)$$

The apparent decomposition rate of the active $Re(L_{N-O})_2$ site is dependent on three reactions: the formation ($K_1 k_2$), reduction (k_3), and hydrolysis (k_4) of $[Re^{VII}(O)_2(L_{N-O})_2]^+$ (**6**). Because the Re−Pd/C catalysts **1a'** and **2b'** showed surprisingly different stabilities, we expected that the rate constants of one or more steps were significantly altered by the minor modifications of ligand with –Me on the oxazoline or –OMe on the phenolate.

Hydrolytic decomposition of $[Re^{VII}(O)_2(L_{N-O})_2]^+$. We first hypothesized that the rate of hydrolysis for **6** (k_4) determines the lifetime of $Re(L_{N-O})_2$ sites. A slow **step iv** could

57

preserve **6** in the catalytic cycle (**Scheme 2.1**). Due to the difficulty of directly probing and modeling molecular transformations at the heterogeneous water-carbon interface, we investigated the hydrolysis of various **6** (**1A$^+$**, **2A$^+$**, and **2B$^+$**) in organic solutions by ^{1}H NMR (**Figures 2.6**, **Figure S2.4**, and **Figure S2.5** in the **Appendix A**). The solutions of **6** were prepared by sequentially treating the Re^V(O)($L_{N–O}$)$_2$Cl precursor **3** (**1a**, **2a**, and **2b**) with 1 equivalent of AgOTf and 0.25 equivalent of LiClO$_4$ in a dry box. In anhydrous CD$_3$CN, **6** was stable for at least three days. The ^{1}H NMR spectra showed symmetry for the two $L_{N–O}$ ligands. Based on the reported crystal structures of similar dioxo Re^{VII} complexes,[45, 51] we postulate a C$_2$-symmetric *cis*-dioxo configuration for [Re^{VII}(O)$_2$($L_{N–O}$)$_2$]$^+$ structures in this study. Although the reported crystal structure of [Re^V(O)(H$_2$O)($L_{N–O}$)$_2$]$^+$ (**4**) has the H$_2$O *trans* to the oxo group,[52] it is reasonable to assume that, during the rapid catalytic cycles, both H$_2$O and ClO$_x^-$ coordinate with Re^V center from the equatorial site *cis* to the oxo.[27] To normalize the peak intensities of the time-dependent spectra, we used 3,4,5-trichloropyridine as an internal standard (δ = 8.6 ppm).[53] The addition of 5% (v/v) D$_2$O initiated the first-order hydrolysis of **6** (**Figure 2.7a**) directly into Re^{VII}O$_4^-$ and double-protonated free ligand [H$_2$$L_{N–O}$]$^+$.[31] Other intermediate structures, such as the previously reported Re^{VII}(O)$_3$($L_{N–O}$),[26] were not observed.

The rate constants of hydrolysis for **2A$^+$** and **2B$^+$** were merely 20% and 33% of that for **1A$^+$** (**Figure 2.7a**). Thus, the –Me substitution on oxazoline significantly slowed down the hydrolysis. The faster decomposition of **2B$^+$** than **2A$^+$** is probably attributed to the increased electron density at the phenolate O, which facilitates the protonation of $L_{N–O}$ and detachment from the metal.[54, 55] Although a slower hydrolytic **step *iv*** can, to some extent,

help preserve **6** in the catalytic cycle, the modestly different rates of hydrolysis for the three structures may not be fully responsible for the markedly different catalyst stability (**Figures 2.3c−2.3e** and **Figures 2.4b−2.4d**).

Generation of $[Re^{VII}(O)_2(L_{N-O})_2]^+$ via OAT oxidations. We measured the kinetics of formation of **6** from the corresponding **4** (dissolved in acetonitrile) via OAT from ClO_4^-, ClO_3^-, and pyridine N-oxide (*Py*O). In anhydrous acetonitrile, **1a⁺** and **2a⁺** exhibit very similar dark green color, whereas **2b⁺** shows a dark brown color (**Figure S2.6** in the **Appendix A**). Because all three Re complexes have the same N,N−*trans* coordination structure, the absorption redshift of **2b⁺** is attributed to the extended conjugation by –OMe substitution on the phenolate moiety.[56, 57] We performed oxidation of **4** with excess oxidants under pseudo-first-order conditions and monitored the fast kinetics with stopped-flow spectrophotometry.[45] After the addition of oxidants, all solutions turned into red color[26] due to the increased absorption of 380−700 nm (**Figure 2.7b**). The maximum increase of absorbance from **4** to **6** (λ_{max} = 440 nm for **1a⁺→1A⁺** and **2a⁺→2A⁺**, and 510 nm for **2b⁺→2B⁺**) were determined by subtracting the initial absorption spectra of **4** (**Figure 2.7b** inset and **Figure S2.7** in the **Appendix A**). The representative time profiles for the absorbance at λ_{max} are shown in **Figure S2.7d** in the **Appendix A**. The initial rate constant (k_φ) from such profiles at varied concentrations of ClO_4^-, ClO_3^-, and *Py*O are shown in **Figures 2.7c−2.7e**. All datasets showed the gradual saturation of kinetics as the oxidant concentrations increased.[45]

To model the oxidation of **4** to **6** (**steps i** and **ii** in **Scheme 2.1**) measured by the stopped-flow experiment, we developed the non-steady-state **Eq. 2.2** (detailed derivation steps provided in **Text S2.2** in the **Appendix A**):

$$\frac{d[\mathbf{6}]}{dt} = \frac{K_1 k_2 [XO][Re]_T}{1 + K_1[XO]} \qquad (Eq.\,2.2)$$

Nonlinear-least-squares fitting of the initial rate data to **Eq. 2.2** provided the constants K_1 and k_2 for individual oxidants and Re complexes (**Table 2.1**). The equilibrium constants for **step i** (K_1, for ligand exchange from the solvent to the oxygen donor) depend on both the oxidant and L_{N-O} structure. Among the three oxidants, ClO_4^- showed the lowest K_1. This result is consistent with the well-known weak coordinating capability of ClO_4^-.[58] The substantially lower K_1 for *Py*O by **2a⁺** and **2b⁺** (17.3 and 12.1 M^{-1}) than by **1a⁺** (191 M^{-1}) is attributed to the steric hindrance by the methyl group on the ligands. The K_1 for ClO_4^- with **1a⁺** (13.2 M^{-1}) is also slightly higher than with **2a⁺** and **2b⁺** (9.2 and 9.8 M^{-1}).

For **step ii**, the three complexes showed very similar k_2 for the OAT from coordinated ClO_4^- to Re^V (0.030−0.032 s^{-1}). However, to our surprise, the OAT from coordinated ClO_3^- to **1a⁺** (12.75 s^{-1}) was two orders-of-magnitude faster than to **2a⁺** (0.109 s^{-1}). For the reaction with ClO_3^-, the overall second-order rate constants ($K_1 k_2$) for **2a⁺** and **2b⁺** (3.6 and 4.4 M^{-1} s^{-1}) were 70- and 57-fold smaller than for **1a⁺** (251.2 M^{-1} s^{-1}, entries 2, 5, and 8 in **Table 2.1**). On the basis of **Eq. 2.1**, the substantially slower formation of **6** is beneficial for its stability. We expected similar trends for the even more reactive ClO_2^- and ClO^- substrates, but experimental attempts were not successful due to (1) the low

solubility of $NaClO_2$ in pure or water-mixed acetonitrile and (2) uncontrolled reactivity of $HClO/ClO^-$ with common organics. Hence, we used pyridine oxide (PyO) as a highly reactive surrogate (entries 3, 6, and 9 in **Table 2.1**). For the OAT from PyO to Re^V, the k_2 for $1a^+$ (10.43 M^{-1}) was one order-of-magnitude higher than for $2a^+$ (1.107 M^{-1}). Therefore, the introduction of –Me on the oxazoline moiety of L_{N-O} not only causes a steric hindrance for Re^V to coordinate with the oxygen donor (e.g., PyO), but also slows down the OAT from the coordinated donor (e.g., ClO_3^- and PyO) to Re^V. The comparison between $2a^+$ and $2b^+$ shows that the $-OMe$ on the phenolate moiety can both decrease K_1 and increase k_2 for ClO_3^- and PyO, but not for ClO_4^- (entries 4–6 versus 7–9 in **Table 2.1**).

Notably, the profiles for the oxidation from **4** to **6** by ClO_3^- contained two phases with different reaction rates (**Figure S2.8** in the **Appendix A**). The fast oxidation in the first phase took only about 0.2 s for $1a^+$, 15 s for $2a^+$, and 12 s for $2b^+$. The much slower oxidation in the second phase took >30 s for $1a^+$, >300 s for $2a^+$, and >150 s for $2b^+$. Both phases exhibited first-order kinetics. A detailed analysis of the time-evolved absorption spectra found the formation of $Re^V(O)(L_{N-O})_2Cl$ (the precursor **3** in **Scheme 2.1**), which is responsible for the relatively slow reaction in the second phase. The reduction of highly reactive ClO_3^- rapidly generates Cl^-, which inhibited the reaction by competing for the coordination site on Re^V (c.f. **Figure S2.3** in the **Appendix A**). In the homogeneous system, the Re−Cl binding in **2a** is much stronger than in **1a**. Spectroscopic evidence and reasoning are provided in **Figures S2.9−S2.11** in the **Appendix A**. Such two-phase kinetics was less pronounced using the much more inert ClO_4^-, and was not observed from the reaction with PyO.

Reduction of [Re^{VII}(O)$_2$(L$_{N-O}$)$_2$]$^+$. Because it is challenging to measure redox transformations of Re in the three-phase system of H$_2$+Pd/C in water, we measured homogeneous reduction of **6** to **4** with dimethyl sulfide (DMS) as the reductant. In a sequential mixing flow circuit, the two solutions containing **4** and *Py*O (equal molar concentration in anhydrous acetonitrile) were first mixed for a preset aging time to ensure complete oxidation of **4** into **6**. The reduction was initiated by the subsequent mixing with excess DMS. The dependence of the reaction rate constants on DMS concentration is shown in **Figure 2.7f**. The second-order rate constants were obtained as the slopes of the linear fittings. The reduction of **2A$^+$** (842.6 M^{-1} s^{-1}) was 82% slower than that of **1A$^+$** (4778 M^{-1} s^{-1}). This is probably caused by the steric repulsion[52] between the ligand methyl group and DMS. We note that in the Re–Pd/C catalyst, Pd-activated hydrogen is much less steric demanding than DMS. However, similar to the two orders-of-magnitude different reactivity of oxidative OAT from coordinated ClO$_3^-$ to Re^V (**Table 2.1**, k_2 of entry 2 versus 5), it is also possible that the –Me substitution decreased the intrinsic reactivity of reductive OAT from Re^{VII} to sulfide. The comparison between **2A$^+$** and **2B$^+$** indicates the electron-donating effect of the –OMe substitution. The reduction of the more electron-rich **2B$^+$** is slower than that of **2A$^+$** by 80% (171.9 versus 842.6 M^{-1} s^{-1}).

The overall stability of [Re^{VII}(O)$_2$(L$_{N-O}$)$_2$]$^+$. The rate constants obtained above allow a quantitative comparison of the decomposition rates for **6** with **Eq. 2.1**. **Table 2.2** shows the apparent rate constants, $k_{dec} = K_1 k_2 k_4 / k_3$, when the substrate is ClO$_4^-$ and ClO$_3^-$. For each Re complex, k_{dec,ClO_4^-} is 1−3 orders-of-magnitude lower than k_{dec,ClO_3^-}, indicating that the oxidative stress mainly comes from the highly reactive ClO$_x^-$

intermediates. The methyl group on the ligand oxazoline moiety slows down the oxidation (K_1k_2) by ClO_3^- for two orders-of-magnitude, while the rate of oxidation by ClO_4^- was not significantly changed (see **Table 2.1** for uncertainties of the model-fit values). We postulate that the rate constants of the reduction step (k_3) measured using Me_2S could be impacted by the steric repulsion. When Pd-activated H_2 is the reductant, it is possible that k_3 for **2a** reaches the same order-of-magnitude as that for **1a** (i.e., about 5-fold higher). In such a case, k_{dec} for **2a** and **2b** could be further lowered for about 5-fold, resulting in much higher catalyst stability than **1a**. Although **2b** exhibited a slower reduction and faster hydrolysis than **2a** due to the electronic effect from –OMe substitution, **2b'** already showed high stability after treating five spikes of 10 mM ClO_4^- (**Figure 2.3f**). Therefore, the methyl group on the ligand oxazoline moiety played the critical role in protecting the Re site from decomposition. It even allowed –OMe substitution for a limited enhancement of the apparent rate of aqueous ClO_4^- reduction (**2b'** versus **2a'** in **Figures 2.2c** and **2.3a**). Due to the methyl group, the relatively limited detrimental effects from the –OMe substitution, such as 64% faster hydrolysis (k_4) and 80% slower reduction (k_3, **2b** versus **2a** in **Table 2.2**), did not cause catalyst decomposition during the reduction of 10 mM ClO_4^- or 0.5 mM ClO_3^-. Although technical challenges prevented us from measuring K_1 and k_2 for the reactions with ClO_2^- and ClO^-, we expect the trends to be similar to the observations using ClO_3^- and PyO. Moreover, the generation of ClO_2^- and ClO^- will not cause significant deactivation of **2b**. The OAT reduction of ClO_3^- (i.e., the generation of ClO_2^-) has already been slowed down for two orders-of-magnitude by the ligand methyl group (**Table 2.1**).
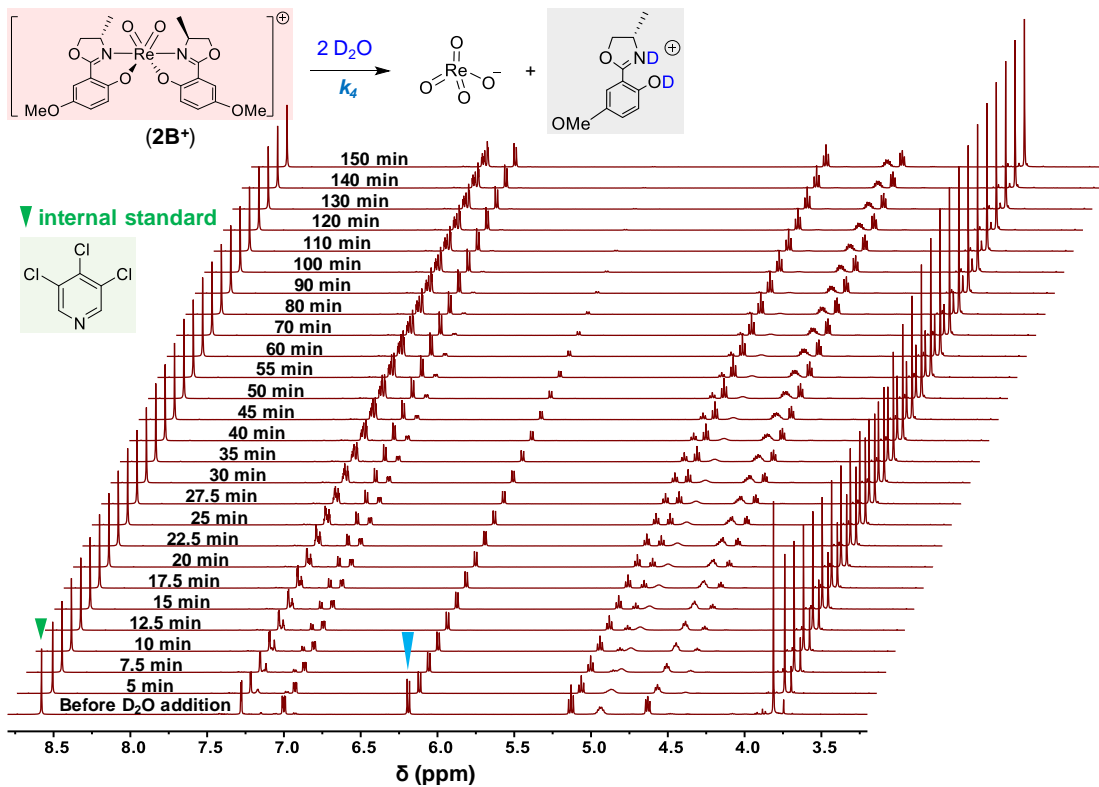
Figure 2.6 Time-dependent 1H NMR (600 MHz) spectra for the hydrolysis of 2B+ (10 mM) in 5/95 (v/v) D2O/CD3CN at 20°C. The resonance indicated by the blue arrow was used for quantitation shown in **Figure 2.7a**.
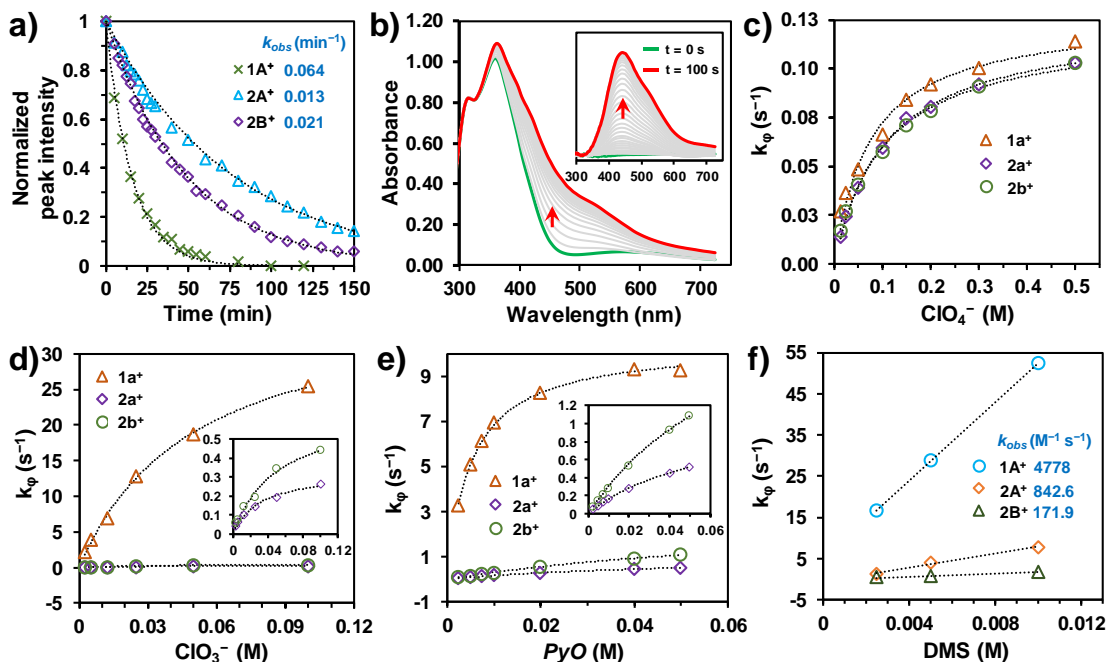
Figure 2.7 (a) Time profiles of ^1H NMR measured hydrolytic decomposition of $[Re^{VII}(O)_2(L_{N–O})_2]^+$ in 5/95 (v/v) D_2O/CD_3CN at 20°C; (b) the time-dependent UV-vis absorption spectra for **1a⁺→1A⁺** upon stopped-flow mixing of 0.5 mM **1a⁺** and 25 mM $LiClO_4$ at 1:1 (v/v). Both species were dissolved in anhydrous CH_3CN. The inset shows the change of absorption after subtracting the initial spectrum (t = 0 s) from all spectra; (c–f) dependence of the initial rate constant (k_φ) on the concentrations of ClO_4^-, ClO_3^-, and PyO (for Re^V oxidation), and of DMS (for Re^{VII} reduction).

Entry	Oxygen donor (XO)	K_1 (M^{-1})	k_2 (s^{-1})	$K_1 k_2$ (M^{-1}s^{-1})
		1a$^+$ (from L1)		
1	ClO$_4^-$	13.2 ± 2.1	0.032 ± 0.004	0.4
2	ClO$_3^-$	19.7 ± 1.8	12.75 ± 0.670	251.2
3	PyO	191.0 ± 7.2	10.43 ± 0.306	1992.1
		2a$^+$ (from L3)		
4	ClO$_4^-$	9.2 ± 0.4	0.031 ± 0.001	0.3
5	ClO$_3^-$	33.2 ± 8.3	0.109 ± 0.018	3.6
6	PyO	17.3 ± 0.4	1.107 ± 0.009	19.2
		2b$^+$ (from L4)		
7	ClO$_4^-$	9.8 ± 0.9	0.030 ± 0.002	0.3
8	ClO$_3^-$	20.1 ± 4.6	0.219 ± 0.029	4.4
9	PyO	12.1 ± 0.6	2.859 ± 0.092	34.6

Table 2.1 Best fitted rate constants from the data in **Figures 2.7c–2.7e** with **Eq. 2.2**.

Re Precursor	$K_1 k_2$ (ClO$_4^-$) (M^{-1}s^{-1})^a	$K_1 k_2$ (ClO$_3^-$) (M^{-1}s^{-1})^a	k_3 (M^{-1}s^{-1})^b	k_4 (M^{-1}s^{-1})^c	k_{dec} (ClO$_4^-$) (M^{-1}s^{-1})	k_{dec} (ClO$_3^-$) (M^{-1}s^{-1})
1a (from L2)	0.4	251.2	4778	3.9×10^{-4}	3.2×10^{-8}	2.0×10^{-5}
2a (from L3)	0.3	3.6	842.6	7.9×10^{-5}	2.8×10^{-8}	3.4×10^{-7}
2b (from L4)	0.3	4.4	171.9	1.3×10^{-4}	2.2×10^{-7}	3.2×10^{-6}

Table 2.2 Rate constants of all steps shown in **Scheme 2.1** and estimated decomposition rate constants for **Eq. 2.1**.
^{a}Measurement of K_1 in acetonitrile solution involved ligand exchange with CH$_3$CN rather than with H$_2$O.
^{b}The reductant was DMS and might have steric hindrance with the ligand methyl groups in **2a** and **2b**.
^{c}Second-order rate constants derived from the first-order k_{obs} for hydrolysis shown in **Figure 2.7a**. The molar concentration of D$_2$O in the 5/95 (v/v) D$_2$O/CD$_3$CN mixture is approximately 2.8 M.

2.5 Conclusion

When a bioinspired catalyst system can reduce the highly inert ClO$_4^-$, the oxidative deactivation by the much more reactive ClO$_x^-$ intermediates can be a major challenge to the reactive metal sites. Our results show that a simple ligand modification provided multiple benefits to the catalyst development. The methyl group on the oxazoline moiety

led to an exclusive formation of *N,N-trans* $Re^V(O)(L_{N-O})_2Cl$ precursors, and protected the $Re(L_{N-O})_2$ site from decomposition after treating multiple spikes of concentrated ClO_4^- (10 mM, or 1 g L^{-1}). In comparison to the original L_{N-O} ligand, the added methyl group decelerated the OAT from ClO_3^- to $Re^V(L_{N-O})_2$ for two orders-of-magnitude and the hydrolysis of $Re^{VII}(L_{N-O})_2$ for several folds. Since the rate of OAT from ClO_4^- to $Re^V(L_{N-O})_2$ was not impacted, the apparent rate for aqueous ClO_4^- reduction by the Re–Pd/C catalyst was not lowered. For comparison, the methoxy substitution on the phenolate moiety slightly enhanced the OAT and hydrolysis steps, but these effects were overweighed by the effects of the methyl group on the oxazoline moiety. Overall, the simple ligand modification with a methyl group significantly enhanced the stability of Re site without sacrificing the rate of ClO_4^- reduction.

Unlike the biological system that uses delicate enzymatic machinery to work against the oxidative stress from ClO_x^- intermediates, a bioinspired catalyst system relies on simplicity and self-sustainability. The self-protection mechanism empowers the catalyst to treat concentrated ClO_4^- solutions using a single metal center, thus greatly simplifying the catalyst design and preparation. We anticipate the mechanistic insights and design strategy to benefit the development of a wider scope of catalytic systems, where the deactivation by reaction intermediates is limiting the overall turnover number and catalyst life.

2.6 Acknowledgement

2.7 References

1. Motzer, W. E., Perchlorate: problems, detection, and solutions. *Environmental Forensics* **2001,** *2* (4), 301-311.

2. Brandhuber, P.; Clark, S.; Morley, K., A review of perchlorate occurrence in public drinking water systems. *Journal-American Water Works Association* **2009,** *101* (11), 63-73.

3. Kucharzyk, K. H.; Crawford, R. L.; Cosens, B.; Hess, T. F., Development of drinking water standards for perchlorate in the United States. *Journal of environmental management* **2009,** *91* (2), 303-310.

4. Cao, F.; Jaunat, J.; Sturchio, N.; Cancès, B.; Morvan, X.; Devos, A.; Barbin, V.; Ollivier, P., Worldwide occurrence and origin of perchlorate ion in waters: A review. *Science of the Total Environment* **2019,** *661*, 737-749.

5. Greer, M. A.; Goodman, G.; Pleus, R. C.; Greer, S. E., Health effects assessment for environmental perchlorate contamination: the dose response for inhibition of thyroidal radioiodine uptake in humans. *Environmental health perspectives* **2002,** *110* (9), 927-937.

6. Agency, U. S. E. P., Steps Water Systems Can Take to Address Perchlorate in Drinking Water **May 2020**, EPA 815-F-20-001.

7. Hecht, M.; Kounaves, S.; Quinn, R.; West, S.; Young, S.; Ming, D.; Catling, D.; Clark, B.; Boynton, W. V.; Hoffman, J., Detection of perchlorate and the soluble chemistry of martian soil at the Phoenix lander site. *Science* **2009,** *325* (5936), 64-67.

8.   Ming, D. W.; Archer, P.; Glavin, D.; Eigenbrode, J.; Franz, H.; Sutter, B.; Brunner, A.; Stern, J.; Freissinet, C.; McAdam, A., Volatile and organic compositions of sedimentary rocks in Yellowknife Bay, Gale Crater, Mars. *Science* **2014,** *343* (6169), 1245267.

9.   Kim, Y. S.; Wo, K. P.; Maity, S.; Atreya, S. K.; Kaiser, R. I., Radiation-induced formation of chlorine oxides and their potential role in the origin of Martian perchlorates. *Journal of the American Chemical Society* **2013,** *135* (13), 4910-4913.

10.   Clark, B. C.; Kounaves, S. P., Evidence for the distribution of perchlorates on Mars. *International Journal of Astrobiology* **2016,** *15* (4), 311-318.

11.   Jackson, W. A.; Davila, A. F.; Sears, D. W.; Coates, J. D.; McKay, C. P.; Brundrett, M.; Estrada, N.; Böhlke, J. K., Widespread occurrence of (per) chlorate in the Solar System. *Earth and Planetary Science Letters* **2015,** *430*, 470-476.

12.   Kounaves, S. P.; Carrier, B. L.; O'Neil, G. D.; Stroble, S. T.; Claire, M. W., Evidence of martian perchlorate, chlorate, and nitrate in Mars meteorite EETA79001: Implications for oxidants and organics. *Icarus* **2014,** *229*, 206-213.

13.   Youngblut, M. D.; Wang, O.; Barnum, T. P.; Coates, J. D., (Per) chlorate in biology on earth and beyond. *Annual review of microbiology* **2016,** *70*.

14.   Davila, A. F.; Willson, D.; Coates, J. D.; McKay, C. P., Perchlorate on Mars: a chemical hazard and a resource for humans. *International Journal of Astrobiology* **2013,** *12* (4), 321-325.

15.   Youngblut, M. D.; Tsai, C.-L.; Clark, I. C.; Carlson, H. K.; Maglaqui, A. P.; Gau-Pan, P. S.; Redford, S. A.; Wong, A.; Tainer, J. A.; Coates, J. D., Perchlorate reductase is distinguished by active site aromatic gate residues. *Journal of Biological Chemistry* **2016,** *291* (17), 9190-9202.

16.   Schwarz, G.; Mendel, R. R.; Ribbe, M. W., Molybdenum cofactors, enzymes and pathways. *Nature* **2009,** *460* (7257), 839.

17.   Bertero, M. G.; Rothery, R. A.; Palak, M.; Hou, C.; Lim, D.; Blasco, F.; Weiner, J. H.; Strynadka, N. C., Insights into the respiratory electron transfer pathway from the structure of nitrate reductase A. *Nature Structural & Molecular Biology* **2003,** *10* (9), 681-687.

18.   Jormakka, M.; Törnroth, S.; Byrne, B.; Iwata, S., Molecular basis of proton motive force generation: structure of formate dehydrogenase-N. *Science* **2002,** *295* (5561), 1863-1868.

19.   Hofbauer, S.; Gruber, C.; Pirker, K. F.; Sündermann, A.; Schaffner, I.; Jakopitsch, C.; Oostenbrink, C.; Furtmüller, P. G.; Obinger, C., Transiently produced hypochlorite is responsible for the irreversible inhibition of chlorite dismutase. *Biochemistry* **2014,** *53* (19), 3145-3157.

20.   de Geus, D. C.; Thomassen, E. A.; Hagedoorn, P.-L.; Pannu, N. S.; van Duijn, E.; Abrahams, J. P., Crystal structure of chlorite dismutase, a detoxifying enzyme producing molecular oxygen. *Journal of molecular biology* **2009,** *387* (1), 192-206.

21.   Melnyk, R. A.; Youngblut, M. D.; Clark, I. C.; Carlson, H. K.; Wetmore, K. M.; Price, M. N.; Iavarone, A. T.; Deutschbauer, A. M.; Arkin, A. P.; Coates, J. D., Novel mechanism for scavenging of hypochlorite involving a periplasmic methionine-rich peptide and methionine sulfoxide reductase. *MBio* **2015,** *6* (3), e00233-15.

22.   Lee, C. C.; Sickerman, N. S.; Hu, Y.; Ribbe, M. W., YedY-a mononuclear molybdenum enzyme with a redox-active ligand? *ChemBioChem* **2016,** *17* (6), 453.

23.   Coates, J. D.; Achenbach, L. A., Microbial perchlorate reduction: rocket-fuelled metabolism. *Nature Reviews Microbiology* **2004,** *2* (7), 569-580.

24.   Ford, C. L.; Park, Y. J.; Matson, E. M.; Gordon, Z.; Fout, A. R., A bioinspired iron catalyst for nitrate and perchlorate reduction. *Science* **2016,** *354* (6313), 741-743.

25.   Drummond, M. J.; Miller, T. J.; Ford, C. L.; Fout, A. R., Catalytic Perchlorate Reduction Using Iron: Mechanistic Insights and Improved Catalyst Turnover. *ACS Catalysis* **2020,** *10* (5), 3175-3182.

26.   Abu-Omar, M. M.; McPherson, L. D.; Arias, J.; Béreau, V. M., Clean and efficient catalytic reduction of perchlorate. *Angewandte Chemie* **2000,** *112* (23), 4480-4483.

27.   Liu, J.; Wu, D.; Su, X.; Han, M.; Kimura, S. Y.; Gray, D. L.; Shapley, J. R.; Abu-Omar, M. M.; Werth, C. J.; Strathmann, T. J., Configuration control in the synthesis of homo-and heteroleptic bis (oxazolinylphenolato/thiazolinylphenolato) chelate ligand complexes of oxorhenium (V): Isomer effect on ancillary ligand exchange dynamics and implications for perchlorate reduction catalysis. *Inorganic chemistry* **2016,** *55* (5), 2597-2611.

28.   Liu, J.; Choe, J. K.; Wang, Y.; Shapley, J. R.; Werth, C. J.; Strathmann, T. J., Bioinspired complex-nanoparticle hybrid catalyst system for aqueous perchlorate reduction: Rhenium speciation and its influence on catalyst activity. *ACS Catalysis* **2015,** *5* (2), 511-522.

29.   Elrod, L. T.; Kim, E., Lewis Acid Assisted Nitrate Reduction with Biomimetic Molybdenum Oxotransferase Complex. *Inorganic chemistry* **2018,** *57* (5), 2594-2602.

30.   Jiang, J.; Holm, R., Reaction systems related to dissimilatory nitrate reductase: nitrate reduction mediated by bis (dithiolene) tungsten complexes. *Inorganic chemistry* **2005,** *44* (4), 1068-1072.

31.   Liu, J.; Chen, X.; Wang, Y.; Strathmann, T. J.; Werth, C. J., Mechanism and mitigation of the decomposition of an oxorhenium complex-based heterogeneous catalyst for perchlorate reduction in water. *Environmental science & technology* **2015,** *49* (21), 12932-12940.

32.   Liu, J.; Su, X.; Han, M.; Wu, D.; Gray, D. L.; Shapley, J. R.; Werth, C. J.; Strathmann, T. J., Ligand design for isomer-selective oxorhenium (V) complex synthesis. *Inorganic chemistry* **2017,** *56* (3), 1757-1769.

33.   Bergeron, R. J., Synthesis and solution structure of microbial siderophores. *Chemical Reviews* **1984,** *84* (6), 587-602.

34.   Hurley, K. D.; Zhang, Y.; Shapley, J. R., Ligand-enhanced reduction of perchlorate in water with heterogeneous Re− Pd/C catalysts. *Journal of the American Chemical Society* **2009,** *131* (40), 14172-14173.

35.   Liu, B. Y.; Wagner, P. A.; Earley, J. E., Reduction of perchlorate ion by (N-(hydroxyethyl) ethylenediaminetriacetato) aquatitanium (III). *Inorganic Chemistry* **1984,** *23* (21), 3418-3420.

36.   Liu, J.; Han, M.; Wu, D.; Chen, X.; Choe, J. K.; Werth, C. J.; Strathmann, T. J., A new bioinspired perchlorate reduction catalyst with significantly enhanced stability via rational tuning of rhenium coordination chemistry and heterogeneous reaction pathway. *Environmental science & technology* **2016,** *50* (11), 5874-5881.

37.   Hurley, K. D.; Shapley, J. R., Efficient heterogeneous catalytic reduction of perchlorate in water. *Environmental science & technology* **2007,** *41* (6), 2044-2049.

38.   Cao, J.; Elliott, D.; Zhang, W.-x., Perchlorate reduction by nanoscale iron particles. *Journal of Nanoparticle Research* **2005,** *7* (4), 499-506.

39.   Xiong, Z.; Zhao, D.; Pan, G., Rapid and complete destruction of perchlorate in water and ion-exchange brine using stabilized zero-valent iron nanoparticles. *Water research* **2007,** *41* (15), 3497-3505.

40.   Moore, A. M.; De Leon, C. H.; Young, T. M., Rate and extent of aqueous perchlorate removal by iron surfaces. *Environmental science & technology* **2003,** *37* (14), 3189-3198.

41.   Hori, H.; Sakamoto, T.; Tanabe, T.; Kasuya, M.; Chino, A.; Wu, Q.; Kannan, K., Metal-induced decomposition of perchlorate in pressurized hot water. *Chemosphere* **2012,** *89* (6), 737-742.

42.   Hori, H.; Kamijo, A.; Inoue, M.; Chino, A.; Wu, Q.; Kannan, K., Efficient decomposition of perchlorate to chloride ions in subcritical water by use of steel slag. *Environmental Science and Pollution Research* **2018,** *25* (8), 7262-7270.

43.   Gu, B.; Dong, W.; Brown, G. M.; Cole, D. R., Complete degradation of perchlorate in ferric chloride and hydrochloric acid under controlled temperature and pressure. *Environmental science & technology* **2003,** *37* (10), 2291-2295.

44.   Wang, C.; Huang, Z.; Lippincott, L.; Meng, X., Rapid Ti (III) reduction of perchlorate in the presence of β-alanine: Kinetics, pH effect, complex formation, and β-alanine effect. *Journal of hazardous materials* **2010,** *175* (1-3), 159-164.

45.   McPherson, L. D.; Drees, M.; Khan, S. I.; Strassner, T.; Abu-Omar, M. M., Multielectron atom transfer reactions of perchlorate and other substrates catalyzed by rhenium oxazoline and thiazoline complexes: Reaction kinetics, mechanisms, and density functional theory calculations. *Inorganic chemistry* **2004,** *43* (13), 4036-4050.

46.   Liu, J.; Choe, J. K.; Sasnow, Z.; Werth, C. J.; Strathmann, T. J., Application of a Re–Pd bimetallic catalyst for treatment of perchlorate in waste ion-exchange regenerant brine. *Water research* **2013,** *47* (1), 91-101.

47.   Choe, J. K.; Boyanov, M. I.; Liu, J.; Kemner, K. M.; Werth, C. J.; Strathmann, T. J., X-ray spectroscopic characterization of immobilized rhenium species in hydrated rhenium–palladium bimetallic catalysts used for perchlorate water treatment. *The Journal of Physical Chemistry C* **2014,** *118* (22), 11666-11676.

48.   Choe, J. K.; Shapley, J. R.; Strathmann, T. J.; Werth, C. J., Influence of rhenium speciation on the stability and activity of Re/Pd bimetal catalysts used for perchlorate reduction. *Environmental science & technology* **2010,** *44* (12), 4716-4721.

49.   Greiner, M. T.; Rocha, T. C.; Johnson, B.; Klyushin, A.; Knop-Gericke, A.; Schlögl, R., The oxidation of rhenium and identification of rhenium oxides during catalytic partial oxidation of ethylene: an in-situ XPS study. *Zeitschrift für Physikalische Chemie* **2014,** *228* (4-5), 521-541.

50.   Deshwal, B. R.; Jo, H. D.; Lee, H. K., Reaction kinetics of decomposition of acidic sodium chlorite. *The Canadian Journal of Chemical Engineering* **2004,** *82* (3), 619-623.

51.   Lippert, C. A.; Arnstein, S. A.; Sherrill, C. D.; Soper, J. D., Redox-Active Ligands Facilitate Bimetallic O2 Homolysis at Five-Coordinate Oxorhenium (V) Centers. *Journal of the American Chemical Society* **2010,** *132* (11), 3879-3892.

52. Arias, J.; Newlands, C. R.; Abu-Omar, M. M., Kinetics and mechanisms of catalytic oxygen atom transfer with oxorhenium (V) oxazoline complexes. *Inorganic chemistry* **2001,** *40* (9), 2185-2192.

53. Rundlöf, T.; Mathiasson, M.; Bekiroglu, S.; Hakkarainen, B.; Bowden, T.; Arvidsson, T., Survey and qualification of internal standards for quantification by 1H NMR spectroscopy. *Journal of pharmaceutical and biomedical analysis* **2010,** *52* (5), 645-651.

54. Polshin, V.; Popescu, D.-L.; Fischer, A.; Chanda, A.; Horner, D. C.; Beach, E. S.; Henry, J.; Qian, Y.-L.; Horwitz, C. P.; Lente, G., Attaining control by design over the hydrolytic stability of Fe-TAML oxidation catalysts. *Journal of the American Chemical Society* **2008,** *130* (13), 4497-4506.

55. Ghosh, A.; Ryabov, A. D.; Mayer, S. M.; Horner, D. C.; Prasuhn, D. E.; Sen Gupta, S.; Vuocolo, L.; Culver, C.; Hendrich, M. P.; Rickard, C. E., Understanding the mechanism of H+-induced demetalation as a design strategy for robust iron (III) peroxide-activating catalysts. *Journal of the American Chemical Society* **2003,** *125* (41), 12378-12379.

56. Wähler, K.; Ludewig, A.; Szabo, P.; Harms, K.; Meggers, E., Rhenium Complexes with Red-Light-Induced Anticancer Activity. *European journal of inorganic chemistry* **2014,** *2014* (5), 807-811.

57. Hasan, K.; Bansal, A. K.; Samuel, I. D.; Roldán-Carmona, C.; Bolink, H. J.; Zysman-Colman, E., Tuning the emission of cationic iridium (III) complexes towards the red through methoxy substitution of the cyclometalating ligand. *Scientific reports* **2015,** *5*, 12325.

58. Cotton, F. A.; Wilkinson, G.; Murillo, C. A.; Bochmann, M.; Grimes, R., *Advanced inorganic chemistry*. Wiley New York: 1988; Vol. 5.

Chapter 3. Catalytic Reduction of Aqueous Chlorate with MoO$_x$ Immobilized on Pd/C

This chapter is based on, or in part a reprint of the material as it appears in Ren, C.; Yang, P.; Gao, J.; Huo, X.; Min, X.; Bi, E. Y.; Liu, Y.; Wang, Y.; Zhu, M.; Liu, J. Catalytic reduction of aqueous chlorate with MoOx immobilized on Pd/C. *ACS Catalysis*, 2020, 10, 8201−8211.

3.1 Abstract

Chlorate (ClO_3^-) is an undesirable byproduct in the Chlor-Alkali process. It is also a heavily used chemical in various industrial and agricultural applications, making it a toxic water pollutant worldwide. Catalytic reduction of ClO_3^- into Cl^- by H_2 is of great interest to both emission control and water purification, but platinum group metal catalysts are either sluggish or severely inhibited by halide anions. Here, we report on the facile preparation, robust performance, and mechanistic investigation of a MoO$_x$−Pd/C catalyst for aqueous ClO_3^- reduction. Under 1 atm H_2 and room temperature, the Na$_2$MoO$_4$ precursor is rapidly immobilized from aqueous solution onto Pd/C as a mixture of low-valent Mo oxides. The catalyst enables complete reduction of ClO_3^- in a wide concentration range (e.g., 1 μM to 1 M) into Cl^-. The addition of Mo to Pd/C not only enhances the catalytic activity by > 55-fold, but also provides strong resistance to concentrated salts. To probe the reaction mechanisms, we conducted a series of kinetic measurements, microscopic and X-ray spectroscopic characterizations, sorption experiments, tests with other oxyanion substrates, and a comparative study using dissolved Mo species. The

catalytic site is the reduced MoO_x species (primarily Mo^{IV}), showing selective and proton-assisted reactivity with ClO_3^-. This work demonstrates a great promise of using relatively abundant metals to expand the functionality of hydrogenation catalysts for environmental and energy applications.

3.2 Introduction

Catalytic reduction of toxic chlorate (ClO_3^-) has significant values for both industrial sustainability and environmental protection. More than 4 million tons of $KClO_3$ are manufactured worldwide each year by the electrochemical Chlorate Process.[1, 2] Heavy uses of chlorate in various industrial and agricultural applications (e.g., pulp bleaching, weed control, pyrotechnics, and water disinfection) have led to widespread environmental pollution[3] and emerging challenges for water systems.[4] The World Health Organization (WHO) has proposed a guideline for limiting the ClO_3^- concentration below 0.7 mg L^{-1} in drinking water.[4] The third Unregulated Contaminant Monitoring Rule (UCMR 3) by the United States Environmental Protection Agency (USEPA) included ClO_3^- as a contaminant monitored by public water systems, with the Minimum Reporting Level at 0.02 mg L^{-1}.[5] On the other hand, the global production of Cl_2 has reached over 70 million tons per year by the electrochemical Chlor-Alkali Process,[1] where on average one kg of ClO_3^- is generated per ton of Cl_2 produced.[6-9] The undesirable ClO_3^- byproduct has negative effects on both the manufacturing processes and the environment.[6, 10] Hence, at least 70,000 tons of ClO_3^- must be treated in Chlor-Alkali plants per year. Typical waste brines from the Chlor-Alkali Process contain up to 10 g L^{-1} of ClO_3^- and up to 5 M of $NaCl$.[6, 10, 11] Other emerging electrochemical technologies such as water splitting,[12]

wastewater treatment,[13] and direct HCl production from seawater desalination waste brines[14] also produce various levels of undesirable ClO_3^- at the anode.[7, 8] Therefore, an efficient and robust approach for ClO_3^- reduction is beneficial for a wide scope of industrial and environmental endeavors.

In Chlor-Alkali plants, the ClO_3^- byproduct is treated by either comproportionation under acidic conditions (**Eq. 3.1**) or catalytic reduction by H_2 (**Eq. 3.2**):

$$ClO_3^- + 6\ H^+ + 5\ Cl^- \rightarrow 3\ H_2O + 3\ Cl_2 \qquad\qquad \textbf{(Eq. 3.1)}$$

$$ClO_3^- + 3\ H_2 \rightarrow Cl^- + 3\ H_2O \qquad\qquad \textbf{(Eq. 3.2)}$$
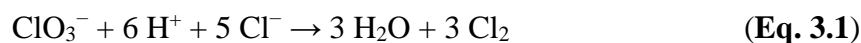
The comproportionation reaction requires $> 85\ °C$ and pH 0 (i.e., 1 M of H^+) to achieve a partial (60−90%) removal of ClO_3^-. The pH adjustment involves large amounts of HCl and NaOH.[6] In comparison, catalytic reduction allows an almost complete conversion of ClO_3^- to Cl^- and requires orders of magnitude less acid (i.e., pH 2−4).[6] In particular, H_2 gas is produced in excess at the cathode of the Chlor-Alkali Process; about 10% of the H_2 is emitted to the atmosphere.[6] Supported platinum group metal (PGM) catalysts have been examined; however, they exhibit limited activity and require high catalyst loadings to achieve a satisfactory reaction rate.[11, 15, 16] Furthermore, PGM catalysts can be severely inhibited by concentrated salts in the brine.[11, 17] It is thus highly desirable to develop a ClO_3^- reduction catalyst with the following features: (i) high activity and robustness, (ii) using a relatively abundant metal, and (iii) having a facile preparation.

Polyoxometalates (POMs) of Group 6 Mo and W have a series of fascinating redox properties and have been used in various chemical catalysis.[18] A century ago, molybdate

was used as a homogeneous catalyst to reduce ClO_3^- by I^- for iodometric analysis.[19] Molybdate was later used in the catalytic polarographic reduction of ClO_3^- to determine Mo contents in metals.[20] For the reduction of ClO_3^- in drinking water sources and in brines, an ideal approach is to immobilize Mo species as an active site on solid supports and utilize H_2 as a clean and readily available electron donor. In this study, by using a Pd/C catalyst platform and conducting a series of material characterizations, we show that Mo^{VI} POMs can be transformed into a heterogeneous MoO_x−Pd/C catalyst which is highly active and robust for ClO_3^- reduction under various challenging conditions.

3.3 Materials and Methods

3.3.1 Reagents and Materials

Ultrahigh purity H_2 gas (99.999%, Airgas), standard 2 N sulfuric acid solution (Alfa Aesar), POM precursors (Sigma−Aldrich or Alfa Aesar) and all other chemicals (Sigma−Aldrich or Fisher Scientific) were used as received. All aqueous solutions were prepared with deionized (DI) water (resistivity >18.2 MΩ cm). The 5 wt% Pd/C (Sigma−Aldrich, catalog #330116, wet paste) was dried and treated prior to use as previously described.[21]

3.3.2 Catalyst Preparation and Chlorate Reduction

For the preparation of a typical 0.2 g/L loading of MoO_x−Pd/C catalyst containing nominally 5 wt% Mo, a 50-mL round bottom flask was sequentially loaded with 50 mL of DI water (pH adjusted to 3.0 with 2N H_2SO_4), 10 mg of Pd/C powder, 0.5 mL of Na_2MoO_4 stock solution (containing 0.5 mg Mo), and a magnetic stir bar. The flask was sealed with a rubber stopper and sonicated for 1 min to disperse the Pd/C in water. The aqueous suspension was stirred at 1600 rpm under 1 atm H_2 headspace for at least 15 min to allow the immobilization of Mo POM species onto the carbon support. The H_2 gas was supplied by two 16-gauge in diameter and 6-inch in length stainless steel needles as gas inlet and outlet to the fume hood. The catalytic reduction of a typical 1 mM ClO_3^- was initiated by adding 0.25 mL of $NaClO_3$ stock solution (200 mM) into the catalyst suspension. For the initial ClO_3^- concentration of 1 M, 5.32 g of solid $NaClO_3$ was added into the suspension.

Aliquots were collected through the H_2 outlet needle with a 3-mL plastic syringe and immediately filtered through a 0.22-μm cellulose membrane to quench reactions.

3.3.3 Aqueous Sample Analysis

The quantitation of ClO_3^-, Cl^-, BrO_3^-, and NO_3^- in aqueous samples were conducted by ion chromatography (Dionex ICS-5000 system with a conductivity detector and a 25 μL sample injection loop). Brine samples were diluted 100 times before analysis. A Dionex IonPac AS19 analytical column was used to separate ClO_3^- from other anions. The most effective separation was achieved by maintaining the column at 30 °C and using 20 mM KOH at 1 mL min^{-1} as the eluent. When Br^- was present, ClO_3^- was separated by an IonPac AS18 column at 30 °C with 16 mM KOH at 1 mL min^{-1} as the eluent. The concentration of total Mo in aqueous samples was analyzed by inductively coupled plasma−mass spectrometry (ICP−MS, Agilent 7700).

3.3.4 Catalyst Collection and Characterization

After disconnection from the H_2 supply, the catalyst suspension (the flask still being sealed by the rubber stopper) was quickly transferred into an anaerobic glove bag (Coy Laboratories, filled with 98% N_2 and 2% H_2) to avoid artifacts from air exposure. The catalyst suspension was filtered through a ceramic funnel covered with filter paper (Whatman qualitative) under vacuum. The filter paper coated by the catalyst was transferred into a 20-mL scintillation vial. The vial was placed in a sand bath at 110 °C to remove moisture from the catalyst powder. The contents of Mo and Pd were measured by inductively coupled plasma−optical emission spectroscopy (ICP−OES, PerkinElmer

Optima 8300) after digestion with HCl/HNO₃. The surface area and pore structure were characterized by N_2 Brunauer-Emmett-Teller (BET) adsorption-desorption isotherms measured at 77 K using a Micromeritics ASAP 2020 analyzer. The surface area of Pd was determined by CO chemisorption.[22] The catalyst sample for microscopy analysis was re-dispersed in distilled water and sonicated for 30 min. A drop of the suspension was loaded onto the copper microgrids and dried under vacuum. The distribution of Mo, Pd, C, and O elements was characterized by high-angle annular dark-field (HAADF) imaging with scanning transmission electron microscopy (STEM, FEI Titan Themis 300, operated at 300 kV).

3.3.5 X-ray Photoelectron Spectroscopy (XPS)

Inside the glove bag, the dried powder was loaded onto a copper conductive tape on the XPS sample holder and stored in an anaerobic chamber secured with Klein Flange for the transfer to the XPS facility. All XPS experiments were performed on the Kratos AXIS Supra surface analysis instrument at the UC Irvine Materials Research Institute (IMRI). The sp^2 C 1s peak (284.5 eV) of the carbon support was used for binding energy calibration. For Mo reference standards that were mixed with Nb_2O_5 powder, the binding energy of Nb $3d_{5/2}$ was set to 207.6 eV. Spectra in the resolution of 0.1 eV were fit using CasaXPS (version 2.3.19). Spectra of Pd 3d (collected with 5 scans), Mo 3d (30 scans), and Nb 3d (30 scans) were fit with the constrained peak separations (5.27 eV for Pd, 3.15 eV for Mo, and 2.75 eV for Nb) and the constrained ratio of peak areas (3:2) of 3d spin-orbital coupling doublets.

3.3.6 X-ray Absorption Spectroscopy (XAS)

The preparation and transfer of XAS samples are the same as mentioned above. Mo K-edge EXAFS data were collected at beamlines 4−1 and 2−2 at Stanford Synchrotron Radiation Light source. During the data collection, the sample chamber was purged with N_2 to minimize sample alteration by atmospheric O_2. Both transmission signals and fluorescence signals were acquired. A Mo metal foil reference was concomitantly measured with the samples for energy calibration (E_0 = 20000 eV). Zirconium (Z–2) metal foil was used as the filter for collecting fluorescence signals. *Athena* was used for energy calibration, raw spectra average, post-edge normalization, and background removal.[23] *Artemis* was used to obtain the structural parameters by fitting k^3-weighted EXAFS spectra to the standard EXAFS equation using several single-scattering paths. The fittings were over a k range of 3–13 $Å^{-1}$ and an R range of 1.0–3.0 Å for the catalyst sample, a k range of 3–12 $Å^{-1}$ and an R range of 1.2–3.9 Å for MoO_2 standard, and a k range of 3–12 $Å^{-1}$ and an R range of 0.9–2.0 Å for $(NH_4)_6Mo_7O_{24}$ standard. Phase and amplitude functions for the scattering paths were generated using FEFF6[24] based on the MoO_2, MoO_3, and monomolybdate structures. In all fittings, the number of independent variables included was fewer than the number of independent data points. The Hanning window was used for the Fourier transform of the EXAFS data.

3.3.7 Homogeneous Reaction

In the anaerobic glove bag, a 15-mL glass reaction tube was loaded with 6 mL of water, 34.8 mg of sodium molybdate dihydrate, 60 μL of aqueous hydrazine solution (15.6 M), and a magnetic stir bar. The resulting aqueous solution thus contained 24 mM of Mo^{VI} and 156 mM of H_2N-NH_2. The solution pH was further adjusted to 3.0 with 1N HCl. The tube was sealed with a Teflon screw cap and heated in a 70 °C oil bath for 24 h. Sodium chlorate (0.5 mM) was then added to monitor the ClO_3^- reduction in the homogeneous solution for another 24 h at 70 °C. Aliquots of 1 mL solution were collected at time intervals. Each sample was diluted with another 1 mL of DI water before IC analysis.

3.4 Results and Discussion

3.4.1 Catalyst Preparation

We developed a simple and straightforward method to immobilize and activate Mo sites on Pd/C. Inspired by the reductive immobilization of Group 7 metal oxyanions ($Tc^{VII}O_4^-$ and $Re^{VII}O_4^-$) from aqueous solutions,[25-28] we hypothesized that Group 6 Mo^{VI} and W^{VI} POM precursors could be similarly immobilized and reduced to insoluble lower-valent oxide species on Pd/C. Hence, two Mo^{VI} POM precursors (nominally 5 wt% as Mo to the weight of Pd/C) were added into the water suspension of Pd/C at room temperature (20 °C), with 1 atm H_2 in the headspace of the reactor flask. After 2 h of stirring, 1 mM of $NaClO_3$ was added into the suspension to probe the catalytic activity. As shown in **Figure 3.1a**, the use of $Na_2Mo^{VI}O_4$ and $(NH_4)_6Mo^{VI}_7O_{24}$ provided rapid ClO_3^- reduction. The pseudo-first-order rate constants are 55-fold higher than that of the original Pd/C. In

comparison, the two W^{VI} POM precursors, $Na_2W^{VI}O_4$ and $Na_6W^{VI}_{12}O_{39}$, provided little activity enhancement.

The immobilization and activation of Mo are both rapid. Inductively coupled plasma mass spectrometry (ICP−MS) analysis of the aqueous phase found >96% of the initial Mo (10 mg/L as Mo element) adsorbed into Pd/C within 5 min on the benchtop. Without exposure to H_2, X-ray photoelectron spectroscopy (XPS) characterization observed only Mo^{VI} in the Pd/C (see **Section 3.4.3 Characterization of Mo speciation**). After 1 atm H_2 was supplied to the water suspension of Mo^{VI}−Pd/C, high activity of ClO_3^- reduction was observed. Prior to the addition of $NaClO_3$, after Mo^{VI}−Pd/C was exposed to H_2 for only 5 min, the profile of ClO_3^- reduction had an induction period at the beginning (**Figure 3.1b**). However, the exposure to H_2 for 15 min or longer eliminated this induction period, providing similar ClO_3^- reduction kinetics. Thus, the reduction of adsorbed Mo^{VI} by Pd-activated H_2 is required to enable ClO_3^- reduction. This process is rapid, taking only 15 min at ambient pressure and temperature. Detailed characterizations of the lower-valent Mo species are provided in later sections.

Upon H_2 exposure for 2 h, the Mo immobilization ratio was further increased to 99.9% (**Figure S3.1** in the **Appendix B**). Throughout the ClO_3^- reduction process, < 15 µg/L of Mo (i.e., < 0.15% of the total added Mo) was detected by ICP−MS in the aqueous solution. Thus, the carbon support of Pd/C has a high capacity to accommodate MoO_x species. It also appears that ClO_3^- reduction occurred on the heterogeneous catalyst-water interface. In contrast, the same Pd/C material provided a poor sorption capacity for WO_x species. ICP−MS analysis showed that only 24% of the added W was immobilized after

exposure to H_2 for 2 h. The reduced W species in the aqueous solution showed a blue color, which faded within one minute after exposure to air. Therefore, the reductive immobilization method applies to Mo^{VI} POMs to yield a highly active MoO_x-Pd/C catalyst. In aqueous solutions, Mo^{VI} POMs have dynamic speciations depending on pH. Both Na_2MoO_4 and $(NH_4)_6Mo_7O_{24}$ added in an acidic solution (e.g., pH 3) transform into a mixture of $Mo_8O_{26}^{4-}$, $H_3Mo_8O_{28}^{5-}$, $HMo_7O_{24}^{5-}$, $H_2Mo_6O_{21}^{4-}$, and other minor polymeric species.[29] To avoid introducing the unnecessary NH_4^+, we used Na_2MoO_4 as the Mo precursor for the following experiments.
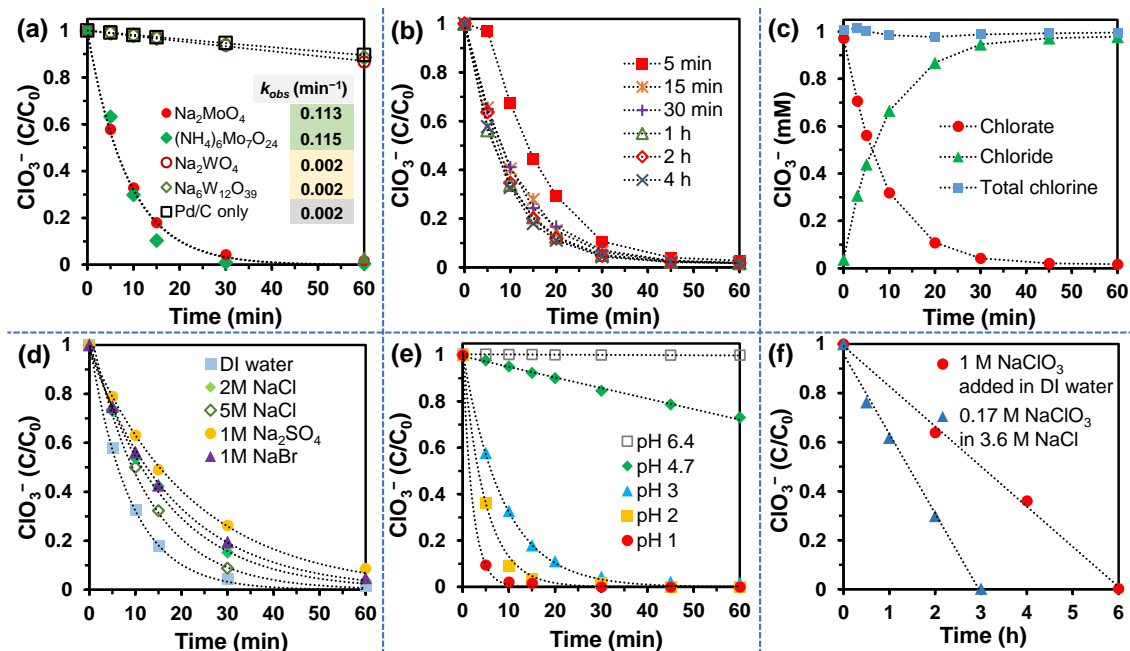
Figure 3.1 (a) Profiles, first-order fittings, and rate constants for the reduction of ClO_3^- by Pd/C added with various POM precursors; (b) profiles of ClO_3^- reduction by the MoO_x-Pd/C catalyst prepared by allowing variable time lengths after adding the Na_2MoO_4 precursor under 1 atm H_2 and before adding the $NaClO_3$ substrate; (c) chlorine mass balance; (d) effects of concentrated salts; (e) effects of proton concentrations; and (f) the reduction of 1 M ClO_3^- in DI water and of 170 mM ClO_3^- in 3.6 M NaCl brine by 0.5 g L^{-1} MoO_x-Pd/C. Unless specified, all reactions used 1 mM ClO_3^-, 0.2 g L^{-1} MoO_x-Pd/C, pH 3.0, 20 °C.

3.4.2 Catalyst Performance

The MoO_x-Pd/C catalyst outperforms multiple reported PGM catalysts in terms of the activity for ClO_3^- reduction, and the robustness in concentrated brines. At 20 °C, a loading of 0.2 g L^{-1} catalyst in water achieved >99.9% reduction of 1 mM ClO_3^- within 1 h (**Figure 3.1a**). The observed rate constant is substantially higher than those of most PGM catalysts at the same or higher temperatures (**Table 3.1**). Calculation suggests that the rate of ClO_3^- reduction is not limited by either internal or external mass transfer of aqueous ClO_3^- with regard to the catalyst particle (see **Appendix B**). The mass balance between ClO_3^- and Cl^- throughout the reaction (**Figure 3.1c**) indicates minimal accumulation of partially deoxygenated intermediates (e.g., ClO_2^-). In real-world situations, ClO_3^- needs to be reduced in acidic and/or brine matrices, such as Chlor-Alkali waste brines,[10, 16] ion-exchange resin regeneration wastes,[30] or HCl produced from waste brine electrolysis.[14] Therefore, we further challenged the performance of MoO_x-Pd/C in solutions containing 2 M and 5 M NaCl, 1 M Na_2SO_4, and 1 M NaBr, respectively. None of the concentrated salts caused a significant loss of activity (**Figure 3.1d** and **Table 3.1, entries 1−5**). We note that Br^- is a much stronger inhibitor than Cl^- for PGM catalysts.[11, 17] The same Pd/C was significantly inhibited by halide anions at low concentrations, as observed in our previous study (**Table 3.1**, **entries 8−12**).[17] Similarly, although a Rh/C catalyst exhibited very high activity in a deionized water matrix (**Table 3.1**, **entry 13**),[15] the performance was significantly affected by Cl^- and Br^- (**Table 3.1**, **entries 20−24**).[11] An Ir/C catalyst showed similar ClO_3^- reduction kinetics to the MoO_x-Pd/C in concentrated brine (**Table 3.1**, **entry 17** versus **7**), whereas the reaction temperature was much higher (70 °C).[16]

Higher rates of ClO_3^- reduction were observed at lower pH conditions (**Figure 3.1e**), suggesting that a proton-assisted mechanism is involved. We note that the pH dependence may be primarily attributed to the reactivity of the active site rather than the surface charge of the catalyst support.[15, 31] Instead, the protonation of an O atom in the ClO_3^- that is bound by the lower-valent Mo may assist the structural distortion.[32] This structural change lowers the LUMO of Mo-bound ClO_3^- and thus promotes the electron transfer from reduced Mo (e.g., Mo^{IV}) to Cl^V. Alternatively, the proton may provide an ancillary hydrogen bonding[33] to facilitate the coordination of ClO_3^- to Mo. Thus, the MoO_x-Pd/C catalyst is expected to be highly robust in reducing ClO_3^- in acidic brines.[14] Because the build-up of Cl^- did not cause a significant inhibition, we further tested the catalyst for treating concentrated ClO_3^- (1 M) at pH 3.0. With a 0.5 g L^{-1} loading of MoO_x-Pd/C catalyst, a > 99.7% reduction of ClO_3^- was achieved within 6 h following zero-order kinetics (**Figure 3.1f**). When ClO_3^- concentrations were high, the reaction rate became controlled by the H_2 availability (**Figure S3.2** in the **Appendix B**). Assuming that the Mo sites reacted with all ClO_x^- (x= 3, 2, and 1) substrates, at pH 3 the corresponding TON for each Mo atom is calculated as 11,510 within 6 h (i.e., TOF = 1,920 h^{-1}). If not all immobilized Mo atoms were directly involved in the reaction (see the catalyst characterization results below), the actual TOF on the reactive Mo sites would be even higher. As shown in **Figure 3.1e**, a higher TOF can also be expected at pH < 3.

We prepared a solution mimicking a real Chlor-Alkali waste brine sample (0.17 M of ClO_3^- in 3.6 M of NaCl).[11] The MoO_x-Pd/C catalyst achieved > 99.8% reduction of ClO_3^- in 3 h (**Figure 3.1f** and **Table 3.1**, **entry 7**). To further examine the catalyst stability

and reusability, we added multiple spikes of 180 mM ClO_3^-, for up to 20 spikes (the final product thus became 3.6 M NaCl), into the catalyst suspension in water (**Figure S3.3** in the **Appendix B**, zero-order rate constants shown in **Table 3.2**). Each spike of ClO_3^- was completely reduced within 4 h. The decrease of the catalytic activity was only caused by the gradual build-up of concentrated Cl^-. In particular, the reduction profile for the 20th $NaClO_3$ spike corresponds to a zero-order rate constant of 0.13 M h^{-1} g$_{cat}^{-1}$. This rate constant, after the catalyst had been used to reduce 19 spikes of 0.18 M ClO_3^- in the gradually concentrated NaCl, is almost identical to that of the freshly prepared catalyst (**Table 3.1**, **entry 7**). The reduction of ClO_3^- did not consume H$^+$, so that the initially added 1 mM H$^+$ (for pH 3.0) maintained the acidic pH throughout the 20 spikes. The final pH reading was ~2.5 because the resulted 3.6 M NaCl decreased the hydration of H$^+$.[34] The Mo and Pd contents in the catalysts collected after 5, 10, and 20 spikes remained consistent (**Table 3.2**), indicating negligible leaching of metals into the high-salinity aqueous solutions. A catalyst recycling operation using the conventional "filtration-collection-redispersion" procedure resulted in a slightly decreased performance (**Figure S3.4a** in the **Appendix B**), most probably due to the loss of a non-recoverable fraction of catalyst during the sample transfer (e.g., held by the filter paper). The filtrate solution contained <0.1% of total Mo. Therefore, the reductively immobilized MoO_x species in Pd/C showed high activity, robustness, and stability for catalytic ClO_3^- reduction.

Entry	Catalyst	Catalyst loading	pH	Temp	Initial ClO_3^- conc.	Other salts added in solution	Time	ClO_3^- removal ratio	1st-order rate constant [a] (L h^{-1} g$_{cat}^{-1}$)	Ref.
					MoO$_x$−Pd/C catalyst					
1						DI [b]	1 h	99.9%	33.9	
2	(5 wt% Mo					2 M NaCl	1 h	97%	18.3	
3	5 wt% Pd)	0.2 g L^{-1}	3	20 ℃	84 mg L^{-1}	5 M NaCl	1 h	99.9%	24.6	
4	MoO$_x$−Pd/C				(1 mM)	1 M NaBr	1 h	95%	16.5	
5						1 M Na$_2$SO$_4$	1 h	91%	13.5	
6	(5 wt% Mo 5 wt% Pd) MoO$_x$−Pd/C	0.5 g L^{-1}	3	20 ℃	84,000 mg L^{-1} (1 M)	DI, KCl built up to 1 M	6 h	99.7%	0.33 M h^{-1} g$_{cat}^{-1}$ [c]	
7					14,280 mg L^{-1} (0.17 M)	3.6 M NaCl	3 h	99.8%	0.11 M h^{-1} g$_{cat}^{-1}$ [c]	
					PGM catalysts					
8						DI	8 h	96%	0.79	[17]
9						10 mM NaCl	8 h	81%	0.41	[17]
10	5 wt% Pd/C	0.5 g L^{-1}	3	20 ℃	84 mg L^{-1} (1 mM)	100 mM NaCl	8 h	49%	0.17	[17]
11						1 M NaCl	8 h	43%	0.14	[17]
12						10 mM NaBr	8 h	42%	0.13	[17]
13	5 wt% Rh/C						¼ h	99.3%	46	[15]
14	5 wt% Ru/C	0.5 g L^{-1}	3	20 ℃	84 mg L^{-1}	DI	1 h	43%	n.a.[d]	[15]
15	5 wt% Pt/C				(1 mM)		1 h	14%	0.33	[15]
16	1 wt% Ir/C						1 h	45%	1.2	[15]
17	5 wt% Ir/C	2.5 g L^{-1}	3.8	70 ℃	22,000 mg L^{-1} (0.26 M)	3.2 M NaCl	¾ h	100%	0.14 M h^{-1} g$_{cat}^{-1}$	[16]
18	0.5 wt% Rh/SiC	0.5 g L^{-1}	4	70 ℃	1000 mg L^{-1} (12 mM)	DI	2 h	85%	1.9 [e]	[11]
19	0.5 wt% Pt/SiC						2 h	90%	2.3	[11]
20	0.5 wt% Rh/SiC	0.5 g L^{-1}	2	50 ℃	1000 mg L^{-1} (12 mM)	DI	2 h	35%	0.43	[11]
21						3.6 M NaCl	2 h	10%	0.11	[11]
22						DI	2 h	89%	0.55	[11]
23	0.5 wt% Rh/ZrO$_2$	2 g L^{-1}	4	70 ℃	1000 mg L^{-1} (12 mM)	0.85 M NaCl	2 h	45%	0.15	[11]
24						78 mM NaBr	2 h	27%	0.079	[11]

Table 3.1. Performance of ClO_3^- reduction by MoOx−Pd/C and reported PGM catalysts.

[a]Normalized to the mass of the whole catalyst (metal + support) for cross-comparison of catalysts with variable metal contents;

[b]Containing HCl or H$_2$SO$_4$ used for pH adjustment;

[c]Zero-order kinetics due to the concentrated ClO_3^- substrate; these two reactions used the same high flow rate of H$_2$ (0.1 L per minute) as used for entries 18−24.

[d]The reaction did not follow first- or zero-order kinetics and the catalyst showed significant loss of activity during the reaction;

[e]First-order rate law reasonably assumed for the initial ClO_3^- concentration at 12 mM (entries 18−24).

Catalyst sample	Mo content	Pd content	Mo wt% : Pd wt%[b]	Zero-order initial rate constant[c] ($M\ h^{-1}\ g_{cat}^{-1}$)
Fresh catalyst	4.48%	5.73%	0.782	0.271 (in DI water)
After 5 spikes	4.38%	5.51%	0.795	0.186 (in 0.9 M NaCl)[d]
After 10 spikes	4.19%	5.61%	0.747	0.141 (in 1.8 M NaCl)[d]
After 20 spikes	4.39%	5.70%	0.771	0.130 (in 3.6 M NaCl)[d]

Table 3.2 Kinetics and metal contents of the freshly prepared and used MoO_x−Pd/C catalysts.

[a]The nominal content for Mo and Pd elements in the freshly prepared catalyst are both 5 wt%. The calculated Mo content assuming the addition of "MoO_4" in Pd/C is ~4.62%. Each spike introduced 180 mM ClO_3^-. At least 4 h of reaction (1 atm H_2, 20 °C, initial pH = 3 by adding 1 mM HCl) was allowed for each spike. The catalyst powder was collected in an anaerobic glove bag by filtering off the aqueous solution, rinsing the catalyst powder cake on the filter paper with DI water, and drying in a 100 °C sand bath.

[b]Because the Mo:Pd mass content ratio is rather consistent, the fluctuation of the absolute values of Mo and Pd contents in these samples should either be within the range of system errors of elemental analysis for heterogeneous materials or be attributed to the residual NaCl salt in the dried catalyst samples.

[c]From the linear fitting of all data points with $C/C_0 > 0.2$ (see **Figure S3.3b** in the **Appendix B** for details).

[d]The NaCl is generated from the reduction of ClO_3^- from all previous spikes (180 mM each).

3.4.3 Characterization of Mo Speciation

The immobilization of Mo POMs in Pd/C decreased both the Brunauer-Emmett-Teller (BET) surface area and the Pd surface area (**Table 3.3**). For a rough estimation of MoO_x coverage on the carbon support, one could assume that each MoO_x unit is six-coordinate and takes a square area at the length of an O–Mo–O. Since the atomic radius of O atom is ~60 pm and the typical Mo–O bond length is ~200 pm (see EXAFS analysis and **Table 3.4** below), the corresponding length of an O–Mo–O is (60 + 200) × 2 = 520 pm. Thus, a single layer of MoO_x at the 5 wt% Mo loading in one gram of carbon support is calculated to be 86 m^2. The carbon support has a sufficient surface area to accommodate a single-layer coverage of MoO_x. The decrease in pore volume (19.4%) was very similar to the decrease in surface area (19.6%), indicating that the loss of BET surface area is probably attributed to both the pore-blocking and surface-covering by the immobilized MoO_x. High-angle annular dark-field scanning transmission electron microscopy

(HAADF-STEM) characterization of the MoO_x−Pd/C catalyst observed Pd nanoparticles in the size of 1−8 nm (**Figure 3.2a**). Individual elements of C, O, Pd, and Mo were observed by the energy-dispersive X-ray (EDX) elemental mapping (**Figures 3.2b−3.2e**). Mo was present throughout the catalyst particle, either being on the carbon support or overlapping with Pd (**Figure 3.2f**).

XPS characterization of the H_2-reduced MoO_x−Pd/C catalyst (kept under an anaerobic atmosphere) identified Pd^0, which showed the characteristic $3d_{5/2}$ binding energy (BE) at 335.2 eV (**Figure S3.5a** in the **Appendix B**) and various oxidation states of Mo (**Figure 3.3a**). Because the MoO_x−Pd/C catalyst and the references such as $Mo^{II}_2(OAc)_4$ contain different carbon species (i.e., graphitic carbon versus acetate), we blended Nb_2O_5 powders with all XPS samples as the internal standard for BE calibration (**Figure S3.5b** in the **Appendix B**, Nb $3d_{5/2}$ BE set to 207.6 eV[35]). Upon deconvoluting the spectrum for MoO_x−Pd/C, we identified four Mo doublets with $3d_{5/2}$ BE of 231.3, 230.5, 229.4, and 228.7 eV. The two dominant $3d_{5/2}$ peaks with BE of 231.3 and 230.5 eV closely match literature values for Mo^V and Mo^{IV} species. The Mo^V reference was generated from a hydrothermal synthesis of a Keggin POM from $Na_2Mo^{VI}O_4$[36, 37] and the Mo^{IV} reference was generated from a direct reduction of $Mo^{VI}O_3$ by H_2 at 400 °C.[38] The observed Mo^V and Mo^{IV} in the MoO_x−Pd/C should be generated by the partial and full hydrogenation of one oxo bond in Mo^{VI} POM precursors.[38] Due to the wide range of BE values for Mo species in lower oxidation states, $Mo^{II}_2(OAc)_4$ was used as a reference. The XPS spectrum revealed two Mo oxidation states on the surface of $Mo^{II}_2(OAc)_4$ (**Figure S3.5c** in the **Appendix B**). The high BE peak (232.3 eV) is characteristic of Mo^{VI}, indicating partial oxidation at the

surface of $Mo^{II}_2(OAc)_4$ powders. The $3d_{5/2}$ BE of Mo^{II} is 228.9 eV, which is close to the lowest BE (228.7 eV) observed in MoO_x−Pd/C. The remaining peak (BE 229.4 eV) in the catalyst is thus assigned as Mo^{III}, although a reference chemical for oxygen-coordinated Mo^{III} was not accessible. Compared to the formation of Mo^V and Mo^{IV} from Mo^{VI}, the formation of the less abundant Mo^{III} and Mo^{II} can be attributed to the deeper but less favorable reduction of Mo^{IV}. Without exposure to H_2, the oxidation state of the adsorbed Mo^{VI} POMs in Pd/C remained the same (Mo $3d_{5/2}$ BE at 232.0 eV, **Figure 3.3a**).

To further probe the valence of Mo species in the bulk MoO_x−Pd/C sample, we conducted Mo K-edge X-ray absorption near-edge structure (XANES) spectroscopic characterization (**Figure 3.3b**). A linear relationship[39] was established between the Mo oxidation state and the Mo K-edge energy (i.e., the energy where the intensity reaches 60% of the absorption maxima) of three references: $(NH_4)_6Mo^{VI}_7O_{24}$, $Mo^{IV}O_2$, and $Mo^{II}_2(OAc)_4$ (**Figure 3.3c**). With this empirical relationship and the measured edge energy of 20012 eV for MoO_x−Pd/C, the average valence of Mo in the bulk sample is calculated to be 4.4. This value roughly agrees with the XPS characterization result for the surface layer, where Mo^{IV} and Mo^V are dominant species. Moreover, the XANES spectrum of $(NH_4)_6Mo^{VI}_7O_{24}$ contains a pre-edge peak at 20003 eV. The presence and absence of this characteristic pre-edge peak indicate the formation and elimination of $Mo^{VI}=O$ bonds, respectively.[39, 40] The significantly weakened pre-edge peak in MoO_x−Pd/C (**Figure 3.3b**) indicates the reduction of Mo=O bonds in Mo^{VI} POM precursors.

To determine whether the reductively immobilized Mo species exist as oxide clusters or as monomers (e.g., stabilized by complexation with functional groups on the

carbon surface), we collected the k^3-weighted Mo K-edge extended X-ray absorption fine structure (EXAFS) spectra from the MoO_x−Pd/C sample and references (**Figures 3.3d** and **3.3e**). The MoO_x−Pd/C spectrum contained two main peaks at 1.5 and 2.2 Å (R + ΔR). Shell-by-shell fitting (**Table 3.4**) showed that they correspond to two atomic shells, Mo^{IV}−O (2.03 Å) and Mo^{IV}−Mo^{IV} (2.56 Å), respectively.[41] Similar EXAFS spectra have been reported in a study on the complete and reversible 24-electron reduction of a well-defined solid-state $[PMo^{VI}_{12}O_{40}]^{3−}$ into $[PMo^{IV}_{12}O_{40}]^{27−}$ on a battery reaction platform,[39] where the Mo−Mo distance was shortened from 3.4 Å to 2.6 Å upon the reduction of all Mo^{VI} into Mo^{IV}. Since Mo^{VI} precursors were transformed into a mixture of multiple POM structures in the aqueous solution and XPS characterization observed mixed oxidation states of Mo at the surface layer, the EXAFS fitting here represents the average bonding environment for the bulk MoO_x−Pd/C sample. The average coordination number (CN) of 6.1 for Mo−O shell indicates that a majority of reduced Mo atoms are in the octahedral MoO_6 coordination structure. The overall CN of 1.7 for Mo−Mo shell confirms the polymeric structures for reductively immobilized Mo species. A majority of Mo atoms likely have two neighboring Mo atoms at a distance of ~2.56 Å. Furthermore, the lack of Mo−Mo pairs with longer interatomic distances as observed in $Mo^{IV}O_2$ reference (>3 Å, **Figure 3.3e** and **Table 3.4**) suggests that the spatial arrangement of Mo atoms in MoO_x−Pd/C is different from that in $Mo^{IV}O_2$. The latter has a three-dimensional distorted rutile structure with alternating short (2.51 Å) and long (3.11 Å) Mo^{IV}–Mo^{IV} distances.[41] The fitting also detects a weak atomic shell at 1.67 Å, which can be assigned to the Mo^{VI}=O bond as observed in $(NH_4)_6Mo^{VI}_7O_{24}$ reference (1.74 Å, **Table 3.4**). Thus, a small fraction

of immobilized Mo remained in +VI valence, but it was not observed by XPS characterization on the catalyst surface. The inclusion of a Mo−Pd shell yielded problematic data fitting (**Table S3.1** in the **Appendix B**), suggesting that the direct bonding between the two metals is not a primary mechanism for the immobilization and activation of Mo. However, chemisorption results show that the immobilization of MoO_x decreased the total surface area and the Pd surface area by 168 m^2 g^{-1} (20%) and 4.6 m^2 g^{-1} (66%), respectively (**Table 3.3**). The higher percent decrease in the Pd surface area suggests a preferred aggregation of MoO_x in the proximity of Pd nanoparticles.[42]

Sample	Surface area ($m^2\ g_{cat}^{-1}$)	Pore volume ($cm^3\ g_{cat}^{-1}$)	Average pore size (nm)	Pd surface area ($m^2\ g_{cat}^{-1}$)	Pd dispersion (%)	Pd particle size (nm)
Pd/C	857.2	0.67	3.11	6.85	30.7	3.7
MoO$_x$–Pd/C	689.0	0.54	3.12	2.29	N/A [a]	N/A [a]

Table 3.3 Physisorption and chemisorption data.

[a]The calculated Pd dispersion and average particle size are 10.3% and 10.8 nm, respectively. This set of data is not meaningful as it is calculated from the reduced Pd surface area by the immobilized MoO$_x$.

Sample	Shell	CN[a]	R (Å)[b]	σ^2 (Å^2)[c]	ΔE (eV)[d]	R-factor
(NH$_4$)$_6$Mo$_7$O$_{24}$	Mo−O	4	1.74 (0.01)	0.004 (0.002)	−4.0 (3.3)	0.012
MoO$_2$	Mo−O	6	1.99 (0.01)	0.002 (0.001)		
	Mo−Mo	1	2.52 (0.01)	0.001 (0.001)	−1.4 (2.0)	0.023
	Mo−Mo	1	3.12 (0.01)	0.002 (0.001)		
	Mo−Mo	8	3.70 (0.01)	0.004 (0.001)		
MoO$_x$−Pd/C	Mo−O	0.4 (0.3)	1.67 (0.04)	0.002[e]		
	Mo−O	6.1 (1.9)	2.03 (0.02)	0.010 (0.004)	−4.1 (2.9)	0.030
	Mo−Mo	1.7 (0.6)	2.56 (0.01)	0.005 (0.002)		

Table 3.4 Mo K-edge EXAFS shell-by-shell fitting parameters of MoO$_x$−Pd/C and references.

[a]Coordination number; [b]Interatomic distance; [c]Debye-Waller factor; [d]Energy shifts. During the EXAFS shell-by-shell fitting for the two references, the CNs were fixed at theoretical values according to their crystal structures. [e]Fixed during the fitting.
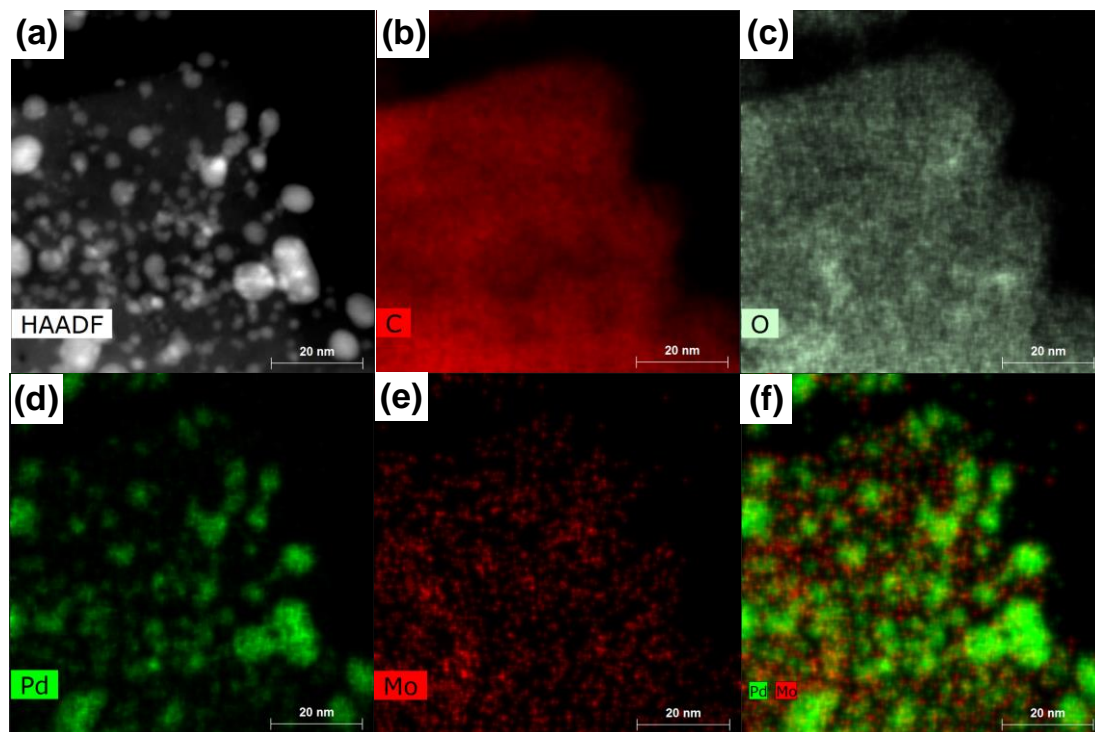
Figure 3.2 (a) HAADF-STEM imaging of the MoO_x−Pd/C catalyst and EDX mapping of (b) C, (c) O, (d) Pd, and (e) Mo. (f) The combined Pd and Mo mapping showing the different distribution of the two elements.
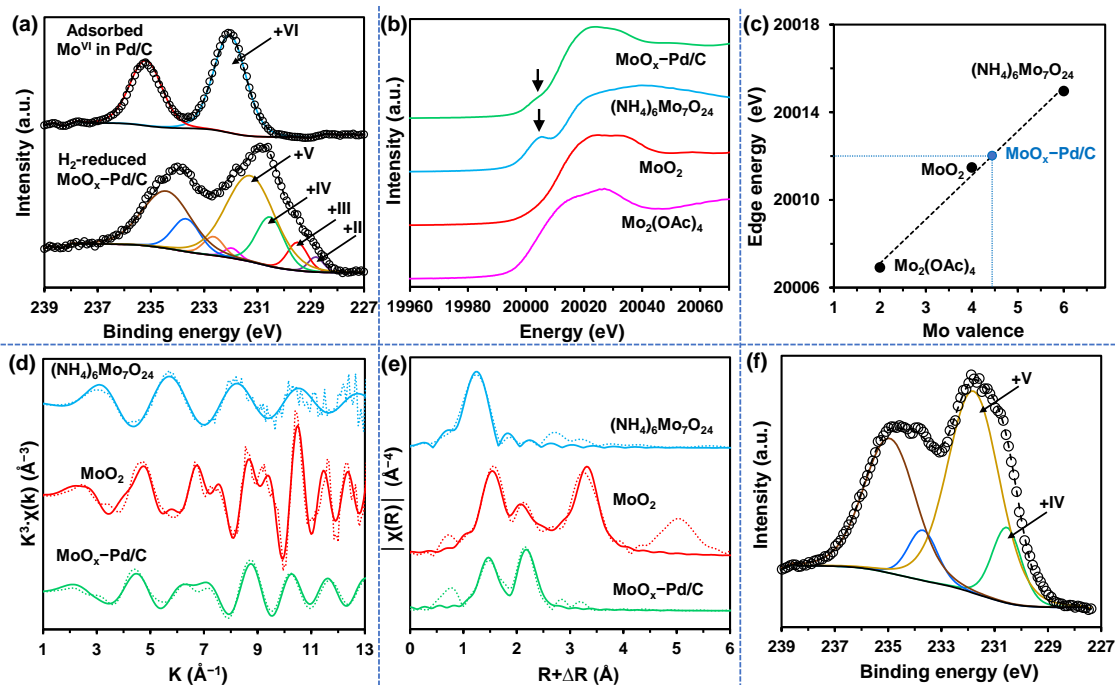
Figure 3.3 (a) Mo 3d XPS spectra of MoO_x−Pd/C samples; (b) Mo K-edge XANES spectra of the reduced MoO_x−Pd/C and references, with the two arrows indicating the characteristic pre-edge peak for oxo-Mo^{VI} species; (c) the correlation between Mo K-edge energies and valences for the references; (d) Mo K-edge EXAFS spectra of the reduced MoO_x−Pd/C and references and their shell-by-shell fits; (e) the EXAFS Fourier transforms and their fits, and (f) Mo 3d XPS spectrum of the solid residue from the dried aqueous solution of Na_2MoO_4 after the reduction using hydrazine. In the XPS and EXAFS spectra (panels a, d, e, and f), the dotted and solid lines represent spectra and their fits, respectively.

3.4.4 Mechanistic Insights

Since a negligible fraction of Mo was detected in aqueous phase throughout the reduction of ClO_3^-, it appears that the catalytic site is surface-immobilized and that the reduction of MoO_x species by H_2 occurs on the carbon support. To further rule out the possibility that the reactive site is dissolved Mo in aqueous solution, we conducted control reactions without involving Pd/C or H_2 in the gas-water-solid three-phase system. In the first experiment, the use of $Na_2Mo^{VI}O_4$ and H_2 (without Pd/C) did not reduce ClO_3^-

(**Figure S3.4b** in the **Appendix B**), indicating the critical role of Pd nanoparticles in harvesting electrons from H_2. In another experiment, the $Na_2Mo^{VI}O_4$ solution was heated with 6.5 equivalents of hydrazine at pH 3 and 70 °C. This system has been reported to reduce Mo^{VI} in the aqueous phase.[43] XPS characterization of the residue (slowly dried at 70 °C under anaerobic conditions) observed two Mo $3d_{5/2}$ peaks at 231.5 and 230.4 eV (**Figure 3.3f**), which can be readily assigned as Mo^V and Mo^{IV}, respectively. However, the aqueous solution containing both reduced Mo species and excess hydrazine did not show any ClO_3^- reduction activity, even after another 24 h of heating at 70 °C. Therefore, a homogeneous reduction of ClO_3^- by the reduced Mo species from $Na_2Mo^{VI}O_4$ is unlikely. The structural and reactivity differences of the reduced Mo species in solution and on carbon support warrant further investigation. Nonetheless, all kinetic and characterization results collectively confirm the heterogeneous nature of the MoO_x-Pd/C catalyst. Furthermore, the change of reaction kinetics from first-order at low ClO_3^- concentrations to zero-order at high ClO_3^- concentrations (**Figure 3.1** and **Figure S3.3a** in the **Appendix B**) can be readily explained by the Langmuir-Hinshelwood mechanism describing heterogeneous catalysis.[44]

For the catalytic reduction of ClO_3^-, we propose that the surface-immobilized MoO_x species and Pd nanoparticles play separate roles (i.e., oxygen atom transfer (OAT) with ClO_x^- by Mo and activation of H_2 by Pd, respectively), rather than POM enhancing the activity of Pd nanoparticles.[42] The original Pd/C has high activity in the reduction of bromate (BrO_3^-) but no activity in the reduction of nitrate (NO_3^-).[15] The immobilization of MoO_x neither increased the BrO_3^- reduction activity (**Figure S3.6a** in the **Appendix B**)

nor enabled NO_3^- reduction (**Figure S3.6b** in the **Appendix B**). Thus, the addition of MoO_x in Pd/C did not increase the "intrinsic" activity of Pd nanoparticles. Instead, the results with BrO_3^- and NO_3^- suggest the unique selectivity of reduced Mo species towards ClO_3^-.

Based on the spectroscopic findings, we propose a representative catalytic cycle in **Scheme 3.1**. The Mo^{VI} POM precursor (multi-acid form **1**, in equilibrium with the oxo-Mo^{VI} structure **1'**) is immobilized onto the carbon support and undergoes the reduction of $Mo^{VI}=O$ to Mo^V-OH (**2**). The electron comes from Pd-activated H_2. A further one-electron reduction generates $Mo^{IV}-OH_2$ (**3**). A similar reduction of a 10-nm layer of $Mo^{VI}O_3$ by H_2 at room temperature to yield Mo^V and Mo^{IV} species and H_2O on a Pd membrane has been reported.[45] The dissociation of H_2O (**3a**) allows the coordination between the Mo^{IV} center and a ClO_3^- (**4**), followed by a two-electron OAT reaction, resulting in the formation of $Mo^{VI}=O$ and the dissociation of ClO_2^-. An H^+ is necessary to facilitate OAT from Cl to Mo. The daughter products ClO_2^- and ClO^- have much higher reactivity than ClO_3^-.[21] Although Pd nanoparticles can also rapidly reduce the daughter products, the more favorable site should still be the reduced Mo because a major fraction of Pd nanoparticles has been "blocked" by MoO_x (**Table 3.3**). Therefore, a complete reduction of ClO_3^- into Cl^- involves up to three OAT redox cycles of Mo. We highlight that the reaction with ClO_x^- should involve the transfer of an oxygen atom to the Mo cluster. Thus, this process is different from the direct electron transfer with the solid-state $[PMo_{12}O_{40}]^{x-}$ structure, which only alters the bond distance within the intact Keggin cluster.[39] Since the average Mo valence in the H_2-reduced bulk MoO_x-Pd/C is 4.4, we propose that the primary catalytic mechanism is the Mo^{VI}/Mo^{IV} redox cycling. This Mo redox pair for OAT has been

confirmed by bioinorganic chemistry studies,[46] including the reduction of nitrate with biomimetic Mo complexes.[47] Other redox cycles such as Mo^{IV}/Mo^{II} and Mo^V/Mo^{III} may have also contributed to the reactions. The Mo^{IV}/Mo^{II} cycle has been employed for OAT from CO_2 and N_2O.[48] The Mo^V/Mo^{III} cycle has been observed for OAT from sulfoxide to phosphine.[49] However, a direct reaction between oxyanions and Mo^{II} or Mo^{III} has not been confirmed and warrants further studies. At the water-catalyst heterogeneous interface, the highly oxophilic reduced Mo species can be readily generated from Mo^{VI} POMs by Pd-catalyzed hydrogenation under ambient temperature and pressure. The Mo sites exhibit excellent binding affinity and unprecedentedly high reactivity with ClO_3^-. Common anions such as Cl^-, Br^-, and SO_4^{2-} in three orders-of-magnitude higher concentrations do not have significant inhibition on the catalytic activity. The significantly decreased surface area of Pd after Mo immobilization (**Table 3.3**) suggests the probable coverage of Pd nanoparticles by MoO_x species. Such coverage is assumed to protect Pd from halide poisoning but does not block the diffusion of H_2.[45]

The findings further contribute to the understanding of the redox transformation of Mo^{VI} POMs added to PGM hydrogenation catalysts. In a recent study on catalytic cyclohexane oxidation with an O_2–H_2 mixture,[50] the $PMo^{VI}_{12}O_{40}^{3-}$ added into a Pt/C suspension in acetonitrile became partially adsorbed. Under the O_2–H_2 atmosphere at 35 °C, up to four of the twelve Mo^{VI} atoms were reduced to Mo^V, forming $PMo^{VI}_8Mo^V_4O_{40}^{7-}$. The Pt-activated O_2 and two equivalents of H^+ were transferred to the Mo^V sites and yielded Mo^V-bound H_2O_2, which further oxidized cyclohexane. Hence, in both bimetallic systems (i.e., PMo_{12}–Pt/C and MoO_x–Pd/C), the Pt or Pd nanoparticles play the role of activating

the dissolved and adsorbed gases (O_2 and/or H_2), and the reduced POMs act as the oxophilic site (for Mo-bound peroxide or ClO_x^-) to enable further steps. Furthermore, the near-complete immobilization and deep reduction of the $Na_2Mo^{VI}O_4$ precursor in this study suggests the influence of specific POM structures and solvents on the extent of adsorption onto support materials and of valence change upon hydrogenation.
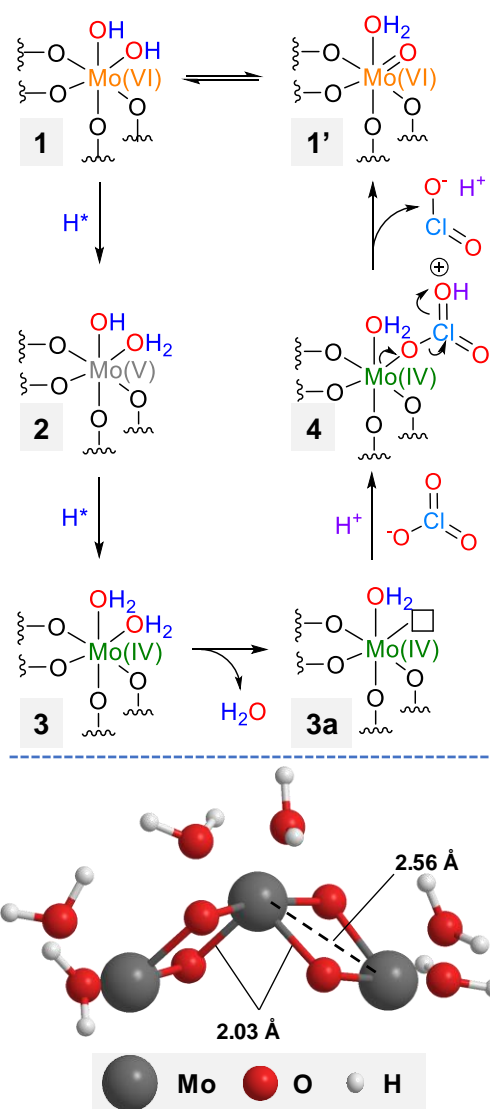
Scheme 3.1 A proposed reaction mechanism and a model local structure of Mo^{IV} species **3** based on EXAFS analysis.

3.5 Conclusion

The incorporation of an abundant Mo^{VI} precursor, $NaMoO_4$, in Pd/C yields a highly active and robust catalyst for the complete reduction of aqueous ClO_3^- into Cl^- by 1 atm H_2 under ambient temperature. The $Na_2Mo^{VI}O_4$ precursor is rapidly adsorbed from the aqueous solution onto the carbon support and reduced by Pd-activated hydrogen into a mixture of low-valent Mo oxide species. The primary mechanism for chlorate reduction is proposed to be the OAT from ClO_x^- substrates to the surface-immobilized Mo^{IV} species. The Mo sites also show a high selectivity toward ClO_3^- over other oxyanions. The high activity and stability, the preference for low pH, and the strong resistance to common salts make the MoO_x-Pd/C catalyst suitable for degrading ClO_3^- in waste brines in the Chlor-Alkali process and other scenarios such as water purification, environmental remediation, and waste brine valorization. This work shows great promise of exploring relatively abundant elements to expand the functionality of hydrogenation catalysts for environmental and energy applications.[51, 52]

3.6 Acknowledgement

3.7 References

1.   Karlsson, R. K.; Cornell, A., Selectivity between oxygen and chlorine evolution in the chlor-alkali and chlorate processes. *Chemical reviews* **2016,** *116* (5), 2982-3028.

2.   Group, I., Sodium Chlorate Market: Global Industry Trends, Share, Size, Growth, Opportunity and Forecast 2019-2024. **April 2019**.

3.   United States Environmental Protection Agency, O. o. W. M., Six-Year Review 3 Technical Support Document for Chlorate. **December 2016,** *EPA-810-R-16-013*.

4.   Organization, W. H., Chlorite and Chlorate in Drinking-water: Background Document for Development of WHO Guidelines for Drinking-water Quality **2005,** *WHO/SDE/WSH/05.08/86*.

5.   Agency, U. S. E. P., Third Unregulated Contaminant Monitoring Rule. **2012**.

6.   Brinkmann, T.; Santonja, G. G.; Schorcht, F.; Roudier, S.; Sancho, L. D., Best Available Techniques (BAT) Reference Document for the Production of Chlor-alkali. *Industrial Emissions Directive, 2010/75/EU (Integrated Pollution Prevention and Control), Luxembourg: Publications Office of the European Union* **2014**.

7.   Ibl, N.; Landolt, D., On the mechanism of anodic chlorate formation in dilute NaCl solutions. *Journal of The Electrochemical Society* **1968,** *115* (7), 713-720.

8.   Landolt, D.; Ibl, N., On the mechanism of anodic chlorate formation in concentrated NaCl solutions. *Electrochimica Acta* **1970,** *15* (7), 1165-1183.

9.   Macounová, K. M.; Simic, N.; Ahlberg, E.; Krtil, P., Electrocatalytic Aspects of the Chlorate Process: A Voltammetric and DEMS Comparison of RuO2 and DSA Anodes. *Journal of The Electrochemical Society* **2018,** *165* (14), E751-E758.

10.   Lakshmanan, S.; Murugesan, T., Adsorption performance of coconut shell activated carbon for the removal of chlorate from chlor-alkali brine stream. *Water Science and Technology* **2016,** *74* (12), 2819-2831.

11.   Van Santen, R.; Klesing, A.; Neuenfeldt, G.; Ottmann, A., Method for removing chlorate ions from solutions. Google Patents: 2001.

12.   Park, H.; Vecitis, C. D.; Hoffmann, M. R., Electrochemical Water Splitting Coupled with Organic Compound Oxidation: The Role of Active Chlorine Species. *The Journal of Physical Chemistry C* **2009,** *113* (18), 7935-7945.

13.   Cho, K.; Qu, Y.; Kwon, D.; Zhang, H.; Cid, C. m. A.; Aryanfar, A.; Hoffmann, M. R., Effects of anodic potential and chloride ion on overall reactivity in electrochemical reactors designed for solar-powered wastewater treatment. *Environmental science & technology* **2014,** *48* (4), 2377-2384.

14.   Kumar, A.; Phillips, K. R.; Thiel, G. P.; Schröder, U.; Lienhard, J. H., Direct electrosynthesis of sodium hydroxide and hydrochloric acid from brine streams. *Nature Catalysis* **2019,** *2* (2), 106.

15.   Chen, X.; Huo, X.; Liu, J.; Wang, Y.; Werth, C. J.; Strathmann, T. J., Exploring beyond palladium: Catalytic reduction of aqueous oxyanion pollutants with alternative platinum group metals and new mechanistic implications. *Chemical Engineering Journal* **2017,** *313*, 745-752.

16.   Kuznetsova, L. I.; Kuznetsova, N. I.; Koscheev, S. V.; Zaikovskii, V. I.; Lisitsyn, A. S.; Kaprielova, K. M.; Kirillova, N. V.; Twardowski, Z., Carbon-supported iridium catalyst for reduction of chlorate ions with hydrogen in concentrated solutions of sodium chloride. *Applied Catalysis A: General* **2012,** *427*, 8-15.

17.   Liu, J.; Chen, X.; Wang, Y.; Strathmann, T. J.; Werth, C. J., Mechanism and mitigation of the decomposition of an oxorhenium complex-based heterogeneous catalyst for perchlorate reduction in water. *Environmental science & technology* **2015,** *49* (21), 12932-12940.

18.   Wang, S.-S.; Yang, G.-Y., Recent advances in polyoxometalate-catalyzed reactions. *Chemical reviews* **2015,** *115* (11), 4893-4962.

19.   Kolthoff, I., Jodometrische Studien (Schluss). *Zeitschr. f. anal. Chem.* **1921,** *60*, 448-457.

20.   Kolthoff, I.; Hodara, I., Polarographic study of the molybdenum catalyzed reduction of chlorate, perchlorate and nitrate. *Journal of Electroanalytical Chemistry (1959)* **1963,** *5* (1), 2-16.

21.   Liu, J.; Choe, J. K.; Wang, Y.; Shapley, J. R.; Werth, C. J.; Strathmann, T. J., Bioinspired complex-nanoparticle hybrid catalyst system for aqueous perchlorate reduction: Rhenium speciation and its influence on catalyst activity. *ACS Catalysis* **2014,** *5* (2), 511-522.

22.   Huo, X.; Liu, J.; Strathmann, T. J., Ruthenium Catalysts for the Reduction of N-Nitrosamine Water Contaminants. *Environmental science & technology* **2018,** *52* (7), 4235-4243.

23.   Ravel, B.; Newville, M., ATHENA, ARTEMIS, HEPHAESTUS: data analysis for X-ray absorption spectroscopy using IFEFFIT. *Journal of synchrotron radiation* **2005,** *12* (4), 537-541.

24.   Zabinsky, S.; Rehr, J.; Ankudinov, A.; Albers, R.; Eller, M., Multiple-scattering calculations of X-ray-absorption spectra. *Physical Review B* **1995,** *52* (4), 2995-3009.

25.   Masters-Waage, N. K.; Morris, K.; Lloyd, J. R.; Shaw, S.; Mosselmans, J. F. W.; Boothman, C.; Bots, P.; Rizoulis, A.; Livens, F. R.; Law, G. T., Impacts of repeated redox cycling on technetium mobility in the environment. *Environmental science & technology* **2017,** *51* (24), 14301-14310.

26.   Wang, L.; Song, H.; Yuan, L.; Li, Z.; Zhang, P.; Gibson, J. K.; Zheng, L.; Wang, H.; Chai, Z.; Shi, W., Effective Removal of Anionic Re (VII) by Surface-Modified Ti2CT x MXene Nanocomposites: Implications for Tc (VII) Sequestration. *Environmental science & technology* **2019,** *53* (7), 3739-3747.

27.   Choe, J. K.; Shapley, J. R.; Strathmann, T. J.; Werth, C. J., Influence of rhenium speciation on the stability and activity of Re/Pd bimetal catalysts used for perchlorate reduction. *Environmental science & technology* **2010,** *44* (12), 4716-4721.

28.   Choe, J. K.; Boyanov, M. I.; Liu, J.; Kemner, K. M.; Werth, C. J.; Strathmann, T. J., X-ray spectroscopic characterization of immobilized rhenium species in hydrated rhenium–palladium bimetallic catalysts used for perchlorate water treatment. *The Journal of Physical Chemistry C* **2014,** *118* (22), 11666-11676.

29.   Oyerinde, O. F.; Weeks, C. L.; Anbar, A. D.; Spiro, T. G., Solution structure of molybdic acid from Raman spectroscopy and DFT analysis. *Inorganica Chimica Acta* **2008,** *361* (4), 1000-1007.

30.   McAdam, E.; Judd, S., Biological treatment of ion-exchange brine regenerant for re-use: A review. *Separation and Purification Technology* **2008,** *62* (2), 264-272.

31.   Clark, C. A.; Reddy, C. P.; Xu, H.; Heck, K. N.; Luo, G.; Senftle, T. P.; Wong, M. S., Mechanistic Insights into pH-Controlled Nitrite Reduction to Ammonia and Hydrazine over Rhodium. *ACS Catalysis* **2019,** *10* (1), 494-509.

32.   Liu, B. Y.; Wagner, P. A.; Earley, J. E., Reduction of perchlorate ion by (N-(hydroxyethyl) ethylenediaminetriacetato) aquatitanium (III). *Inorganic Chemistry* **1984,** *23* (21), 3418-3420.

33. Hurley, K. D.; Shapley, J. R., Efficient heterogeneous catalytic reduction of perchlorate in water. *Environmental science & technology* **2007,** *41* (6), 2044-2049.

34. Liu, J.; Choe, J. K.; Sasnow, Z.; Werth, C. J.; Strathmann, T. J., Application of a Re–Pd bimetallic catalyst for treatment of perchlorate in waste ion-exchange regenerant brine. *Water research* **2013,** *47* (1), 91-101.

35. Sanz, J.; Hofmann, S., Auger electron spectroscopy and X-ray photoelectron spectroscopy studies of the oxidation of polycrystalline tantalum and niobium at room temperature and low oxygen pressures. *Journal of the Less Common Metals* **1983,** *92* (2), 317-327.

36. Iyer, A. K.; Peter, S. C., Two-Dimensional Bicapped Supramolecular Hybrid Semiconductor Material Constructed from the Insulators α-Keggin Polyoxomolybdate and 4, 4′-Bipyridine. *Inorganic chemistry* **2013,** *53* (1), 653-660.

37. Haushalter, R. C.; Mundi, L. A., Reduced molybdenum phosphates: octahedral-tetrahedral framework solids with tunnels, cages, and micropores. *Chemistry of materials* **1992,** *4* (1), 31-48.

38. Choi, J.-G.; Thompson, L., XPS study of as-prepared and reduced molybdenum oxides. *Applied Surface Science* **1996,** *93* (2), 143-149.

39. Wang, H.; Hamanaka, S.; Nishimoto, Y.; Irle, S.; Yokoyama, T.; Yoshikawa, H.; Awaga, K., In operando X-ray absorption fine structure studies of polyoxometalate molecular cluster batteries: polyoxometalates as electron sponges. *Journal of the American Chemical Society* **2012,** *134* (10), 4918-4924.

40. Jalilehvand, F.; Lim, B. S.; Holm, R.; Hedman, B.; Hodgson, K. O., X-ray absorption spectroscopy of a structural analogue of the oxidized active sites in the sulfite oxidase enzyme family and related molybdenum (V) complexes. *Inorganic chemistry* **2003,** *42* (18), 5531-5536.

41. Brandt, B. G.; Skapski, A., A refinement of the crystal structure of molybdenum dioxide. *Acta Chem. Scand* **1967,** *21* (3).

42. Wang, Y.; Weinstock, I. A., Polyoxometalate-decorated nanoparticles. *Chemical Society Reviews* **2012,** *41* (22), 7479-7496.

43. Maksimovskaya, R. I., Molybdophosphate heteropoly blues: electron-transfer reactions in aqueous solutions as studied by NMR. *Polyhedron* **2013,** *65*, 54-59.

44. Wee, H.-Y.; Cunningham, J. A., Palladium-catalyzed hydrodehalogenation of 1, 2, 4, 5-tetrachlorobenzene in water–ethanol mixtures. *Journal of hazardous materials* **2008,** *155* (1-2), 1-9.

45.   Borgschulte, A.; Sambalova, O.; Delmelle, R.; Jenatsch, S.; Hany, R.; Nüesch, F., Hydrogen reduction of molybdenum oxide at room temperature. *Scientific reports* **2017,** *7*, 40761.

46.   Sugimoto, H.; Tsukube, H., Chemical analogues relevant to molybdenum and tungsten enzyme reaction centres toward structural dynamics and reaction diversity. *Chemical Society Reviews* **2008,** *37* (12), 2609-2619.

47.   Elrod, L. T.; Kim, E., Lewis Acid Assisted Nitrate Reduction with Biomimetic Molybdenum Oxotransferase Complex. *Inorganic chemistry* **2018,** *57* (5), 2594-2602.

48.   Reeds, J. P.; Yonke, B. L.; Zavalij, P. Y.; Sita, L. R., Carbon Monoxide-Induced N–N Bond Cleavage of Nitrous Oxide That Is Competitive with Oxygen Atom Transfer to Carbon Monoxide As Mediated by a Mo (II)/Mo (IV) Catalytic Cycle. *Journal of the American Chemical Society* **2011,** *133* (46), 18602-18605.

49.   Schindler, T.; Sauer, A.; Spaniol, T. P.; Okuda, J., Oxygen Atom Transfer Reactions with Molybdenum Cofactor Model Complexes That Contain a Tetradentate OSSO-Type Bis (phenolato) Ligand. *Organometallics* **2018,** *37* (23), 4336-4340.

50.   Kuznetsova, L.; Kuznetsova, N., Cyclohexane oxidation with an O 2–H 2 mixture in the presence of a two-component Pt/C–heteropoly acid catalyst and ionic liquids. *Kinetics and Catalysis* **2017,** *58* (5), 522-532.

51.   Chaplin, B. P.; Reinhard, M.; Schneider, W. F.; Schüth, C.; Shapley, J. R.; Strathmann, T. J.; Werth, C. J., Critical review of Pd-based catalytic treatment of priority contaminants in water. *Environmental science & technology* **2012,** *46* (7), 3655-3670.

52.   Yin, Y. B.; Guo, S.; Heck, K. N.; Clark, C. A.; Coonrod, C. L.; Wong, M. S., Treating water by degrading oxyanions using metallic nanostructures. *ACS Sustainable Chemistry & Engineering* **2018,** *6* (9), 11160-11175.

Chapter 4. A Bioinspired Molybdenum Catalyst for Aqueous Perchlorate Reduction

4.1 Abstract

Perchlorate (ClO_4^-) is a pervasive, harmful, and inert anion on both Earth and Mars. Current technologies for ClO_4^- reduction entail either harsh conditions or multi-component enzymatic processes. Herein, we report a heterogeneous Mo−Pd/C catalyst directly prepared from Na_2MoO_4, a bidentate nitrogen ligand (*L*), and Pd/C to reduce aqueous ClO_4^- into Cl^- with 1 atm H_2 at room temperature. A suite of instrument characterizations and probing reactions suggest that the Mo^{VI} precursor and *L* at the optimal 1:1 ratio are transformed *in situ* into oligomeric Mo^{IV} active sites at the carbon-water interface. For each Mo site, the initial turnover frequency (TOF_0) for oxygen atom transfer from ClO_x^- substrates reached 165 h^{-1}. The turnover number (TON) reached 3,840 after a single batch reduction of 100 mM ClO_4^-. This study provides a water-compatible, efficient, and robust catalyst to degrade and utilize ClO_4^- for water purification and space exploration.

4.2 Introduction

Perchlorate (ClO_4^-) is a pervasive water contaminant on Earth[1] and a major salt component in the surface soil on Mars.[2, 3] The uptake of ClO_4^- through water and food can cause thyroid gland malfunction,[4] and a recent study has identified that ClO_4^- in drinking water is more dangerous than previously thought.[5] NASA has identified Martian ClO_4^- as both a potential hazard to humans and an oxygen source to supply exploration activities.[6] However, the oxidizing power of ClO_4^- is primarily utilized via rocket fuels, munitions, or pyrotechnics.[7] Without ignition, ClO_4^- is a well-known inert anion and commonly used for ionic strength adjustment in various chemical systems.[8] Abiotic reduction of aqueous ClO_4^- usually requires harsh conditions and large excesses of reducing agents.[9, 10] Herein, we report on a bioinspired heterogeneous Mo catalyst for aqueous ClO_4^- reduction with 1 atm H_2 at room temperature.

Microbes can use ClO_4^- for respiration via a multifactor metalloenzyme system (**Figure 4.1a**).[11, 12] The reduction of ClO_4^- and ClO_3^- is achieved by oxygen atom transfer (OAT)[13] to a dithiolate-coordinated Mo cofactor (**Figure 4.1b**), which is biosynthesized from molybdate.[14] Amino acid residues mediate the binding and stabilization of ClO_x^- substrates.[15] The redox cycling between Mo^{IV} and Mo^{VI} (**Figure 4.1c**) is sustained by the electron transfer from H_2 or acetate via multiple enzymes containing Fe-S clusters and *heme* complexes, and electron shuttling compounds.[16] The complexity of biological systems challenges the design of an artificial ClO_4^- reduction system, especially in the aqueous phase under ambient conditions. For example, a Fe complex relies on hydrogen bonds in the secondary coordination sphere to reduce ClO_4^- (**Figure 4.1d**) and thus requires

an anhydrous environment.[17, 18] Moreover, a single-function metal complex or isolated reductase requires special electron donors (e.g., methyl viologen, hydrazine, ferrocene, and phosphine) to sustain the redox cycle of OAT metals.[17, 19, 20] Hence, a robust catalyst that can reduce aqueous ClO_4^- with H_2 is highly desirable.[21, 22] Although the immobilization of Re complexes (**Figure 4.1e**)[23, 24] onto Pd/C has achieved this function,[25, 26] Re is a rare metal, and the pre-synthesized Re complexes are subject to irreversible decomposition.[27]
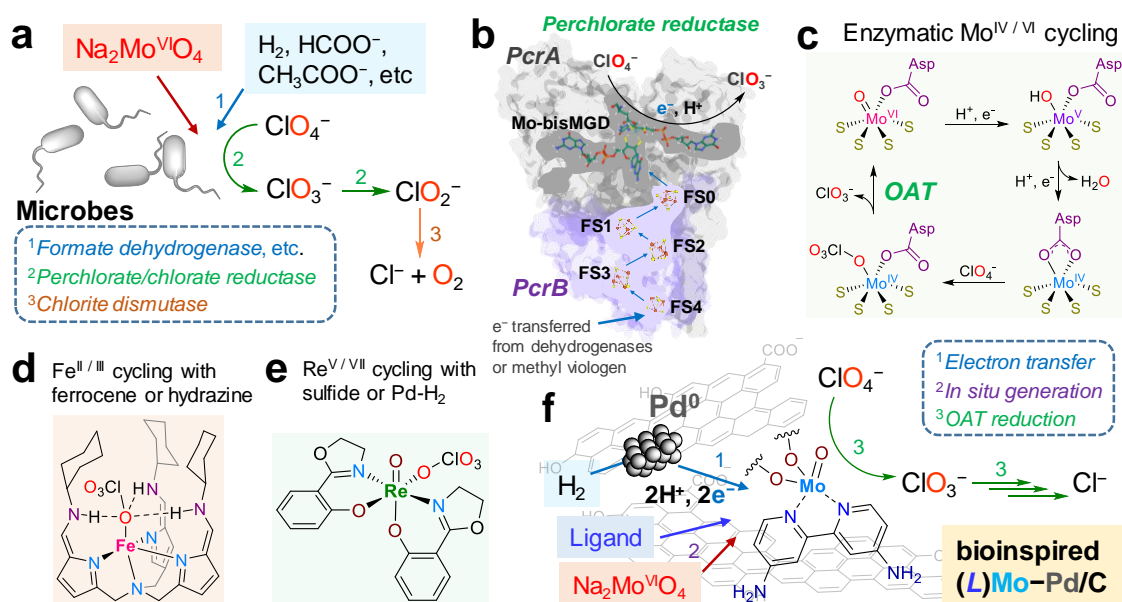
Figure 4.1 Microbial and abiotic systems for perchlorate reduction. (a) Microbial ClO_4^- reduction processes; (b) electron transfer and metal centers in perchlorate reductase (*Pcr*); (c) redox cycling of the Mo cofactor proposed in literature;[15] (d) a bioinspired Fe complex for ClO_4^- reduction;[17] (e) a Re complex for ClO_4^- reduction;[23] (f) the overall design rationale for the (*L*)MoO$_x$−Pd/C catalyst.

4.3 Materials and Methods

4.3.1 Reagents and Materials

Sodium molybdate dihydrate ($Na_2MoO_4 \cdot 2H_2O$), ammonium molybdate tetrahydrate [$(NH_4)_6Mo_7O_{24} \cdot 4H_2O$], molybdenum(IV) oxide (MoO_2), and molybdenum(II) acetate dimer [$Mo_2(OCOCH_3)_4$] were purchased from Sigma−Aldrich. The nitrogen ligands were purchased from Alfa Aesar, Ark Pharm, Combi-Blocks, Oakwood Chemical, Sigma−Aldrich, and TCI. Inorganic salts (e.g., $NaClO_4$, $NaCl$, and Na_2SO_4) in ≥99% purities were purchased from Fisher Chemical. Sulfuric acid solution (2 N standard) was purchased from Alfa Aesar. Triphenylphosphine (PPh_3, 99%) and trisodium triphenylphosphine-3,3′,3″-trisulfonate (TPPTS, ≥95%) were purchased from Sigma−Aldrich. All chemicals were used as received. Aqueous solutions were prepared with deionized (DI) water (resistivity >18.2 MΩ cm). The 5 wt% Pd/C (Sigma−Aldrich, catalog #330116) was wet sieved to obtain the <37 µm fraction, dried under air at 110°C for 2 h and heated under H_2 flow at 250°C for 1 h.[25] The treated Pd/C had the surface area of 860 $m^2 g_{cat}^{-1}$, the pore volume of 0.67 $cm^3 g^{-1}$, the average pore size of 3.1 nm, and the Pd surface area of 6.9 $m^2 g_{cat}^{-1}$ (Pd dispersion of 31% and average Pd particle size of 3.7 nm).[28] Control experiments suggest that the (**L**)MoO_x−Pd/C catalysts prepared from the Pd/C with and without the sieving and reducing treatments showed very similar performance in ClO_4^- reduction. The activated carbon without Pd[29] was purchased from Alfa Aesar (Norit GSX; steam activated and acid-washed; surface area 1300 $m^2 g^{-1}$) and used as received.

4.3.2 (*L*)MoO$_x$−Pd/C Catalyst Preparation

This procedure describes the *in situ* preparation of the typical 0.2 g L^{-1} loading of [(NH$_2$)$_2$*bpy*]MoO$_x$−Pd/C catalyst with 5 wt% Mo and the same molar amount of the (NH$_2$)$_2$*bpy* ligand. A 50-mL round bottom flask was sequentially loaded with 49 mL of DI water (pH adjusted to 3.0 with H$_2$SO$_4$), 10 mg of Pd/C powder, 0.5 mL of Na$_2$MoO$_4$ stock solution (containing 0.5 mg or 5.2 µmol of Mo), 0.5 mL of aqueous (NH$_2$)$_2$*bpy* stock solution (containing 5.2 µmol of ligand), and a magnetic stir bar. The flask was sealed with a rubber stopper and sonicated for 1 min, and then placed in the fume hood. H$_2$ gas (99.999%, Airgas) was supplied by two 16-gauge (diameter) and 6-inch (length) stainless steel needles penetrating the stopper as the gas inlet and outlet, respectively. The aqueous suspension was stirred at 1600 rpm under 1 atm H$_2$ headspace for 1 h to afford the suspension of [(NH$_2$)$_2$*bpy*]MoO$_x$−Pd/C catalyst. All parameters such as Mo concentration, catalyst loading, solution pH, and ligand structure can be readily adjusted.

4.3.3 Perchlorate Reduction

The reduction of the typical 1 mM ClO$_4^-$ was initiated by adding 0.25 mL of NaClO$_4$ stock solution (200 mM) into the catalyst suspension. For the initial ClO$_4^-$ concentration of 100 mM, 612.5 mg of solid NaClO$_4$ was added into the suspension. All reactions were carried out at room temperature (20°C) and under 1 atm H$_2$ atmosphere. The flow rate of H$_2$ was about 1−2 bubbles per second coming out from the 16-gauge needle tip to maintain a slightly positive pressure of the H$_2$ headspace inside the flask. The solution pH remained at pH 2.9−3.0 throughout the reaction because the reduction of ClO$_4^-$

does not consume H^+. Aliquots were collected through the H_2 outlet needle with a 3-mL plastic syringe and immediately filtered through a 0.22-μm cellulose membrane to quench reactions.

4.3.4 Aqueous Sample Analysis

The quantitation of ClO_4^- and Cl^- was conducted by ion chromatography (Dionex ICS-5000 system with a conductivity detector and a 25 μL sample injection loop). Samples from the reduction of 100 mM of ClO_4^- were diluted 100 times before analysis. A Dionex IonPac AS16 analytical column was used at 30 °C, with 65 mM KOH at the flow rate of 1 mL min^{-1} as the eluent. The concentration of total Mo in aqueous samples was analyzed by inductively coupled plasma−mass spectrometry (ICP−MS, Agilent 7700). The concentration of free N ligand in aqueous samples was quantified by high-performance liquid chromatography (HPLC) with a photodiode array (PDA) detector (Shimadzu Nexera XR).

4.3.5 Catalyst Collection and Characterization

After disconnection from the H_2 supply, the flask was kept sealed by the rubber stopper and immediately transferred into an anaerobic glove bag (Coy Laboratories, filled with 98% N_2 and 2% H_2) to avoid artifacts from air exposure. The catalyst suspension was filtered through a ceramic funnel covered with filter paper (Whatman qualitative) under vacuum. The filter paper was transferred into a 20-mL scintillation vial and dried in a sand bath at 110 °C to remove moisture. The dried catalyst powder was collected and stored in the glove bag until XPS and XAS analysis (see below). For microscopy analysis, the

catalyst powder was re-dispersed in distilled water and sonicated for 30 min. A drop of the suspension was loaded onto the copper microgrids and dried under vacuum. The distribution of Mo, Pd, N, O, and C elements was characterized by high-angle annular dark-field (HAADF) imaging with scanning transmission electron microscopy (STEM, FEI Titan Themis 300, operated at 300 kV) at the UC Riverside Central Facility for Advanced Microscopy and Microanalysis (CFAMM).

4.3.6 X-ray Photoelectron Spectroscopy (XPS)

Inside the glove bag, the dried powder was loaded onto a copper conductive tape on the XPS sample holder and stored in an anaerobic chamber secured with Klein Flange before transferring to the XPS facility at the UC Irvine Materials Research Institute (IMRI). All XPS experiments were performed on the Kratos AXIS Supra surface analysis instrument. The sp^2 C 1s peak (284.5 eV) of the carbon support was used for binding energy (BE) calibration. The BE of Mo^{II}, Mo^{IV}, and Mo^{VI} standards were acquired in our previous study.[28] Spectra in the resolution of 0.1 eV were fit using CasaXPS (version 2.3.19). Spectra of Mo 3d (30 scans) were fit with the constrained peak separations (3.15 eV) and the constrained ratio of peak areas (3:2) of 3d spin-orbital coupling doublets.

4.3.7 X-ray Absorption Spectroscopy (XAS)

The preparation and transfer of XAS samples are the same as mentioned above. Mo K-edge EXAFS data were collected at beamlines 4−1 and 2−2 at Stanford Synchrotron Radiation Light source. The sample chamber was purged with N_2 during data collection to minimize the artifact caused by atmospheric O_2. Both transmission and fluorescence

signals were acquired. A Mo metal foil reference was concomitantly measured with the samples for energy calibration (E_0 = 20000 eV). Zirconium (Z–2) metal foil was used as the filter for collecting fluorescence signals. *Athena* was used for energy calibration, raw spectra average, post-edge normalization, and background removal.[28] *Artemis* was used to obtain the structural parameters by fitting k^3-weighted EXAFS spectra to the standard EXAFS equation using several single-scattering paths. The fittings were over a k range of 3–13 Å^{-1} and an R range of 1.0–3.0 Å for the catalyst sample, a k range of 3–12 Å^{-1} and an R range of 1.2–3.9 Å for MoO_2 standard, and a k range of 3–12 Å^{-1} and an R range of 0.9–2.0 Å for $(NH_4)_6Mo_7O_{24}$ standard as reported previsouly.[28] Phase and amplitude functions for the scattering paths were generated using FEFF6[30] based on the structures of MoO_2, MoO_3, and monomolybdate. In all fittings, the number of independent variables included was fewer than the number of independent data points. The Hanning window was used for the Fourier transform of the EXAFS data.

4.3.8 Synthesis and Testing of Model Mo-Ligand Complexes

The synthesis of the Mo : $(NH_2)_2bpy$ = 1 : 1 complex and the reported complex $Mo_8O_{22}(OH)_4((t\text{-Bu})_2bpy)_4$ (Mo : $(NH_2)_2bpy$ = 1 : 0.5) followed the literature method.[31] Briefly, MoO_3 (68 mg, 0.48 mmol), $(NH_2)_2bpy$ or $(t\text{-Bu})_2bpy$ (0.48 mmol), and deionized water (5 mL) were loaded in a Teflon-lined stainless steel autoclave. The autoclave was heated in an oven at 160°C for 3 days. The resulting products were light pink crystalline solid and amorphous white powder from the use of $(t\text{-Bu})_2bpy$ and $(NH_2)_2bpy$, respectively. The products were collected by filtration and washed with deionized water and diethyl ether. ^{1}H NMR characterization and other experiments found that the complexes fully

decomposed to free ligands upon dissolution (See **Figures S4.12−S4.16** in the **Appendix C** and figure captions for details).

4.3.9 Electrochemical Study

Samples for electrochemical studies were prepared by immobilizing Na_2MoO_4, free $(NH_2)_2bpy$, and the 1:1 mixture of $(NH_2)_2bpy$ + Na_2MoO_4 onto activated carbon powder with the same adsorption procedures used for the *in situ* preparation of $[(NH_2)_2bpy]MoO_x$−Pd/C. The activated carbon did not contain Pd because Pd^0 nanoparticles can catalyze the hydrogen evolution reaction[32] and interfere with the reduction of $[(NH_2)_2bpy]MoO_x$. Catalyst ink was prepared by dispersing 5 mg of each carbon powder sample in the mixture of 5 ml Nafion, 500 ml ethanol, and 250 ml deionized water. Aliquots of 2 ml of the catalyst ink were applied twice onto the glassy carbon electrode. After the ink was dried in air, the working electrode was ready for use. The electrochemical cell was purged with Ar gas before measurement to prevent the artifacts from atmospheric oxygen. Cyclic voltammetry was performed at pH 3.0 using an Ag/AgCl reference electrode and platinum wire counter electrode.

4.4 Results and Discussion

4.4.1 Bioinspired Design and Catalyst Performance

We used Pd/C as the platform for our bioinspired catalyst (**Figure 4.1f**). The porous carbon mimics the enzyme protein pocket to accommodate the OAT metal site. The Pd^0 nanoparticles directly harvest electrons from H_2 to simplify the biological electron transfer chain. Then the critical task was to construct a highly active Mo site from molybdate

($Mo^{VI}O_4{}^{2-}$), the same Mo source for the biosynthesized Mo cofactor.[14] Polyoxometalates of aqueous molybdate[33] were readily adsorbed onto Pd/C within 30 min (**Figure S4.1**). The resulting heterogeneous MoO_x−Pd/C showed rapid reduction of $ClO_3{}^{-}$ [28] but negligible activity with $ClO_4{}^{-}$. Hence, we sought to enhance the OAT activity of Mo sites by incorporating an organic ligand like the biological Mo cofactors. Because biomimetic Mo complexes with thiolate ligands are typically water- and oxygen-sensitive, we attempted to prepare an active Mo site *in situ*. We added Na_2MoO_4 and a variety of neutral nitrogen ligands (*L*) to the water suspension of Pd/C under 1 atm H_2. This simple strategy achieved highly active $ClO_4{}^{-}$ reduction by a series of (*L*)MoO_x−Pd/C catalysts (**Table 4.1**, **Figures S4.2** and **S4.3** in the **Appendix C**).

Bipyridine (*bpy*, **Table 4.1 entry 1**) was superior to phenanthroline and other aromatic ligands with an imidazoline or oxazoline half moiety (**Table 4.1 entries 17−19**) as well as pyridines, diamines, and terpyridine (**Table 4.1 entries 10−16** and **23**). Ligands with steric hindrance (**Table 4.1 entries 8**, **9**, and **20**) or a strain on the *bpy* backbone (**Table 4.1 entry 22** versus **21**) resulted in low activities. Electron-donating groups on the *para* positions[34] further enhanced the activity (**Table 4.1 entries 2−7**). At ambient temperature and pressure, the [$(NH_2)_2bpy$]MoO_x−Pd/C catalyst (**Table 4.1 entry 6**) outperformed other abiotic $ClO_4{}^{-}$ reduction catalysts reported to date (**Table S4.1 in the Appendix C**). The chlorine balance was closed by $ClO_4{}^{-}$ and Cl^{-}, indicating a negligible buildup of $ClO_x{}^{-}$ intermediates (**Figure 4.2a**). The optimal molar ratio between $(NH_2)_2bpy$ and Mo was 1:1 (**Figure 4.2b**), and the optimal Mo content in the catalyst was 5 wt% (see below). While enzymes use amino acid residues to assist the reduction of metal-bound

oxyanions,[15, 35] the $[(NH_2)_2bpy]MoO_x$–Pd/C needs external protons to enable ClO_4^- reduction.[28, 34] The optimal activity was observed at pH 3.0 (1 mM H^+ from H_2SO_4). The pK_a values for $-NH_3^+$ and pyridyl NH^+ are around 2 and 7, respectively (**Figure S4.4** in the **Appendix C**). The coordination between $(NH_2)_2bpy$ and Mo is competed by the protonation of pyridyl N at pH 3.0. Thus, the active $[(NH_2)_2bpy]Mo$ sites may be in the solid phase rather than in the aqueous solution (see below). The reduced performance at pH 2.0 and 1.0 (**Figure 4.2c**) can be attributed to the protonation of $-NH_2$.

Catalyst reuse for ten times did not cause a noticeable loss of activity (**Figure S4.5** in the **Appendix C**). The leached Mo and $(NH_2)_2bpy$ into water throughout the catalysis were <1.5% and <0.2% of the total amount, respectively (**Figure 4.2d**). The apparent first-order kinetics with 0.01−1 mM ClO_4^- and zeroth-order kinetics at 1−100 mM ClO_4^- (**Figures S4.6** and **S4.7** in the **Appendix C**) support the Langmuir–Hinshelwood model, which is characteristic for heterogeneous catalysis (See **Texts S4.1** and **S4.2** in the **Appendix C** for kinetic modeling and mass transfer analysis). Notably, a 0.2 g L^{-1} loading of the catalyst reduced 99.99% of 100 mM ClO_4^- (~10 g L^{-1}) within 48 h (**Figure S4.6c** in the **Appendix C**). Due to the high oxidative stress caused by ClO_x^- intermediates,[15, 27] complete reduction of 100 mM ClO_4^- in water has not been reported by either microbial or abiotic systems. Assuming the Mo sites catalyze the OAT from ClO_4^- and all ClO_x^- intermediates, the turnover number (TON) for that single batch and the initial turnover frequency (TOF_0) reached 3,840 and 165 h^{-1}, respectively, for each Mo atom.

In the presence of 0.1 M Cl^-, 2.0 M Cl^-, and 1.0 M SO_4^{2-}, the catalyst retained 57%, 5%, and 36% of the control activity, respectively (**Figure S4.8** and **Table S4.2** in the

Appendix C), showing the promise for reducing ClO_4^- in brine solutions produced from ion exchange or reverse osmosis for water purification.[36] Furthermore, exposing the catalyst suspension to air did not cause irreversible deactivation. The same ClO_4^- reduction activity was recovered after resuming the H_2 supply (**Figure S4.9a** in the **Appendix C**), suggesting that the *in situ* prepared catalyst can be handled in air. In comparison, Re−Pd/C catalysts using pre-synthesized Re^V precursors (**Figure 4.1e**) are highly sensitive to air and irreversibly deactivated (**Figure S4.9b** in the **Appendix C**).[25, 37]

Entry	Ligand	TOF$_0$ (h^{-1})[b]	Entry	Ligand	TOF$_0$ (h^{-1})[b]
			17		3.1
1	R = H	14.3			
2	R = Me	12.4			
3	R = OH	11.7	18		4.6
4	R = OMe	20.8			
5	R = NMe$_2$	53.9			
6	R = NH$_2$	106	19		2.8
7	R = Cl	0.63			
8		0.78			
9		0.13	20		0.31
10	R = H	0.16	21		11.2
11	R = OH	0.16			
12	R = NH$_2$	0.090			
13	R = NMe$_2$	0.79			
14		0.43	22		0.40
15		0.18			
16		0.22	23		0.85

Table 4.1 Perchlorate reduction activity of Mo−Pd/C catalysts enabled by various ligands.[a]
[a]Reaction conditions: 1 mM ClO$_4^-$ in water, 0.5 g L^{-1} catalyst (5 wt% Mo and 5 wt% Pd on carbon), molar ratio of Ligand:Mo = 1:1 (bidentate and tridentate) or 2:1 (monodentate), pH 3.0, 1 atm H$_2$, 20°C. Entries 5 and 6 used 0.2 g L^{-1} catalyst.
[b]Calculated using the degradation of the first 5% of 1 mM ClO$_4^-$ and four OAT cycles to reduce each ClO$_4^-$ into Cl$^-$.
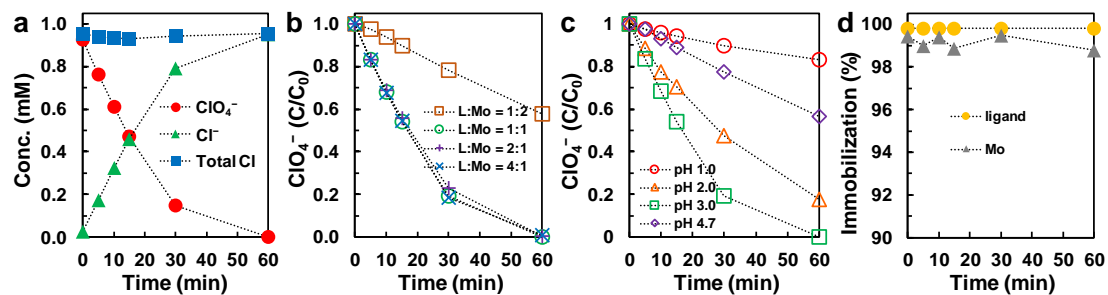
Figure 4.2 Kinetic data. (a) Chlorine balance for ClO_4^- reduction; (b) the effect of $(NH_2)_2bpy$:Mo molar ratio; (c) the effect of solution pH; (d) the ratio of immobilized $(NH_2)_2bpy$ and Mo during ClO_4^- reduction. Default reaction conditions: 0.2 g L^{-1} catalyst (5 wt% Mo in 5 wt% Pd/C, molar ratio of $(NH_2)_2bpy$:Mo=1:1), 1 mM ClO_4^-, pH 3.0, 1 atm H_2, 20 °C.
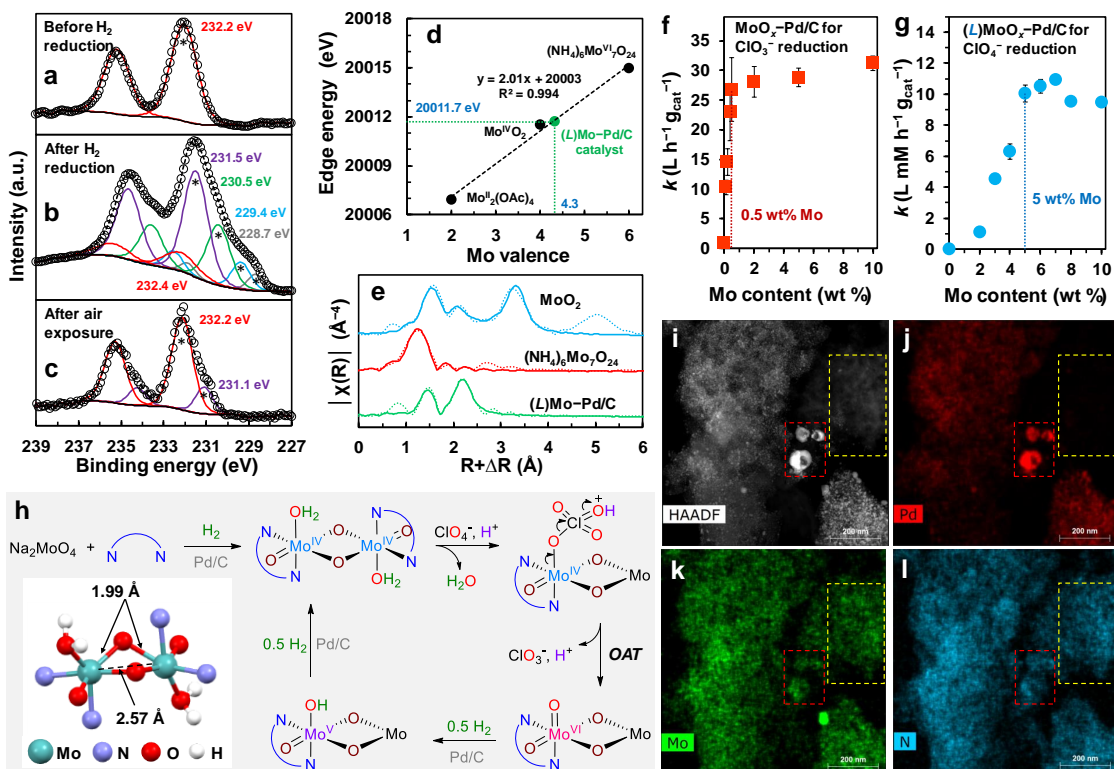
Figure 4.3 Characterization data and proposed reaction mechanisms. (a−c) Mo 3d XPS spectra (empty dots) and fits (solid lines) of the $[(NH_2)_2bpy]MoO_x$−Pd/C catalyst. The 3d5/2 peaks are indicated by asterisks; (d) the correlation between Mo K-edge XANES energies and valences for the catalyst and Mo references; (e) the EXAFS Fourier transforms (dotted lines) and their fits (solid lines); (f−g) the effect of Mo content in the catalysts with and without $(NH_2)_2bpy$; (h) a proposed structure of the reduced $[(NH_2)_2bpy]MoO_x$ species and representative redox transformations for ClO_4^- reduction; (i−l) HAADF-STEM imaging of the catalyst and EDX mapping of Pd, Mo, and N. The two dotted areas show the heterogeneity of $[(NH_2)_2bpy]MoO_x$ species immobilized on both the carbon support and Pd particles.

4.4.2 Catalyst Characterization and Homogeneous Reaction

X-ray photoelectron spectroscopy (XPS) characterization identified the reduction of Mo^{VI} precursor into multiple oxidation states (+V, +IV, +III and +II) (**Figure 4.3a** versus 4.**3b**). Air exposure reoxidized the low-valent species to Mo^{V} and Mo^{VI} (**Figure 4.3c**). For the reduced bulk catalyst sample, Mo K-edge X-ray absorption near-edge structure (XANES) spectroscopic analysis found the average valence of Mo to be 4.3 from the edge energy of 20011.7 eV (**Figure 4.3d** and **Figure S4.10** in the **Appendix C**)[38]. Fitting of the extended X-ray absorption fine structure (EXAFS) spectra found three major atomic shells for Mo=O (1.67 Å), Mo−O (1.99 Å) and Mo−Mo (2.57 Å) (**Figure 4.3e**, **Table S4.3**, and **Figure S4.11** in the **Appendix C**). This short Mo−Mo distance also indicates the reduction of Mo^{IV} into Mo^{IV} by hydrogenation. In a previous study, the reduction of $[PMo^{VI}_{12}O_{40}]^{3-}$ in a battery electrolyte with 24 electrons into $[PMo^{IV}_{12}O_{40}]^{27-}$ shortended the Mo−Mo distance from 3.4 Å to 2.6 Å.[38] The Mo−Mo coordination number (CN) of 0.9 ± 0.5 suggests the heterogeneity of the surface Mo species as a mixture of monomers (CN = 0), dimers (CN = 1), and polymers (CN > 1).

Notably, the use of $(NH_2)_2bpy$ ligand not only enhanced the activity but also altered the structure of MoO_x species. Without the ligand, the MoO_x−Pd/C catalyst could not reduce ClO_4^-, and the highest ClO_3^- reduction activity was achieved with merely 0.5 wt% of Mo (**Figure 4.3f**). Thus, the additional 4.5 wt% of Mo in the 5 wt% MoO_x−Pd/C served as the structural building block of polymeric MoO_x clusters rather than catalytic sites. The CN for Mo−Mo in MoO_x−Pd/C (1.7 ± 0.6, **Table S4.3** in the **Appendix C**) also indicated the dominance of polymeric MoO_x clusters.[28] In stark comparison, the ClO_4^- reduction

activity of [(NH$_2$)$_2$*bpy*]MoO$_x$−Pd/C kept increasing with the Mo content until 5 wt% (**Figure 4.3g** in the **Appendix C**). Thus, most Mo atoms in the 5 wt% [(NH$_2$)$_2$*bpy*]MoO$_x$−Pd/C served as catalytic sites. Because the average CN for Mo−Mo and Mo=O were 0.9 and 1.1, respectively (**Table S4.3** in the **Appendix C**) and the optimal ratio between (NH$_2$)$_2$*bpy* and Mo was 1:1 (**Figure 4.2b**), we propose a representative dimer structure for the active Mo site (**Figure 4.3h**). This configuration is based on the crystal structure of Mo$^{VI}_2$O$_6$[(*t*-Bu)$_2$*bpy*]$_2$, a minor product from the hydrothermal reaction using MoO$_3$ and 4,4'-(*t*-Bu)$_2$*bpy*.[31] This dimer structure also allows for multi-valent transformation of Mo between +VI and +II (**Figure 4.3b**) via the reduction of Mo=O into Mo−OH and Mo−OH$_2$.

We attempted to synthesize a molecular framework for the [(NH$_2$)$_2$*bpy*]MoO$_x$ site; however, both [(*t*-Bu)$_2$*bpy*]Mo^{VI} and [(NH$_2$)$_2$*bpy*]Mo^{VI} complexes from hydrothermal synthesis[31] decomposed into free ligands upon dissolution (**Figures S4.12** and **S4.13** in the **Appendix C**). Although PPh$_3$ reduced Mo^{VI} to Mo^{IV} and yielded OPPh$_3$ by OAT,[13] the homogeneous ClO$_4^-$ reduction did not occur (**Figure S4.14** in the **Appendix C**). The heating of Na$_2$MoO$_4$, (NH$_2$)$_2$*bpy*, and P(PhSO$_3$Na)$_3$ (TPPTS) in water yielded a green solid, confirming the reduction of Mo^{VI} and the coordination with (NH$_2$)$_2$*bpy* (**Figure S4.15** in the **Appendix C**). Still, this product dissolved poorly in water and did not reduce aqueous ClO$_4^-$ (**Figure S4.16a** in the **Appendix C**). In comparison, the use of activated carbon (without Pd^0 nanoparticles)[29] together with Na$_2$MoO$_4$, (NH$_2$)$_2$*bpy*, and TPPTS resulted in a slow but significant ClO$_4^-$ reduction at pH 3.0 (**Figure S4.16b** and **S4.16c** in the **Appendix C**). Although an exact molecular structure for the active Mo sites remains

elusive, the above findings have collectively confirmed the heterogeneous nature of the catalyst. The critical role of the carbon support may be to provide a large surface area (>900 m^2 g^{-1})[28, 29] to disperse the insoluble $[(NH_2)_2bpy]MoO_x$ structure for up to 5 wt% Mo (**Figure 4.3g**), or to stabilize the specific coordination structure that is reactive with ClO_4^-. In addition, since $(NH_2)_2bpy$ is strongly prone to pyridyl protonation, the $[(NH_2)_2bpy]MoO_x$ coordination structure is less likely to remain intact upon dissolution in the aqueous phase.

Scanning transmission electron microscopy (STEM) and energy dispersive X-ray spectrometry (EDS) element mapping images indicate the ubiquitous distribution of Mo and N on either carbon support or Pd^0 nanoparticles (**Figures 4.3i−4.3l** and **S4.17** in the **Appendix C**). The poor EXAFS fittings considering Mo−Pd bonding (**Table S4.4** in the **Appendix C**) suggest isolated aggregation and distinct roles of the $[(NH_2)_2bpy]MoO_x$ site (OAT for ClO_x^- reduction) and Pd nanoparticles (electron transfer from H_2). Both the phosphine reduction via OAT and Pd-mediated hydrogenation could transform polymeric Mo^{VI} precursors[28] into specific $[(NH_2)_2bpy]MoO_x$ structures for ClO_4^- reduction. For comparison, our cyclic voltammetry studies on the mixture of Na_2MoO_4, $(NH_2)_2bpy$, and activated carbon (without Pd^0 nanoparticles) between 0.37 and −1.1 V (versus the reversible hydrogen electrode) did not observe ClO_4^- reduction (**Figure S4.18** in the **Appendix C**) but showed the reduction peaks of MoO_x and $(NH_2)_2bpy$ ligand (**Figure S4.19** in the **Appendix C**). The potential allows the reduction of Mo^{VI} into Mo^V, Mo^{IV}, and Mo^{III},[39, 40] but the potential $[(NH_2)_2bpy]MoO_x$ formed upon electrochemical reduction[38] were probably in different structures and thus not reactive with ClO_4^-.

4.5 Conclusion

In conclusion, we have developed a highly active and robust heterogeneous (L)MoO$_x$−Pd/C catalyst for aqueous ClO$_4^-$ reduction. The catalysis proceeded at 20°C with 1 atm H$_2$ and fully reduced a wide concentration range (10 µM to 0.1 M) of ClO$_4^-$ into Cl$^-$. On the carbon support, the oligomeric Mo site was generated *in situ* via the reduction of Na$_2$MoO$_4$ and coordination with a bidentate nitrogen ligand. This study highlights a new strategy for designing bioinspired systems with common chemicals and simple preparation. We anticipate that this water-compatible catalyst will advance environmental and energy technologies to degrade or utilize ClO$_4^-$ on Earth and Mars.

4.6 Acknowledgement

4.7 Reference

1.   Brandhuber, P.; Clark, S.; Morley, K., A review of perchlorate occurrence in public drinking water systems. *Journal-American Water Works Association* **2009,** *101* (11), 63-73.

2.   Hecht, M.; Kounaves, S.; Quinn, R.; West, S.; Young, S.; Ming, D.; Catling, D.; Clark, B.; Boynton, W. V.; Hoffman, J., Detection of perchlorate and the soluble chemistry of martian soil at the Phoenix lander site. *Science* **2009,** *325* (5936), 64-67.

3.   Jackson, W. A.; Davila, A. F.; Sears, D. W.; Coates, J. D.; McKay, C. P.; Brundrett, M.; Estrada, N.; Böhlke, J. K., Widespread occurrence of (per) chlorate in the Solar System. *Earth and Planetary Science Letters* **2015,** *430*, 470-476.

4.   Greer, M. A.; Goodman, G.; Pleus, R. C.; Greer, S. E., Health effects assessment for environmental perchlorate contamination: the dose response for inhibition of thyroidal radioiodine uptake in humans. *Environmental health perspectives* **2002,** *110* (9), 927-937.

5.   Llorente-Esteban, A.; Manville, R. W.; Reyna-Neyra, A.; Abbott, G. W.; Amzel, L. M.; Carrasco, N., Allosteric regulation of mammalian Na+/I− symporter activity by perchlorate. *Nature Structural & Molecular Biology* **2020**, 1-7.

6.   Davila, A. F.; Willson, D.; Coates, J. D.; McKay, C. P., Perchlorate on Mars: a chemical hazard and a resource for humans. *International Journal of Astrobiology* **2013,** *12* (4), 321-325.

7.   Rehwoldt, M. C.; Yang, Y.; Wang, H.; Holdren, S.; Zachariah, M. R., Ignition of nanoscale titanium/potassium perchlorate pyrotechnic powder: reaction mechanism study. *The Journal of Physical Chemistry C* **2018,** *122* (20), 10792-10800.

8.   Gayen, P.; Sankarasubramanian, S.; Ramani, V. K., Fuel and oxygen harvesting from Martian regolithic brine. *Proceedings of the National Academy of Sciences* **2020,** *117* (50), 31685-31689.

9.   Gu, B.; Dong, W.; Brown, G. M.; Cole, D. R., Complete degradation of perchlorate in ferric chloride and hydrochloric acid under controlled temperature and pressure. *Environmental science & technology* **2003,** *37* (10), 2291-2295.

10.   Cao, J.; Elliott, D.; Zhang, W.-x., Perchlorate reduction by nanoscale iron particles. *Journal of Nanoparticle Research* **2005,** *7* (4), 499-506.

11.   Coates, J. D.; Achenbach, L. A., Microbial perchlorate reduction: rocket-fuelled metabolism. *Nature Reviews Microbiology* **2004,** *2* (7), 569-580.

12.   Youngblut, M. D.; Wang, O.; Barnum, T. P.; Coates, J. D., (Per) chlorate in biology on earth and beyond. *Annual review of microbiology* **2016,** *70*.

13.   Holm, R., Metal-centered oxygen atom transfer reactions. *Chemical Reviews* **1987,** *87* (6), 1401-1449.

14.   Schwarz, G.; Mendel, R. R.; Ribbe, M. W., Molybdenum cofactors, enzymes and pathways. *Nature* **2009,** *460* (7257), 839.

15.   Youngblut, M. D.; Tsai, C.-L.; Clark, I. C.; Carlson, H. K.; Maglaqui, A. P.; Gau-Pan, P. S.; Redford, S. A.; Wong, A.; Tainer, J. A.; Coates, J. D., Perchlorate reductase is distinguished by active site aromatic gate residues. *Journal of Biological Chemistry* **2016,** *291* (17), 9190-9202.

16.   Bertero, M. G.; Rothery, R. A.; Palak, M.; Hou, C.; Lim, D.; Blasco, F.; Weiner, J. H.; Strynadka, N. C., Insights into the respiratory electron transfer pathway from the structure of nitrate reductase A. *Nature Structural & Molecular Biology* **2003,** *10* (9), 681-687.

17.   Ford, C. L.; Park, Y. J.; Matson, E. M.; Gordon, Z.; Fout, A. R., A bioinspired iron catalyst for nitrate and perchlorate reduction. *Science* **2016,** *354* (6313), 741-743.

18.   Drummond, M. J.; Miller, T. J.; Ford, C. L.; Fout, A. R., Catalytic Perchlorate Reduction Using Iron: Mechanistic Insights and Improved Catalyst Turnover. *ACS Catalysis* **2020,** *10* (5), 3175-3182.

19.   Hutchison, J. M.; Poust, S. K.; Kumar, M.; Cropek, D. M.; MacAllister, I. E.; Arnett, C. M.; Zilles, J. L., Perchlorate reduction using free and encapsulated Azospira oryzae enzymes. *Environmental science & technology* **2013,** *47* (17), 9934-9941.

20.   Elrod, L. T.; Kim, E., Lewis Acid Assisted Nitrate Reduction with Biomimetic Molybdenum Oxotransferase Complex. *Inorganic chemistry* **2018,** *57* (5), 2594-2602.

21.   Yin, Y. B.; Guo, S.; Heck, K. N.; Clark, C. A.; Coonrod, C. L.; Wong, M. S., Treating water by degrading oxyanions using metallic nanostructures. *ACS Sustainable Chemistry & Engineering* **2018,** *6* (9), 11160-11175.

22.   Chaplin, B. P.; Reinhard, M.; Schneider, W. F.; Schüth, C.; Shapley, J. R.; Strathmann, T. J.; Werth, C. J., Critical review of Pd-based catalytic treatment of priority contaminants in water. *Environmental science & technology* **2012,** *46* (7), 3655-3670.

23.   Abu-Omar, M. M.; McPherson, L. D.; Arias, J.; Béreau, V. M., Clean and efficient catalytic reduction of perchlorate. *Angewandte Chemie* **2000,** *112* (23), 4480-4483.

24.   Liu, J.; Wu, D.; Su, X.; Han, M.; Kimura, S. Y.; Gray, D. L.; Shapley, J. R.; Abu-Omar, M. M.; Werth, C. J.; Strathmann, T. J., Configuration control in the synthesis of homo-and heteroleptic bis (oxazolinylphenolato/thiazolinylphenolato) chelate ligand complexes of oxorhenium (V): Isomer effect on ancillary ligand exchange dynamics and implications for perchlorate reduction catalysis. *Inorganic chemistry* **2016,** *55* (5), 2597-2611.

25.   Liu, J.; Choe, J. K.; Wang, Y.; Shapley, J. R.; Werth, C. J.; Strathmann, T. J., Bioinspired complex-nanoparticle hybrid catalyst system for aqueous perchlorate reduction: Rhenium speciation and its influence on catalyst activity. *ACS Catalysis* **2015,** *5* (2), 511-522.

26.   Liu, J.; Han, M.; Wu, D.; Chen, X.; Choe, J. K.; Werth, C. J.; Strathmann, T. J., A new bioinspired perchlorate reduction catalyst with significantly enhanced stability via rational tuning of rhenium coordination chemistry and heterogeneous reaction pathway. *Environmental science & technology* **2016,** *50* (11), 5874-5881.

27.   Liu, J.; Chen, X.; Wang, Y.; Strathmann, T. J.; Werth, C. J., Mechanism and mitigation of the decomposition of an oxorhenium complex-based heterogeneous catalyst for perchlorate reduction in water. *Environmental science & technology* **2015,** *49* (21), 12932-12940.

28.   Ren, C.; Yang, P.; Gao, J.; Huo, X.; Min, X.; Bi, E. Y.; Liu, Y.; Wang, Y.; Zhu, M.; Liu, J., Catalytic Reduction of Aqueous Chlorate With MoO x Immobilized on Pd/C. *ACS Catalysis* **2020,** *10* (15), 8201-8211.

29.   Gao, J.; Ren, C.; Huo, X.; Ji, R.; Wen, X.; Guo, J.; Liu, J., Supported Palladium Catalysts: A Facile Preparation Method and Implications to Reductive Catalysis Technology for Water Treatment. *ACS ES&T Engineering* **2021,** *1* (3), 562–570.

30.   Zabinsky, S.; Rehr, J.; Ankudinov, A.; Albers, R.; Eller, M., Multiple-scattering calculations of X-ray-absorption spectra. *Physical Review B* **1995,** *52* (4), 2995-3009.

31.   Amarante, T. R.; Neves, P.; Paz, F. A. A.; Pillinger, M.; Valente, A. A.; Gonçalves, I. S., A dinuclear oxomolybdenum (VI) complex,[Mo2O6 (4, 4′-di-tert-butyl-2, 2′-bipyridine) 2], displaying the {MoO2 (μ-O) 2MoO2} 0 core, and its use as a catalyst in olefin epoxidation. *Inorganic Chemistry Communications* **2012,** *20*, 147-152.

32.   Ghasemi, S.; Hosseini, S. R.; Nabipour, S.; Asen, P., Palladium nanoparticles supported on graphene as an efficient electrocatalyst for hydrogen evolution reaction. *International Journal of Hydrogen Energy* **2015,** *40* (46), 16184-16191.

33.   Oyerinde, O. F.; Weeks, C. L.; Anbar, A. D.; Spiro, T. G., Solution structure of molybdic acid from Raman spectroscopy and DFT analysis. *Inorganica Chimica Acta* **2008,** *361* (4), 1000-1007.

34.   Hurley, K. D.; Zhang, Y.; Shapley, J. R., Ligand-Enhanced Reduction of Perchlorate in Water with Heterogeneous Re− Pd/C Catalysts. *Journal of the American Chemical Society* **2009,** *131* (40), 14172-14173.

35.   Mirts, E. N.; Petrik, I. D.; Hosseinzadeh, P.; Nilges, M. J.; Lu, Y., A designed heme-[4Fe-4S] metalloenzyme catalyzes sulfite reduction like the native enzyme. *Science* **2018,** *361* (6407), 1098-1101.

36.   Liu, J.; Choe, J. K.; Sasnow, Z.; Werth, C. J.; Strathmann, T. J., Application of a Re–Pd bimetallic catalyst for treatment of perchlorate in waste ion-exchange regenerant brine. *Water research* **2013,** *47* (1), 91-101.

37.   Zhang, Y.; Hurley, K. D.; Shapley, J. R., Heterogeneous catalytic reduction of perchlorate in water with Re− Pd/C catalysts derived from an oxorhenium (V) molecular precursor. *Inorganic chemistry* **2011,** *50* (4), 1534-1543.

38.   Wang, H.; Hamanaka, S.; Nishimoto, Y.; Irle, S.; Yokoyama, T.; Yoshikawa, H.; Awaga, K., In operando X-ray absorption fine structure studies of polyoxometalate molecular cluster batteries: polyoxometalates as electron sponges. *Journal of the American Chemical Society* **2012,** *134* (10), 4918-4924.

39.   Anbananthan, N.; Rao, K. N.; Venkatesan, V., Cyclic voltammetric investigations of the reduction of Mo (VI) to Mo (IV) in 1 M sulphuric acid. *Journal of Electroanalytical Chemistry* **1994,** *374* (1-2), 207-214.

40.   You, J.; Wu, D.; Liu, H., Electrochemical studies of molybdate and thiomolybdates. *Polyhedron* **1986,** *5* (1-2), 535-537.

Chapter 5. Molybdenum-Catalyzed Perchlorate Reduction: Robustness, Challenges, and Solutions

The text of this chapter is based on, or in part a reprint of the material as it appears in Ren, C.; Bi, Y. E.; Gao, J.; Liu, J. Molybdenum-catalyzed perchlorate reduction: robustness, challenges, and solutions. *ACS ES&T Engineering*, 2021, DOI: 10.1021/acsestengg.1c00290.

5.1 Abstract

We have recently developed a highly active ligand-enabled (L)Mo−Pd/C catalyst (L = 4,4'-diamino-2,2'-bipyridine) for aqueous perchlorate (ClO_4^-) reduction with 1 atm H_2 at room temperature. This study reports on a series of satisfactory properties of this catalyst closely relevant to ClO_4^- treatment in waste brines resulting from ion-exchange resin regeneration. In the presence of concentrated salts and humic acid, the catalyst experienced limited inhibition but completed ClO_4^- reduction in a few hours with an adjustable loading between 0.2 and 2 g/L. The catalyst was not deactivated by the high oxidative stress from multiple spikes of 100 mM ClO_4^-. The challenge of deactivation by nitrate was solved by pretreating the brine with In−Pd/Al_2O_3. The loss of activity upon ligand hydrogenation was overcome by regenerating the Pd/C at pH 12. We also optimized the catalyst formulation and saved 70% of Pd without sacrificing the activity. The substantially enhanced performance and lowered adverse environmental impacts of (L)Mo−Pd/C make the catalytic treatment competitive to microbial reactors for ClO_4^- reduction. We showcase the power of coordination chemistry in environmental technology

innovation and expect this catalyst to promote the reuse of ClO_4^--selective resins for sustainable water treatment.

5.2 Introduction

The excess uptake of perchlorate (ClO_4^-) through contaminated water and food can disrupt thyroid hormone production, which is critical for the growth, development, metabolism, and mental function of humans.[1] In the United States, California[2] and Massachusetts[3] set the maximum contamination level for ClO_4^- in drinking water at 6 and 2 µg/L, respectively. In China, the proposed 2021 revision of the National Standards for Drinking Water Quality included ClO_4^- at 70 µg/L.[4] With the improved understanding of ClO_4^- toxicity[5] and the discovery of ClO_4^- on Mars,[6] the remediation of ClO_4^- contamination is an imperative research topic for environmental engineering[7-9] and space explorations.[10, 11]

Although ion-exchange (IX) resins can readily remove ClO_4^- from water,[12] achieving a rapid reduction of enriched ClO_4^- has been a challenge for over two decades. Microbial reactors can take days to weeks to stabilize the function of ClO_4^- reduction,[13, 14] and most abiotic methods require harsh conditions and a large excess of reducing agents.[15-19] The use of rhenium (Re) for ClO_4^- activation together with palladium (Pd) for H_2 activation (Re−Pd/C) realized rapid and complete reduction of ClO_4^- into Cl^- at ambient conditions.[9, 20-24] Recently, we have replaced Re with a highly reactive molybdenum (Mo) species, which was formed *in situ* from a common fertilizer, Na_2MoO_4, and a common bipyridine ligand (*L*) (**Figure 5.1**).[25] In comparison to Re−Pd/C catalysts, the new

(*L*)Mo−Pd/C shows even higher activity, does not involve specialized preparation procedures and is not deactivated by air exposure.[25] Spectroscopic evidence suggested a dimeric structure of the surface-immobilized Mo site, with each Mo coordinating with an *N,N*-bidentate ligand.[25] The coordination of Mo with the electron-rich ligand enables the rapid reaction with highly inert ClO_4^- via oxygen atom transfer to the reduced Mo^{IV} site:

$$ClO_x^- + (L)Mo^{IV}(O) \rightarrow (L)Mo^{VI}(O)_2 + ClO_{x-1}^-$$
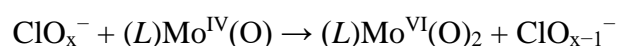
The oxidized Mo^{VI} is then reduced back to Mo^{IV} by Pd-catalyzed hydrogenation:

$$(L)Mo^{VI}(O)_2 + H_2 \rightarrow (L)Mo^{IV}(O) + H_2O$$
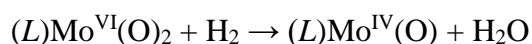
The overall reaction is the complete and clean reduction of ClO_4^- :

$$ClO_4^- + 4\,H_2 \rightarrow Cl^- + 4\,H_2O$$
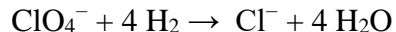
To promptly transfer the exciting invention into engineering solutions, herein we report on systematic evaluation and improvement of the (*L*)Mo−Pd/C catalyst in terms of various conventional and novel properties closely relevant to practical applications, including i) performance in water matrices of concentrated salts and natural organics, ii) longevity in challenging and continuous oxidative and reducing environments, and iii) cost-effectiveness optimized through catalyst formulation. In particular, we provide viable solutions to catalyst deactivation challenges. The results will guide the application of this catalyst and exemplify lab-scale evaluations of new water treatment catalysis.

Figure 5.1 Illustrated experimental procedures for (a) preparation of (*L*)Mo−Pd/C with adjustable Pd and Mo contents, (b) sequential reduction of NO_3^- by In−Pd/Al$_2$O$_3$ and ClO_4^- by (*L*)Mo−Pd/C, and **(c)** hydrogenation deactivation and regeneration of (*L*)Mo−Pd/C.

5.3 Materials and Methods

5.3.1 Chemicals and Materials

Na$_2$MoO$_4$•2H$_2$O (≥99%), Na$_2$PdCl$_4$ (98%), and humic acid were purchased from Sigma−Aldrich. The ligand 4,4'-diamino-2,2'-bipyridine ((NH$_2$)$_2$*bpy*, >98%) was purchased from TCI America. NaClO$_4$, NaCl, Na$_2$SO$_4$, NaH$_2$PO$_4$, NaNO$_3$, NH$_4$Cl, and NaOH in ≥99% purities were purchased from Fisher Chemical. Ultrahigh purity (99.999%) H$_2$ gas was purchased from Airgas. The standard 2 N sulfuric acid solution was purchase from Alfa Aesar. All chemicals were used as received. Aqueous solutions were prepared with deionized (DI) water (resistivity >18.2 MΩ cm). The carbon support was purchased from Alfa Aesar (Norit GSX; steam activated and acid-washed; surface area 1300 m^2/g) and used as received.

5.3.2 Preparation and Use of (*L*)Mo−Pd/C Catalyst

In this study, we prepared the catalyst with various formulations from pristine activated carbon, Pd^{II} and Mo^{VI} precursors, and free ligand (**Figure 5.1a**). The first step followed our previously developed *in situ* method to prepare Pd/C.[26] The amounts of carbon and Pd are adjustable based on the specific catalyst powder loading in water (0.2−2.0 g/L) and the specific Pd content in the catalyst (0.1−5.0 wt%). In a 50-mL flask, activated carbon powder was added to 50 mL of DI water. The flask was capped with a rubber stopper, and the mixture was sonicated for 1 min. Under magnetic stirring, Na_2PdCl_4 solution was added dropwise into the carbon suspension. Stirring for another 5 min was sufficient for Pd^{II} immobilization onto carbon support. H_2 gas was supplied through a 16-gauge stainless steel needle. Another needle was used as the gas outlet so that the H_2 pressure in the flask was maintained at 1 atm. The exposure to H_2 for 5 min was sufficient to reduce all Pd^{II} into Pd^0 nanoparticles.[26] The resulting Pd/C catalyst could be either immediately added with Mo or filtered and dried under vacuum for future use. In the second step, stock solutions of Na_2MoO_4 and $(NH_2)_2bpy$ were sequentially added in the Pd/C suspension. The solution pH was adjusted to 3.0 using 2N H_2SO_4. The amount of Mo is adjustable for specific Mo content in the catalyst (0.5−5.0 wt%), whereas the molar ratio of *L*:Mo was kept at 1:1. The following exposure to 1 atm H_2 for 1 h afforded the final (*L*)Mo−Pd/C catalyst.[25] The addition of $NaClO_4$ (1−100 mM) initiated the catalytic reduction at room temperature (20 °C). Aliquots were collected intermittently from the gas outlet needle and immediately filtered by 0.22-μm cellulose acetate membrane to quench reactions.

5.3.3 Perchlorate Reduction in the Synthetic Brine

After (L)Mo−Pd/C was prepared, solid salts were added to the catalyst suspension following the composition of a previously studied waste brine (**Table 5.1**) collected from a Californian water treatment plant using a regenerable ion-exchange system.[21] Because the reduction of NO_3^- consumes H^+:[21]

$$NO_3^- + 2.5\ H_2 + H^+ \rightarrow 0.5\ N_2 + 3\ H_2O$$

$$NO_3^- + 4\ H_2 + 2\ H^+ \rightarrow NH_4^+ + 3\ H_2O$$
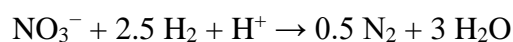
A 50-mL double-neck flask was used to monitor and maintain the solution pH during the reaction. Both necks were capped with rubber stoppers, one of which accommodated a Fisherbrand accumet gel-filled pencil-thin pH combination electrode (**Figure 5.1b**). The other stopper accommodated the two stainless needles for H_2 supply and sampling. H_2SO_4 (0.1 M) was added through the sampling needle to adjust the pH back to the working range for the catalyst (3.0 ± 0.1).

Component[a]	Concentration
Chloride	0.9 M (32.3 g/L as Cl$^-$, ~5 wt% NaCl)
Perchlorate	1 mM (100 mg/L as ClO$_4^-$)[b]
Nitrate	38 mM (2.36 g/L as NO$_3^-$)
Sulfate	48 mM (4.70 g/L as SO$_4^{2-}$)
Phosphate	0.22 mM (20.9 mg/L as PO$_4^{3-}$)

Table 5.1 Composition of the synthetic IX regenerant brine.
[a]Na$^+$ was the only cation introduced with the above anionic species because K$^+$, Ca^{2+}, and Mg^{2+} (taking a small portion of total cations in the real brine) did not significantly impact reaction kinetics.[23] Although present in the real waste brine, carbonate was not added to the synthetic brine because it was fully removed as CO$_2$ bubbles during pH adjustment to 3.0.[21]
[b]The ClO$_4^-$ concentration in the real brine was 0.02 mM (~2 mg L^{-1} as ClO$_4^-$) because the IX resin was not perchlorate-selective. We increased the concentration to 1 mM for (i) ensuring the accuracy of ClO$_4^-$ quantitation in the concentrated salt matrix, (ii) comparing the catalyst performance with most experiments that used 1 mM ClO$_4^-$ as the probe. The catalyst is capable of reducing as low as 0.01 mM (~1 mg/L) ClO$_4^-$ by >99% (i.e., <10 µg/L in the treated water).[25]

5.3.4 Preparation and Use of In−Pd/Al$_2$O$_3$ Catalyst

A 5 wt % Pd on γ-Al$_2$O$_3$ (Pd/Al$_2$O$_3$) catalyst and InCl$_3$ (98%) were purchased from Sigma−Aldrich and used as received. The InCl$_3$ was dissolved in ethanol and added in Pd/Al$_2$O$_3$ via incipient wetness following a reported method.[27] The solid was dried in air at 120 °C for 4 h and reduced with H$_2$ for 12 h. Then the catalyst was collected and used at 2 g/L to reduce NO$_3^-$ in the synthetic brine. Due to the scope of this work, the preparation and formulation of In−Pd/Al$_2$O$_3$ were not further optimized. The pH monitoring and adjustment during NO$_3^-$ reduction (5.6±0.2) followed the same reactor configuration as described above. After NO$_3^-$ reduction was complete, In−Pd/Al$_2$O$_3$ was filtered out, and the treated brine was added with 0.2 g/L of (*L*)Mo−Pd/C to reduce ClO$_4^-$ (**Figure 5.1b**).

5.3.5 Aqueous Sample Analysis

The concentrations of ClO_4^- and NO_3^- were measured on an ion chromatography (Dionex ICS-5000) with a conductivity detector and 25 μL sample loop. The best separation of ClO_4^- from other anions was achieved by using a Dionex IonPac AS16 analytical column at 30 °C with 1 mL/min of 65 mM KOH eluent. A Dionex IonPac AS 19 analytical column was used to separate NO_3^-. 20 mM KOH eluent was used to achieve the best separation. The concentration of Mo in aqueous samples was analyzed by inductively coupled plasma−mass spectrometry (ICP−MS, Agilent 7700). The concentration of the free $(NH_2)_2bpy$ ligand was quantified by high-performance liquid chromatography (Shimadzu Nexera XR) with a photodiode array detector.

5.3.6 Catalyst Collection and Elemental Analyses

The catalyst powders, either freshly prepared or used after reactions, were collected by vacuum filtration through a ceramic funnel covered with Whatman qualitative filter paper. The filter paper was transferred into a 20-mL scintillation vial and dried in an oven at 70 °C to remove moisture. The contents of Mo, Pd, C, H, and N in the catalyst powders were determined by inductively coupled plasma−optical emission spectrometry (ICP−OES, PerkinElmer Optima 8300) after microwave digestion in $HNO_3−H_2O_2$ (performed by the Microanalysis Laboratory at the University of Illinois at Urbana-Champaign).

5.3.7 Regeneration of (*L*)Mo−Pd/C Catalyst

This set of procedures is illustrated in **Figure 5.1c**. After the catalyst was deactivated by hydrogenation, the pH of the water suspension was adjusted to 12.0 with

NaOH. The suspension was stirred for 10 min and filtered under vacuum. The collected solid was redispersed in DI water and added with new stock solutions of Na_2MoO_4 and $(NH_2)_2bpy$ to regenerate the $(L)Mo-Pd/C$ following the procedures described above.

5.4 Results and Discussion

5.4.1 Catalyst Performance for Brine Treatment

We prioritize the evaluation of $(L)Mo-Pd/C$ by assessing its performance in a practical scenario: ClO_4^- reduction in a waste brine resulting from IX resin regeneration. Further assessment and development will be meaningful only if the catalyst can demonstrate satisfactory activity under challenging conditions. We prepared the synthetic brine containing all anion constituents in a previously studied brine (**Table 5.1**). Because early IX resins were not highly selective for ClO_4^-, the waste brines produced from resin regeneration typically contained sulfate, nitrate, and even phosphate at orders of magnitude higher concentrations than ClO_4^-.[21, 28-30] We added 1 mM ClO_4^- in the synthetic brine (**Table 5.1**, **footnote b**). The ClO_4^- reduction was conducted at the optimized pH of 3.0, and the complete conversion into Cl^- has been confirmed.[25] Most abiotic ClO_4^- reduction systems require H^+ to enable oxygen atom transfer (OAT) in the aqueous phase.[9, 18, 20-25, 31-34]

In comparison to the performance in deionized (DI) water (i.e., no concentrated brine constituents added), the synthetic brine matrix substantially retarded ClO_4^- reduction (**Figure 5.2a**). During the relatively fast reaction in the first 2 h, the barely fit first-order rate constant was only 1.9% of that observed in DI water (**Table 5.2 entry 5** versus **1**). The

gradually flattened kinetics suggested catalyst deactivation (i.e., loss of intrinsic activity).

The simultaneous reduction of NO_3^- in the synthetic brine followed a similar trend (**Figure 5.2a**). To identify the deactivating species, we examined the effect of individual constituents on ClO_4^- reduction. In comparison to the DI water control, the addition of 80 mM $H_2PO_4^-$, 1 M SO_4^{2-}, and 1 M Cl^- lowered the rate constant by 37%, 64%, and 86%, respectively (**Table 5.2 entries 2−4** versus **1**). However, these anions merely caused inhibition (i.e., decrease of reaction rate by reaction site competition) rather than deactivation. First, the ClO_4^- reduction followed the 1st-order kinetics well (**Figure S5.1**). The most inhibited catalyst in 1 M NaCl still achieved >99.5% ClO_4^- reduction within 15 h (**Figure S5.2**). Second, recycling the catalyst from the previous use in 80 mM NaH_2PO_4, 1 M Na_2SO_4, or 1 M NaCl by filtration fully restored the activity (**Figure S5.3**). Although the catalyst was significantly inhibited by concentrated Cl^-, increasing the catalyst loading from 0.2 g/L to 2.0 g/L achieved >99.99% ClO_4^- reduction within 1 h (**Figure S5.4**). Notably, the activity was >13 times higher than that of the previously developed salt-resistant ReO_x−Pd/C (**Table 5.2 entry 4** versus **8** and **9**).[21]

Hence, NO_3^- was the only remaining suspect for catalyst deactivation. We prepared a new synthetic brine that only excluded NO_3^-. In this brine, the ClO_4^- reduction profile resembled that in 1 M NaCl (**Figure S5.2**, **Table 5.2 entry 4** versus **6**), confirming that NO_3^- is responsible for catalyst deactivation. The slight inhibition in the presence of 40 mM NH_4Cl (assuming complete reduction of NO_3^- into NH_4^+)[35] is primarily attributed to Cl^- (**Table 5.2 entry 7** versus **1** and **4**) rather than NH_4^+. In a separate experiment, we used (*L*)Mo−Pd/C to first treat 40 mM NO_3^- for 48 h. The water-rinsed catalyst only retained

11% of the original activity for ClO_4^- reduction (**Figure S5.5**). Because Pd-based catalysts integrating In, Cu, or Sn as the second metal have shown excellent NO_3^- reduction activities,[36] the severe deactivation of (*L*)Mo−Pd/C is attributed to the reaction between NO_3^- (or intermediates such as NO_2^-, NO, and N_2O) with the (*L*)Mo site rather than with Pd. Inorganic chemistry studies using molecular Mo species for NO_3^- reduction have observed inhibition by those nitrogen intermediates.[37, 38] Similar deactivation of the Re site has been observed from the ReO_x−Pd/C catalyst.[21] While deeper mechanistic insights into the deactivation phenomenon warrant further investigation, in this study, we prioritize the research effort as solving this challenge by preventing NO_3^- from reacting with the Mo catalytic site.
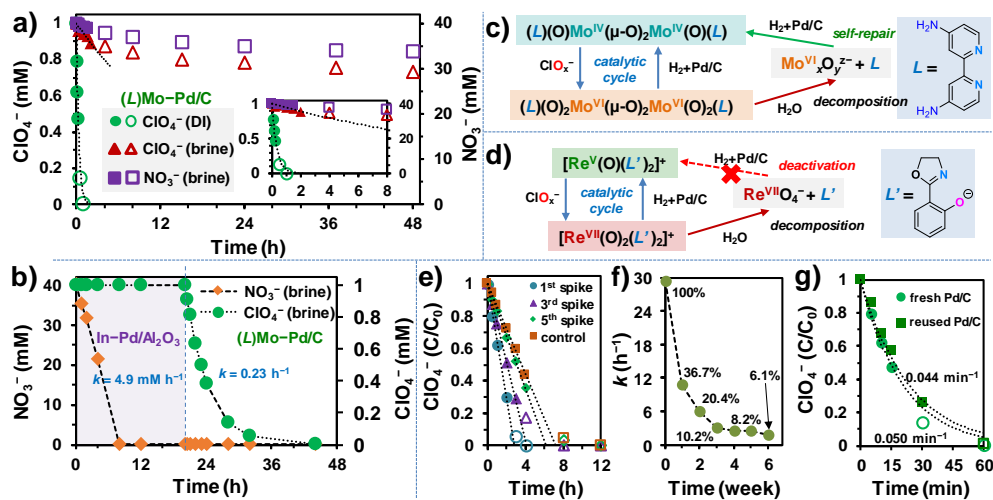
Figure 5.2 Degradation of ClO_4^- and NO_3^- in the synthetic brine by (a) (L)Mo−Pd/C only and (b) sequential application of In−Pd/Al$_2$O$_3$ (2 g/L at pH 5.6) and (L)Mo−Pd/C; mechanistic schemes for (c) self-repair of (L)Mo−Pd/C and (d) deactivation of $(L')_2$Re−Pd/C caused by concentrated ClO_4^-; (e) reduction of continuous spikes of 100 mM ClO_4^- by 2 g/L of (L)Mo−Pd/C; (f) the decrease of ClO_4^- reduction rate constants after continuous H$_2$ exposure; and (g) ClO_4^- reduction by (L)Mo−Pd/C prepared from reused Pd/C after treatment at pH 12. Default reaction conditions: 0.2 g/L of (L)Mo−Pd/C (5 wt% Mo, 5 wt% Pd), pH 3.0, 1 atm H$_2$, 20 °C. In panels a, e, and g, filled symbols were used to fit the 1st- or 0th-order model, whereas hollow ones were either not appropriate for fitting (i.e., C/C$_0$ < 0.2) or indicating the deviation from models.

Entry	Other constituents in the solution	k (L h^{-1} g$_{cat}$$^{-1}$) ^{a}
	[(NH$_2$)$_2$bpy]MoO$_x$−Pd/C (5 wt% Mo, 5 wt% Pd)	
1	DI ^{b}	14.83 ± 0.37
2	80 mM NaH$_2$PO$_4$	12.26 ± 0.81
3	1 M Na$_2$SO$_4$	5.47 ± 0.23
4	1 M NaCl	2.19 ± 0.14
5	Synthetic waste brine (see **Table 5.1**)	0.25 ± 0.04
6	Synthetic waste brine without NO$_3$$^-$	2.12 ± 0.16
7	40 mM NH$_4$Cl	9.88 ± 0.39
	ReO$_x$−Pd/C (5 wt% Re, 5 wt% Pd)	
8	DI ^{b}	0.047 ± 0.003 ^{c}
9	1 M NaCl	0.16 ± 0.01 ^{c}
10	Synthetic waste brine (see **Table 5.1**)	0.0079 ± 0.0003 ^{c}
11	Synthetic waste brine without NO$_3$$^-$	0.18 ± 0.01 ^{c}

Table 5.2 Rate constants for ClO$_4$$^-$ reduction by Mo and Re catalysts
^{a}Apparent first-order rate constants (h^{-1}) for 1 mM ClO$_4$$^-$ reduction (pH 3.0, 1 atm H$_2$, 20 °C) normalized by the loading of catalyst powder in water (g$_{cat}$ L^{-1}) to facilitate cross-comparison. The loading of Mo- and Re-based catalysts used in experiments were 0.2 and 2.0 g/L, respectively.
^{b}Containing ~1 mM H$_2$SO$_4$ (for pH adjustment to 3.0) and cations introduced with Na$_2$MoO$_4$ or KReO$_4$ precursor.
^{c}Data reported in Ref 21.

5.4.2 The Solution to Catalyst Deactivation by Nitrate

We proposed a two-stage treatment to protect (*L*)Mo−Pd/C from reacting with NO$_3$$^-$ (**Figure 5.1b**). In the first stage, NO$_3$$^-$ in the synthetic brine was reduced with a well-established In−Pd/Al$_2$O$_3$ catalyst.[39] Similar to the previous report,[21] 2 g/L of In−Pd/Al$_2$O$_3$ reduced >99.98% of the 38 mM of NO$_3$$^-$ within 8 h (**Figure 5.2b**) with a <30% product selectivity toward NH$_4$$^+$, whereas no ClO$_4$$^-$ reduction was observed. Then we filtered out In−Pd/Al$_2$O$_3$ and added 0.2 g/L of (*L*)Mo−Pd/C into the nitrate-removed brine. As expected, the reduction of 1 mM ClO$_4$$^-$ proceeded rapidly and achieved 99.9% reduction within 24 h. The (*L*)Mo−Pd/C showed the highest ClO$_4$$^-$ reduction activity in both DI water and brine among the hydrogenation catalysts studied to date (**Table S5.1**).

5.4.3 Catalyst Stability against Oxidative Stress

After solving the nitrate deactivation challenge, we evaluated the stability of (L)Mo−Pd/C during the treatment of concentrated ClO_4^-. The regeneration of ClO_4^--selective resins can produce highly concentrated ClO_4^- up to 10 g/L (~100 mM) within one bed volume of waste brine.[12, 15] Although ClO_4^- is highly inert, the ClO_x^- intermediates are much more reactive with the (L)Mo site,[33] where the ligand carries two strong electron-donating −NH$_2$ groups. For Re−Pd/C catalysts prepared from presynthesized $[Re^V(O)(L')_2]^+$ (L'=various oxazoline-phenolate ligands) as the active site, concentrated ClO_x^- could cause the accumulation of $[Re^{VII}(O)_2(L')_2]^+$ and irreversible decomposition into ReO_4^- and free L' (i.e., deactivation, **Figure 5.2d**).[23, 24] In contrast, the active $[(L)(O)Mo^{IV}]_2(\mu\text{-}O)_2$ site in (L)Mo−Pd/C is prepared *in situ* from inorganic molybdate and free $(NH_2)_2bpy$ ligand. If similar hydrolysis of oxidized $[(L)(O)Mo^{VI}]_2(\mu\text{-}O)_2$ occurs, the products would be the starting materials, allowing the active site to form again (i.e., self-repair, **Figure 5.2c**). To verify this hypothesis, we challenged (L)Mo−Pd/C with five spikes of 100 mM ClO_4^-. The reduction of the fifth ClO_4^- spike was not slower than the control, where the fresh (L)Mo−Pd/C reduced 100 mM ClO_4^- in the presence of 400 mM Cl^- (**Figure 5.2e** and **Table S5.2**). Therefore, the gradual activity loss is attributed to the accumulation of Cl^- from ClO_4^- reduction. After five spikes, each (L)Mo site had undergone 1,920 redox turnovers without deactivation. Notably, the removal of 100 mM ClO_4^- reached >99.99%, more effective than the previously reported thermal treatment (92−98%).[12]

5.4.4 Catalyst Longevity under Reducing Atmosphere

It has been well documented that pyridine structures are susceptible to Pd^0-catalyzed hydrogenation, and those with electron-donating substitutions (e.g., $-NH_2$) have the lowest reactivity.[40, 41] To evaluate the catalyst longevity under extended hydrogenating conditions, we exposed the water suspension of (*L*)Mo$-$Pd/C to 1 atm H_2 atmosphere for up to 1000 h (6 weeks, **Figure 5.1c**). The rate constants for ClO_4^- reduction decreased exponentially by 90% in the first three weeks (0.113 day^{-1}, **Figure 5.2f** and **Figure S5.6**). The activity loss in weeks 4$-$6 was less pronounced and remained at 6% of the original activity after 1000 h. We attribute the rapid activity decrease to the hydrogenation of pyridyl rings in Mo-coordinated (NH$_2$)$_2$*bpy*. After that, the hydrogenation product still coordinated with Mo and enabled ClO_4^- reduction to a limited extent. This interpretation is supported by the limited ClO_4^- reduction activity using selected aliphatic diamine ligands and no activity without using any organic ligand.[25]

Elemental analyses of solid catalysts found that long-term exposure to H_2 caused roughly 20% and 50% loss of Mo and N, respectively (**Table 5.3 entry 4** versus **2**). In comparison, the redox transformation during ClO_4^- reduction is not the cause for the leaching (**Table 5.3 entry 3**). In general, aliphatic amines have 5$-$6 units higher pKa values than pyridines (i.e., much more prone to be protonated). The hydrogenation of pyridyl structures might also eliminate the π-π stacking interaction with carbon support and thus enhance dissolution. The original (NH$_2$)$_2$*bpy* ligand was not detected in the water. In contrast, the Pd content did not significantly change in the solid, and ICP$-$MS analysis

detected up to 0.01% of the total Pd dissolved in various water samples. Such stability is as expected because solid-state Pd^0 can be readily maintained under H_2 atmosphere.[26]

Entry	Sample	Pd	Mo	Pd:Mo[b]	C	H	N
1	Pd/C without Mo[a]	3.86	0.01	-	83.61	1.14	0.52
2	fresh (L)Mo−Pd/C[a]	3.25	3.58	0.91:1	77.92	1.24	2.82
3	used (L)Mo−Pd/C after 1 mM ClO_4^- treatment	3.09	3.23	0.96:1	77.30	1.24	2.74
4	after 6-week exposure under 1 atm H_2	3.30	2.95	1.12:1	79.14	1.03	1.37
5	after regeneration at pH 12	3.53[c]	0.03	-	83.41	1.29	2.04

Table 5.3 Elemental analyses of solid catalysts (Unit: weight percentage, wt%).
[a]Pd/C and (L)Mo−Pd/C had the nominal 5 wt% loadings for both Pd and Mo.
[b]Because elemental analyses of solid samples always have deviations and can be significantly impacted by the addition of other constituents in the solid, the ratio between the two metals is a more meaningful indicator of metal leaching than the absolute weight percentage of each metal. Recall that Pd leaching is minimal under the H_2 atmosphere.[26]
[c]For the same reason as footnote b, this value is slightly lower than that in the original Pd/C (3.86% for Pd and 0.52 for % N) because of the residual N (2.04%).

### 5.4.5 Catalyst Regeneration after Ligand Hydrogenation

The above findings suggest that the loss of the most precious component, Pd, is minimal. To restore the catalyst activity, we investigated the regeneration of Pd/C platform by removing Mo and hydrogenated ligand residues. Inspired by an early study on molybdate desorption from carbon,[42] we elevated the pH to 12 under air and achieved quantitative dissolution of Mo within 10 min (**Figure S5.7**). Elemental analysis of the solid confirmed the complete removal of Mo but incomplete removal of N-containing residues (**Table 5.3 entry 5** versus **1**). After adding fresh Na_2MoO_4 and $(NH_2)_2bpy$ to the regenerated Pd/C (**Figure 5.1c**), the "refurbished" (L)Mo−Pd/C showed only slightly diminished activity (**Figure 5.2g**), probably due to the N-containing residues left on the carbon support. Hence, after several rounds of such regeneration, a complete recovery of Pd via chemical extractions[43-45] could be necessary.

5.4.6 Optimization of Catalyst Formulation

To further reduce the use of Pd and maximize cost-effectiveness, we examined the effect of variable Pd and Mo contents on ClO_4^- reduction activity. Our recently developed method enables "instant" preparation of Pd/C with any metal content and significantly reduces the technical efforts for fine-tuning the metal contents.[26] With the Mo content fixed at 5 wt%, the decrease of Pd content by 90% (i.e., from 5 to 0.5 wt%) only lowered the rate constant by 71% (**Figure 5.3a** and **Figure S5.8a**), suggesting the feasibility of using less Pd to achieve the same catalytic activity at an increased loading of catalyst.[26] However, if the Mo content is kept at 5 wt%, the increased catalyst loading will involve more Mo and ligand. Interestingly, after the Pd content was lowered to 0.5 wt%, the initially optimized 5 wt% of Mo (using 5 wt% Pd/C)[25] became excessive, and 3 wt% was found to be the optimal content (**Figure 5.3b** and **Figure S5.8b**). The tripled loading of 3 wt% Mo−0.5 wt% Pd/C exhibited the same rate of ClO_4^- reduction as the original 5 wt% Mo−5 wt% Pd/C (**Figure 5.3c**). Hence, the new formulation involved a tripled amount of carbon and 80% more (*L*)Mo but saved 70% of Pd, the most expensive component.

A life cycle assessment (LCA) study comparing microbial and catalytic (using ReO_x−Pd/C) reduction of ClO_4^- found that the mining and refining of Pd and Re contributed to the majority of adverse environmental impacts.[46] Because Re is a minor component in Mo minerals, we assume that the adverse impacts from Mo are not higher than from Re. The activity of (*L*)Mo−Pd/C is 290- and 10-fold higher than ReO_x−Pd/C in DI water and NO_3^--free synthetic brine, respectively (**Table 5.2**). Furthermore, catalyst optimization has saved 70% Pd to achieve the same activity. Based on all of these

advancements, the environmental impacts from Pd can be reduced by at least 970 and 33 folds for use in DI water and brine, respectively. With the same LCA metrics and 33-fold decrease of Pd consumption, the new catalytic ClO_4^- reduction module using (L)Mo−Pd/C coupled with ion-exchange resin has become comparable to microbial reduction (**Figure 5.3e** and **Text 5.S1**).
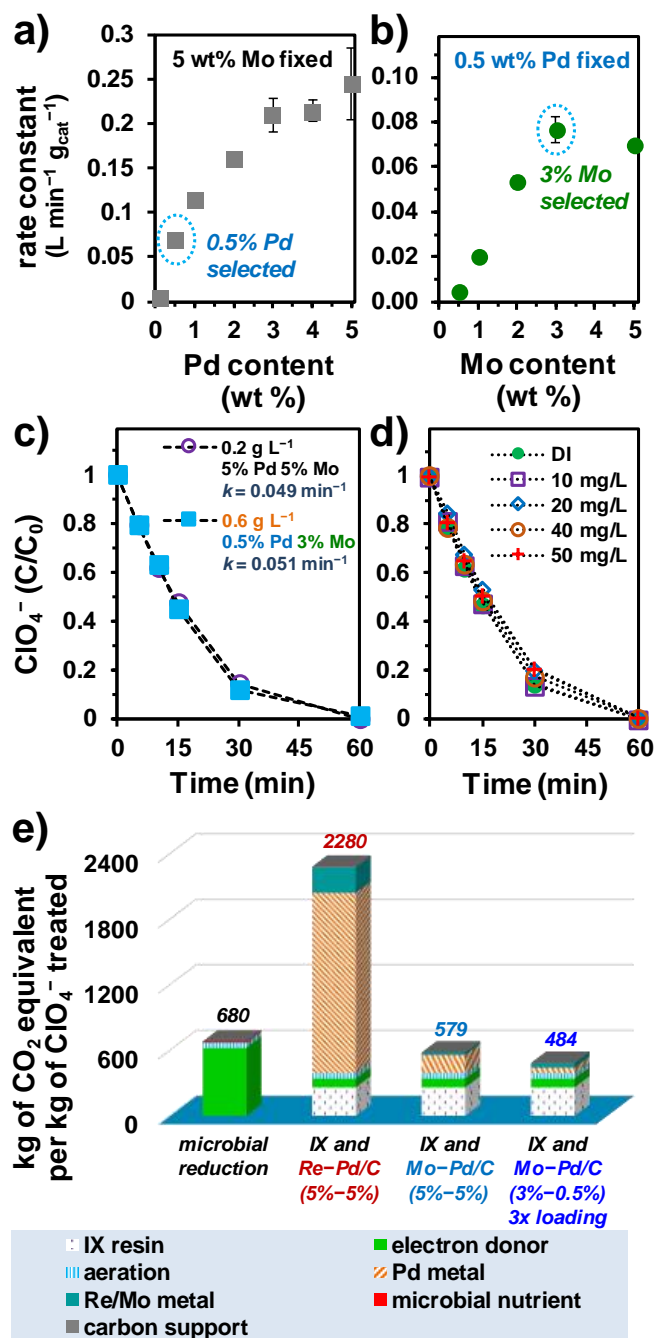
Figure 5.3 Optimization of (a) Pd and (b) Mo content in the (*L*)Mo−Pd/C catalyst, and the ClO_4^- reduction performance (c) with two catalyst formulations and (d) in the presence of 10−50 mg/L humic acid (0.2 g/L, 5 wt% Mo and 5 wt% Pd). Common reaction conditions: 1 mM ClO_4^-, pH 3.0, 1 atm H_2, and 20 °C. Panel **e** shows the comparison of "global warming" impacts by microbial reduction and sequential IX-catalysis treatment based on the data in a previous LCA study.[46]

5.5 Environmental Implementation

5.5.1 Implication to Perchlorate Treatment

The above results showcase a highly active, robust, and cost-effective heterogeneous catalyst for ClO_4^- reduction. Regarding practical application, it is essential to highlight four technical points. First, the treatment of resin regeneration waste is separated from the drinking water treatment loop. Any concern of the non-neutral pH and minimal leaching of Mo and ligand in the treated brine can be further addressed if necessary. More importantly, cost-effective degradation of concentrated pollutants will advance drinking water treatment technologies by allowing sustainable reuse of ClO_4^--selective IX resins instead of incineration.[12, 47, 48] Highly selective resins do not require frequent regeneration; thus, a continuous operation for ClO_4^- reduction may not be needed, alleviating catalyst deactivation caused by ligand hydrogenation and allowing the use of a batch reactor configuration. In such cases, abiotic catalysts also have unique advantages over microbial reactors, which usually require continuous operation. The U.S. EPA has included Mo on the Third Unregulated Contaminant Monitoring Rule (UCMR-3) with the minimum reporting level of 1 μg/L in drinking water.[49] If the treated brine is recycled for resin regeneration, further studies are warranted to evaluate the potential transfer of leached Mo from waste brine treatment to drinking water. Second, the use of H_2 gas for reductive pollutant degradation has been widely adopted in environmental engineering projects.[50-55] Third, inorganic sulfide, a potent Pd poison that may be present in the wastes, can be instantly oxidized into inert SO_4^{2-} using common oxidants[56] to avoid catalyst fouling. Fourth, although dissolved organics might not be significant constituents in the waste

brine,[21] our data show that 10−50 mg/L of humic acid did not inhibit the (L)Mo−Pd/C catalyst (**Figure 5.3d**). Although humic acid is a well-known inhibitor to Pd catalysts,[36] it appears that the $(NH_2)_2bpy$-coordinated Mo sites are not sensitive to external ligands (e.g., the carboxylate groups in humic acid) and thus preserved the overall activity of (L)Mo−Pd/C. We will continue the study on the treatment of waste brines from the regeneration of perchlorate-selective resins. The brine has been reported to contain concentrated ClO_4^- (~100 mM) and $[FeCl_4]^-$ (from 1 M $FeCl_3$ and 4 M HCl).[12] Natural organic matters released from the resin are also expected to be abundant due to the long enrichment for six months. We will report unexpected case-specific challenges and technical solutions from pilot-scale testing of the (L)Mo−Pd/C catalyst used for the regeneration of perchlorate-selective resins.

5.5.2 Implication to Catalyst Development

The (L)Mo site is generated *in situ* via non-covalent Mo−N bonding and immobilized on carbon support via non-covalent interactions. The structure is also subject to decomposition upon dissolution[25] or significant pH adjustment from 3 to 12. However, under optimized conditions, the (L)Mo−Pd/C catalyst exhibits satisfactory performance in various parameters regarding practical applications, including unprecedentedly high activity for ClO_4^- reduction and resistance to oxidative stress. Moreover, the dynamic property of the (L)Mo complex also enables facile catalyst regeneration. Besides our continuous research efforts for Re-based catalysts,[24, 57-59] this study highlights the value of coordination metal complexes for environmental technology innovation aiming at practical engineering treatment.

5.6 Acknowledgement

5.7 Reference

1.   Greer, M. A.; Goodman, G.; Pleus, R. C.; Greer, S. E., Health effects assessment for environmental perchlorate contamination: the dose response for inhibition of thyroidal radioiodine uptake in humans. *Environmental health perspectives* **2002,** *110* (9), 927-937.

2.   Short, J. *HMS TIRELESS Self Contained Oxygen Generator (SCOG) Explosion-20 March 2007*; 0148-7191; SAE Technical Paper: 2008.

3.   Ford, C. L.; Park, Y. J.; Matson, E. M.; Gordon, Z.; Fout, A. R., A bioinspired iron catalyst for nitrate and perchlorate reduction. *Science* **2016,** *354* (6313), 741-743.

4.   National   Standard   of the People's Republic of China: GB 5749-XXXX (to replace   GB   5749-2006)   Standards   for   Drinking   Water   Quality.   **2021**, http://www.cuwa.org.cn/Uploads/file/20210715/20210715225950_71443.pdf.

5.   Llorente-Esteban, A.; Manville, R. W.; Reyna-Neyra, A.; Abbott, G. W.; Amzel, L. M.; Carrasco, N., Allosteric regulation of mammalian Na+/I− symporter activity by perchlorate. *Nature Structural & Molecular Biology* **2020**, 1-7.

6.   Hecht, M.; Kounaves, S.; Quinn, R.; West, S.; Young, S.; Ming, D.; Catling, D.; Clark, B.; Boynton, W. V.; Hoffman, J., Detection of perchlorate and the soluble chemistry of martian soil at the Phoenix lander site. *Science* **2009,** *325* (5936), 64-67.

7.   Hatzinger, P. B., Perchlorate biodegradation for water treatment. ACS Publications: 2005.

8.   Khera, R.; Ransom, P.; Guttridge, M.; Speth, T. F., Estimating costs for nitrate and perchlorate treatment for small drinking water systems. *AWWA Water Science* **2021,** *3* (2), e1224.

9.   Hurley, K. D.; Zhang, Y.; Shapley, J. R., Ligand-Enhanced Reduction of Perchlorate in Water with Heterogeneous Re− Pd/C Catalysts. *Journal of the American Chemical Society* **2009,** *131* (40), 14172-14173.

10.   Davila, A. F.; Willson, D.; Coates, J. D.; McKay, C. P., Perchlorate on Mars: a chemical hazard and a resource for humans. *International Journal of Astrobiology* **2013,** *12* (4), 321-325.

11.   Schuttlefield, J. D.; Sambur, J. B.; Gelwicks, M.; Eggleston, C. M.; Parkinson, B., Photooxidation of chloride by oxide minerals: Implications for perchlorate on Mars. *Journal of the American Chemical Society* **2011,** *133* (44), 17521-17523.

12.   Gu, B.; Brown, G. M.; Chiang, C.-C., Treatment of perchlorate-contaminated groundwater using highly selective, regenerable ion-exchange technologies. *Environmental science & technology* **2007,** *41* (17), 6277-6282.

13.   Coates, J. D.; Achenbach, L. A., Microbial perchlorate reduction: rocket-fuelled metabolism. *Nature Reviews Microbiology* **2004,** *2* (7), 569-580.

14.   Lai, C.-Y.; Wu, M.; Lu, X.; Wang, Y.; Yuan, Z.; Guo, J., Microbial perchlorate reduction driven by ethane and propane. *Environmental Science & Technology* **2021,** *55* (3), 2006-2015.

15.   Gu, B.; Dong, W.; Brown, G. M.; Cole, D. R., Complete degradation of perchlorate in ferric chloride and hydrochloric acid under controlled temperature and pressure. *Environmental science & technology* **2003,** *37* (10), 2291-2295.

16.   Cao, J.; Elliott, D.; Zhang, W.-x., Perchlorate reduction by nanoscale iron particles. *Journal of Nanoparticle Research* **2005,** *7* (4), 499-506.

17.   Xiong, Z.; Zhao, D.; Pan, G., Rapid and complete destruction of perchlorate in water and ion-exchange brine using stabilized zero-valent iron nanoparticles. *Water research* **2007,** *41* (15), 3497-3505.

18.   Wang, C.; Huang, Z.; Lippincott, L.; Meng, X., Rapid Ti (III) reduction of perchlorate in the presence of β-alanine: Kinetics, pH effect, complex formation, and β-alanine effect. *Journal of hazardous materials* **2010,** *175* (1-3), 159-164.

19.   Hori, H.; Sakamoto, T.; Tanabe, T.; Kasuya, M.; Chino, A.; Wu, Q.; Kannan, K., Metal-induced decomposition of perchlorate in pressurized hot water. *Chemosphere* **2012,** *89* (6), 737-742.

20.   Hurley, K. D.; Shapley, J. R., Efficient heterogeneous catalytic reduction of perchlorate in water. *Environmental science & technology* **2007,** *41* (6), 2044-2049.

21.   Liu, J.; Choe, J. K.; Sasnow, Z.; Werth, C. J.; Strathmann, T. J., Application of a Re–Pd bimetallic catalyst for treatment of perchlorate in waste ion-exchange regenerant brine. *Water research* **2013,** *47* (1), 91-101.

22.   Liu, J.; Choe, J. K.; Wang, Y.; Shapley, J. R.; Werth, C. J.; Strathmann, T. J., Bioinspired complex-nanoparticle hybrid catalyst system for aqueous perchlorate reduction: Rhenium speciation and its influence on catalyst activity. *ACS Catalysis* **2015,** *5* (2), 511-522.

23.   Liu, J.; Chen, X.; Wang, Y.; Strathmann, T. J.; Werth, C. J., Mechanism and mitigation of the decomposition of an oxorhenium complex-based heterogeneous catalyst for perchlorate reduction in water. *Environmental science & technology* **2015,** *49* (21), 12932-12940.

24.   Ren, C.; Liu, J., Bioinspired Catalytic Reduction of Aqueous Perchlorate by One Single-Metal Site with High Stability against Oxidative Deactivation. *ACS Catalysis* **2021,** *11*, 6715-6725.

25.   Ren, C.; Yang, P.; Sun, J.; Bi, E. Y.; Gao, J.; Palmer, J.; Zhu, M.; Wu, Y.; Liu, J., A Bioinspired Molybdenum Catalyst for Aqueous Perchlorate Reduction. *Journal of the American Chemical Society* **2021,** *143* (21), 7891-7896.

26.   Gao, J.; Ren, C.; Huo, X.; Ji, R.; Wen, X.; Guo, J.; Liu, J., Supported palladium catalysts: A facile preparation method and implications to reductive catalysis technology for water treatment. *ACS ES&T Engineering* **2020,** *1* (3), 562-570.

27.   Chaplin, B. P.; Shapley, J. R.; Werth, C. J., Regeneration of sulfur-fouled bimetallic Pd-based catalysts. *Environmental science & technology* **2007,** *41* (15), 5491-5497.

28.   Batista, J. R.; McGarvey, F. X.; Vieira, A. R., The removal of perchlorate from waters using ion-exchange resins. In *Perchlorate in the Environment*, Springer: 2000; pp 135-145.

29.   Gingras, T. M.; Batista, J. R., Biological reduction of perchlorate in ion exchange regenerant solutions containing high salinity and ammonium levels. *Journal of environmental monitoring* **2002,** *4* (1), 96-101.

30.   Lehman, S. G.; Badruzzaman, M.; Adham, S.; Roberts, D. J.; Clifford, D. A., Perchlorate and nitrate treatment by ion exchange integrated with biological brine treatment. *Water research* **2008,** *42* (4-5), 969-976.

31.   Abu-Omar, M. M.; Espenson, J. H., Facile abstraction of successive oxygen atoms from perchlorate ions by methylrhenium dioxide. *Inorganic chemistry* **1995,** *34* (25), 6239-6240.

32.   Rechnitz, G. A.; Laitinen, H., A Study of the Molybdenum Catalyzed Reduction of Perchlorate. *Analytical Chemistry* **1961,** *33* (11), 1473-1477.

33.   Ren, C.; Yang, P.; Gao, J.; Huo, X.; Min, X.; Bi, E. Y.; Liu, Y.; Wang, Y.; Zhu, M.; Liu, J., Catalytic Reduction of Aqueous Chlorate With MoO x Immobilized on Pd/C. *ACS Catalysis* **2020,** *10* (15), 8201-8211.

34.   Liu, B. Y.; Wagner, P. A.; Earley, J. E., Reduction of perchlorate ion by (N-(hydroxyethyl) ethylenediaminetriacetato) aquatitanium (III). *Inorganic Chemistry* **1984,** *23* (21), 3418-3420.

35.   Chen, X.; Huo, X.; Liu, J.; Wang, Y.; Werth, C. J.; Strathmann, T. J., Exploring beyond palladium: Catalytic reduction of aqueous oxyanion pollutants with alternative platinum group metals and new mechanistic implications. *Chemical Engineering Journal* **2017,** *313*, 745-752.

36.   Chaplin, B. P.; Reinhard, M.; Schneider, W. F.; Schüth, C.; Shapley, J. R.; Strathmann, T. J.; Werth, C. J., Critical review of Pd-based catalytic treatment of priority contaminants in water. *Environmental science & technology* **2012,** *46* (7), 3655-3670.

37.   Majumdar, A.; Pal, K.; Sarkar, S., Selectivity of thiolate ligand and preference of substrate in model reactions of dissimilatory nitrate reductase. *Inorganic chemistry* **2008,** *47* (8), 3393-3401.

38.   Ehweiner, M. A.; Wiedemaier, F.; Belaj, F.; Mösch-Zanetti, N. C., Oxygen Atom Transfer Reactivity of Molybdenum (VI) Complexes Employing Pyrimidine-and Pyridine-2-thiolate Ligands. *Inorganic Chemistry* **2020,** *59* (19), 14577-14593.

39.   Prüsse, U.; Vorlop, K.-D., Supported bimetallic palladium catalysts for water-phase nitrate reduction. *Journal of Molecular Catalysis A: Chemical* **2001,** *173* (1-2), 313-328.

40.   Cui, Y.; Kwok, S.; Bucholtz, A.; Davis, B.; Whitney, R. A.; Jessop, P. G., The effect of substitution on the utility of piperidines and octahydroindoles for reversible hydrogen storage. *New Journal of Chemistry* **2008,** *32* (6), 1027-1037.

41.   Irfan, M.; Petricci, E.; Glasnov, T. N.; Taddei, M.; Kappe, C. O., Continuous flow hydrogenation of functionalized pyridines. Wiley Online Library: 2009.

42.   Namasivayam, C.; Sangeetha, D., Removal of molybdate from water by adsorption onto ZnCl2 activated coir pith carbon. *Bioresource technology* **2006,** *97* (10), 1194-1200.

43.   Fotouhi-Far, F.; Bashiri, H.; Hamadanian, M.; Keshavarz, M. H., A New Approach for the Leaching of Palladium from Spent Pd/C Catalyst in HCl–H 2 O 2 System. *Protection of Metals and Physical Chemistry of Surfaces* **2021,** *57* (2), 297-305.

44.   Fontana, D.; Pietrantonio, M.; Pucciarmati, S.; Torelli, G. N.; Bonomi, C.; Masi, F., Palladium recovery from monolithic ceramic capacitors by leaching, solvent extraction and reduction. *Journal of Material Cycles and Waste Management* **2018,** *20* (2), 1199-1206.

45.   Nogueira, C. A.; Paiva, A. P.; Costa, M. C.; da Costa, A. M. R., Leaching efficiency and kinetics of the recovery of palladium and rhodium from a spent auto-catalyst in HCl/CuCl2 media. *Environmental technology* **2019**.

46.   Choe, J. K.; Mehnert, M. H.; Guest, J. S.; Strathmann, T. J.; Werth, C. J., Comparative assessment of the environmental sustainability of existing and emerging perchlorate treatment technologies for drinking water. *Environmental science & technology* **2013,** *47* (9), 4644-4652.

47.   Sharbatmaleki, M.; Batista, J. R., Multi-cycle bioregeneration of spent perchlorate-containing macroporous selective anion-exchange resin. *Water research* **2012,** *46* (1), 21-32.

48.   Faccini, J.; Ebrahimi, S.; Roberts, D. J., Regeneration of a perchlorate-exhausted highly selective ion exchange resin: kinetics study of adsorption and desorption processes. *Separation and Purification Technology* **2016,** *158*, 266-274.

49.   AGENCY, E. P., 77 FR 26072 - Revisions to the Unregulated Contaminant Monitoring Regulation (UCMR 3) for Public Water Systems. *Federal Register* **2012,** *77* (85), 26072-26101.

50.   Zhou, D.; Luo, Y.-H.; Zheng, C.-W.; Long, M.; Long, X.; Bi, Y.; Zheng, X.; Zhou, C.; Rittmann, B. E., H2-Based Membrane Catalyst-Film Reactor (H2-MCfR) Loaded with Palladium for Removing Oxidized Contaminants in Water. *Environmental Science & Technology* **2021,** *55* (10), 7082-7093.

51.   Luo, Y.-H.; Long, X.; Wang, B.; Zhou, C.; Tang, Y.; Krajmalnik-Brown, R.; Rittmann, B. E., A Synergistic Platform for Continuous Co-removal of 1, 1, 1-Trichloroethane, Trichloroethene, and 1, 4-Dioxane via Catalytic Dechlorination Followed by Biodegradation. *Environmental Science & Technology* **2021,** *55* (9), 6363-6372.

52.	Zhao, H.-P.; Ontiveros-Valencia, A.; Tang, Y.; Kim, B. O.; Ilhan, Z. E.; Krajmalnik-Brown, R.; Rittmann, B., Using a two-stage hydrogen-based membrane biofilm reactor (MBfR) to achieve complete perchlorate reduction in the presence of nitrate and sulfate. *Environmental science & technology* **2013,** *47* (3), 1565-1572.

53.	McNab, W. W.; Ruiz, R.; Reinhard, M., In-situ destruction of chlorinated hydrocarbons in groundwater using catalytic reductive dehalogenation in a reactive well: Testing and operational experiences. *Environmental Science & Technology* **2000,** *34* (1), 149-153.

54.	Schüth, C.; Kummer, N.-A.; Weidenthaler, C.; Schad, H., Field application of a tailored catalyst for hydrodechlorinating chlorinated hydrocarbon contaminants in groundwater. *Applied Catalysis B: Environmental* **2004,** *52* (3), 197-203.

55.	Davie, M. G.; Cheng, H.; Hopkins, G. D.; Lebron, C. A.; Reinhard, M., Implementing heterogeneous catalytic dechlorination technology for remediating TCE-contaminated groundwater. *Environmental science & technology* **2008,** *42* (23), 8908-8915.

56.	Tomar, M.; Abdullah, T. H., Evaluation of chemicals to control the generation of malodorous hydrogen sulfide in waste water. *Water Research* **1994,** *28* (12), 2545-2552.

57.	Liu, J.; Wu, D.; Su, X.; Han, M.; Kimura, S. Y.; Gray, D. L.; Shapley, J. R.; Abu-Omar, M. M.; Werth, C. J.; Strathmann, T. J., Configuration control in the synthesis of homo-and heteroleptic bis (oxazolinylphenolato/thiazolinylphenolato) chelate ligand complexes of oxorhenium (V): Isomer effect on ancillary ligand exchange dynamics and implications for perchlorate reduction catalysis. *Inorganic chemistry* **2016,** *55* (5), 2597-2611.

58.	Liu, J.; Han, M.; Wu, D.; Chen, X.; Choe, J. K.; Werth, C. J.; Strathmann, T. J., A new bioinspired perchlorate reduction catalyst with significantly enhanced stability via rational tuning of rhenium coordination chemistry and heterogeneous reaction pathway. *Environmental science & technology* **2016,** *50* (11), 5874-5881.

59.	Liu, J.; Su, X.; Han, M.; Wu, D.; Gray, D. L.; Shapley, J. R.; Werth, C. J.; Strathmann, T. J., Ligand design for isomer-selective oxorhenium (V) complex synthesis. *Inorganic chemistry* **2017,** *56* (3), 1757-1769.

Chapter 6. Conclusion

The overarching goal of this doctoral research is to design an effective, robust, and practical catalyst for aqueous ClO_4^- reduction. The insights gained through this work have advanced the understanding of (1) the stability of organometallic rhenium complexes and (2) the oxygen atom transfer activity of molybdate.

In **Chapter 2**, we investigated the structure-stability relationship of $Re^V(O)(L_{N-O})_2Cl$ complexes. We surprisingly found that the introduction of a methyl group on the ligand oxazoline moiety can achieve a substantial enhancement of catalyst stability without sacrificing the performance of the ClO_4^- reduction rate. The enhanced stability has been confirmed by kinetic measurements and X-ray photoelectron spectroscopy characterizations. The results from reaction modeling, stopped-flow photo spectrometry, and ^1H NMR spectra have revealed that the addition of a methyl group decelerates the oxygen atom transfer reaction from ClO_3^- to $[Re^V(O)(\mathbf{Me}hoz)_2]^+$ for two orders of magnitude. Furthermore, the modification on the oxazoline moiety allows the introduction of the methoxy group onto the phenolate to further accelerate ClO_4^- reduction. This study highlights the power of rational ligand design and has gained valuable insights into heterogeneous catalyst design.

Chapter 3 describes our initial attempts to employ an earth-abundant metal for oxyanion reductions. Because of the notorious kinetic inertness of ClO_4^-, direct application of Mo species to ClO_4^- reduction may lead to sluggish reaction kinetics. As a result, the individual difference of each precursor in reaction activity can be minified or overlooked.

Chlorate is an ideal probe for Mo precursor screening because of its moderate kinetic inertness. We have screened a series of commercially available molybdate precursors. It has been found that sodium molybdate can be rapidly immobilized from an aqueous solution onto the heterogeneous Pd/C support. The catalyst is ready for ClO_3^- reduction after 15 min of pretreatment. Compared to the virgin Pd/C catalyst, the addition of Mo not only enhances the catalytic activity by over 55-fold but also shows strong resistance to concentrate salts. Results indicate the potential of using relatively abundant metals for toxic oxyanion reduction.

With the heterogeneous platform built in **Chapter 3**, we describe a way to enhance the oxygen atom transfer activity of the Mo−Pd/C catalyst in **Chapter 4**. A variety of commercially available nitrogen ligands (**L**) were added with Na_2MoO_4 solution and Pd/C suspension under 1 atm of H_2. The catalysts ((**L**)MoO_x−Pd/C) prepared from this simple strategy are highly active for ClO_4^- reduction. The best catalyst has been shown effective to reduce a wide concentration range (10 μM to 0.1 M) of ClO_4^-. The initial turnover frequency of each Mo site reached 165 h^{-1}, which is the highest among all reported abiotic ClO_4^- reduction catalysts. The turnover number reached 3840 after a single batch reduction of 100 mM ClO_4^-. The XPS and Mo K-edge XANES results indicate that the active Mo species are mostly in the +4 oxidation state. Based on the fitting of EXAFS results, a dimeric structure was proposed for the active Mo sites. This work highlights a new strategy for designing bioinspired catalysts with common chemicals and simple preparation.

Having seen the excellence of the (**L**)MoO_x−Pd/C catalyst in the pure water matrix, in **Chapter 5**, we evaluate its performance in waste brines resulting from ion-exchange

resin regeneration. In synthetic brine, slight inhibition on reduction rate was observed, but all reactions were completed in a few hours. A common co-contaminant of ClO_4^-, NO_3^-, was identified to inhibit the catalyst severely. However, we demonstrated that a simple pretreatment of brine by In−Pd/Al_2O_3 can effectively prevent deactivation. We also assessed the stability of the catalyst under the high oxidation and reducing environment. No performance loss was observed after five spikes of 100 mM ClO_4^- reductions. In order to mimic the long-term continuous operation, the catalyst was kept under the reducing environment for up to 1000 hours. We found that the first-order rate constant quickly decreased to around 6% of its original value. The hydrogenation of organic ligand most likely causes the loss of activity, and we showcased that the used catalyst can be easily regenerated by sodium hydroxide solution at a pH of 12.

This doctoral research highlights the power of coordination chemistry in environmental technology innovation and has a series of broad impacts. The research findings provide a highly efficient and cost-effective ClO4− reduction technology for water and wastewater treatment for environmental engineering. For chemical science, ligand design rationales from **Chapters 2** and **4** will guide ongoing efforts to develop molybdenum and rhenium-based oxygen atom transfer catalysts for a wide range of reactions, including epoxidation and sulfoxidation, and biomass deoxygenation. For the water treatment industry, **Chapter 5** provides preliminary results pertaining to applying (**L**)MoO$_x$−Pd/C catalyst in the regeneration of the ion-exchange resin. Future works may focus on designing ligands that are more resistant to hydrogenation under the reaction condition and explore other earth-abundant metals for ClO_4^- reduction.

Appendix A

Supplementary Information for Chapter 2

Entry	Re–Pd/C catalyst (1 atm H_2, 20°C, pH 3.0, 0.5 g L^{-1}) (5 wt% Re in the same 5 wt% Pd/C)	k_{obs}	Single-run turnover number (TON)	Initial turnover frequency (TOF$_0$) [a] for ClO_4^-	TOF$_0$ for removing all four oxygens	Ref.
			1 mM ClO_4^-			
1	**Re(*hoz*)$_2$–Pd/C (1a')**	2.2 h^{-1}	30	16 h^{-1}	64 h^{-1}	this study [b]
2	**Re(Me*hoz*)$_2$–Pd/C (2a')**	2.2 h^{-1}	30	16 h^{-1}	64 h^{-1}	this study
3	**Re(MeO-Me*hoz*)$_2$–Pd/C (2b')**	3.7 h^{-1}	30	27 h^{-1}	108 h^{-1}	this study
4	**Re(*htz*)$_2$–Pd/C** [c]	0.51 h^{-1}	30	3.7 h^{-1}	15 h^{-1}	ref. [1]
5	**Re(*hoz*)(*htz*)–Pd/C**	1.0 h^{-1}	30	7.3 h^{-1}	29 h^{-1}	ref. [1]
6	ReO$_4$–Pd/C	0.014 h^{-1}	30	0.10 h^{-1}	0.41 h^{-1}	ref. [2] [d]
7	4-dimethylaminopyridine +**ReO$_4$–Pd/C**	0.32 h^{-1}	30	2.3 h^{-1}	9.3 h^{-1}	ref. [3] [e]
			10 mM ClO_4^-			
8	**Re(*hoz*)$_2$–Pd/C (1a')**	0.14 h^{-1}	300	10 h^{-1}	41 h^{-1}	this study [f]
9	**Re(Me*hoz*)$_2$–Pd/C (2a')**	1.4 h^{-1}	300	102 h^{-1}	407 h^{-1}	this study
10	**Re(MeO-Me*hoz*)$_2$–Pd/C (2b')**	1.5 h^{-1}	300	109 h^{-1}	436 h^{-1}	this study
11	**Re(*hoz*)(*htz*)–Pd/C**	0.13 h^{-1}	300	9.4 h^{-1}	38 h^{-1}	ref. [1]

Table S2.1 Performances of various Re−Pd/C catalysts for aqueous perchlorate reduction.

[a]Calculated using model-fit time for the degradation of the first 5% of ClO_4^-, see Experimental Section for details.

[b]The k measured in this study was slightly lower than the previously reported value (2.5 h^{-1}).[4]

[c]*Htz* is the analogous structure of *hoz*, with the thiazoline moiety replacing the oxazoline.

[d]The k was measured in this study to allow the comparison under the same reaction settings. The original report[2] used different catalyst loading, initial concentration of ClO_4^-, and solution pH.

[e]The molar ratio between DMAP ligand and Re was 2:1. The k was measured in this study. The original report used different catalyst loading, Re content, initial concentration of ClO_4^-, and solution pH.

[f]The k measured in this study was slightly lower than the previously reported value (0.22 h^{-1}).[1]

Entry	Reducing agent	Temp.	Loading of the reducing agent	$[ClO_4^-]_0$	pH	k_{obs} or percentage of reduction	Ref.
			Heterogeneous reduction				
1	Nano Fe^0	75°C	10 g L^{-1}	1 mM	6.0−8.0	0.056 h^{-1}	ref. [5 b]
2	CMC-stabilized nano Fe^0	110°C	1.8 g L^{-1}	0.1 mM	7.5−7.8	0.98 h^{-1}	ref. [6 c]
3	Iron filings (40 mesh)	r.t.	1.25 kg L^{-1}	0.1 mM	7.0−7.2	66% after 14 days	ref. [7 d]
4	Fe powder	150°C	14.5 g L^{-1}	0.1 mM	NA [e]	85% after 6 h	ref. [8 f]
5	Steel slag	200°C	85 g L^{-1}	0.1 mM	NA [e]	0.27 h^{-1}	ref. [9 g]
			Homogeneous reduction				
5	$FeCl_2$	195 °C	1.4 M	87 mM	4 M HCl	5.2 h^{-1}	ref. [10 h]
6	$TiCl_3$/β-alanine (1:3)	50 °C	40 mM Ti^{III}	1 mM	2.3	1.1 h^{-1}	ref. [11 i]

Table S2.2 Performances of other chemical systems for aqueous perchlorate reduction.[a]

[a]Limited by the scope of discussion, this table does not include early literature before 2000 on theoretical inorganic chemistry investigations or homogeneous ClO_4^- reduction systems in non-aqueous media.

[b]Kinetic data extracted from Figure 3 of the reference.[5]

[c]Kinetic data obtained from Table 2 of the reference.[6] CMC= carboxymethyl cellulose.

[d]Kinetic data obtained from Abstract of the reference.[7]

[e]Not available from the reference.

[f]Kinetic data obtained from Abstract of the reference.[8]

[g]Kinetic data obtained from Figure 3 of the reference.[9]

[h]Kinetic data obtained from Table 1 of the reference.[10]

[i]Kinetic data obtained from Figure 1 of the reference.[11]

Entry	Condition	Re^{VII}	Re^V	Re^{III}	Re^I
	KReO₄−Pd/C				
1	As prepared	ND	ND	8.5	91.5
	(KReO₄+*L4*)−Pd/C				
2	As prepared	15.0	ND	10.2	74.8
	1a−Pd/C (1a')				
3	As prepared	23.3	28.1	48.6	ND
4	After 10 mM ClO₄⁻ reduction	13.4	27.4	17.7	41.5
5	After 0.5 mM ClO₃⁻ reduction	25.7	25.7	14.1	34.6
6	After 1 mM ClO₃⁻ reduction	19.9	11.7	12.1	56.3
	2a−Pd/C (1b')				
7	As prepared	25.9	70.5	3.6	ND
8	After 10 mM ClO₄⁻ reduction	19.1	63.6	11.8	5.5
9	After 0.5 mM ClO₃⁻ reduction	26.1	65.1	8.8	ND
10	After 1 mM ClO₃⁻ reduction	26.9	41.2	14.4	17.6
	2b−Pd/C (2b')				
11	As prepared	14.5	70.4	8.3	6.8
12	After 10 mM ClO₄⁻ reduction	19.0	69.9	6.4	4.6
13	After 0.5 mM ClO₃⁻ reduction	30.1	62.3	4.7	2.9
14	After 1 mM ClO₃⁻ reduction	28.9	55.4	5.9	9.9

Table S2.3 Summary of XPS characterized relative abundance (%) of each Re species in Re−Pd/C catalysts.
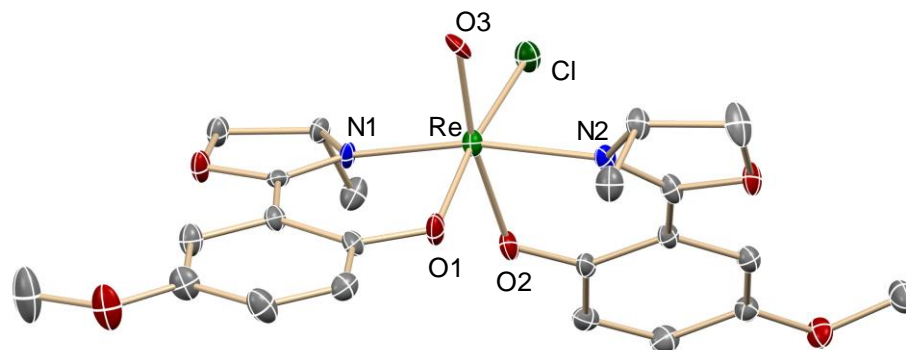
Figure S2.1 The molecular structure of complex **2b** by single crystallography analysis. Although multiple attempts were given to obtain better crystals, there were still problems with the collected data of the best crystal, which prevented further refinement. However, the *N,N-trans* configuration can be confirmed (also see the comparison of ^{1}H NMR data for **2a** and **2b** in **Figure 2.2b**).
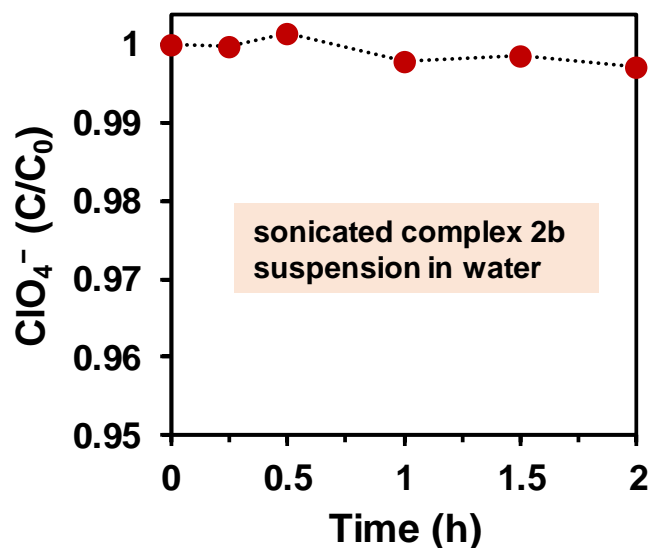
Figure S2.2 The negligible reduction (<0.3% after 2 h) of 1 mM ClO_4^- using suspended particles of Re complex **2b** (pH 3.0, 20°C, 1100 rpm stirring). Note that the y-axis starts from $C/C_0 = 0.95$. Before the addition of ClO_4^-, the complex **2b** in water was sonicated for 5 min and turned from as-prepared green powders into a milky suspension. The dose of Re is the same as used for 0.5 g L^{-1} of 5 wt% Re in Pd/C (i.e., 0.134 mM Re if fully dissolved).
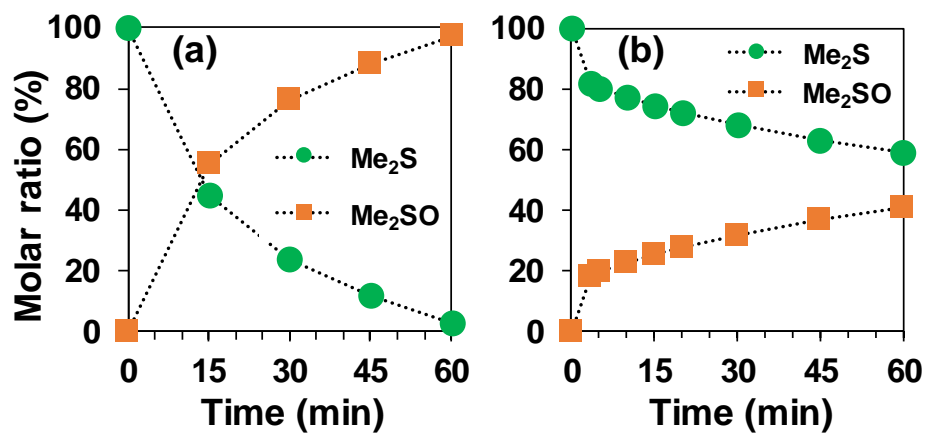
Figure S2.3 Homogeneous ClO_4^- reduction (as indicated by ^1H NMR-monitored Me_2S oxidation to Me_2SO) catalyzed with dissolved (a) **1a$^+$** and (b) **2a$^+$**. Reaction conditions: Re (4 mM), $LiClO_4$ (100 mM) and Me_2S (400 mM) in 95/5 (v/v) CD_3CN/D_2O at 25°C.
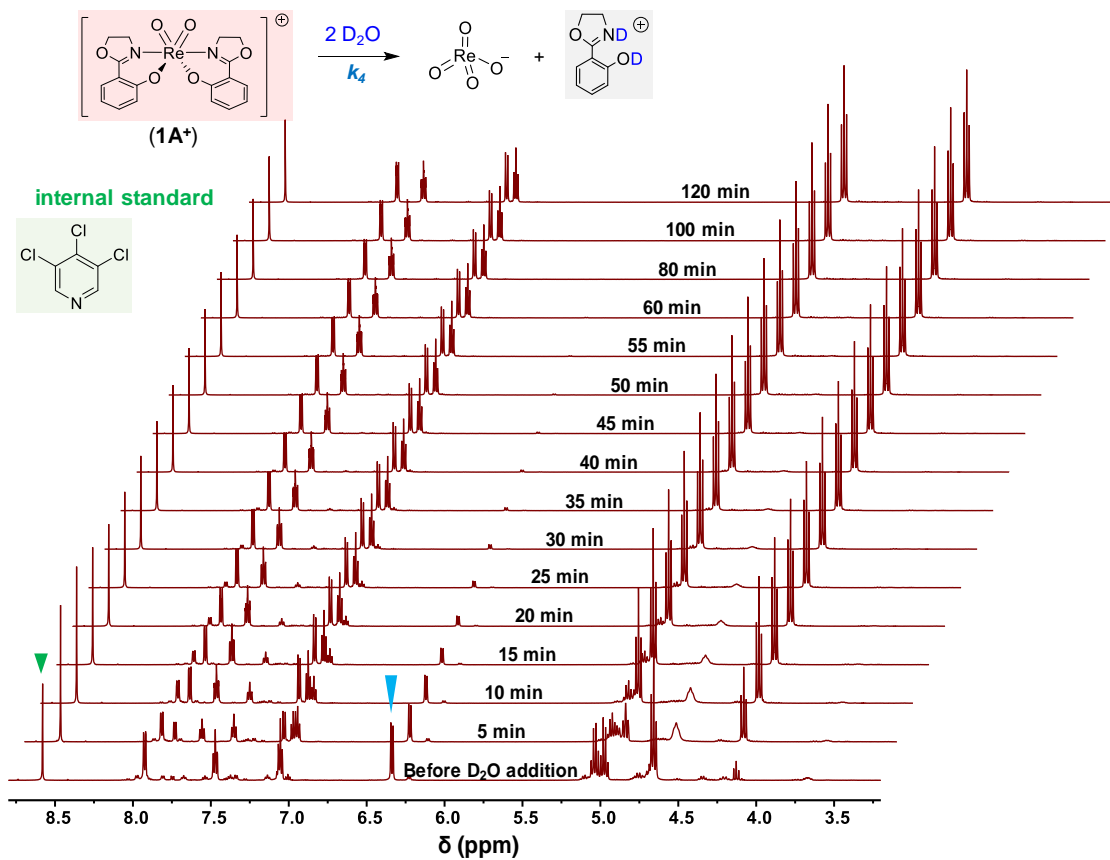
Figure S2.4 Time-dependent ^{1}H NMR (600 MHz) spectra for the hydrolysis of **1A$^+$** (10 mM) in 5/95 (v/v) D$_2$O/CD$_3$CN at 20°C. The resonance indicated by the blue arrow was used for quantitation shown in **Figure 2.7a**.
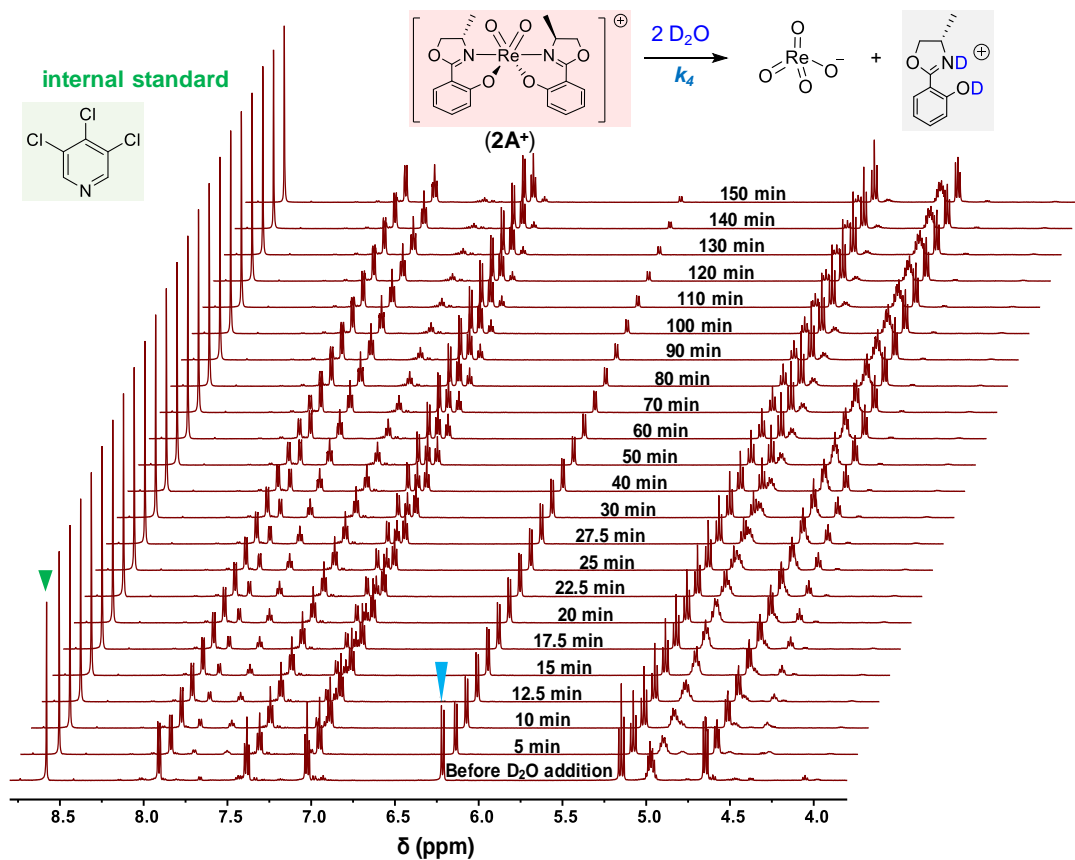
Figure S2.5 Time-dependent ^{1}H NMR (600 MHz) spectra for the hydrolysis of **2A$^+$** (10 mM) in 5/95 (v/v) D$_2$O/CD$_3$CN at 20°C. The resonance indicated by the blue arrow was used for quantitation shown in **Figure 2.7a**.
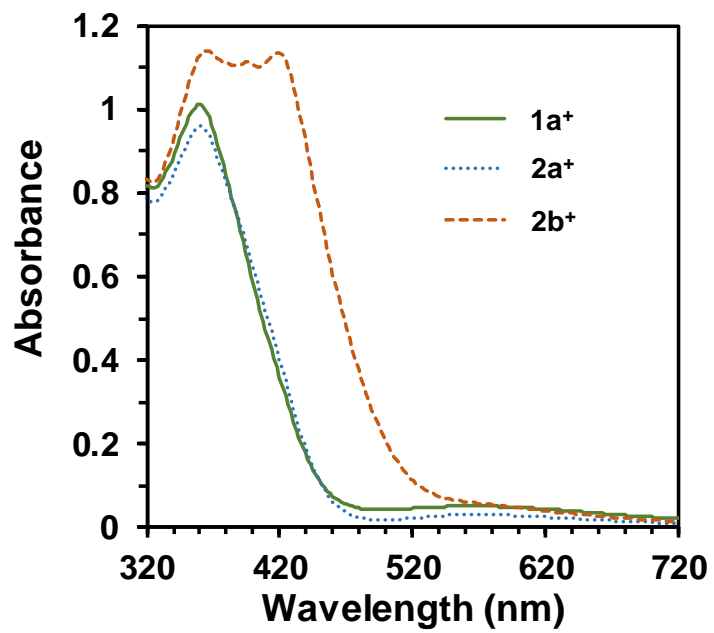
Figure S2.6 UV-vis absorbance of 0.5 mM **1a**$^+$, **2a**$^+$, and **2b**$^+$ in anhydrous CH$_3$CN.
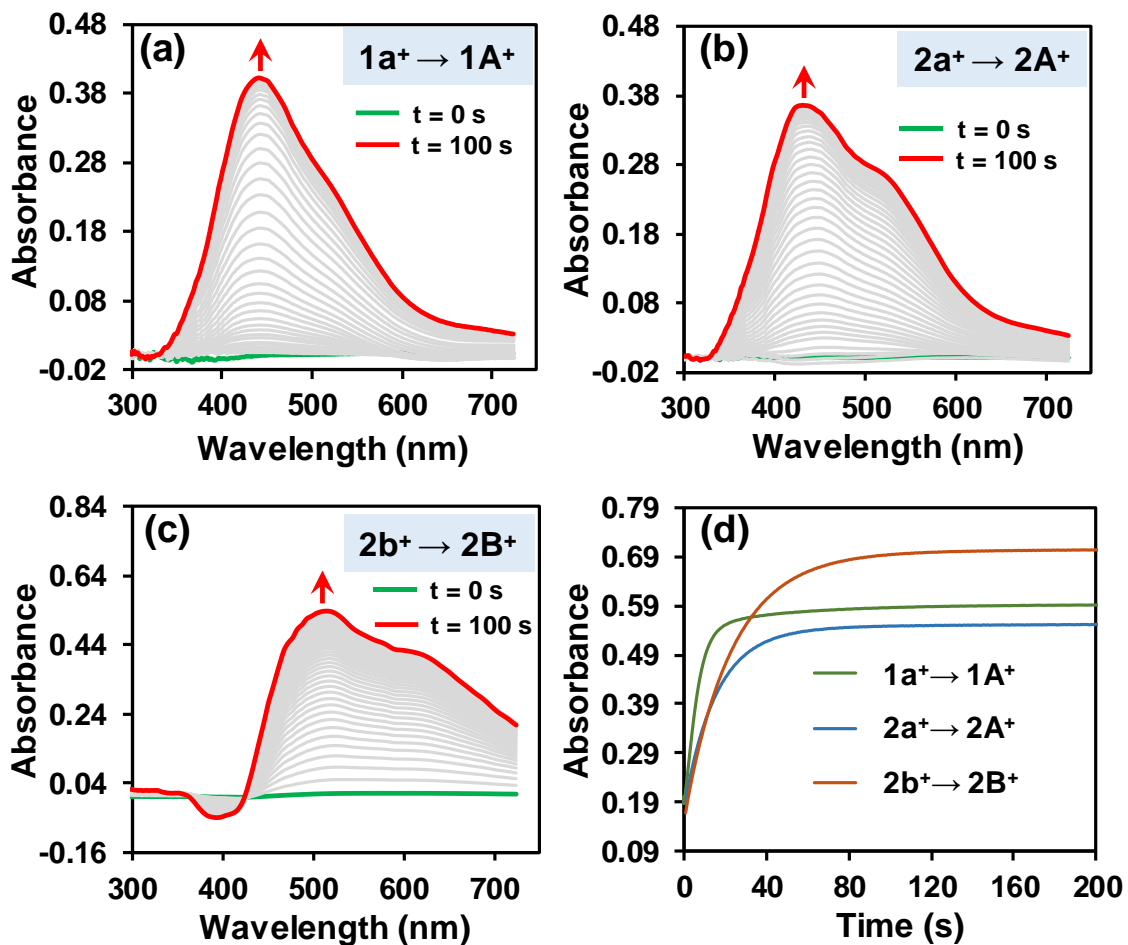
Figure S2.7 (a–c) The change of UV-vis absorption (i.e., by subtracting the initial t = 0 spectrum from all spectra) during the oxidation of 0.5 mM **1a$^+$**, **2a$^+$**, and **2b$^+$** by 25 mM LiClO$_4$ in anhydrous CH$_3$CN; (d) time profiles of the absorption change at individual λ_{max} for the oxidation of 0.5 mM **1a$^+$**, **2a$^+$**, and **2b$^+$** by 50 mM LiClO$_4$ in anhydrous CH$_3$CN.
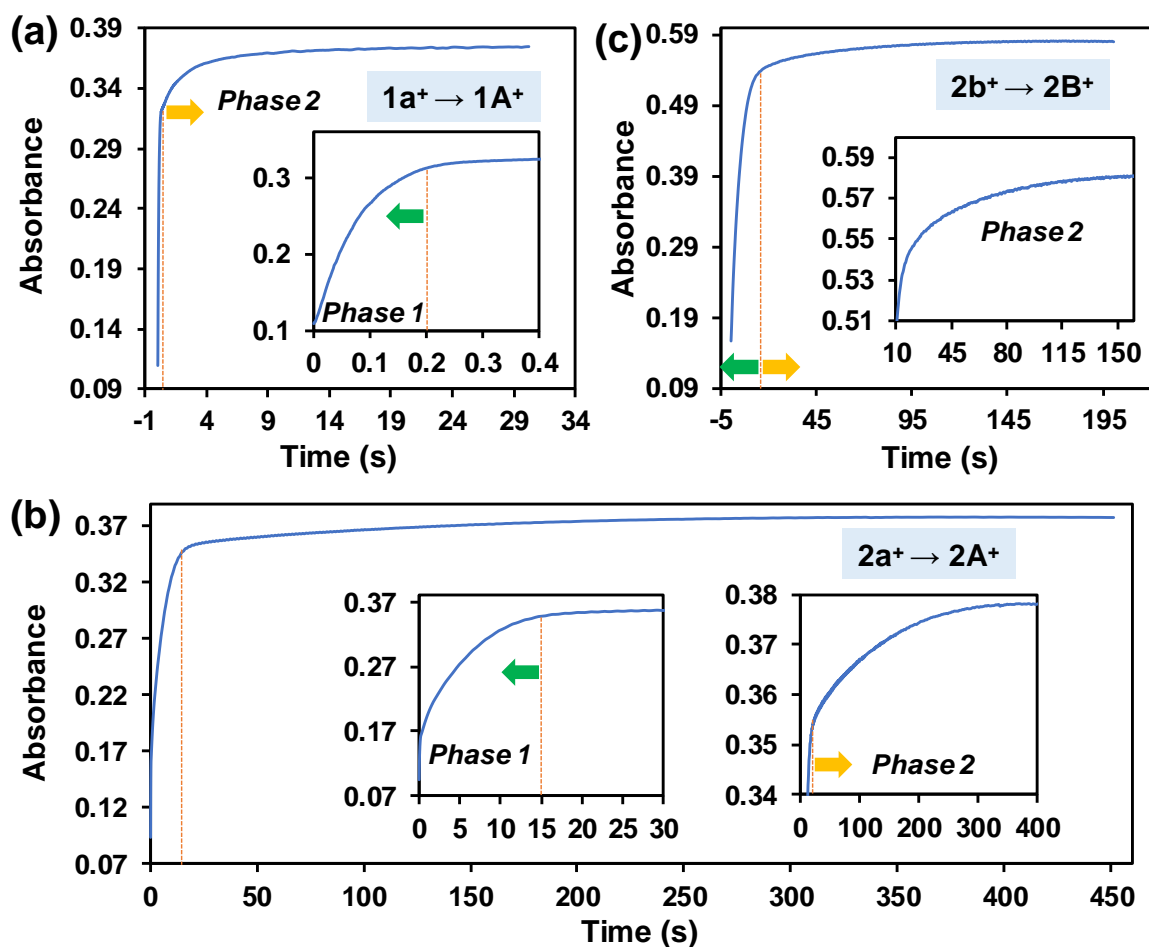
Figure S2.8 Two-phase time profiles for the oxidation of 0.5 mM **1a⁺**, **2a⁺**, and **2b⁺** complexes by 25 mM NaClO₃ in 95/5 (v/v) CH₃CN/H₂O. Insert shows the first or second phase of the reactions.
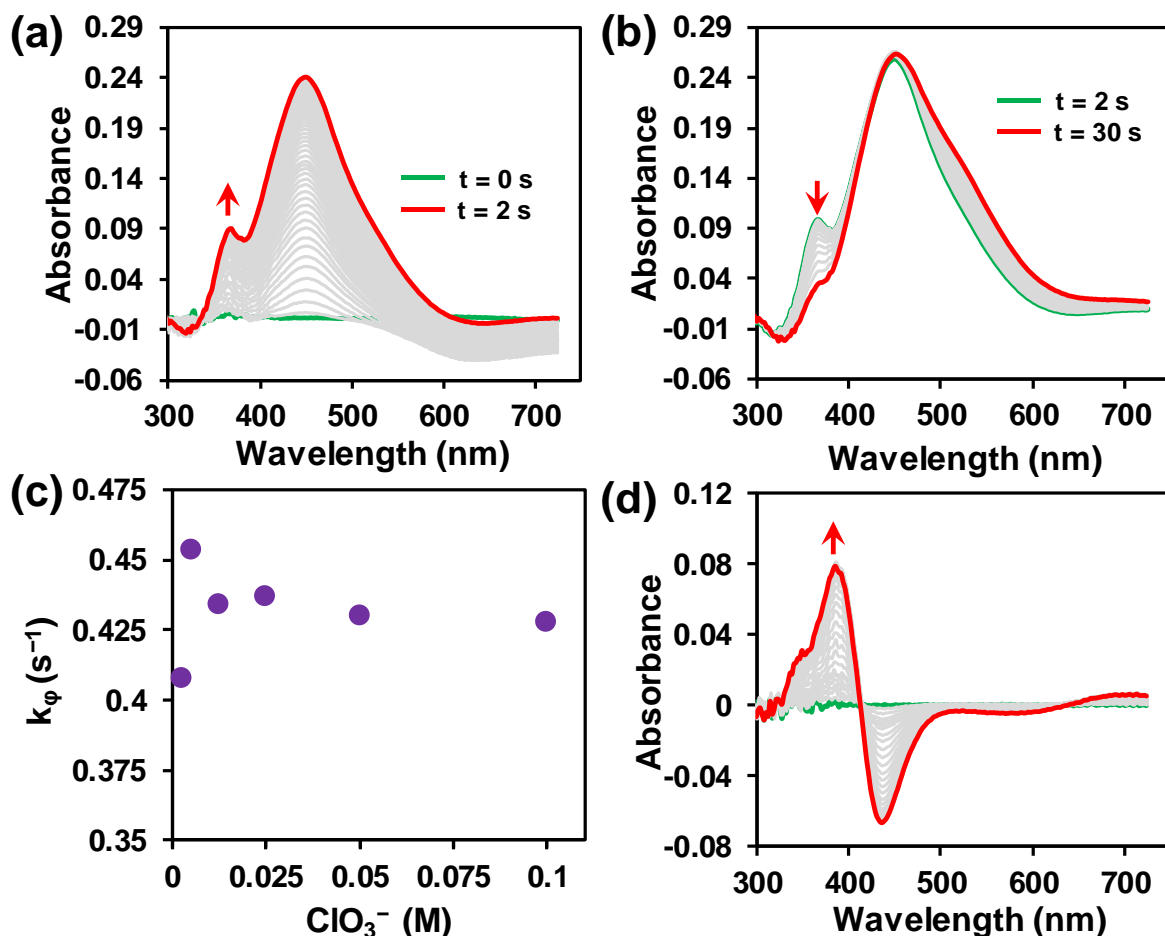
Figure S2.9 The change of UV-vis absorption during (a) the first phase and (b) the second phase during the oxidation of 0.5 mM **1a**$^+$ by 25 mM NaClO$_3$; (c) measured initial rate constants *from the second reaction phase* during the oxidation of 0.5 mM **1a**$^+$ by 25 mM NaClO$_3$ in 95/5 (v/v) CH$_3$CN/H$_2$O; (d) the change of UV-vis absorption of 0.5 mM **1a**$^+$ upon addition of 0.5 mM LiCl in anhydrous CH$_3$CN. Compared to the first reaction phase data shown in Figure 7d, the much lower reaction rate and the insensitivity to varying ClO$_3^-$ concentrations in panel c suggest a low reactivity of chloride-bound Re^V(O)(L_{N-O})$_2$Cl. The absorption spectra in panel d support the formation of Re^V(O)(L_{N-O})$_2$Cl due to the rapid generation of Cl$^-$ from ClO$_3^-$.
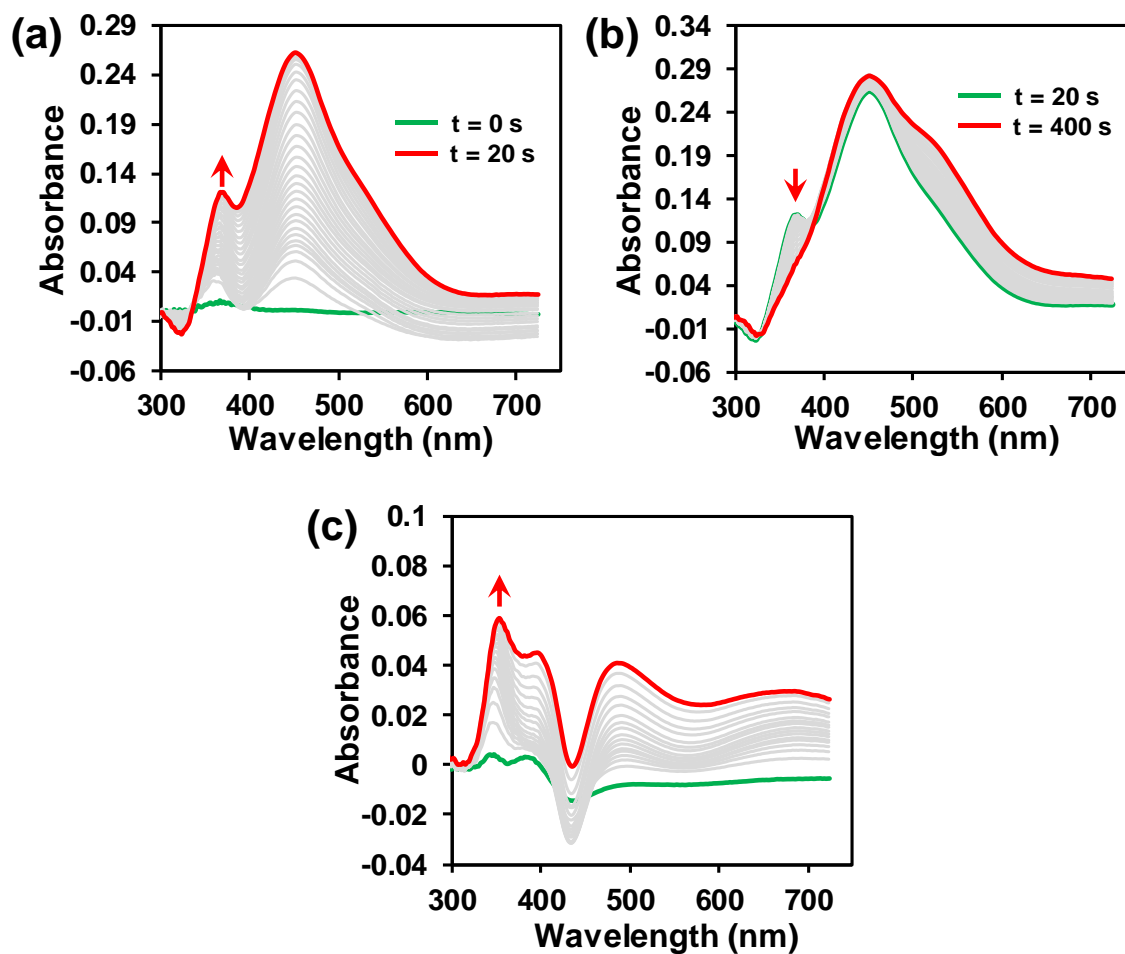
Figure S2.10 The change of UV-vis absorption during (a) the first phase and (b) the second phase during the oxidation of 0.5 mM **2a**$^+$ by 25 mM NaClO$_3$ in 95/5 (v/v) CH$_3$CN/H$_2$O; (c) the change of UV-vis absorption of 0.5 mM **1a**$^+$ upon addition of 0.5 mM LiCl in anhydrous CH$_3$CN.
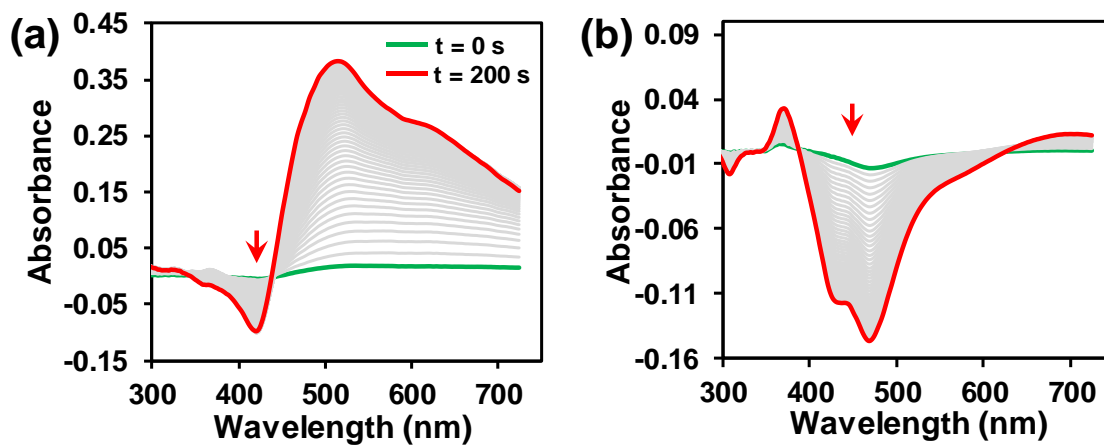
Figure S2.11 The change of UV-vis absorption during the oxidation of 0.5 mM **2b⁺** by 25 mM $NaClO_3$ in 95/5 (v/v) CH_3CN/H_2O; (b) the change of UV-vis absorption of 0.5 mM **2b⁺** upon addition of 0.5 mM LiCl in anhydrous CH_3CN.

Text S2.1. Derivation of the quasi-steady-state Eq. 2.1 in the main text.

Scheme 2.1 in the main text shows the key reaction steps for modeling the hydrolytic decomposition of $[Re^{VII}(O)_2(L_{N-O})_2]^+$ during ClO_x^- reduction. Additional steps such as chloride binding to **4** and the reduction of **7** into Re^I species are not included. The rate of hydrolytic decomposition (r_4) is defined by

$$r_4 = \frac{d[\mathbf{7}]}{dt} = k_4[\mathbf{6}] \tag{S2.1}$$

where $[number]$ represents the concentration of the corresponding Re species at any given time. Because the oxygen atom transfer (OAT) reaction between ClO_4^- and Re^V is the rate-limiting step, the quasi-steady-state approximation is applied to species **4** and **5**. The time-dependent evolution of these species is expressed as

$$\frac{d[\mathbf{4}]}{dt} = k_3[\mathbf{6}] + k_{-1}[\mathbf{5}][Solv] - k_1[\mathbf{4}][XO] = 0 \tag{S2.2}$$

$$\frac{d[\mathbf{5}]}{dt} = k_1[\mathbf{4}][XO] - k_2[\mathbf{5}] - k_{-1}[\mathbf{5}][XO] = 0 \tag{S2.3}$$

where $[XO]$ represents the concentration of the oxidant (e.g., ClO_4^- and ClO_3^-) and $[Solv]$ denotes the concentration of the solvent, which is assumed to be unity. At the beginning of the reaction, the following conservation law holds for the total amount of Re species ($[Re]_T$)

$$[Re]_T \approx [\mathbf{4}] + [\mathbf{5}] + [\mathbf{6}] \tag{S2.4}$$

From **Eq. S2.2** and **Eq. S2.3**, $[\mathbf{4}]$ and $[\mathbf{5}]$ can be expressed with respect to $[\mathbf{6}]$ by

$$[\mathbf{5}] = \frac{k_3}{k_2}[\mathbf{6}] \tag{S2.5}$$

$$[\mathbf{4}] = \left(\frac{k_{-1} + k_2}{k_1 k_2}\right)\frac{k_3}{[XO]}[\mathbf{6}] \tag{S2.6}$$

Substitution of **Eq. S2.5** and **Eq. S2.6** into **Eq. S2.4** affords the relation between $[Re]_T$ and $[\mathbf{6}]$

$$\begin{aligned}[Re]_T &= \left(\frac{k_{-1} + k_2}{k_1 k_2}\right)\frac{k_3}{[XO]}[\mathbf{6}] + \frac{k_3}{k_2}[\mathbf{6}] + [\mathbf{6}] \\ &= \frac{k_3}{k_2}[\mathbf{6}]\left(\left(\frac{k_{-1} + k_2}{k_1 k_2}\right)\frac{k_2}{[XO]} + 1 + \frac{k_2}{k_3}\right) \end{aligned} \tag{S2.7}$$

Since we assume that the OAT reaction is the rate-limiting step (i.e., $k_2 \ll k_3, k_1$, and k_{-1}), the last term in the parentheses of **Eq. S2.7**, $\frac{k_2}{k_3}$, is approximately zero, and **Eq. S2.7** can be further simplified to

$$[Re]_T = \frac{k_3}{k_2}[\mathbf{6}]\left(\frac{k_1[XO] + k_{-1} + k_2}{k_1[XO]}\right) \tag{S2.8}$$

Similarly, k_2 can be removed from the equation as it is small compared to other rate constants. Therefore, **Eq. S2.8** is converted to

$$[Re]_T = \frac{k_3}{k_2}[\mathbf{6}]\left(\frac{K_1[XO] + 1}{K_1[XO]}\right) \tag{S2.9}$$

where $K_1 = k_1/k_{-1}$ is the equilibrium constant.

Finally, the decomposition rate (r_4) can be expressed in terms of $[Re]_T$ by substituting **Eq. S2.9** into **Eq. S2.1**.

$$r_4 = \frac{d[7]}{dt} = \frac{k_2 k_4}{k_3}\left(\frac{K_1[XO]}{K_1[XO]+1}\right)[Re]_T \qquad\qquad (S2.10)$$

For most cases discussed in this study, $[XO]$ is relatively low (i.e., $[XO]$ is much lower than 1 M). Thus, **Eq. S2.10** is further simplified by assuming $K_1[XO] \ll 1$.

$$r_4 = \frac{d[7]}{dt} = -\frac{d[6]}{dt} = \frac{K_1 k_2 k_4}{k_3}[XO][Re]_T \qquad\qquad (S2.11)$$

Eq. S2.11 is **Eq. 2.1** in the main text.

Test S2.2. Derivation of the non-steady-state Eq. 2.2 in the main text.

In the single-turnover stopped-flow experiments, the reaction terminates at $[Re^{VII}(O)_2(L_{N-O})_2]^+$. The concentration variation of $[Re^{VII}(O)_2(L_{N-O})_2]^+$ with respect to time is expressed as

$$\frac{d[6]}{dt} = k_2[5] \qquad\qquad (S2.12)$$

At the beginning of the reaction, we assume that species **4** is in pre-equilibrium with **5**, and the concentration of **6** is close to zero. Therefore, the following equations are valid.

$$K_1 = \frac{k_1}{k_{-1}} = \frac{[5][Solv]}{[4][XO]} \qquad\qquad (S2.13)$$

$$[Re]_T \approx [4] + [5] \qquad\qquad (S2.14)$$

where $K_1 = k_1/k_{-1}$ is the equilibrium constant and $[Solv]$ is assumed to be unity. Based on **Eq. S2.13** and **S2.14**, $[Re]_T$ is related to **5** by

$$[Re]_T = \left(\frac{K_1[XO] + 1}{K_1[XO]}\right) [5] \qquad (S2.15)$$

The combination of **Eq. S2.15** into **Eq. S2.12** yields

$$\frac{d[6]}{dt} = \frac{K_1 k_2 [XO][Re]_T}{1 + K_1[XO]} \qquad (S2.16)$$

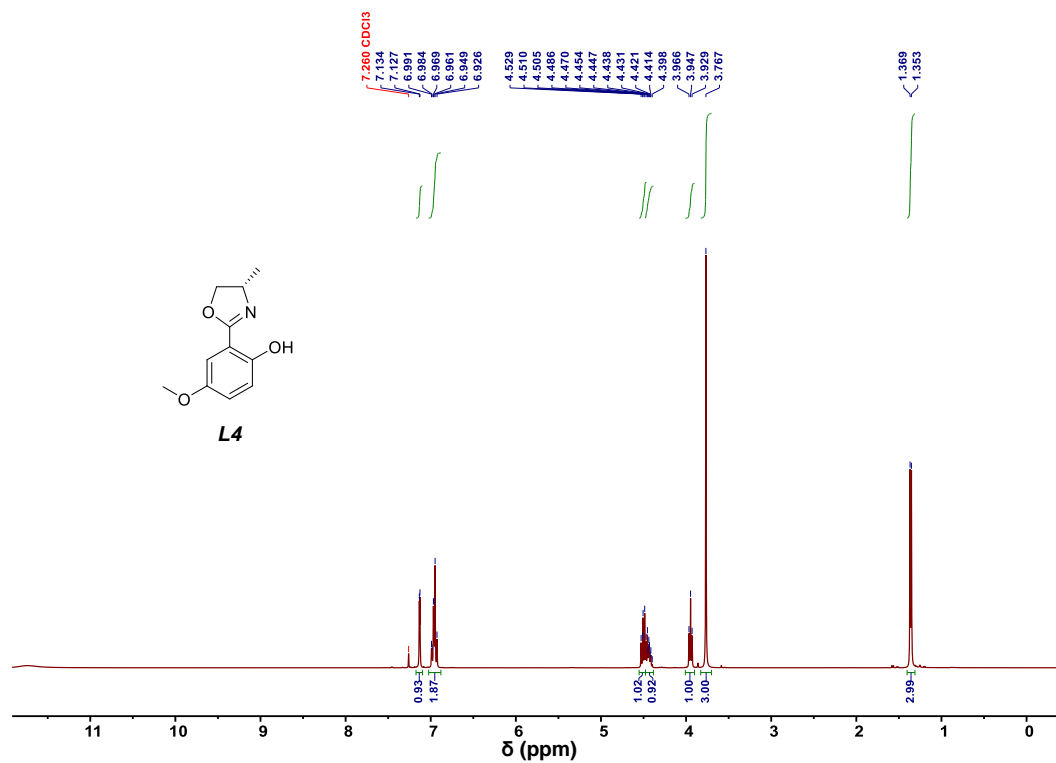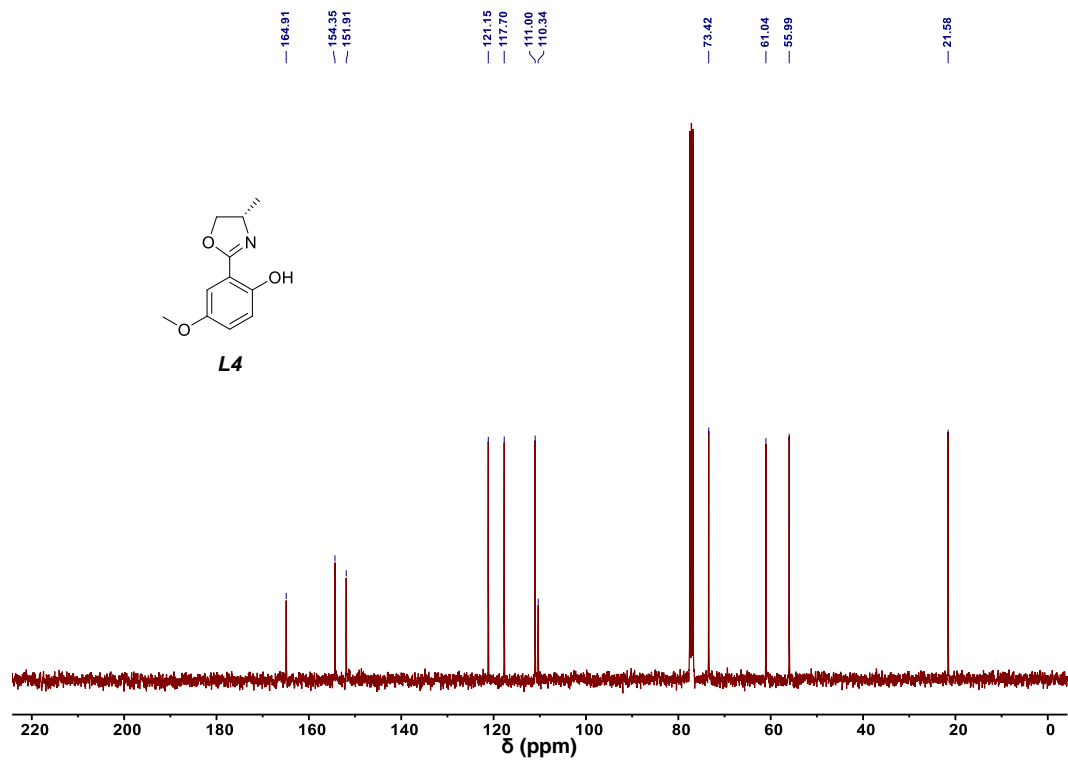**Eq. S2.16** is **Eq. 2.2** in the main text.
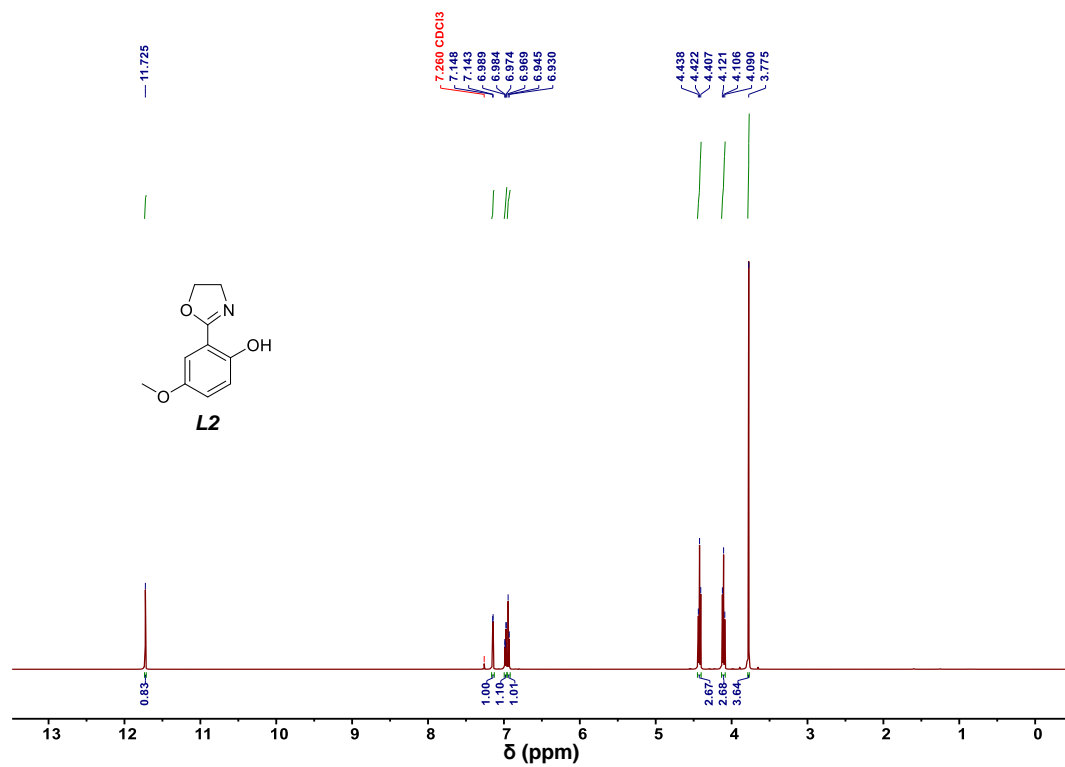
Figure S2.12 ^{1}H NMR (600 MHz, CDCl$_3$) spectrum of H*hoz*(5MeO) (**L2**).
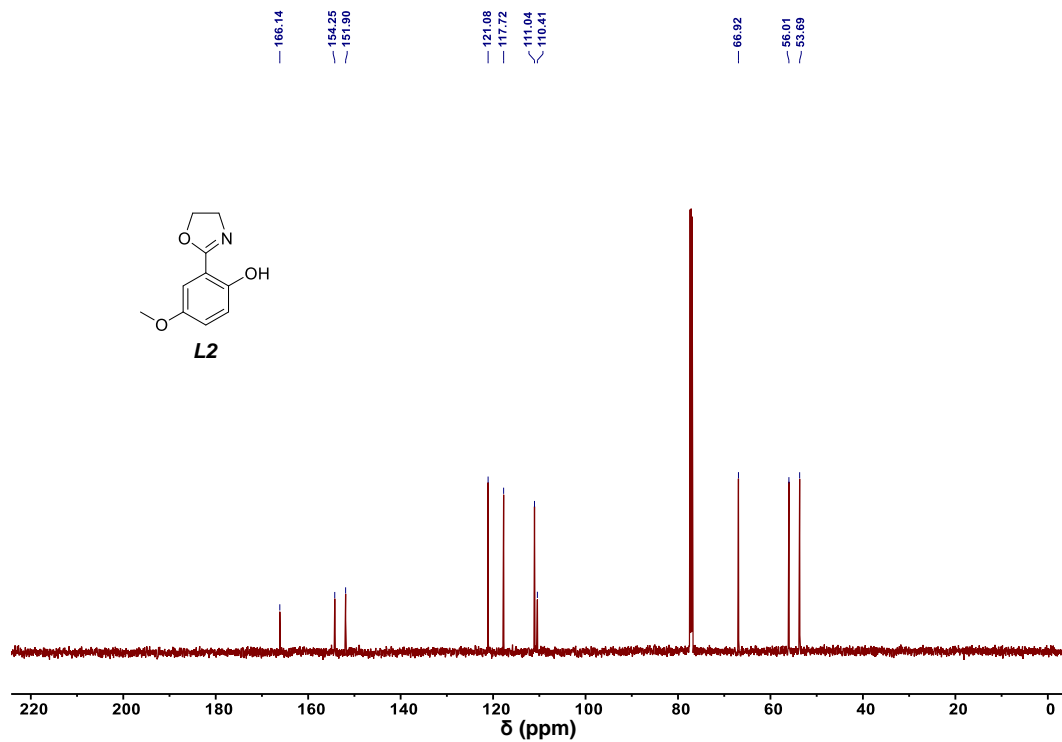
Figure S2.14. ^{13}C NMR (151 MHz, CDCl$_3$) spectrum of H*hoz*(5MeO) (**L2**).

Figure S2.13 ^{1}H NMR (400 MHz, CDCl$_3$) spectrum of HMe*hoz*(5MeO) (**L4**).

Figure S2.15 ^{13}C NMR (101 MHz, CDCl$_3$) spectrum of HMe*hoz*(5MeO) (*L4*).
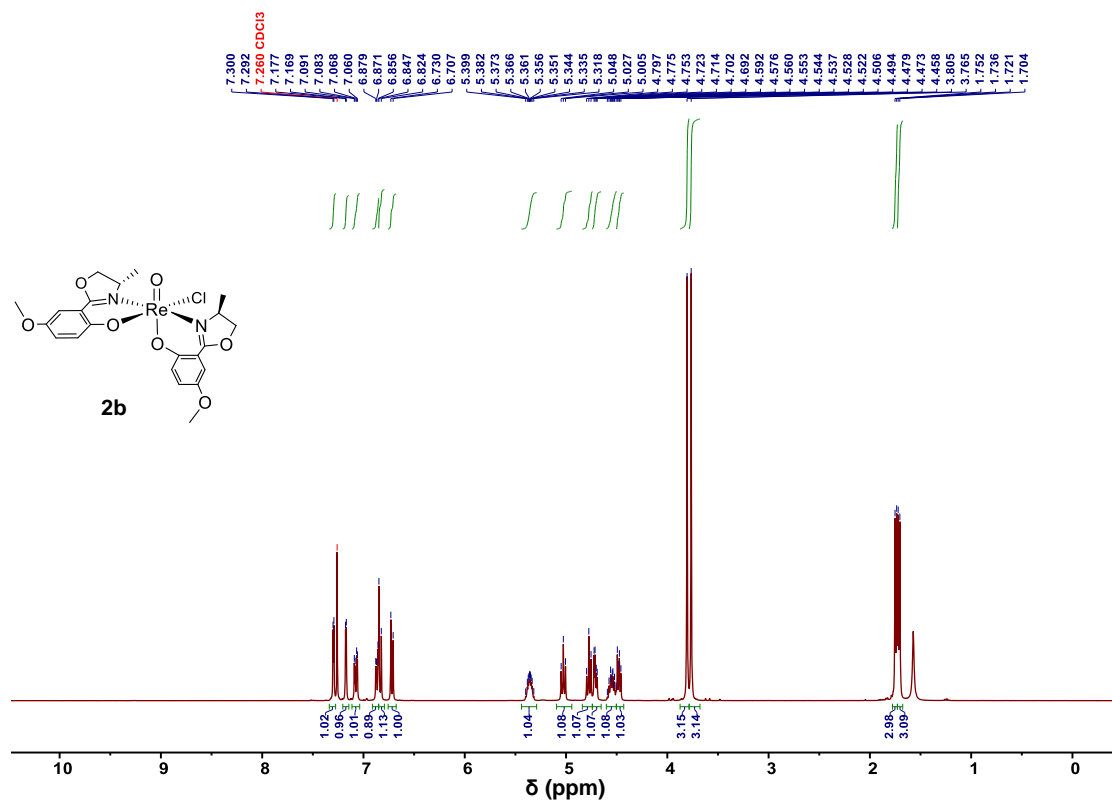
Figure S2.16 ^{1}H NMR (400 MHz, CDCl$_3$) spectrum of Re(O)[Me*hoz*(5MeO)]$_2$Cl (**2b**).

References

1.	Liu, J.; Han, M.; Wu, D.; Chen, X.; Choe, J. K.; Werth, C. J.; Strathmann, T. J. A new bioinspired perchlorate reduction catalyst with significantly enhanced stability via rational tuning of rhenium coordination chemistry and heterogeneous reaction pathway. *Environ. Sci. Technol.* **2016**, *50*, 5874-5881.

2.	Hurley, K. D.; Shapley, J. R. Efficient heterogeneous catalytic reduction of perchlorate in water. *Environ. Sci. Technol.* **2007**, *41*, 2044-2049.

3.	Hurley, K. D.; Zhang, Y.; Shapley, J. R. Ligand-enhanced reduction of perchlorate in water with heterogeneous Re−Pd/C catalysts. *J. Am. Chem. Soc.* **2009**, *131*, 14172-14173.

4.	Liu, J.; Choe, J. K.; Wang, Y.; Shapley, J. R.; Werth, C. J.; Strathmann, T. J. Bioinspired complex-nanoparticle hybrid catalyst system for aqueous perchlorate reduction: Rhenium speciation and its influence on catalyst activity. *ACS Catal.* **2015**, *5*, 511-522.

5.	Cao, J.; Elliott, D.; Zhang, W.-X. Perchlorate reduction by nanoscale iron particles. *J. Nanopart. Res.* **2005**, *7*, 499-506.

6.	Xiong, Z.; Zhao, D.; Pan, G. Rapid and complete destruction of perchlorate in water and ion-exchange brine using stabilized zero-valent iron nanoparticles. *Water Res.* **2007**, *41*, 3497-3505.

7.	Moore, A. M.; De Leon, C. H.; Young, T. M. Rate and extent of aqueous perchlorate removal by iron surfaces. *Environ. Sci. Technol.* **2003**, *37*, 3189-3198.

8.	Hori, H.; Sakamoto, T.; Tanabe, T.; Kasuya, M.; Chino, A.; Wu, Q.; Kannan, K. Metal-induced decomposition of perchlorate in pressurized hot water. *Chemosphere* **2012**, *89*, 737-742.

9.	Hori, H.; Kamijo, A.; Inoue, M.; Chino, A.; Wu, Q.; Kannan, K. Efficient decomposition of perchlorate to chloride ions in subcritical water by use of steel slag. *Environ. Sci. Pollut. Res.* **2018**, *25*, 7262-7270.

10.	Gu, B.; Dong, W.; Brown, G. M.; Cole, D. R. Complete degradation of perchlorate in ferric chloride and hydrochloric acid under controlled temperature and pressure. *Environ. Sci. Technol.* **2003**, *37*, 2291-2295.

11.	Wang, C.; Huang, Z.; Lippincott, L.; Meng, X. Rapid Ti(III) reduction of perchlorate in the presence of β-alanine: Kinetics, pH effect, complex formation, and β-alanine effect. *J. Hazard. Mater.* **2010**, *175*, 159-164.

Appendix B

Supplementary Information for Chapter 3

Evaluation of Internal Mass Transfer

For heterogeneous catalytic reactions, the Weisz-Prater Criterion is commonly used to evaluate the effect of pore diffusion on the measured reaction rates.[1-2] Weisz-Prater parameter (C_{WP}) is defined as

$$C_{WP} = \frac{k_{obs}\tau R^2}{D\theta} \qquad (Eq. S3.1)$$

where k_{obs} is the observed pseudo-first-order rate constant of heterogeneous reaction (min^{-1}), R is the radius of the catalyst particle (m), τ is the tortuosity factor of the catalyst particle, θ is the porosity of the catalyst particle, and D is the diffusion coefficient of reactant in bulk solution ($m^2 s^{-1}$).

The C_{WP} of MoO$_x$–Pd/C was evaluated by choosing the largest k_{obs} from this study ($0.115\ min^{-1}$) and $37\ \mu m$ as the diameter of the catalyst particle because the commercial Pd/C powder was filtered through a 400 mesh sieve before use.[3] The parameters τ and θ typically vary in the range of 2−10 and 0.2−0.7, respectively.[4-5] To conservatively estimate C_{WP}, we choose $\tau = 10$ and $\theta = 0.2$, as these values lead to a smaller internal mass transfer rate than what is calculated from $\tau = 2$ and $\theta = 0.7$. The diffusion coefficient of ClO$_3^-$ ($D_{ClO_3^-}$) is $1.5 \times 10^{-9}\ m^2 s^{-1}$ in bulk solution.[6] Thus the Weisz-Prater parameter was calculated as

$$C_{WP} = \frac{k_{obs}\tau R^2}{D\theta} = \frac{0.115\ min^{-1} \times 10 \times \left(\frac{37}{2} \times 10^{-6}\ m\right)^2}{1.5 \times 10^{-9}\ m^2\ s^{-1} \times 60\ s\ min^{-1} \times 0.2} = 0.02 < 1 \quad (Eq. S3.2)$$

The calculated C_{WP} for MoO$_x$−Pd/C is 0.02, which is much less than 1, suggesting that the internal mass transfer limitation is negligible.

Evaluation of External Mass Transfer

We applied a correlation (**Eq. S3.3**) derived from Kolmogoroff's theory for agitated and aerated particle suspensions:[7-8]

$$Sh = \left[2 + 0.4 \left(\frac{\varepsilon d_p^4}{\nu^3} \right)^{0.25} Sc^{0.33} \right] \cdot \phi_c \qquad (Eq.\,S3.3)$$

where Sh is Sherwood number, Sc is Schmidt number, ϕ_c is Carman's surface factor (assume the catalyst particle is spherical, $\phi_c = 1$), ν is the kinematic viscosity of water ($\nu_{H_2O} = 1.003 \times 10^{-6}\ m^2 s^{-1}$ at 20°C), d_p is the diameter of catalyst particle (m), and ε is the rate of flow energy supply per unit mass of liquid ($m^2 s^{-3}$). The model does not require the measurement of the relative velocity between the particle and the fluid, which is not readily available for heterogeneous systems. To apply the above correlation, we evaluated Sc and ε with the following equation:

$$Sc = \frac{\nu_{H_2O}}{D_{ClO_3^-}} = \frac{1.003 \times 10^{-6}\ m^2\ s^{-1}}{1.5 \times 10^{-9}\ m^2\ s^{-1}} = 668.67 \qquad (Eq.\,S3.4)$$

For agitated reactors, ε was calculated with the following equation:

$$\varepsilon = \frac{N_p \cdot l^5 \cdot n^3}{V} \qquad (Eq.\,S3.5)$$

where N_p is power number (normally $N_p \approx 5.0$),[9] l is the diameter of the stir bar ($l \approx 3\ cm$), n is the rotating speed of the stir bar ($n = 1600\ round\ min^{-1} = 27\ round\ s^{-1}$), and V is the volume of the reactor ($V = 50\ cm^3$). Thus, ε was calculated as

$$\varepsilon = \frac{N_p \cdot l^5 \cdot n^3}{V} = \frac{5 \times (3\ cm)^5 \times (27\ s^{-1})^3}{50\ cm^3} = 48\ m^2\ s^{-3} \qquad (Eq.\,S3.6)$$

With the values obtained from **Eq. S3.4** and **Eq. S3.6**, the Sherwood number was

calculated as

$$Sh = \left[2 + 0.4 \left(\frac{48\ m^2\ s^{-3} \times (3.7 \times 10^{-5}\ m)^4}{(1.003 \times 10^{-6}\ m^2\ s^{-1})^3}\right)^{0.25} 668.67^{0.33}\right] \cdot 1 = 12.5$$

Next, the aqueous/solid mass transfer coefficient ($k_{aq/s}$) was estimated by **Eq. S3.7**:

$$k_{aq/s} = \frac{D_{ClO_3^-}}{d_p} \cdot Sh = \frac{1.5 \times 10^{-9}\ m^2\ s^{-1}}{3.7 \times 10^{-5}\ m} \times 12.5 = 5.1 \times 10^{-4}\ m\ s^{-1} \qquad (Eq.\,S3.7)$$

The geometric surface area of the catalyst per volume of solution (a) was calculated

by **Eq. S3.8**:[10]

$$a = \frac{total\ surface\ area}{total\ volume} = \frac{SA_p \times M}{\rho_p \times V_p} \times \frac{1}{V_R} \qquad (Eq.\,S3.8)$$

in which SA_p is the geometric surface area of one catalyst particle (m^2), M is the mass of

catalyst in the reduction test ($0.01\ g$), V_p is the volume of one catalyst particle (m^3), and

V_R is the volume of the reactor ($50\ mL$).

$$a = \frac{4\pi \times (18.5 \times 10^{-6}\ m)^2 \times 0.01\ g}{2 \times 10^6\ g\ m^{-3} \times \frac{4\pi}{3}(18.5 \times 10^{-6}\ m)^3} \times \frac{1}{50 \times 10^{-6}\ m^3} = 16.22\ m^{-1}$$

The mass transfer rate was then calculated by multiplying the mass transfer

coefficient by the geometric surface area of the catalyst per volume of the solution:

$$k_{aq/s} \cdot a = 5.1 \times 10^{-4} \; m \; s^{-1} \times 16.22 \; m^{-1} = 82.72 \times 10^{-4} \; s^{-1} = 0.5 \; min^{-1} \quad (Eq. S3.9)$$

This estimated external mass transfer rate was larger than the observed rate constant for ClO_3^- reduction ($k_{obs} = 0.115 \; min^{-1}$). Therefore, the reaction rate exhibited by the MoO_x−Pd/C catalyst in our reactor settings is less likely limited by the external mass transfer.

Fitting Method	Shell	CN[a]	R (Å)[b]	σ² (Å²)[c]	ΔE (eV)[d]	R-factor
1	Mo−O	0.7 (3.4)	1.602 (0.228)	0.0003 (0.033)		
	Mo−O	2.7 (5.6)	1.927 (0.088)	−0.0009 (0.024)	−12.4 (7.6)	0.009
	Mo−Pd	1.3 (4.1)	1.919 (0.113)	0.004 (0.030)		
	Mo−Mo	2.0 (2.0)	2.534 (0.025)	0.006 (0.006)		
2	Mo−O	51.8 (249.1)	1.495 (0.134)	0.064 (0.089)		
	Mo−Pd	12.2 (9.0)	1.849 (0.012)	0.024 (0.006)	−16.5 (2.7)	0.013
	Mo−Mo	2.2 (0.6)	2.525 (0.009)	0.006 (0.001)		
3	**Mo−Pd**	11.4 (3.2)	1.827 (0.014)	0.023 (0.003)	−21.9 (2.2)	0.045
	Mo−Mo	1.7 (0.7)	2.509 (0.009)	0.005 (0.002)		

Table S3.1 Mo K-edge EXAFS Shell-by-shell Fitting Parameters of MoO$_x$−Pd/C Using a Mo−Pd Shell. Values Highlighted in Red Color and Gray Shade are Problematic.
[a]Coordination number; [b]Interatomic distance; [c]Debye-Waller factor; [d]Energy shifts.
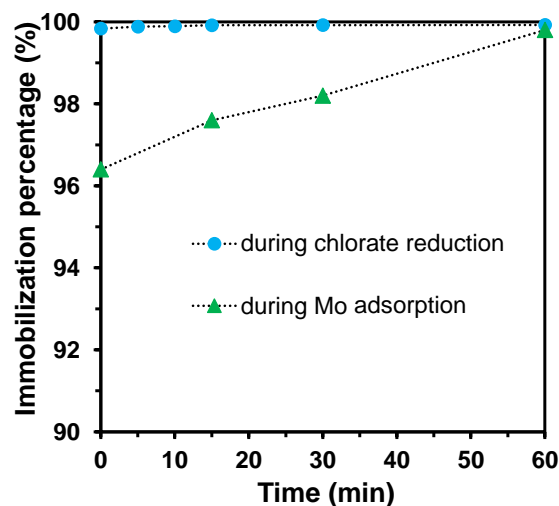
Figure S3.1 The percentage of Mo immobilized in the Pd/C support upon the addition of Na_2MoO_4 precursor into the Pd/C suspension under 1 atm H_2 (i.e., "during Mo adsorption") and during the reduction of 1 mM ClO_3^-. Note that the y-axis starts from 90%. Reaction conditions: 0.2 g/L Pd/C, initial Mo concentration at 10 mg/L, pH =3 (adjusted by H_2SO_4), and 20 °C.
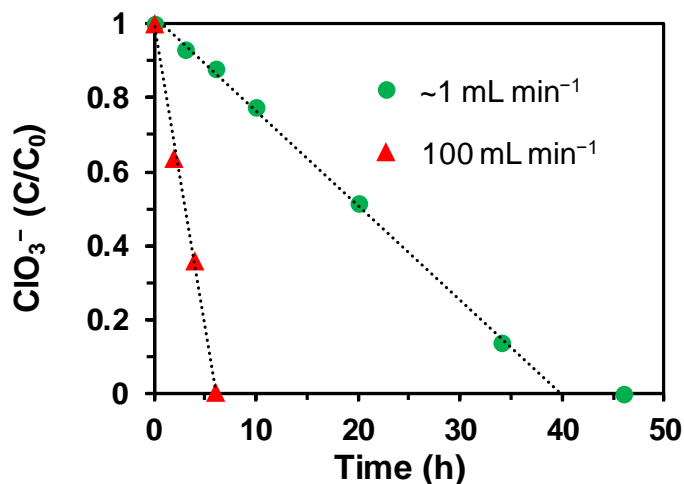

Figure S3.2 Profiles of 1 M ClO_3^- reduction by the MoO_x-Pd/C catalyst. Reaction conditions: 0.5 g/L MoO_x-Pd/C, pH =3, 20 °C. The "~1 mL/min" was estimated from the low H_2 flow rate (1−2 bubbles per second from the 16-gauge needle tip). This flow rate was used for all other experiments on the reduction of 1 mM ClO_3^-, where a higher H_2 flow rate did not accelerate the reactions. The "100 mL/min" refers to 0.1 L per minute, as indicated by the gas flow meter. This flow rate has been previously used for PGM catalysts.[11] In the 50-mL flask, this flow rate generated a vigorous gas flow so that the availability of dissolved H_2 had been maximized for the reduction of concentrated ClO_3^-.
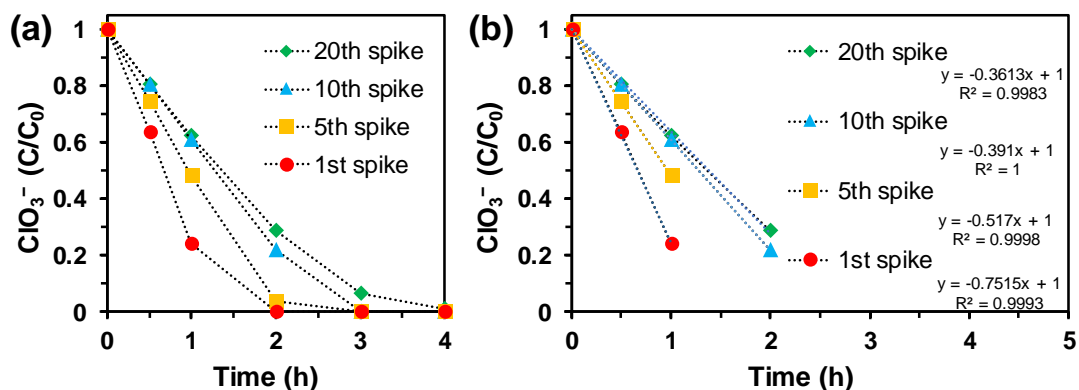
Figure S3.3 (a) Profiles of the reduction of 180 mM ClO_3^- spikes by the MoO_x-Pd/C catalyst in a multiple-spike reaction series. Reaction conditions: 0.5 g/L MoO_x-Pd/C, pH =3, 20 °C, and 1 atm H_2 at 100 mL/min. The increment of NaCl concentrations in the solution was 180 mM after each spike of $NaClO_3$. The total accumulation of Cl^- was 3.6 M; (b) zero-order reaction model fittings of data points with $C/C_0 > 0.2$.
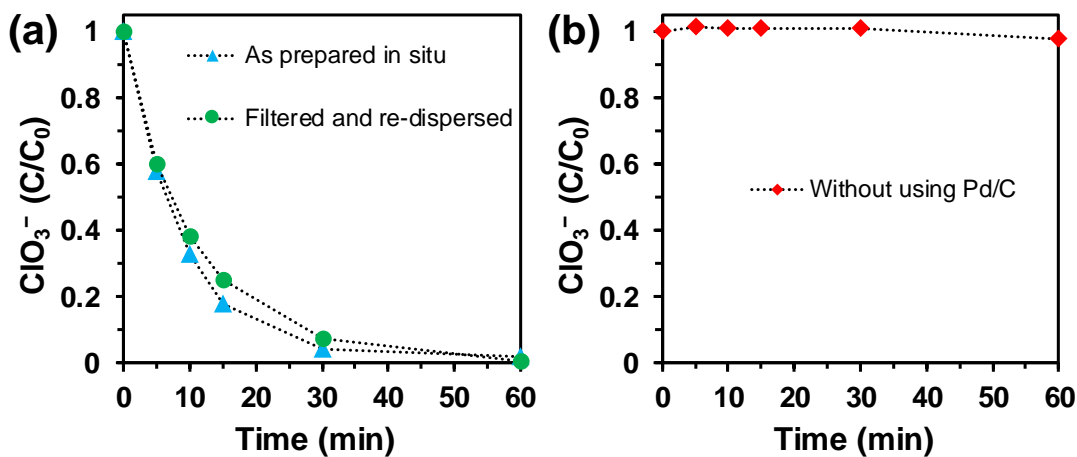
Figure S3.4 (a) Profiles of 1 mM ClO_3^- reduction by the *in situ* prepared MoO_x-Pd/C catalyst and the "recycled" catalyst after the "filtration-collection-redispersion" steps. Note that this recycling operation caused an unavoidable loss of some catalyst powders on the filter paper and other labware such as the funnel, the spoon, and the glass vial during the sample transfer. Reaction conditions: 0.2 g/L MoO_x-Pd/C, pH =3, 20 °C, 1 atm H_2 at ~1 mL/min. (b) the profile of 1 mM ClO_3^- reduction by using dissolved $NaMoO_4$ only (without Pd/C), under the same reaction conditions.

191
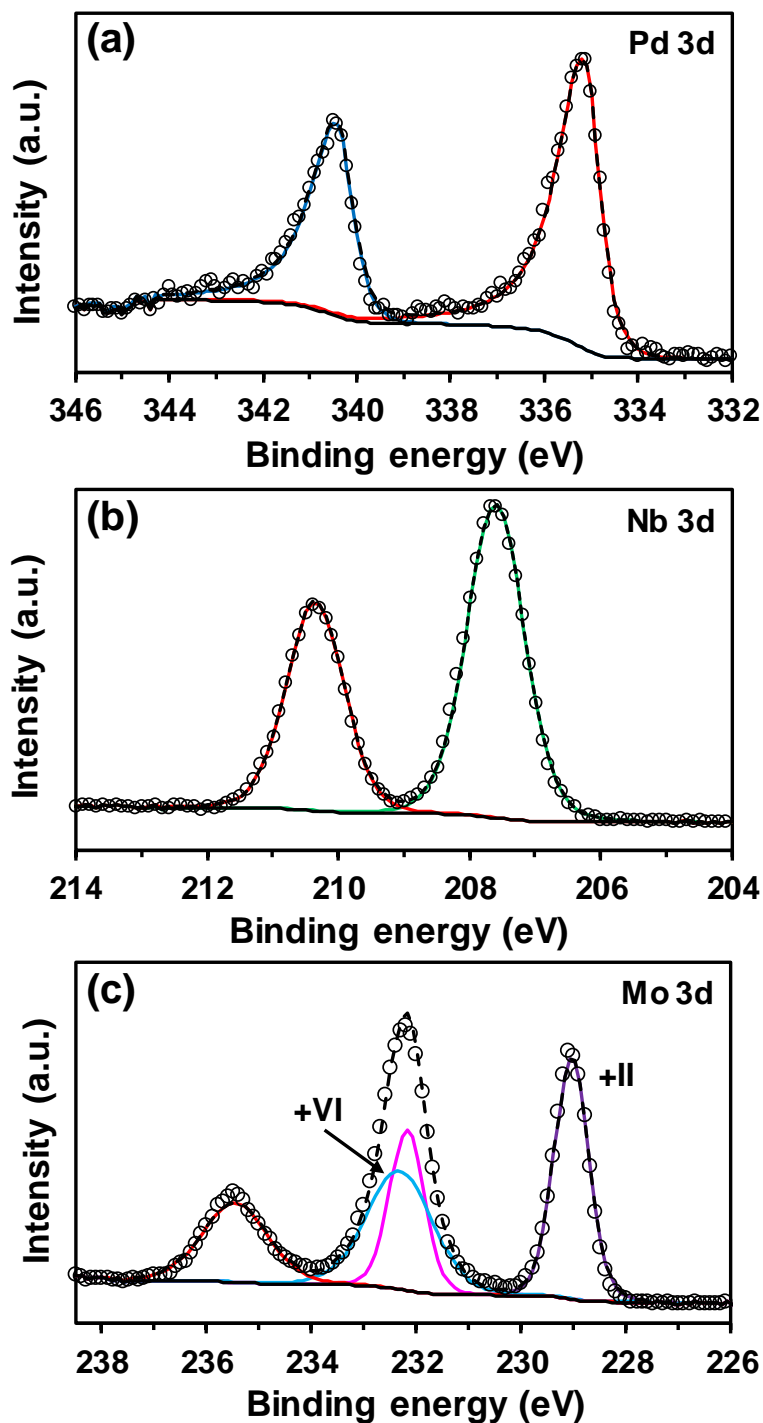
Figure S3.5 XPS spectra for (a) Pd 3d region of the MoO_x−Pd/C catalyst, (b) Nb 3d region of Nb_2O_5 as the internal standard blended in Mo XPS samples, and **(c)** Mo 3d region of the $Mo_2(OAc)_4$ reference. Note that the detection of Mo^{VI} in $Mo_2(OAc)_4$ indicates partial oxidation of Mo^{II} on the surface layer (nanometer-level thickness) of the bulk chemical.
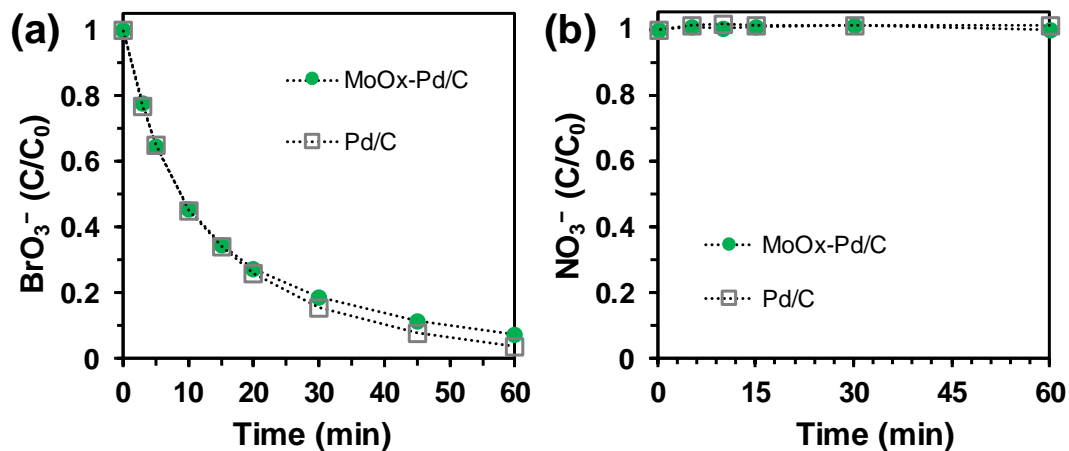
Figure S3.6 The reduction profiles for (a) 1 mM BrO_3^- at pH 6.2 and (b) 1 mM NO_3^- at pH 3 with MoO_x−Pd/C and Pd/C. Reaction conditions: 0.2 g/L Pd/C (with or without Mo), 20 °C, 1 atm H_2 at ~1 mL/min. The reduction of BrO_3^- at pH 3 was too fast to monitor.

References

1.   Shuai, D.; Choe, J. K.; Shapley, J. R.; Werth, C. J. Enhanced activity and selectivity of carbon nanofiber supported Pd catalysts for nitrite reduction. *Environ. Sci. Technol.* **2012,** *46*, 2847-2855.

2.   Weisz, P.; Prater, C. Interpretation of measurements in experimental catalysis. *Adv. Catal.* **1954,** *6*, 143-196.

3.   Liu, J.; Choe, J. K.; Wang, Y.; Shapley, J. R.; Werth, C. J.; Strathmann, T. J. Bioinspired complex-nanoparticle hybrid catalyst system for aqueous perchlorate reduction: Rhenium speciation and its influence on catalyst activity. *ACS Catal.* **2015,** *5*, 511-522.

4.   Satterfield, C. *Mass Transport in Heterogeneous Catalysis*; MIT Press: Cambridge, MA, 1970.

5.   Davie, M. G.; Reinhard, M.; Shapley, J. R. Metal-catalyzed reduction of N-nitrosodimethylamine with hydrogen in water. *Environ. Sci. Technol.* **2006,** *40*, 7329-7335.

6.   Campbell, A.; Oliver, B. Diffusion coefficients of sodium and lithium chlorates in water, at 25°. *Can. J. Chem.* **1969,** *47*, 2681-2685.

7.   Sänger, P.; Deckwer, W.-D. Liquid-solid mass transfer in aerated suspensions. *Chem. Eng. J.* **1981,** *22*, 179-186.

8.   Sano, Y.; Yamaguchi, N.; Adachi, T. Mass transfer coefficients for suspended particles in agitated vessels and bubble columns. *J. Chem. Eng. Jpn.* **1974,** *7*, 255-261.

9.   Bates, R. L.; Fondy, P. L.; Corpstein, R. R. Examination of some geometric parameters of impeller power. *Ind. Eng. Chem. Process Des. Dev.* **1963,** *2*, 310-314.

10.   Liu, B.; Yao, H.; Song, W.; Jin, L.; Mosa, I. M.; Rusling, J. F.; Suib, S. L.; He, J. Ligand-free noble metal nanocluster catalysts on carbon supports via "soft" nitriding. *J. Am. Chem. Soc.* **2016,** *138*, 4718-4721.

11.   Van Santen, R.; Klesing, A.; Neuenfeldt, G.; Ottmann, A. Method for removing chlorate ions from solutions. U.S. Patent 6,270,682, Aug 7, 2001.

Appendix C

Supplementary Information for Chapter 4

Text S4.1. Langmuir-Hinshelwood Mechanism

The kinetic data of $[(NH_2)_2bpy]MoO_x-Pd/C$ catalyst was analyzed with the Langmuir-Hinshelwood (LH) model. Previous works suggest that the reduction of ClO_4^- to ClO_3^- by the active sites is the rate-limiting step.[1, 2] The surface reactions can be simplified with the one-site model[3] shown in **Scheme S4.1**. At the water-catalyst interface, aqueous ClO_4^- reversibly coordinates with the surface Mo center in the first step (i.e., the adsorption of ClO_4^-). The carbon surface has a very low affinity to ClO_4^-. Then, the reduction of Mo-coordinated ClO_4^- is enabled by the two-electron oxygen atom transfer (OAT) reaction, resulting in the formation of Mo=O and the dissociation of ClO_3^-.

$$ClO_4^- (aq) + Mo^{IV} (s) \underset{k_{-1}}{\overset{k_1}{\rightleftharpoons}} Mo^{IV}-ClO_4^- (s) \xrightarrow{k_2} Mo^{VI}=O (s) + ClO_3^- (aq)$$

A $\quad$ **S**$_{empty}$ $\quad\quad$ **AS** $\quad\quad\quad$ **S**$_{used}$
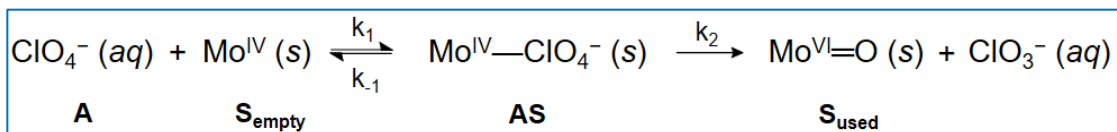
Scheme S4.1 Langmuir-Hinshelwood model for ClO_4^- reduction by $[(NH_2)_2bpy]MoO_x-Pd/C$. The catalytic reduction proceeds on the surface of the solid catalyst. First, aqueous phase ClO_4^- (**A**) reversibly coordinates with the unoccupied Mo^{IV} active sites (**S**$_{empty}$), forming a $Mo^{IV}-ClO_4^-$ (**AS**) intermediate. Then, the OAT reaction affords the reduction of ClO_4^- and the formation of $Mo^{VI}=O$ (**S**$_{used}$). The following assumptions are made: (i) the reduction of ClO_4^- is the rate-limiting step, (ii) the regeneration of **S**$_{used}$ by Pd/C and H_2 is fast and complete; therefore, the number of total active sites (**S**) is approximately equal to the summation of **S**$_{empty}$ and **AS** (i.e., the surface concentration of **S**$_{used}$ is close to zero), (iii) there is no activity loss of the Mo sites, and (iv) the adsorption of ClO_4^- on activated carbon is minimal.

The global reaction rate (r) is defined by

$$r = k_2[AS] = k_2\theta[S] \qquad\qquad (Eq. S4.1)$$

where $[S]$ and $[AS]$ denote the surface concentration of total active sites and occupied sites, respectively. θ is the surface coverage, which is defined as $\theta = [AS]/[S]$. Because the adsorption and desorption of ClO_4^- are assumed to be fast, the steady-state approximation

is applied to AS. Therefore, the concentration variation of AS with respect to time is expressed as

$$\frac{d[AS]}{dt} = k_1[A][S](1-\theta) - k_{-1}[S](\theta) - k_2[S](\theta) = 0 \qquad (Eq.S4.2)$$

θ is solved as

$$\theta = \frac{k_1[A]}{k_1[A] + k_{-1} + k_2} \qquad (Eq.S4.3)$$

Because the OAT reaction is assumed to be the rate-limiting step (i.e., $k_2 \ll k_1[A]$ and k_{-1}), θ can be simplified to

$$\theta = \frac{k_1[A]}{k_1[A] + k_{-1}} \qquad (Eq.S4.4)$$

From **Eq. S4.4** and **Eq. S4.1**, r can be expressed in terms of $[A]$ and $[S]$ by

$$r = \frac{K_1 k_2[A][S]}{K_1[A] + 1} \qquad (Eq.S4.5)$$

in which $K_1 = k_1/k_{-1}$ is the equilibrium constant and $[A]$ is the aqueous concentration of ClO_4^- at any given time. Based on the kinetic results, we notice that the observed rate constant, k_{obs}, varies in terms of the initial concentration of ClO_4^- (i.e., $[A_0]$). Hence, we define a new term φ, in which $\varphi = [A]/[A_0]$, and replace $[A]$ with $\varphi[A_0]$ in **Eq. S4.5**.

$$r = \frac{K_1 k_2[A_0][S]\varphi}{K_1[A_0]\varphi + 1} \qquad (Eq.S4.6)$$

At ***high initial concentrations***, in which $K_1[A_0]\varphi \gg 1$, **Eq. S4.6** can be further simplified to

$$r = k_2[S] \qquad (Eq.\,S4.7)$$

Eq. S4.7 demonstrates that the reaction is <u>zeroth-order</u> with respect to ClO_4^-. This rate law is in good agreement with our kinetic results, in which zeroth-order fitting provides >0.99 R^2 values (i.e., coefficient of determination) for 1, 10 and 100 mM ClO_4^- reduction by the [(NH$_2$)$_2$*bpy*]MoO$_x$–Pd/C catalyst (**Figure S4.6**). Furthermore, the concentration variations of ClO_4^- can be described by

$$\frac{d[A]}{dt} = -k_2[S] \qquad (Eq.\,S4.8)$$

Upon integration and rearrangement, we can obtain the following kinetic equation:

$$\varphi = -\frac{k_2[S]}{[A_0]}t + 1 \qquad (Eq.\,S4.9)$$

Eq. S4.9 shows that $k_{obs} = k_2[S]/[A_0]$ at high ClO_4^- concentrations. This kinetic pattern agrees with our experimental observations. When the initial concentration of ClO_4^- increased from 1 to 100 mM and the catalyst loading remained constant (i.e., $[S]$ does not change), the k_{obs} decreased from 2.01 to 0.043 mM h^{-1} (**Figure S4.6**, panels **a**–**c**). In addition, k_{obs} values were almost identical when we scaled up the reaction proportionally (e.g., reduction of 10 mM ClO_4^- by 0.2 g L^{-1} catalyst and reduction of 100 mM ClO_4^- by 2 g L^{-1} catalyst, **Figure S4.6**, panel **c** versus **d**).

At *low initial concentrations*, in which $K_1[A_0]\varphi \ll 1$, **Eq. S4.6** becomes

$$r = K_1 k_2 [A_0][S]\varphi \qquad\qquad (Eq. S4.10)$$

Now the reaction is <u>first-order</u> in φ (i.e., first-order in $[ClO_4^-]$). Similarly, the reduction of ClO_4^- can be described by

$$\frac{d[A]}{dt} = -K_1 k_2 [A_0][S]\varphi \qquad\qquad (Eq. S4.11)$$

And the following equation holds for low concentrations scenarios

$$\varphi = e^{-K_1 k_2 [S]t} \qquad\qquad (Eq. S4.12)$$

Eq. S4.12 shows that k_{obs} is not a function of $[A_0]$. In other words, k_{obs} remains constant regardless of $[A_0]$. This kinetic pattern agrees with our experimental results, in which k_{obs} remained the same when the initial concentration of ClO_4^- varied from 0.1 to 0.01 mM (**Figure. S4.7**, panels **a−c**).

Text S4.2. Mass Transfer Analysis

A prerequisite of the LH kinetic model is the assumption that surface reactions constitute the rate-limiting step. This assumption implies that the diffusion of ClO_4^- from the bulk solution phase to the liquid-solid interface is much faster than the chemical reactions on the surface. Therefore, evaluations of external and internal mass transfer are essential to verify the assumption.

To evaluate the effect of pore diffusion resistance (i.e., ***internal mass transfer***) on the measured reaction rates, we applied Weisz-Prater (WP) criterion for the system under consideration here.[4, 5] In general, the WP criterion and WP parameter (C_{WP}) are described below:

If $C_{WP} = \frac{k_{obs}\tau R^2}{D\theta} < 1$, the internal mass transfer limitation is negligible

If $C_{WP} = \frac{k_{obs}\tau R^2}{D\theta} > 1$, the internal mass transfer limitation is significant

In the expression of $C_{WP} = \frac{k_{obs}\tau R^2}{D\theta}$, k_{obs} is the observed pseudo-first-order rate constant of heterogeneous reaction (min^{-1}), R is the radius of the catalyst particle (m), τ is the tortuosity factor of the catalyst particle, θ is the porosity of the catalyst particle, and D is the diffusion coefficient of reactant in bulk solution ($m^2 s^{-1}$).

To conservatively evaluate C_{WP}, we used the largest observed reaction rate (i.e., $0.185\ min^{-1}$) from this study. The diameter of the catalyst particle is $37\ \mu m$ because the commercial Pd/C powder was wet-filtered through a 400-mesh sieve before use.[6] Previous

studies suggest that the parameters τ and θ are typically in the range of 2−10 and 0.2−0.7, respectively.[7, 8] In our conservative calculation, 10 and 0.2 were used as the estimated values for τ and θ, respectively. The diffusion coefficient of ClO_4^- is ($D_{ClO_4^-}$) is 1.79×10^{-9} $m^2 s^{-1}$ in bulk solution.[9] Therefore, C_{WP} is calculated as

$$C_{WP} = \frac{k_{obs}\tau R^2}{D\theta} = \frac{0.185 \ min^{-1} \times 10 \times \left(\frac{37}{2} \times 10^{-6} \ m\right)^2}{1.79 \times 10^{-9} \ m^2 \ s^{-1} \times 60 \ s \ min^{-1} \times 0.2} = 0.029 < 1$$

The above calculation shows that the WP criterion is satisfied for the system under consideration. Therefore, the pore diffusion resistance is negligible.

The evaluation of the **external mass transfer** rate is conducted following our recently reported method.[10] First, we calculated the Sherwood number (Sh) and used it to estimate the mass transfer coefficient ($k_{aq/s}$) of ClO_4^- between the aqueous solution and the catalyst surface.[11, 12]

$$Sh = \left[2 + 0.4\left(\frac{\varepsilon d_p^4}{\nu^3}\right)^{0.25} Sc^{0.33}\right] \cdot \phi_c \qquad (Eq.\,S4.13)$$

$$k_{aq/s} = \frac{D_{ClO_3^-}}{d_p} \cdot Sh \qquad (Eq.\,S4.14)$$

In **Eq. S4.13**, ε is the rate of flow energy supply per unit mass of liquid ($m^2 s^{-3}$), d_p is the diameter of the catalyst particle (m), ν is the kinematic viscosity of water ($\nu_{H_2O} = 1.003 \times 10^{-6} \ m^2 s^{-1}$ at 20°C), Sc is Schmidt number, and ϕ_c is Carman's surface factor (assume the catalyst particle is spherical, $\phi_c = 1$). We evaluated Sc and ε with the following equations:

$$Sc = \frac{\nu_{H_2O}}{D_{ClO_4^-}} = \frac{1.003 \times 10^{-6} \ m^2 \ s^{-1}}{1.79 \times 10^{-9} \ m^2 \ s^{-1}} = 560.34$$

$$\varepsilon = \frac{N_p \cdot l^5 \cdot n^3}{V} = \frac{5 \times (3 \ cm)^5 \times (27 \ s^{-1})^3}{50 \ cm^3} = 48 \ m^2 \ s^{-3}$$

where N_p is the power number (normally $N_p \approx 5.0$)[13], l is the length of the stir bar ($l \approx$ 3 cm), n is the rotating speed of the stir bar ($n = 1600 \ round \ min^{-1} = 27 \ round \ s^{-1}$), and V is the volume of the reactor ($V = 50 \ cm^3$). Thus, ε has the value of $48 \ m^2 \ s^{-3}$.

With the calculated values for Sc and ε, the Sherwood number was calculated as

$$Sh = \left[2 + 0.4 \left(\frac{48 \ m^2 \ s^{-3} \times (3.7 \times 10^{-5} \ m)^4}{(1.003 \times 10^{-6} \ m^2 \ s^{-1})^3} \right)^{0.25} 560.34^{0.33} \right] \cdot 1 = 11.944$$

And $k_{aq/s}$ was estimated by **Eq. 4.14**.

$$k_{aq/s} = \frac{D_{ClO_3^-}}{d_p} \cdot Sh = \frac{1.79 \times 10^{-9} \ m^2 \ s^{-1}}{3.7 \times 10^{-5} \ m} \times 11.944 = 5.78 \times 10^{-4} \ m \ s^{-1}$$

The geometric surface area of the catalyst per volume of solution (a)[14] is calculated as

$$a = \frac{SA_p \times M}{\rho_p \times V_p} \times \frac{1}{V_R} = \frac{4\pi \times (18.5 \times 10^{-6} \ m)^2 \times 0.01 \ g}{2 \times 10^6 \ g \ m^{-3} \times \frac{4\pi}{3}(18.5 \times 10^{-6} \ m)^3} \times \frac{1}{50 \times 10^{-6} \ m^3} = 16.22 \ m^{-1}$$

in which SA_p is the geometric surface area of one catalyst particle (m^2), M is the mass of catalyst in the reduction test ($0.01 \ g$), V_p is the volume of one catalyst particle (m^3), and V_R is the volume of the reactor ($50 \ mL$).

The mass transfer rate was then calculated by taking the product of the mass transfer coefficient and the geometric surface area of the catalyst per volume of the solution:

$$k_{aq/s} \cdot a = 5.78 \times 10^{-4}\ m\ s^{-1} \times 16.22\ m^{-1} = 9.375 \times 10^{-3}\ s^{-1} = 0.563\ min^{-1}$$

The above estimation indicates that the external mass transfer rate is larger than the observed rate constant $k_{obs} = 0.185\ min^{-1}$ for ClO_4^- reduction. Therefore, <u>the impact of external mass transfer on the reaction rates is negligible</u>.
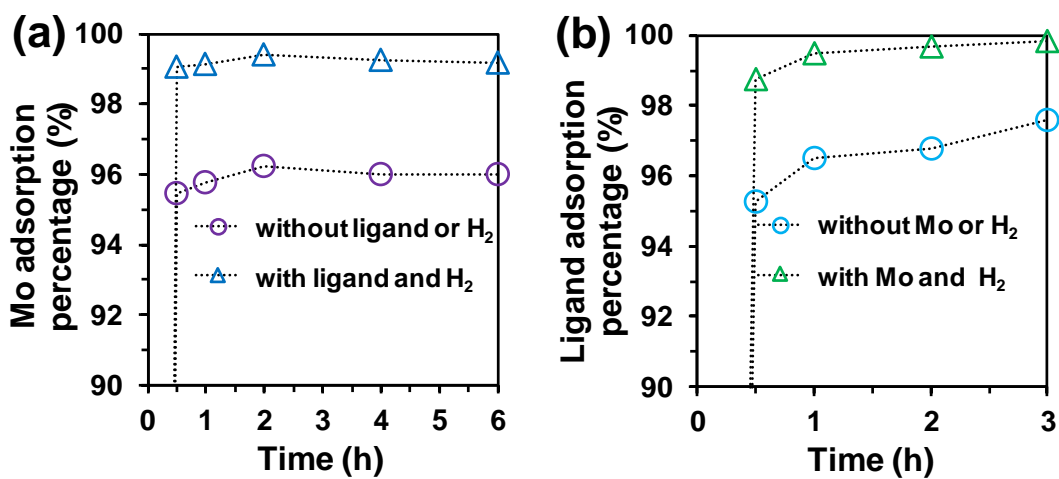
Figure S4.1 The adsorption of (a) Mo and (b) ligand during the preparation of the [(NH$_2$)$_2$*bpy*]MoO$_x$–Pd/C catalyst. All dotted lines start from 0% adsorption at 0 h. Results show that under air (legend ***without ligand or H$_2$*** and ***without Mo or H$_2$***) >95% of either Mo or ligand can be adsorbed onto Pd/C within 30 min. When all components (i.e., 1 atm H$_2$, Mo, and ligand) were supplied together for *in situ* catalyst preparation (legend ***with ligand and H$_2$*** and ***with Mo and H$_2$***), the adsorption of Mo and ligand reached >99 and >99.5%, respectively, within 1 h. Reaction condition: 0.2 g L^{-1} Pd/C, 0.1 mM Mo from Na$_2$MoO$_4$ (for 5 wt% Mo in catalyst), 0.1 mM (NH$_2$)$_2$*bpy*, pH 3.0, 1 atm H$_2$, 20 °C.
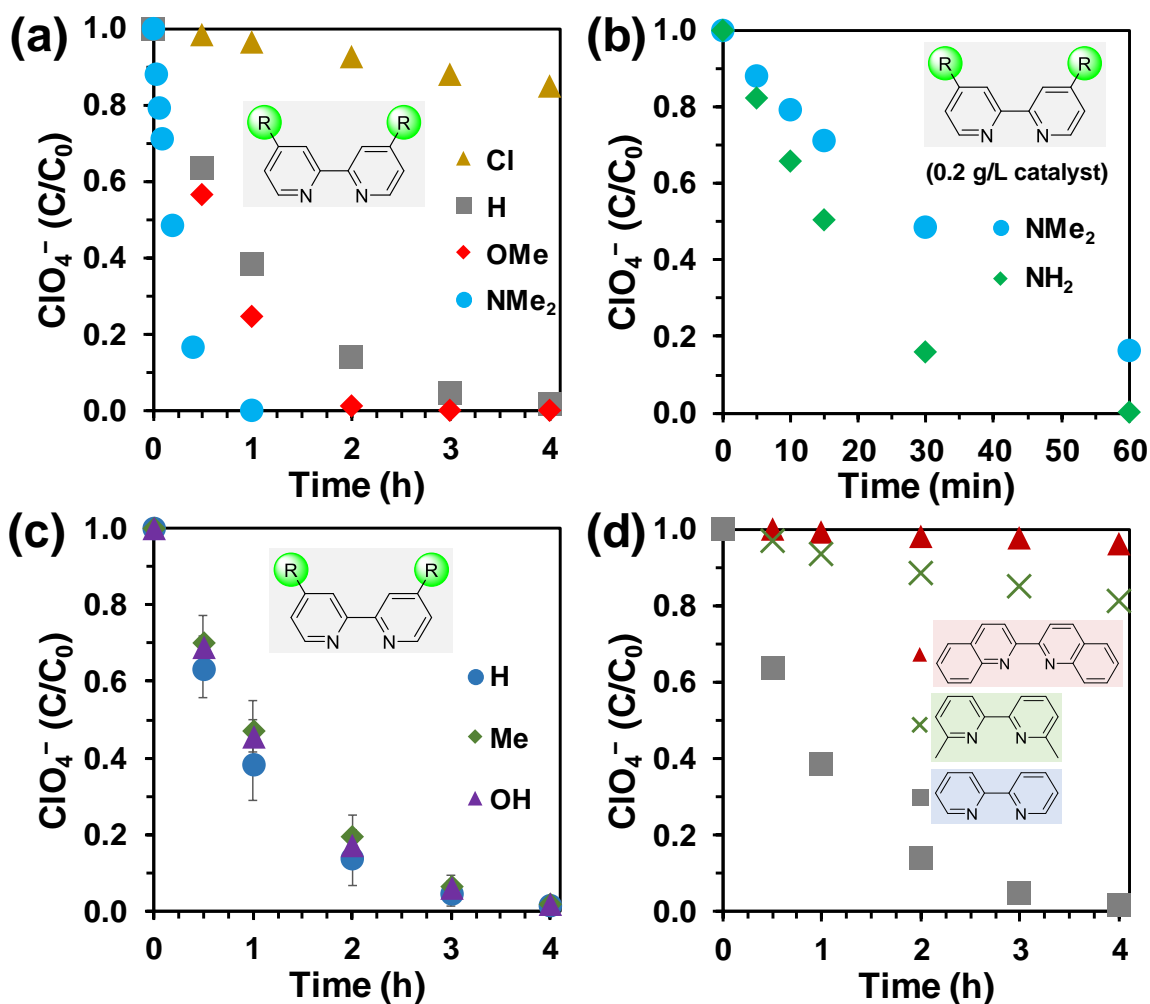
Figure S4.2 Profiles for aqueous ClO_4^- reduction by $(L)MoO_x-Pd/C$ catalysts using bipyridine derivative ligands. Reaction conditions: 0.5 g L^{-1} of $(L)MoO_x-Pd/C$ (5 wt% Mo in 5 wt% Pd/C, the molar ratio of L:Mo=1:1), 1 mM ClO_4^-, pH 3.0, 1 atm H_2, 20 °C. Panel **b** used 0.2 g L^{-1} of catalysts.
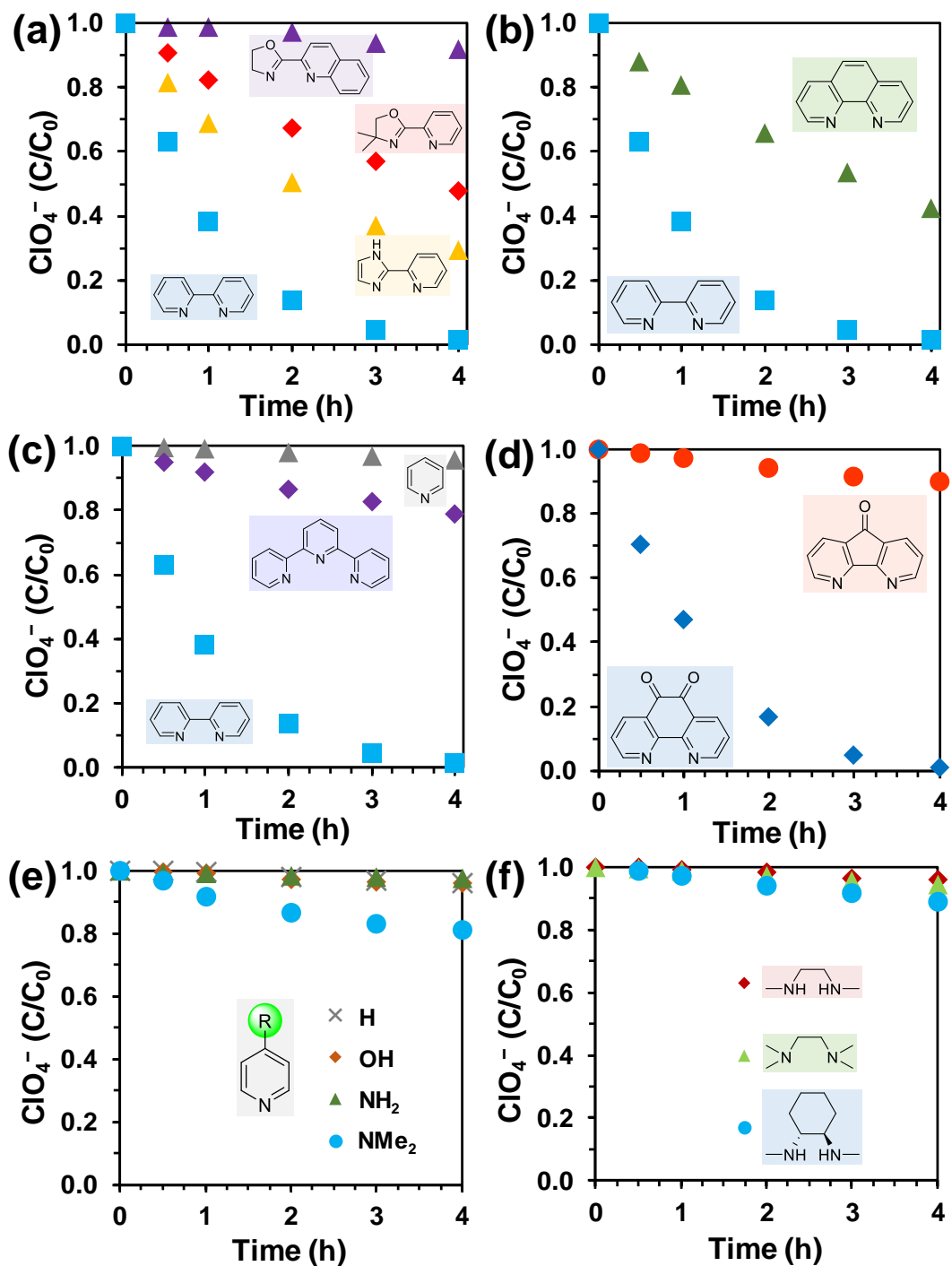
Figure S4.3 Profiles for aqueous ClO_4^- reduction by $(L)MoO_x$–Pd/C catalysts using various ligands. Reaction conditions: 0.5 g L^{-1} of $(L)MoO_x$–Pd/C (5 wt% Mo in 5 wt% Pd/C, the molar ratio of L:Mo=1:1), 1 mM ClO_4^-, pH 3.0, 1 atm H_2, 20 °C. In panel **e**, the molar ratio between the monodentate pyridine and Mo was 2:1.
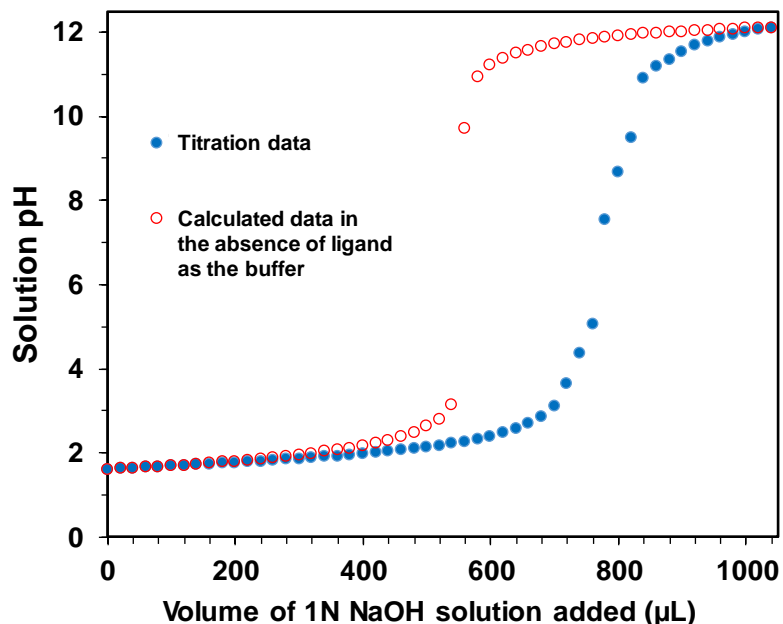
Figure S4.4 The pH titration curve for $(NH_2)_2bpy$ in aqueous solution (0.4 g L^{-1}, or 2.15 mM). Due to the limited solubility of $(NH_2)_2bpy$ in water, the titration started from pH 1.60 where both the pyridyl N and $-NH_2$ were protonated. The $(NH_2)_2bpy$ concentration higher than 0.4 g L^{-1} resulted in precipitation when pH went higher. The titration stopped at pH 12 as the high end of accurate measurement by the pH electrode. The low concentration of $(NH_2)_2bpy$ as the buffer made it challenging to locate the pH turning points as pK_a. However, the comparison with the calculated pH (assuming the absence of buffer) suggested that pK_{a1} (deprotonation from $-NH_3^+$) is below 3.0 to delay the pH rising and pK_{a2} (deprotonation from pyridyl $-NH^+=$) is above 5.0 to reduce the slope of the steep pH increase. This estimation agrees with the reported pK_{a1} of 2.2 and pK_{a2} of 6.7 for the analogous 6,6'-diamino-2,2'-bipyridine.[15]
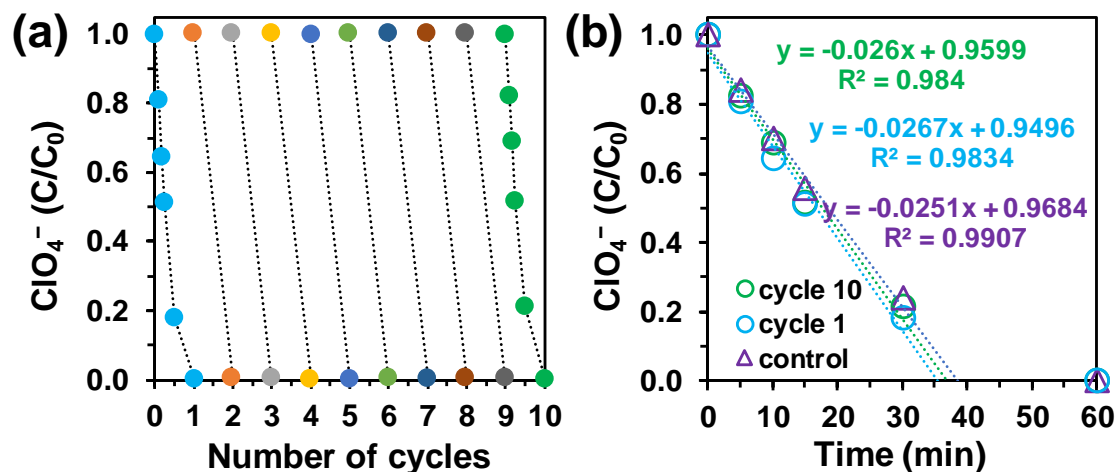
Figure S4.5 The reduction of 1 mM ClO_4^- by the freshly prepared (*cycle 1*) and reused (*cycle 10*, with nine previous spikes of 1 mM ClO_4^-) [(NH₂)₂*bpy*]MoO$_x$−Pd/C catalyst. The 0th order fittings were conducted with all data points at $C/C_0 > 0.2$. Due to the low catalyst loading (0.2 g L^{-1}) and the inevitable loss of catalyst powder from each filtration-redispersion procedure, the continuous spike experiments were conducted. Each ClO_4^- spike was allowed at least 2 h to achieve complete reduction into Cl^-. The ten spikes took two days to finish because no experimentation was performed during the night. The dataset *control* indicates an experiment using the freshly prepared catalyst in the presence of 9 mM NaCl, which simulated the scenario of complete reduction of nine spikes of 1 mM ClO_4^-. The almost overlapping time profiles of the three data sets suggest that the catalyst performance is insensitive to <10 mM of Cl^- and resistant to the acidic and hydrogenating aqueous environment. Reaction condition: 0.2 g L^{-1} catalyst (5 wt% Mo in 5 wt% Pd/C), 1 mM ClO_4^- per spike, pH 3.0, 1 atm H₂, 20 °C.
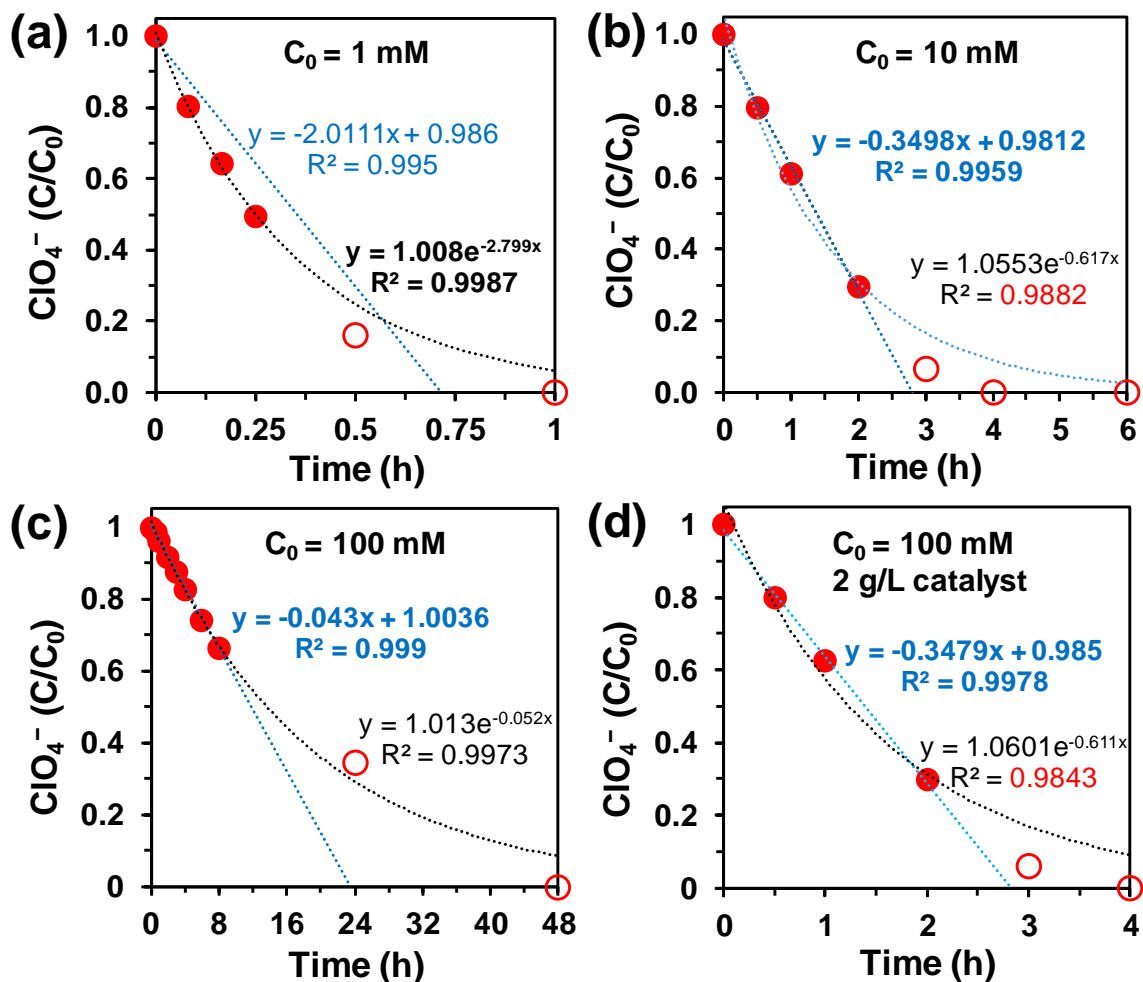
Figure S4.6 Catalytic reduction of high concentrations (C_0 = 1, 10, and 100 mM) of ClO_4^- by the $[(NH_2)_2bpy]MoO_x$–Pd/C catalyst (5 wt% Mo in 5 wt% Pd/C, pH 3.0, 1 atm H_2, 20 °C). Panels **a**, **b**, and **c** used 0.2 g L^{-1} catalyst. Panel **d** used 2.0 g L^{-1} catalyst. The data with $C/C_0 > 0.2$ were fit with both 0th- and 1st-order models. The better fit has the equation highlighted in bold. The slope of the linear fitting (in the unit of h^{-1}) indicates the 0th-order rate constant (mM h^{-1}) divided by C_0 (mM). The discussion in the **Text S4.1** regarding $k_{obs} = k_2[S]/[A_0]$ corresponds to the slopes shown in these figures (i.e., $C_0 = [A_0]$). The first highlight is the decreasing k_{obs} with the increasing $[A_0]$ for ClO_4^- (panels **a**–**c**). Since the overall reaction model is simplified, the decrease of k_{obs} is not strictly in proportion with the increase of $[A_0]$. The second highlight is the very similar k_{obs} for the reduction of 10 mM ClO_4^- using 0.2 g L^{-1} catalyst and the reduction of 100 mM ClO_4^- using 2.0 g L^{-1} catalyst (i.e., the same ratio of $[S]/[A_0]$) shown in panels **b** and **d**. See **Text S4.1** for more details.
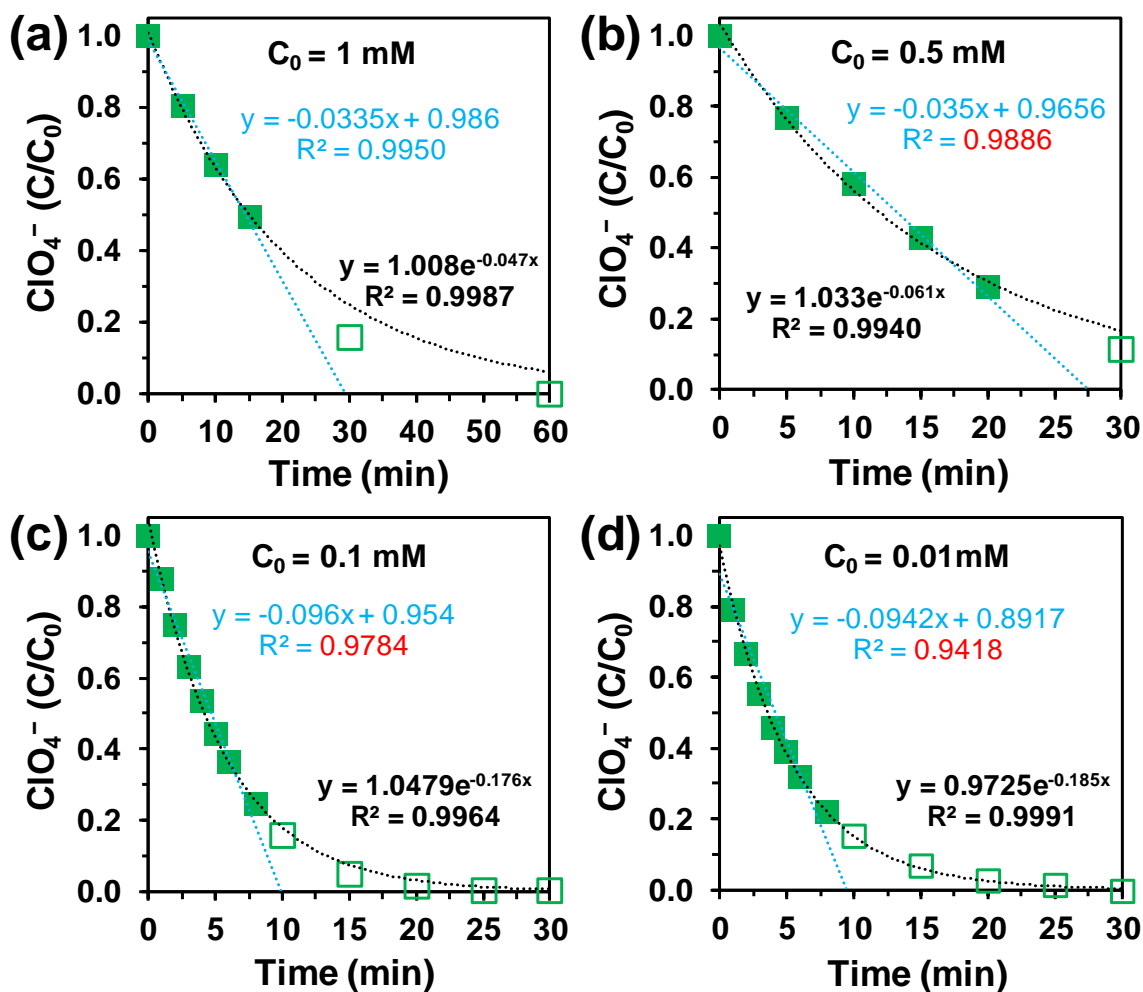
Figure S4.7 Catalytic reduction of low concentrations (C_0 = 1, 0.5, 0.1, and 0.01 mM) of ClO_4^- by 0.2 g L^{-1} of [(NH$_2$)$_2$*bpy*]MoO$_x$−Pd/C catalyst (5 wt% Mo in 5 wt% Pd/C, pH 3.0, 1 atm H$_2$, 20 °C). The data with C/C_0 > 0.2 were fit with both 0th- and 1st-order models. The better fit has the equation highlighted in bold. The power of the exponential fitting indicates the first-order rate constant (min^{-1}, independent from C_0). The highlight is the consistent 1st-order k_{obs} values when the kinetics cannot be fit by the 0th-order model (i.e., R^2<0.98 when C_0 = 0.1 and 0.01 mM). See **Text S4.1** for more details.
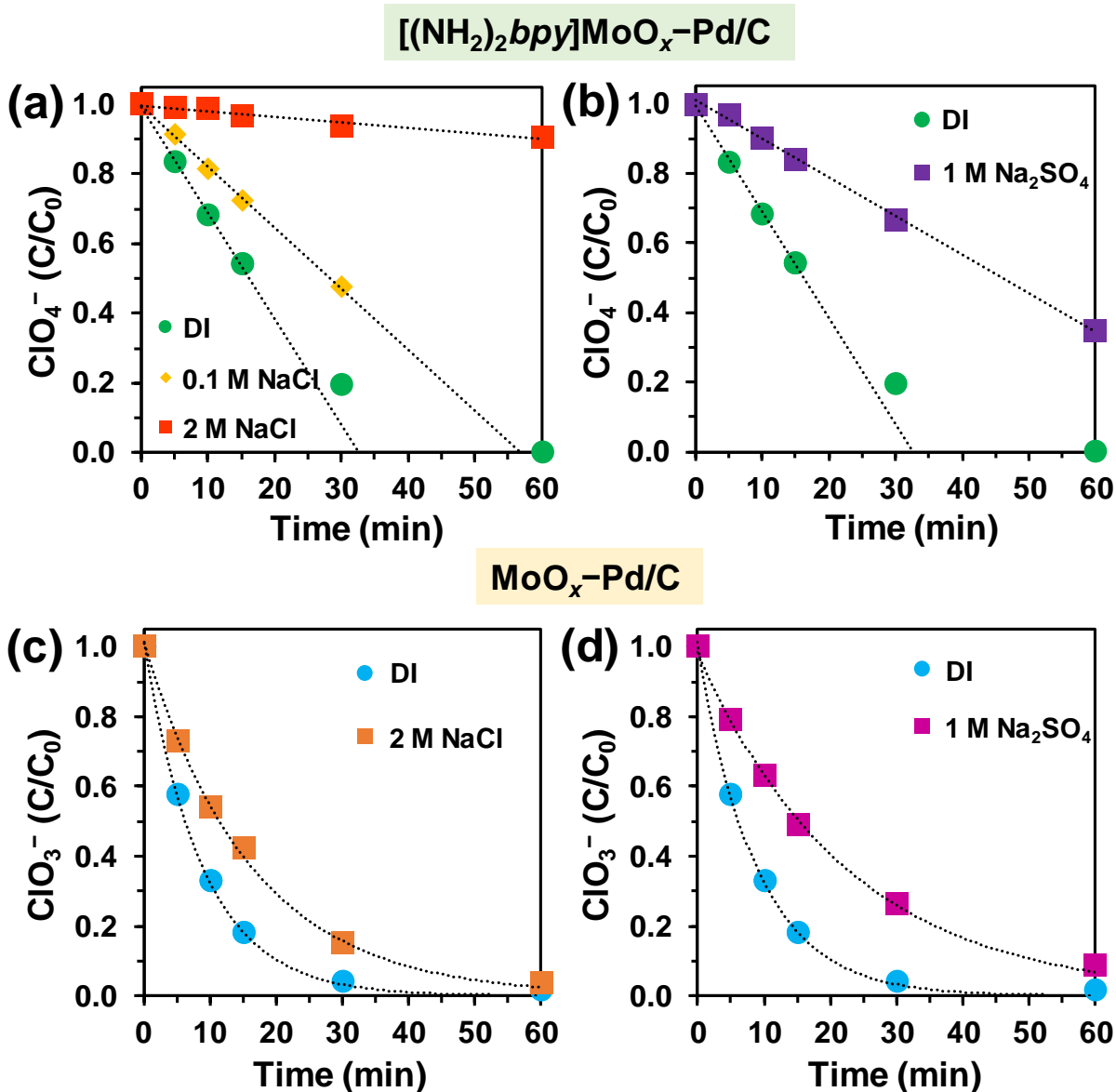
Figure S4.8. Inhibition of ClO_4^- reduction using $[(NH_2)_2bpy]MoO_x$–Pd/C (panels a and b) and of ClO_3^- reduction using ligand-free MoO_x–Pd/C (panels c and d) by chloride and sulfate anions. Dotted lines indicate the 0th- or 1st-order fittings using the data with $C/C_0 > 0.2$. Fitting results and catalyst activity comparisons are shown in **Table S4.2**. Reaction conditions: 0.2 g L^{-1} catalyst (5 wt% Mo in 5 wt% Pd/C), 1 mM ClO_4^- or ClO_3^-, pH 3.0, 1 atm H_2, 20 °C. "DI" indicates control solutions without additions of NaCl or Na_2SO_4.
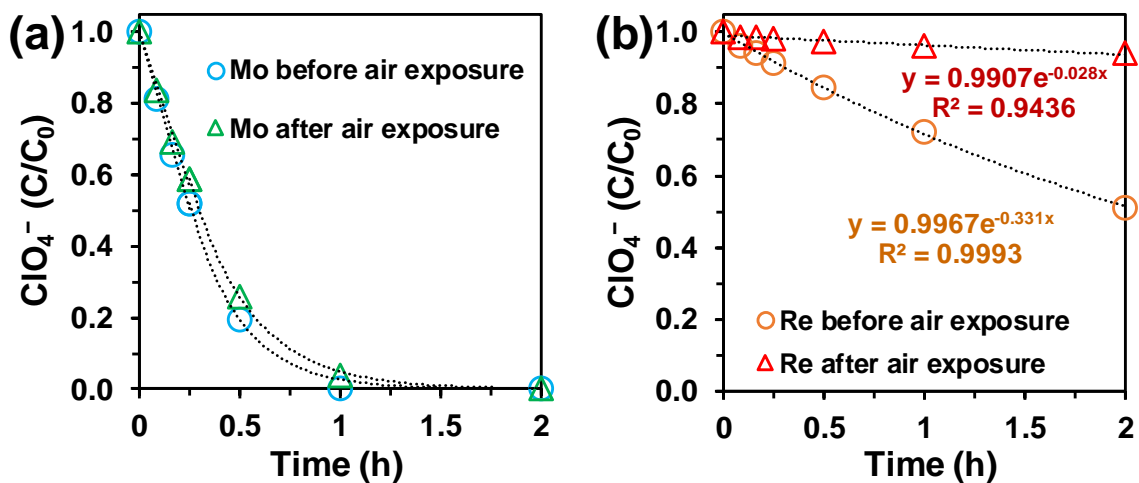
Figure S4.9. The change of ClO_4^- reduction activity by (a) $[(NH_2)_2bpy]MoO_x$−Pd/C and (b) $Re(hoz)_2$−Pd/C[6] before and after air exposure for 1 h. Reaction conditions: 0.2 g L^{-1} catalyst (5 wt% Mo or 5 wt% Re on the same 5 wt% Pd/C material), 1 mM ClO_4^-, pH 3.0, 1 atm H_2, 20 °C. The preparation of both catalysts took 1 h under 1 atm H_2. After air exposure, the catalyst suspensions were treated under 1 atm H_2 for another 1 h before adding ClO_4^-.
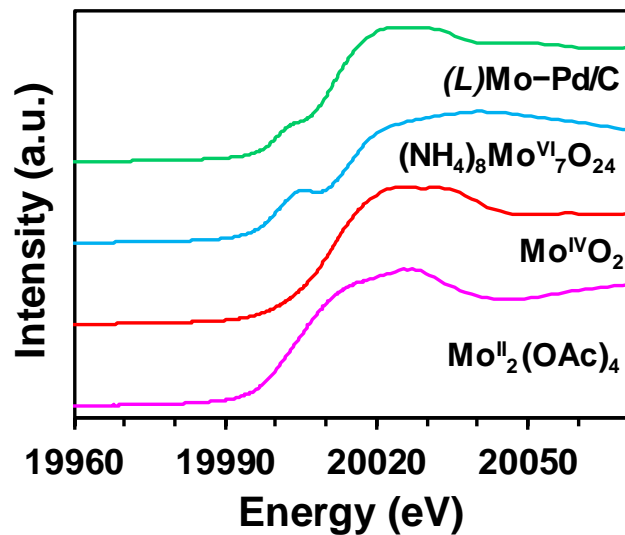
**Figure S4.10** Mo K-edge X-ray absorption near-edge structure (XANES) spectra of the reduced [(NH$_2$)$_2$*bpy*]MoO$_x$−Pd/C and Mo^{II}, Mo^{IV}, and Mo^{VI} references.
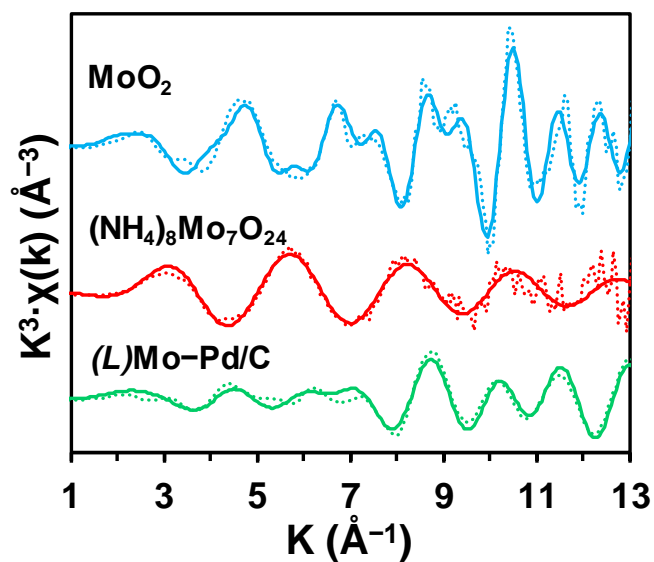
Figure S4.11 Mo K-edge extended X-ray absorption fine structure (EXAFS) spectra (dotted line) of the reduced [(NH$_2$)$_2$*bpy*]MoO$_x$−Pd/C, Mo^{II} and Mo^{IV} references, and their shell-by-shell fits (solid line).
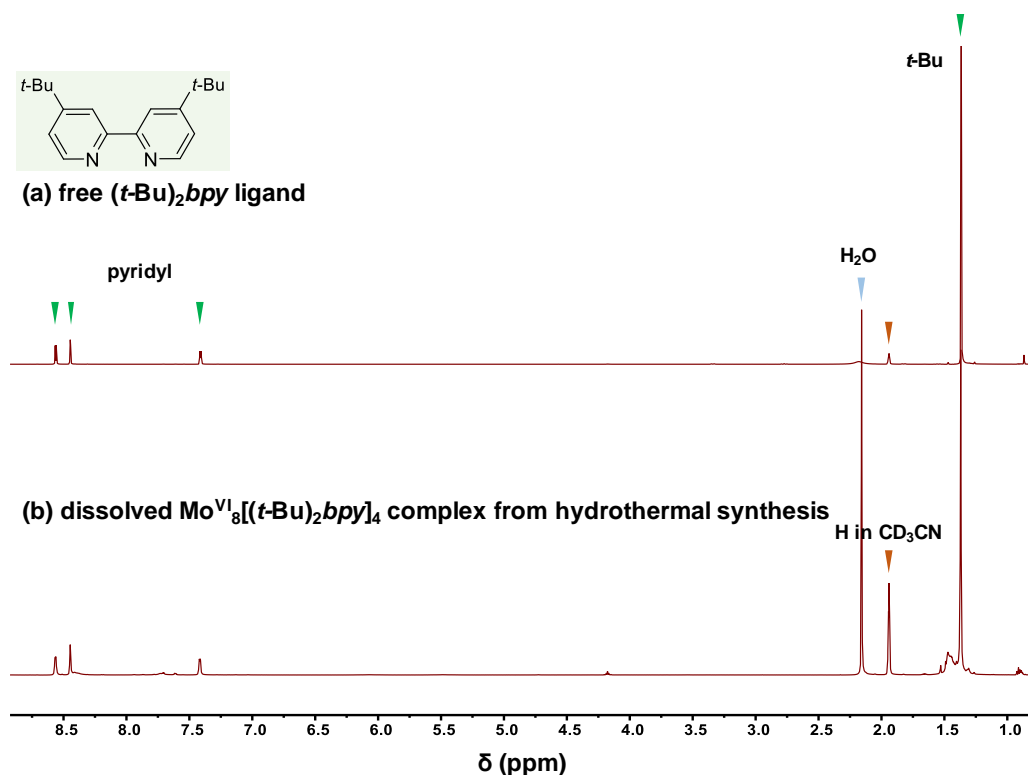
Figure S4.12 ^{1}H NMR (CD$_3$CN, 600 MHz) spectra of (a) 4,4'-di-*tert*-butyl-2,2'-bipyridine [(*t*-Bu)$_2$*bpy*] ligand and (b) Mo$^{VI}_8$O$_{22}$(OH)$_4$[(*t*-Bu)$_2$*bpy*]$_4$ from hydrothermal synthesis. The same spectra indicate complete dissociation of the complex into the free (*t*-Bu)$_2$*bpy* ligand upon dissolution in acetonitrile. The NMR data is consistent with the original report on Mo$^{VI}_8$O$_{22}$(OH)$_4$[(*t*-Bu)$_2$*bpy*]$_4$,[16] suggesting that the original study also observed free (*t*-Bu)$_2$*bpy* ligand rather than a dissolved Mo$^{VI}_8$O$_{22}$(OH)$_4$[(*t*-Bu)$_2$*bpy*]$_4$ structure.
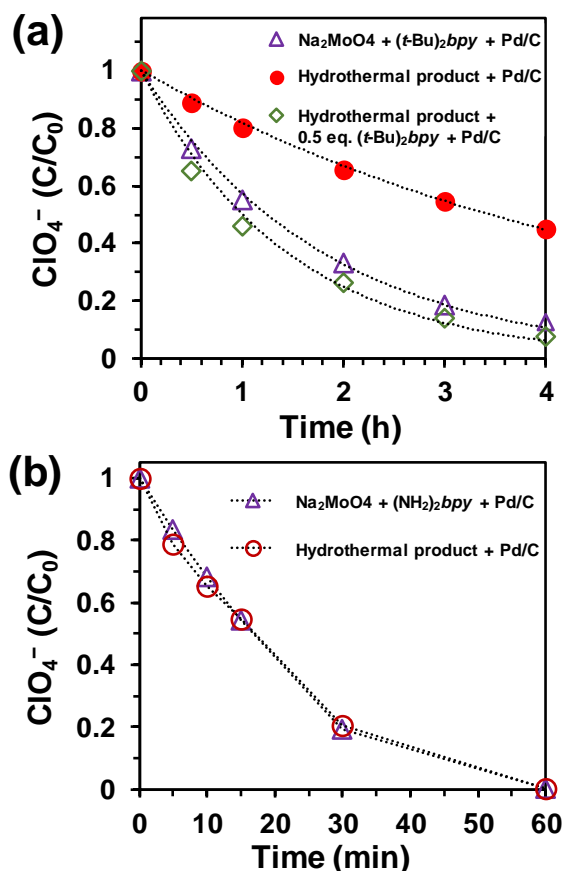
Figure S4.13 Aqueous ClO_4^- reduction using (L)MoO$_x$–Pd/C catalysts prepared from different Mo+L precursors. Reaction conditions: 0.2 g L^{-1} catalyst (5 wt% Mo in 5 wt% Pd/C), 1 mM ClO_4^-, pH 3.0, 1 atm H$_2$, 20 °C. Before adding ClO_4^-, all catalysts were prepared by stirring the mixture of Pd/C and Mo precursors in water suspension for 12 h under 1 atm H$_2$ at 20 °C.

In panel **a** where L = (t-Bu)$_2$*bpy*, the hydrothermal synthesis product was reported as Mo$^{VI}_8$O$_{22}$(OH)$_4$[(t-Bu)$_2$*bpy*]$_4$ with Mo : (t-Bu)$_2$*bpy* = 1 : 0.5.[16] The (L)MoO$_x$–Pd/C catalyst prepared directly from 1:1 Na$_2$MoO$_4$ and (t-Bu)$_2$*bpy* showed a much higher activity. The addition of another 0.5 equivalent of (t-Bu)$_2$*bpy* together with the hydrothermal product also yielded a similarly higher activity. These results confirm that the pre-synthesized Mo$^{VI}_8$O$_{22}$(OH)$_4$[(t-Bu)$_2$*bpy*]$_4$ complex decomposed upon dissolution in water. The Mo^{VI} species and free (t-Bu)$_2$*bpy* reassembled in Pd/C, similar to the direct use of Na$_2$MoO$_4$ + (t-Bu)$_2$*bpy*. The extra (t-Bu)$_2$*bpy* filled the 50% of ligand deficit in the pre-synthesized complex to match the optimal 1:1 ratio between Mo and L (also compare **Figure 4.2b** in the main text). In panel **b** where L = (NH$_2$)$_2$*bpy*, the use of the pre-synthesized [(NH$_2$)$_2$*bpy*]Mo complex achieved the same ClO$_4^-$ reduction activity as the standard preparation from Na$_2$MoO$_4$ + (NH$_2$)$_2$*bpy* at 1:1 ratio. Although the structure of the hydrothermally synthesized [(NH$_2$)$_2$*bpy*]MoO$_x$ product remained unknown, the 1:1 ratio between Mo^{VI} and (NH$_2$)$_2$*bpy* in the product is confirmed by this kinetic comparison. The direct use of hydrothermally synthesized [(t-Bu)$_2$*bpy*]Mo or [(NH$_2$)$_2$*bpy*]Mo complexes without carbon support did not reduce ClO$_4^-$ (see **Figures S4.14** and **S4.16**).
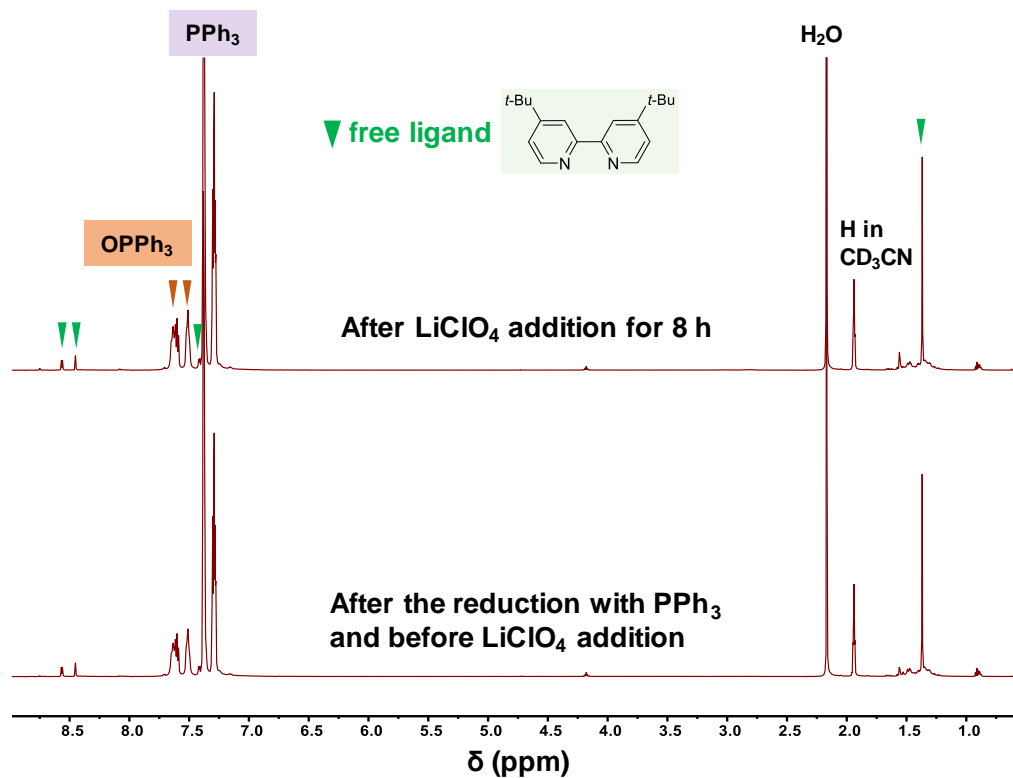
Figure S4.14 ^{1}H NMR spectra (CD$_3$CN, 600 MHz) demonstrating the oxygen atom transfer from pre-synthesized Mo$^{VI}_8$O$_{22}$(OH)$_4$[(t-Bu)$_2$bpy]$_4$ to PPh$_3$ and the lack of ligand coordination in solution after the reaction with excess PPh$_3$ in acetonitrile at 70 °C for 12 h. The formation of OPPh$_3$ is attributed to the reduction of Mo^{VI} into Mo^{IV} via oxygen atom transfer. The lack of resonances for other (t-Bu)$_2$bpy species suggests that all pre-synthesized [(t-Bu)$_2$bpy]Mo structures decomposed into free (t-Bu)$_2$bpy ligand upon dissolution. After LiClO$_4$ addition and heating at 70 °C for another 8 h, no significant change of OPPh$_3$: PPh$_3$ ratio was observed, indicating no ClO$_4^-$ reduction. The same experimental approach using the hydrothermally synthesized [(NH$_2$)$_2$bpy]MoO$_x$ complex observed a much lower amount of OPPh$_3$ and no resonance of (NH$_2$)$_2$bpy ligand because both the complex and free (NH$_2$)$_2$bpy ligand dissolved poorly in acetonitrile.

Experimental details: In an anaerobic glove bag (97% N$_2$ and 3% H$_2$), a 15 mL glass reaction tube was sequentially loaded with 5 mg of the pre-synthesized white powder of Mo$^{VI}_8$O$_{22}$(OH)$_4$[(t-Bu)$_2$bpy]$_4$, 27.5 mg of PPh$_3$, 6 mL of acetonitrile, and a magnetic stir bar. The resulting suspension thus contained 3.0 mM of Mo^{VI}, 1.5 mM of (t-Bu)$_2$bpy, and 17.5 mM of PPh$_3$. The suspension was sealed with a Teflon screw cap and heated in a 70 °C oil bath for 12 h to yield a yellow solution. LiClO$_4$ (1 mM) was then added, and

homogeneous ClO_4^- reduction was monitored by measuring PPh_3 versus $OPPh_3$ for another 8 h at 70 °C. Aliquots of 1 mL solution were collected at 0 and 8h, dried under vacuum, and redissolved in CD_3CN (1 mL) for ^1H NMR characterization.
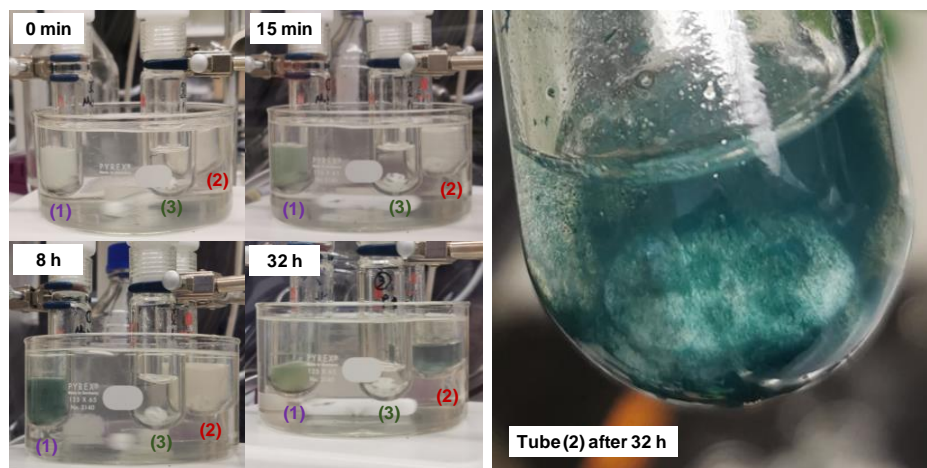
**Figure S4.15** Synthesis of phosphine-reduced [(NH$_2$)$_2$*bpy*]Mo^{IV} complex in the aqueous environment. Tube 1 started from Na$_2$MoO$_4$, (NH$_2$)$_2$*bpy*, and trisodium triphenylphosphine-3,3′,3″-trisulfonate (TPPTS). Tube 2 started from the pre-synthesized Mo^{VI} : (NH$_2$)$_2$*bpy* = 1 : 1 complex (by hydrothermal method) and TPPTS. Tube 3 only contained TPPTS for comparison as a clear solution. In Tube 1, the mixing of Na$_2$MoO$_4$ and (NH$_2$)$_2$*bpy* at the beginning yielded a white suspension, which gradually turned green at 70 °C. The the pre-synthesized [(NH$_2$)$_2$*bpy*]Mo complex needed a much longer time to turn green. The photo on the right side shows the final product as a green powder and colorless liquid. The green powder did not dissolve in common solvents. At pH 3.0, this suspension could not reduce ClO$_4^-$ (see **Figure S4.16a**).

Experimental details: In the anaerobic glove bag, a 15 mL glass reaction tube was sequentially loaded with 2.9 mg of Na$_2$MoO$_4$•2H$_2$O, 2.3 mg of (NH$_2$)$_2$*bpy*, 37 mg of TPPTS, 6.5 mL of deionized water, and a magnetic stir bar. For tube 2, 4.3 mg of the hydrothermally pre-synthesized Mo^{VI} : (NH$_2$)$_2$*bpy* = 1 : 1 complex (assumed as Mo^{VI}$_2$O$_6$[(NH$_2$)$_2$*bpy*]$_2$) was used instead of Na$_2$MoO$_4$ and (NH$_2$)$_2$*bpy*. The resulting white suspension thus contained 2 mM of Mo^{VI}, 2 mM of (NH$_2$)$_2$*bpy*, and 10 mM of TPPTS. The suspension was sealed with a Teflon screw cap and heated in a 70 °C oil bath. After 8 h, the pH was adjusted to 3.0 by H$_2$SO$_4$ and added with NaClO$_4$ (0.5 mM) to monitor ClO$_4^-$ reduction for another 24 h at 70 °C. Aliquots of 2 mL solution were collected at intervals. Samples were immediately analyzed by ion chromatography.
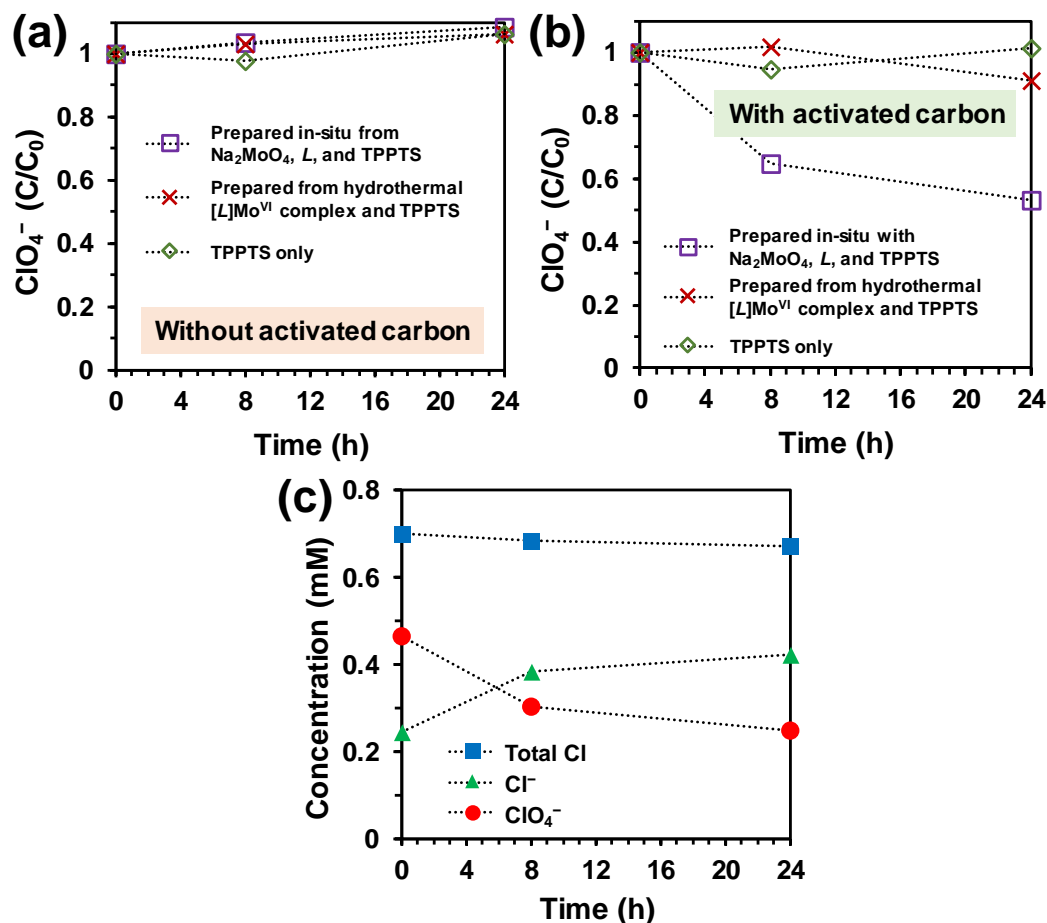
Figure S4.16 Time profiles for aqueous ClO_4^- reduction by TPPTS using different Mo sources with and without carbon support. The three settings in panel **a** correspond to the three reaction tubes described in **Figure S4.15**. The same three settings in panel **b** were added with activated carbon (no Pd nanoparticles or H_2) at the beginning of catalyst preparation. Panel **c** shows the chlorine mass balance for the ClO_4^- reduction enabled by Na_2MoO_4 + $(NH_2)_2bpy$ + TPPTS + carbon at 70°C. The background chloride ion at 0 h (0.24 mM) was from the impurity in carbon (3.5 g L^{-1} in water).

Experimental details: The reaction settings in panel **a** followed the method described for **Figure S15**. For the settings in panel **b**, 23 mg of activated carbon was added in each tube. The corresponding Mo content if fully immobilized on the carbon support was 5 wt%. The loading of the whole Mo/C catalyst in water was approximately 3.5 g L^{-1}.
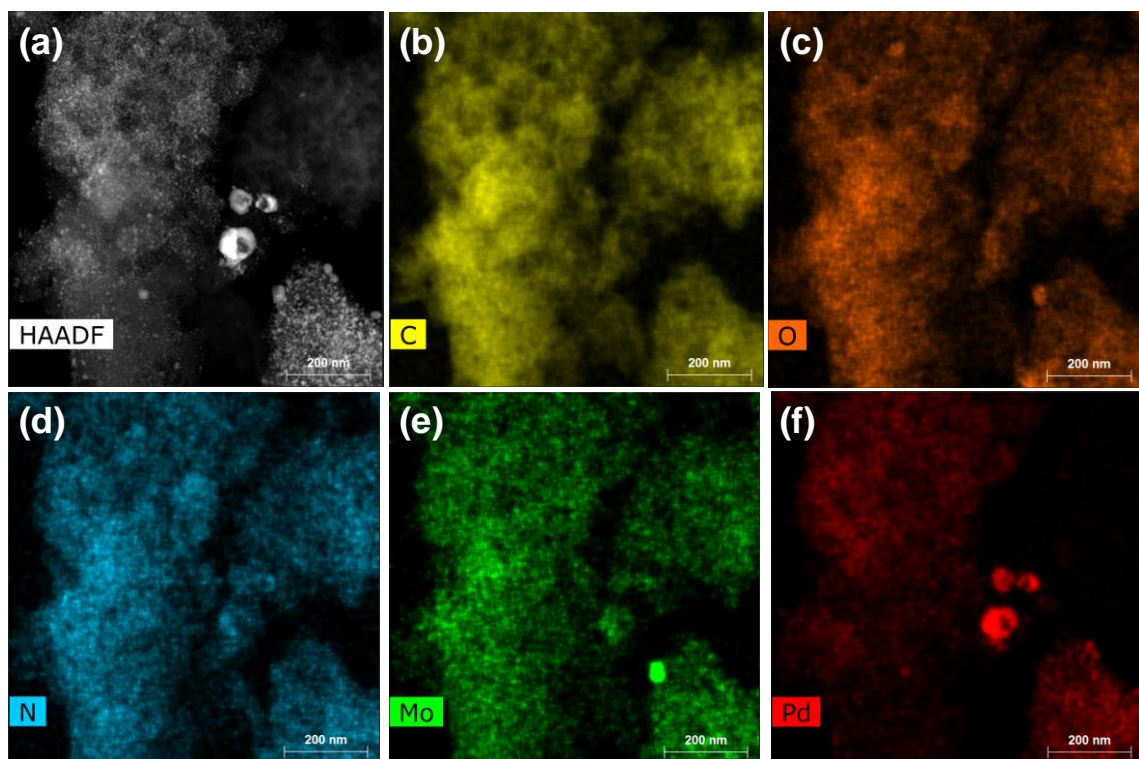
Figure S4.17. Original HAADF-STEM imaging and EDX mapping of another μm-sized particle of the [(NH$_2$)$_2$*bpy*]MoO$_x$−Pd/C catalyst. This particle shows the heterogeneity of metal distribution in the porous carbon (see **Figures 4.3i−4.3l** in the main text).
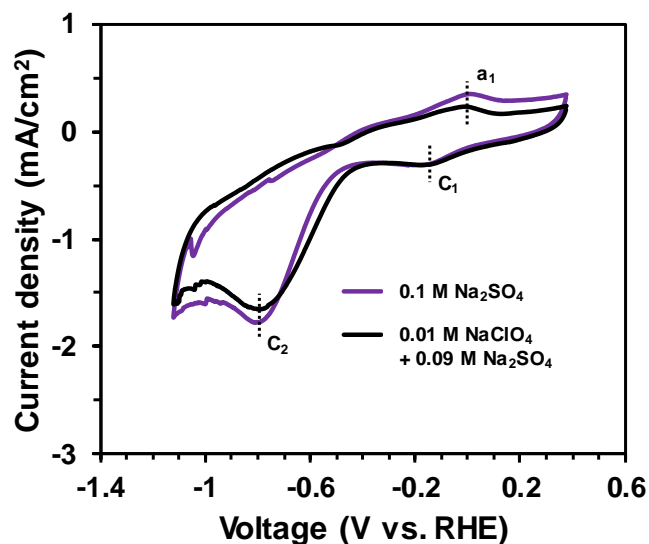
Figure S4.18. Cyclic voltammograms (CVs) of $[(NH_2)_2bpy]MoO_x/C$ (no Pd) in the absence and presence of $NaClO_4$. The working electrode was prepared by drop-casting $[(NH_2)_2bpy]MoO_x/C$ onto the glassy carbon electrode. The cyclic voltammetry was performed at pH 3.0 using a Ag/AgCl reference electrode and Pt wire counter electrode. Two cathodic peaks (labeled as c_1 and c_2, at -0.15 V and -0.8 V) were observed from the scanning in the negative direction. These two peaks are similar to the CVs of aqueous molybdate anions.[17] The anodic counterpart (a_1) of c_1 was observed at 0.0 V. The large potential difference between a_1 and c_1 (0.15 V) indicates the electrochemical irreversibility. After the addition of 0.01 M $NaClO_4$ into the electrolyte (black trace), there was no formation of a new reduction peak, nor a significant change in current densities at c_1 and c_2. Therefore, electrochemical ClO_4^- reduction with $[(NH_2)_2bpy]MoO_x/C$ is unlikely to occur. The reduction using H_2+Pd or phosphine seems necessary to enable ClO_4^- reduction.
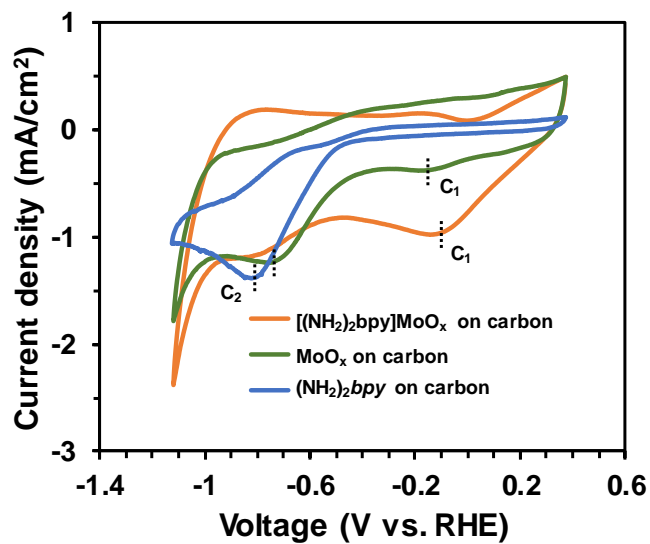
Figure S4.19. CVs of [(NH$_2$)$_2$*bpy*]MoO$_x$/C, MoO$_x$/C, and (NH$_2$)$_2$*bpy*/C in 0.1 M NaClO$_4$. The results confirm that the reduction peak c$_1$ in **Figure S4.18** arises mainly from the reduction of MoO$_x$ and the reduction peak c$_2$ is a combination of the reduction of MoO$_x$ and (NH$_2$)$_2$*bpy*.

Table S4.1. Performance of Abiotic Metal-Catalyzed Perchlorate Reduction Systems.

Entry	Catalyst	Catalyst loading	Reaction medium	Reductant	Moisture sensitivity	Air sensitivity	$[ClO_4^-]_0$ (mM)	TON	TOF[a] (h^{-1})	Apparent rate constant or ClO_4^- conversion	Ref.
Heterogeneous Catalysts- Mo and Re											
1							0.01	0.4	4.2	11.1 h^{-1}	
2	[(NH$_2$)$_2$*bpy*]MoO$_x$–Pd/C	0.2 g L$^{-1,b}$	Water (pH 3.0)	H$_2$ (1 atm)	No	No[e]	1	38.5	106	2.8 h^{-1}	this study
3							10	385	137	3.5 mM h$^{-1,h}$	
4							100	3850	165	4.3 mM h$^{-1,h}$	
5	ReO$_x$–Pd/C	2.0 g L$^{-1,c}$	Water (pH 2.7)	H$_2$ (1 atm)	No	Yes[f]	2	13	4.2	0.33 h^{-1}	18
6	[Re(O)$_2$(Me$_2$N*py*)$_4$]–Pd/C	1.0 g L$^{-1,d}$	Water (pH 2.7)	H$_2$ (1 atm)	No	N/A	2	40	31	0.80 h^{-1}	1
7	Re(O)(*hoz*)$_2$–Pd/C	0.5 g L$^{-1,b}$	Water (pH 3.0)	H$_2$ (1 atm)	No	Yes[g]	1	30	72	2.5 h^{-1}	6
8							10	300	64	0.22 h^{-1}	19
Homogeneous Catalysts- Re and Fe											
9	[Re(O)(*hoz*)$_2$(OH$_2$)]$^+$	0.03 equiv	CH$_3$CN/H$_2$O (v/v 95/5)	CH$_3$SCH$_3$ (5.4 equiv)	No	No	92	31	7.8	100% after 4h	20
10	[N(afa^{Cy})$_3$Fe(OTf)]$^+$	1 equiv	CH$_3$CN (anhydrous)	Diphenylhydrazine (4.0 equiv)	Yes	Yes	0.03	3	0.19	75% after 16h	21
11		0.05 equiv	THF (anhydrous)				0.02	76[i]	3.2	86% after 24h	22

[a] Turnover frequencies are either calculated using the degradation of the first 5% of the initial ClO_4^- concentration or as reported in the cited literature.
[b] These catalysts contained ~5 wt % Mo or Re, and 5 wt % Pd.
[c] This catalyst contained 5.7 wt% Re and 5 wt% Pd. ReO$_x$ catalysts were prepared from KReO$_4$.
[d] This catalyst contained 3.7 wt% Re and 5 wt% Pd. The catalyst can also be prepared *in situ* with 2:1 molar ratio of Me$_2$N*py*:KReO$_4$ added into Pd/C.
[e] Air exposure oxidized the reduced Mo, but metal leaching was minimal (<1.5%) and the catalytic activity was fully restored upon the re-application of 1 atm H$_2$. See **Figure S4.9a.**
[f] Air exposure oxidized the reduced Re and caused significant leaching (>50%), but the catalytic activity was fully restored upon the re-application of 1 atm H$_2$.[23]
[g] Air exposure caused irreversible decomposition of the Re(*hoz*)$_2$ complex into ReO$_4^-$ and free *hoz* ligand. The activity could not be restored. See **Figure S4.9b.**
[h] Zero-order kinetics shown at high ClO_4^- concentrations. See **Text S4.1** for details.
[i] TON was increased from **entry 10** due to the addition of [N(afa^{Cy})$_3$Zn(OTf)]$^+$ as a sacrificial agent to remove Cl$^-$ from the poisoned catalyst, [N(afa^{Cy})$_3$FeCl]$^+$.

Salt added	Fitting equation	R^2 value	Rate constant	Relative activity
	ClO_4^- reduction by [(NH$_2$)$_2$bpy]MoO$_x$−Pd/C			
DI	y = 0.9932−0.0305x	0.9985	0.0305 mM min^{-1}	1
0.1 M NaCl	y = 0.9955−0.0175x	0.9983	0.0175 mM min^{-1}	0.57
2.0 M NaCl	y = 0.9975−0.0016x	0.9628	0.0016 mM min^{-1}	0.052
1.0 M Na$_2$SO$_4$	y = 1.0099−0.0111x	0.9985	0.0111 mM min^{-1}	0.36
	ClO_3^- reduction by MoO$_x$−Pd/C			
DI	y = 1.0126e$^{-0.114x}$	0.9996	0.114 min^{-1}	1
2.0 M NaCl	y = 1.0106e$^{-0.062x}$	0.9978	0.062 min^{-1}	0.54
1.0 M Na$_2$SO$_4$	y = 0.9858e$^{-0.045x}$	0.9988	0.045 min^{-1}	0.39

Table S4.2 Salt Inhibition of Mo Catalysts with and without the Organic Ligand.[a]

[a] Source data are shown in **Figure S8**.

Sample	Shell	CN[a]	R (Å)[b]	σ^2 (Å^2)[c]	ΔE (eV)[d]	R-factor
MoO$_2$	Mo−O	6	1.99 (0.01)	0.002 (0.001)	−1.4 (2.0)	0.023
	Mo−Mo	1	2.52 (0.01)	0.001 (0.001)		
	Mo−Mo	1	3.12 (0.01)	0.002 (0.001)		
	Mo−Mo	8	3.70 (0.01)	0.004 (0.001)		
(NH$_4$)$_6$Mo$_7$O$_{24}$	Mo−O	4	1.74 (0.01)	0.004 (0.002)	−4.0 (3.3)	0.012
[(NH$_2$)$_2$bpy]MoO$_x$−Pd/C	Mo−O	1.1 (1.1)	1.67 (0.03)	0.002 (0.006)	−6.1 (4.9)	0.055
	Mo−O	5.1 (3.1)	1.99 (0.03)	0.012 (0.008)		
	Mo−Mo	0.9 (0.5)	2.57 (0.02)	0.002 (0.002)		
MoO$_x$−Pd/C	Mo−O	0.4 (0.3)	1.67 (0.04)	0.002[e]	−4.1 (2.9)	0.030
	Mo−O	6.1 (1.9)	2.03 (0.02)	0.010 (0.004)		
	Mo−Mo	1.7 (0.6)	2.56 (0.01)	0.005 (0.002)		

Table S4.3 Mo K-edge EXAFS Shell-by-Shell Fitting Parameters of Mo Standards and Mo−Pd/C Catalyst Samples.

[a] Coordination number; [b] Interatomic distance; [c] Debye-Waller factor; [d] Energy shift; [e] Fixed during the fitting.

Fitting Method	shell	CN[a]	R (Å)[b]	σ^2 (Å^2)[c]	ΔE (eV)[d]	R-factor
1	Mo−O	0.5 (16.5)	1.64 (0.80)	0.001 (0.135)		
	Mo−O	1.2 (26.3)	1.95 (0.17)	−0.00002 (0.081)	−10.2 (25.6)	0.046
	Mo−Pd	1.5 (25.3)	1.92 (0.70)	0.015 (0.166)		
	Mo−Mo	1.0 (1.8)	2.55 (0.08)	0.002 (0.009)		
2	Mo−O	−3.1 (43.5)	1.76 (0.46)	0.031 (0.233)		
	Mo−Pd	2.4 (5.0)	1.84 (0.04)	0.014 (0.014)	−13.9 (6.5)	0.121
	Mo−Mo	1.1 (0.8)	2.54 (0.02)	0.002 (0.003)		
3	**Mo−Pd**	2.5 (1.1)	1.83 (0.02)	0.014 (0.004)	−17.6 (3.1)	0.132
	Mo−Mo	0.9 (0.5)	2.53 (0.01)	0.002 (0.003)		

Table S4.4 Mo K-edge EXAFS Shell-by-shell Fitting Parameters of [(NH$_2$)$_2$bpy]MoO$_x$−Pd/C Using a Mo−Pd Shell. Values Highlighted in Red Color and Gray Shade are Problematic.

[a] Coordination number; [b] Interatomic distance; [c] Debye-Waller factor; [d] Energy shifts.

References

1.   Hurley, K. D.;   Zhang, Y.; Shapley, J. R., Ligand-Enhanced Reduction of Perchlorate in Water with Heterogeneous Re− Pd/C Catalysts. *Journal of the American Chemical Society* **2009,** *131* (40), 14172-14173.

2.   McPherson, L. D.;   Drees, M.;   Khan, S. I.;   Strassner, T.; Abu-Omar, M. M., Multielectron atom transfer reactions of perchlorate and other substrates catalyzed by rhenium oxazoline and thiazoline complexes: Reaction kinetics, mechanisms, and density functional theory calculations. *Inorganic chemistry* **2004,** *43* (13), 4036-4050.

3.   Ainsworth, S., Michaelis-Menten Kinetics. In *Steady-State Enzyme Kinetics*, Macmillan Education UK: London, 1977; pp 43-73.

4.   Shuai, D.;   Choe, J. K.;   Shapley, J. R.; Werth, C. J., Enhanced activity and selectivity of carbon nanofiber supported Pd catalysts for nitrite reduction. *Environmental science & technology* **2012,** *46* (5), 2847-2855.

5.   Weisz, P.; Prater, C., Interpretation of measurements in experimental catalysis. *Adv. Catal* **1954,** *6* (143), 60390-9.

6.   Liu, J.;   Choe, J. K.;   Wang, Y.;   Shapley, J. R.;   Werth, C. J.; Strathmann, T. J., Bioinspired complex-nanoparticle hybrid catalyst system for aqueous perchlorate reduction: Rhenium speciation and its influence on catalyst activity. *ACS Catalysis* **2015,** *5* (2), 511-522.

7.   Satterfield, C., Mass transport in heterogeneous catalysis. MIT Press, Cambridge, MA: 1970.

8.   Davie, M. G.;   Reinhard, M.; Shapley, J. R., Metal-catalyzed reduction of N-nitrosodimethylamine with hydrogen in water. *Environmental science & technology* **2006,** *40* (23), 7329-7335.

9.   Heil, S. R.;   Holz, M.;   Kastner, T. M.; Weingärtner, H., Self-diffusion of the perchlorate ion in aqueous electrolyte solutions measured by 35 Cl NMR spin–echo experiments. *Journal of the Chemical Society, Faraday Transactions* **1995,** *91* (12), 1877-1880.

10.   Ren, C.;   Yang, P.;   Gao, J.;   Huo, X.;   Min, X.;   Bi, E. Y.;   Liu, Y.;   Wang, Y.; Zhu, M.; Liu, J., Catalytic Reduction of Aqueous Chlorate With MoO x Immobilized on Pd/C. *ACS Catalysis* **2020,** *10* (15), 8201-8211.

11.   Sänger, P.; Deckwer, W.-D., Liquid—solid mass transfer in aerated suspensions. *The Chemical Engineering Journal* **1981,** *22* (3), 179-186.

12.   SANO, Y.; YAMAGUCHI, N.; ADACHI, T., Mass transfer coefficients for suspended particles in agitated vessels and bubble columns. *Journal of Chemical Engineering of Japan* **1974,** *7* (4), 255-261.

13.   Bates, R. L.; Fondy, P. L.; Corpstein, R. R., Examination of some geometric parameters of impeller power. *Industrial & Engineering Chemistry Process Design and Development* **1963,** *2* (4), 310-314.

14.   Liu, B.; Yao, H.; Song, W.; Jin, L.; Mosa, I. M.; Rusling, J. F.; Suib, S. L.; He, J., Ligand-free noble metal nanocluster catalysts on carbon supports via "soft" nitriding. *Journal of the American Chemical Society* **2016,** *138* (14), 4718-4721.

15.   Kishii, N.; Araki, K.; Shiraishi, S., The Changes in Conformation and Complexability of 6, 6′-Diamino-2, 2′-bipyridine by Protonation. *Bulletin of the Chemical Society of Japan* **1984,** *57* (8), 2121-2126.

16.   Amarante, T. R.; Neves, P.; Tomé, C. t.; Abrantes, M.; Valente, A. A.; Paz, F. A. A.; Pillinger, M.; Gonçalves, I. S., An octanuclear molybdenum (VI) complex containing coordinatively bound 4, 4′-di-tert-butyl-2, 2′-bipyridine,[Mo8O22 (OH) 4 (di-t Bu-bipy) 4]: synthesis, structure, and catalytic epoxidation of bio-derived olefins. *Inorganic chemistry* **2012,** *51* (6), 3666-3676.

17.   You, J.; Wu, D.; Liu, H., Electrochemical studies of molybdate and thiomolybdates. *Polyhedron* **1986,** *5* (1-2), 535-537.

18.   Hurley, K. D.; Shapley, J. R., Efficient heterogeneous catalytic reduction of perchlorate in water. *Environmental science & technology* **2007,** *41* (6), 2044-2049.

19.   Liu, J.; Han, M.; Wu, D.; Chen, X.; Choe, J. K.; Werth, C. J.; Strathmann, T. J., A new bioinspired perchlorate reduction catalyst with significantly enhanced stability via rational tuning of rhenium coordination chemistry and heterogeneous reaction pathway. *Environmental science & technology* **2016,** *50* (11), 5874-5881.

20.   Abu-Omar, M. M.; McPherson, L. D.; Arias, J.; Béreau, V. M., Clean and efficient catalytic reduction of perchlorate. *Angewandte Chemie* **2000,** *112* (23), 4480-4483.

21.   Ford, C. L.; Park, Y. J.; Matson, E. M.; Gordon, Z.; Fout, A. R., A bioinspired iron catalyst for nitrate and perchlorate reduction. *Science* **2016,** *354* (6313), 741-743.

22.   Drummond, M. J.; Miller, T. J.; Ford, C. L.; Fout, A. R., Catalytic Perchlorate Reduction Using Iron: Mechanistic Insights and Improved Catalyst Turnover. *ACS Catalysis* **2020,** *10* (5), 3175-3182.

23.   Choe, J. K.; Shapley, J. R.; Strathmann, T. J.; Werth, C. J., Influence of rhenium speciation on the stability and activity of Re/Pd bimetal catalysts used for perchlorate reduction. *Environmental science & technology* **2010,** *44* (12), 4716-4721.

Appendix D

Supplementary Information for Chapter 5

Entry	Catalyst formulation	Typical loading	pH in DI water [a]	$[ClO_4^-]_0$	Other constituents	Normalized rate constant [b] $(L\ h^{-1}\ g_{cat}^{-1})$	ref.
					$(L)MoO_x$−Pd/C (L = 4,4'-diamino-2,2'-bipyridine)		
1					DI [c]	14.0	
2					1 M Na_2SO_4	5.4	
3					0.1 M NaCl	7.5	
4	5 wt% Mo	0.2 g/L	3.0	1 mM (~100 mg/L)	0.4 M NaCl	4.1	this study
5	5 wt% Pd				1 M NaCl	2.2	
6					waste brine mimic [d]	0.2	
7					waste brine mimic w/o NO_3^-	2.1	
8					40 mM NH_4Cl	10.1	
					ReO_x−Pd/C (no organic ligand added)		
9					DI [c]	0.047	
10	5 wt% Re	2.0 g/L	3.0	1 mM	1 M NaCl	0.16	[1]
11	5 wt% Pd				waste brine mimic [d]	0.008	
12					waste brine mimic w/o NO_3^-	0.18	
					$(L)ReO_x$−Pd/C (L = 4-dimethylaminopyridine)		
13	7 wt% Re 5 wt% Pd	1.0 g/L	2.7	2 mM	DI [c]	0.73	[2]
					$(L')_2Re$−Pd/C (L' = oxazoline-phenolate ligand, hoz)		
14	5 wt% Re	0.5 g/L	3.0	1 mM	DI [c]	5.8	[3]
15	5 wt% Pd				1 M NaCl	0.14	

Table S5.1 Comparison between (L)Mo−Pd/C with Previously Reported Re−Pd/C Catalysts Regarding the Performance of ClO_4^- Reduction in Brines.

[a]The pH value slightly decreased in concentrated electrolytes. See the previous study[1] for details.
[b]Apparent first-order rate constants (h^{-1}) for ClO_4^- reduction (1 atm H_2, 20 °C) normalized by the loading of catalyst powder in water ($g_{cat}\ L^{-1}$) to facilitate cross-comparison.
[c]Containing SO_4^{2-} or Cl^- from the acid for pH adjustment and Na^+/K^+ introduced with the Mo or Re precursor.
[d]Containing 0.9 M Cl^-, 48 mM SO_4^{2-}, 38 mM NO_3^-, 0.22 mM $H_2PO_4^-/HPO_4^{2-}$, and the balancing Na^+. More details of the real brine are provided in Table 1.

| Entry	Condition	Added ClO_4^-	Dissolved Cl^- before reaction	0th-order rate constant (mM h^{-1})
1	1st spike	100 mM	0 M	0.358
2	3rd spike	100 mM	0.2 M	0.239
3	5th spike	100 mM	0.4 M	0.161
4	control	100 mM	0.4 M[b]	0.138

Table S5.2 Reduction Kinetics and Solution Conditions for Five Spikes of 100 mM ClO_4^- [a].

[a]Reaction conditions: 2 g/L of (L)Mo−Pd/C (5 wt% Mo, 5 wt% Pd), pH 3.0, 1 atm H_2, 20 °C. No filtration or DI water rinse was conducted between spikes.
[b]NaCl was added to simulate the reduction of four previous spikes of 100 mM ClO_4^- without oxidative deactivation.
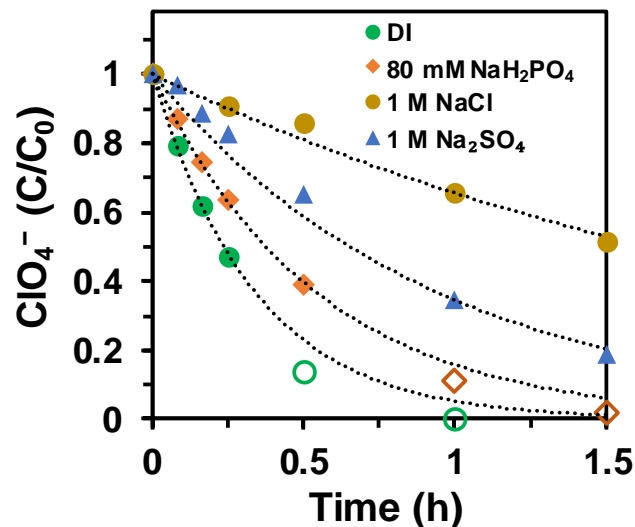
Figure S5.1 Time profiles for 1 mM ClO_4^- reduction by (L)Mo−Pd/C in the presence of various salts. Dotted lines indicate the fitting with the 1st-order model. Filled symbols were used to fit the model, whereas hollow ones ($C/C_0 < 0.2$) were not used. Reaction conditions: 0.2 g/L of (L)Mo−Pd/C (5 wt% Mo, 5 wt% Pd), pH 3.0, 1 atm H_2, 20 ℃.
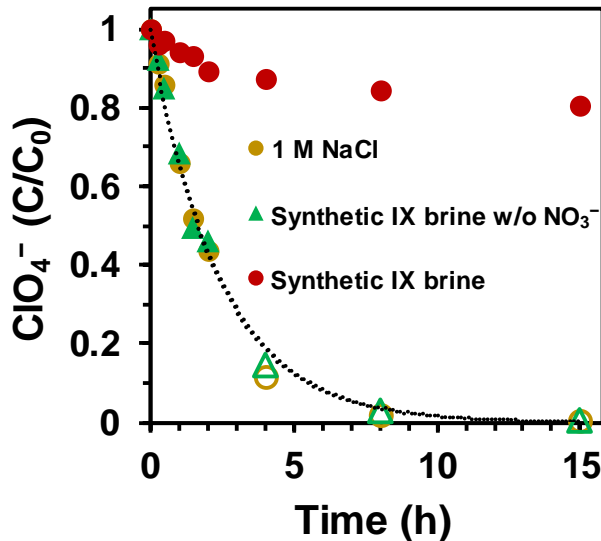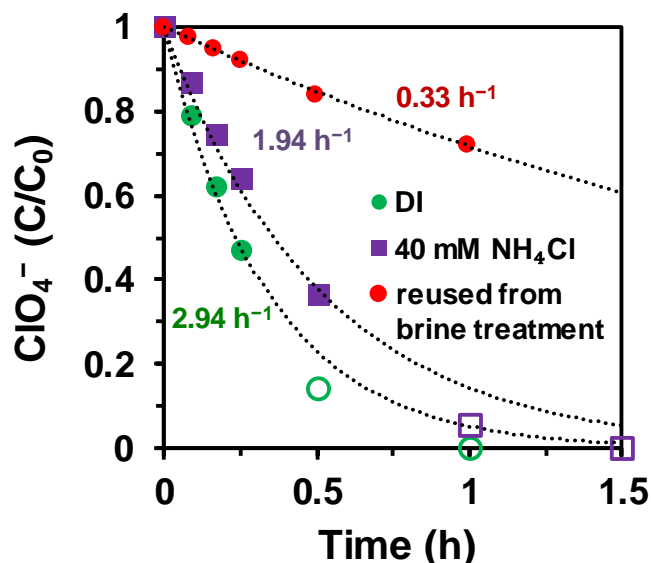

Figure S5.2 Time profiles for 1 mM ClO_4^- reduction by (L)Mo−Pd/C in the presence of 1 M NaCl or mixed salts in the synthetic IX regeneration brine. Dotted lines indicate the fitting with the 1st-order model using $C/C_0 > 0.2$ data. Reaction conditions: 0.2 g/L of (L)Mo−Pd/C (5 wt% Mo, 5 wt% Pd), pH 3.0, 1 atm H_2, 20 ℃.
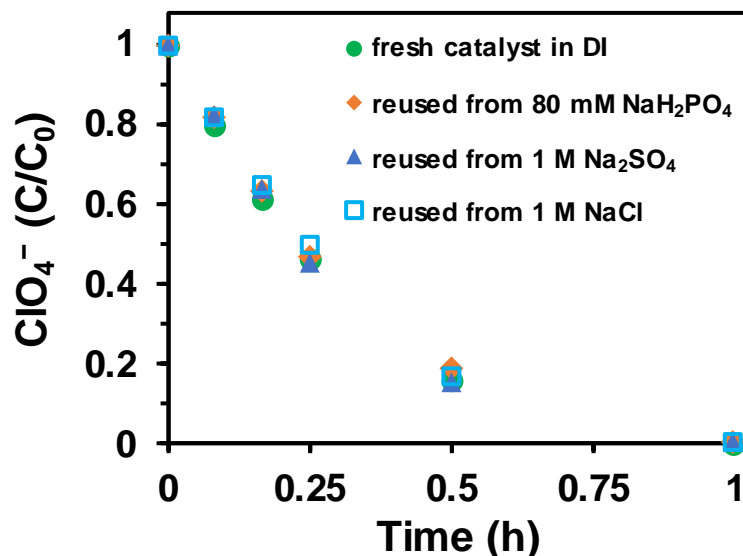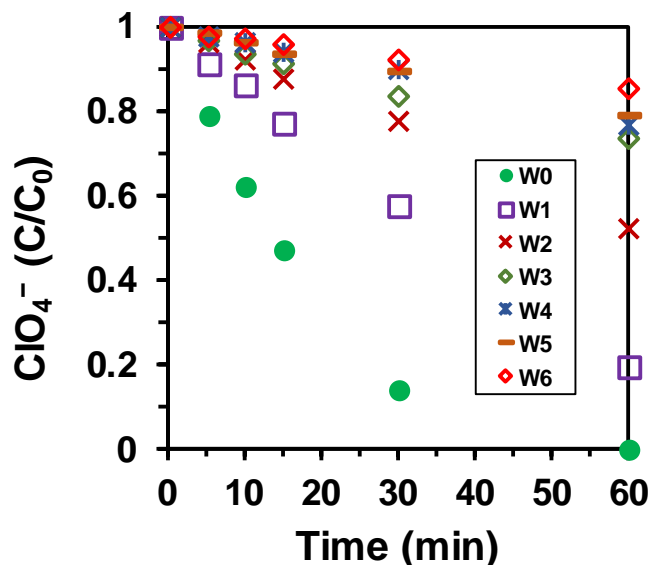
Figure S5.3 Time profiles for 1 mM ClO_4^- reduction by freshly prepared and reused (*L*)Mo−Pd/C in DI water. The "reused" catalyst was collected after a complete reduction of 1 mM ClO_4^- in 80 mM NaH_2PO_4, 1 M Na_2SO_4, or 1 M NaCl and then rinsed with DI water. Reaction conditions: 0.2 g/L of (*L*)Mo−Pd/C (5 wt% Mo, 5 wt% Pd), pH 3.0, 1 atm H_2, 20 °C.
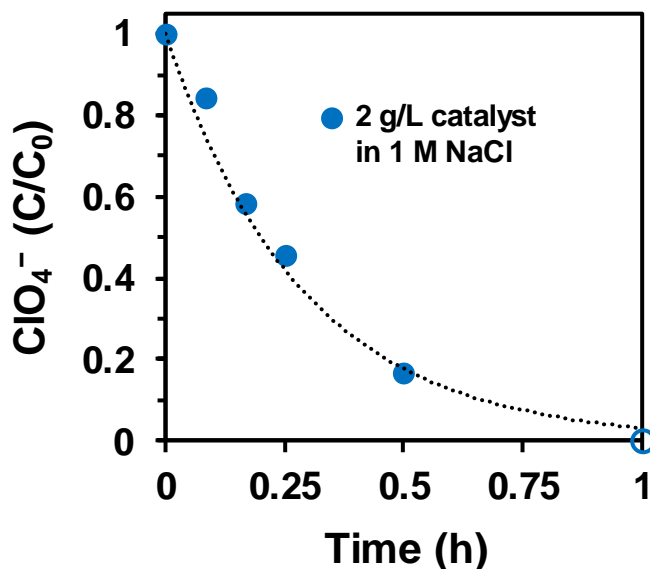
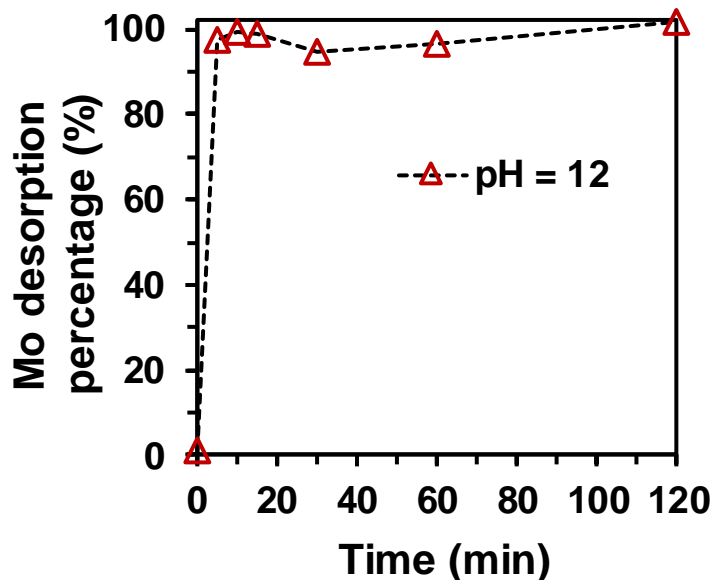**Figure S5.4** Time profile for 1 mM ClO_4^- reduction by 2 g/L of (*L*)Mo−Pd/C in 1 M NaCl. The filled data points (C/C$_0$ > 0.2) were used to fit the 1st-order model. Reaction conditions: pH 3.0, 1 atm H_2, 20 °C.
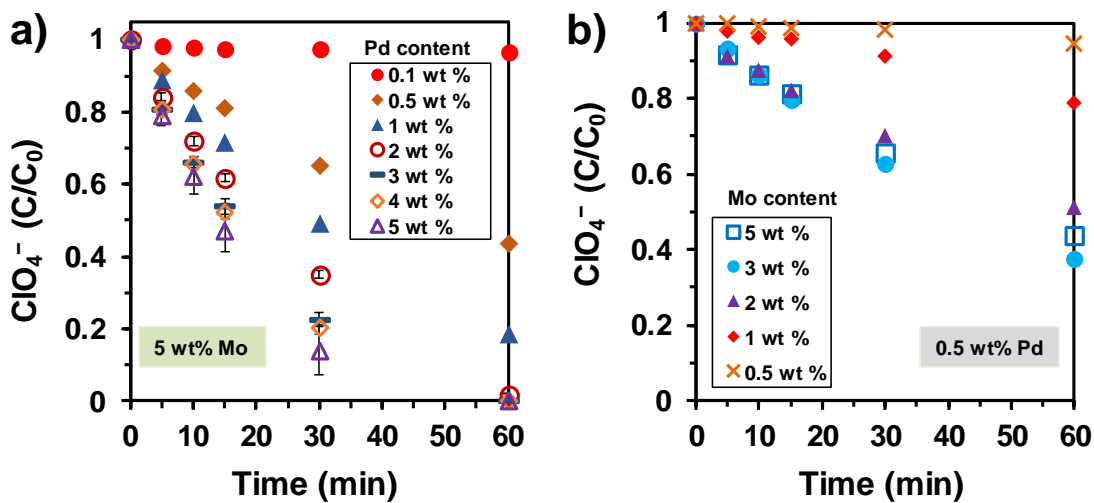
Figure S5.5 Time profiles for 1 mM ClO_4^- reduction by fresh (L)Mo−Pd/C in DI water and in the presence of 40 mM NH_4Cl, and by the "reused" catalyst from treating the synthetic brine containing 40 mM of NO_3^-. The reused catalyst was collected by filtration and rinsed with DI water. The filled data points ($C/C_0 > 0.2$) were used to fit the 1st-order model. Reaction conditions: 0.2 g/L catalyst, pH 3.0, 1 atm H_2, 20 °C.

Figure S5.6 Time profiles for 1 mM ClO_4^- reduction using (L)Mo−Pd/C after different durations of H_2 exposure. Reaction conditions: 0.2 g/L catalyst, pH 3.0, 1 atm H_2, 20 °C. Fresh (L)Mo−Pd/C catalysts were prepared and kept under 1 atm H_2 in a series of sealed serum bottles (50 mL of liquid and ~20 mL of headspace). The serum bottles were stored in a glove bag (98% N_2 and 2% H_2, Coy Laboratories). The headspace in the serum bottle was flushed with 1 atm H_2 once per week until the use for ClO_4^- reduction.

Figure S5.7 The time profile for Mo desorption from (*L*)Mo−Pd/C (after six weeks of continuous H_2 exposure) into water at pH 12.0.

Figure S5.8 Time profiles of 1 mM ClO_4^- reduction using (*L*)Mo−Pd/C with various (a) Pd and (b) Mo contents. Reaction conditions: 0.2 g/L catalyst, pH 3.0, 1 atm H_2, 20 °C.

Text S5.1 Estimation of the environmental impacts based on reported LCA data.

A previous LCA study[4] compared the environmental impacts of ion exchange, microbial reduction, and catalytic reduction of ClO_4^- (using the original ReO_x-Pd/C containing 5 wt% Re and 5 wt% Pd). The hypothetical source water used for the LCA contained 50 μg/L of perchlorate, 20 mg/L of nitrate, 30 mg/L of sulfate, and 5 mg/L of dissolved oxygen as a typical formulation of contaminated groundwater. Because of the time duration, pH requirement, and other factors, direct use of abiotic catalysts for treating drinking water is not feasible. Therefore, we propose to couple ion-exchange resin with catalytic treatment. Perchlorate-selective resin can concentrate ClO_4^- from >37,000 bed volumes of source water into just one bed volume of waste brine from resin regeneration. The regeneration frequency can be as low as once every six months.[5] We assume that the LCA study has obtained minimal environmental impact parameters (i.e., leaving minimal room for further improvement) for the original ReO_x-Pd/C formulation.

In the synthetic brine matrix, the $(L)Mo-Pd/C$ containing 5 wt% Mo and 5 wt% Pd was 10-fold more active than ReO_x-Pd/C (**Table 5.2 entry 6** versus **11**). Moreover, further optimization of the catalyst formulation suggested that 70% of Pd can be saved if the carbon loading is tripled (**Figure 5.3c**). Therefore, the saving factor for Pd can be further elevated to 10/(100%−70%) = 33. The contribution of Pd to the "global warming" impact shown in **Figure 5.3e** can be lowered by a factor of 33 by switching from the original ReO_x-Pd/C to the optimized $(L)Mo-Pd/C$ (3 wt% Mo and 0.5 wt% Pd) without sacrificing the rate of ClO_4^- reduction. Because the Mo content can be reduced from 5 wt% to 3 wt% while the catalyst loading needs to be tripled to achieve the same rate of ClO_4^- reduction,

the amount of involved Mo is $3 \times 3/5 = 1.8$ (i.e., 80% more Mo is used to save 70% of Pd). Thus, the saving factor for Mo is $10/1.8 = 5.6$. Similarly, the saving factor for activated carbon as the catalyst support is $10/3 = 3.3$. Lacking detailed LCA metrics for Mo, we simply assume that the environmental impact of Mo is the same as Re, although this simplification might lead to a significant overestimation.

In **Figure 5.3e**, the data for "microbial reduction" and "IX and Re−Pd/C" followed the original report.[4] The data for "IX and Mo−Pd/C" only changed the values of the three components discussed above (**Table A5.1**).

	For "IX and Re−Pd/C"	Saving factor for 5% Mo−5% Pd/C	For "IX and 5% Mo−5% Pd/C"	Saving factor for the optimized 3% Mo−0.5% Pd/C	For "IX and optimized 3% Mo−0.5% Pd/C" at 3x loading
-Pd metal	1650 [a]	10	165	33	50
-Re/Mo metal	230 [a]	10	23	5.6	41
-Carbon support	10 [a]	10	1	3.3	3
-IX resin	260 [a]	1	260	1	260
-Electron donor	80 [a]	1	80	1	80
-Aeration	50 [a]	1	50	1	50
-Total	2280		579		484

Table A5.1. Adjustment of LCA values (unit: kg of CO_2 equivalent per kg of ClO_4^- treated).
[a]These values were extracted from **Figure 5.6** of the LCA study.[4]

References

1.   Liu, J.; Choe, J. K.; Sasnow, Z.; Werth, C. J.; Strathmann, T. J. Application of a Re–Pd bimetallic catalyst for treatment of perchlorate in waste ion-exchange regenerant brine. *Water Res.* **2013**, *47*, 91-101.

2.   Hurley, K. D.; Zhang, Y.; Shapley, J. R. Ligand-enhanced reduction of perchlorate in water with heterogeneous Re−Pd/C catalysts. *J. Am. Chem. Soc.* **2009**, *131*, 14172-14173.

3.   Liu, J.; Chen, X.; Wang, Y.; Strathmann, T. J.; Werth, C. J. Mechanism and mitigation of the decomposition of an oxorhenium complex-based heterogeneous catalyst for perchlorate reduction in water. *Environ. Sci. Technol.* **2015**, *49*, 12932-12940.

4.   Choe, J. K.; Mehnert, M. H.; Guest, J. S.; Strathmann, T. J.; Werth, C. J. Comparative assessment of the environmental sustainability of existing and emerging perchlorate treatment technologies for drinking water. *Environ. Sci. Technol.* **2013**, *47*, 4644-4652.

5.   Gu, B.; Brown, G. M.; Chiang, C.-C. Treatment of perchlorate-contaminated groundwater using highly selective, regenerable ion-exchange technologies. *Environ. Sci. Technol.* **2007**, *41*, 6277-6282.